DISSERTATION

Synthetic Methods to Control the Structure of Titania – Polymer Hybrid Materials and Nanocomposites

ausgeführt zum Zwecke der Erlangung des akademischen Grades eines Doktors der technischen Wissenschaften unter der Leitung von

Ao. Univ.-Prof. Dr. Guido Kickelbick

Institut für Materialchemie

E165

eingereicht an der Technischen Universität Wien

Fakultät für Technische Chemie

von

Dipl. Ing. Sorin Ivanovici

Matr. Nr. 0527710

Schlüsselgasse 2/16, 1040 Wien

Wien, am 30.06.2008

...for my Grandfather and for Punga

Acknowledgements

First of all, I am very grateful to my supervisor, *Ao. Univ. Prof. Guido Kickelbick*, for giving me the opportunity to undertake my thesis in his research group. His support, guidance, and his confidence in my scientific skills throughout the last years helped me develop both as a scientist and as a person.

Furthermore I want to thank *Ao. Univ. Prof Herwig Peterlik* for the help with the SAXS measurements and productive and interesting discussions, *Dr. Michael Puchberger* for the help with the NMR measurements and for his advices, *Prof. Ulrich Schubert* for scientific support, *Dr. Johannes Bernardi* and *Dr. Sabine Schwarz* for their support on transmission electron microscopy, *Dr. Thomas Koch* and *Elisabeth Eitenberger* for the SEM measurements, *Dr. Silvia Gross* for the XPS measurements, *Dr. Matthias Bauer* and *Benjamin Marchetti* for the EXAFS and Raman measurements, *Dr. Erich Halwax* and *Dipl. Ing. Berthold Stöger* for the XRD measurements, and *Dr. Helmut Fric* for measuring my three crystals, and *Dr. Olivier Lorret* and *Dr. Georg Waldner* for the photocatalytic studies.

My sincere thanks go to all my (former) colleagues/friends and co-workers in Vienna:

Akira, Ana (for her positive attitude)*, Angelika* (for her brightness)*, Berthold* (the real chemist)*, Bernhard, Christian, Christina, Christoph R.* (for solving all my computer problems and for AFM measurements)*, Christoph & Marina L., Claudia F.* (the never-ending sunshine, for her friendship and scientific support)*, Claudia V., Dini, Dieter H., Denisa* (for the phosphonates)*, Denise, Doris B*. (my favorite flat-mate)*, Doris E., Elena* (for the great time in Barcelona)*, Fatmir, Grace, Harald, Helmut, Horst, Jakob, Jim, Maia, Majka, Marco* (for reading parts of this work)*, Melitta, Mirka, Mohsin, Philipp, Ralf* (for great dancing nights out in Chelsea)*, René* (for his flat, friendship and support)*, Robert L., Robert P., Rupert* (for repairing everything)*, Sandra* (for the perpetual smile), *Simas, Stefan B., Stephan, Van An,*

for a pleasant working and scientific atmosphere, and to most of them, for their friendship.

To Antoine and Carlos, who volunteered to do lab work for my thesis.

I gratefully acknowledge the *Fonds zur Förderung der wissenschaftlichen Forschung (FWF)* (project nr.: P17424) and the *Austrian Nanoinitiative* (project nr.: N1001) for financial support of this work.

My greatest debt is to *my parents*, who supported me throughout my study time and my wild years, and who never stopped believing in me. Special thanks to *my grandmother* and to *my brother, Bogdan.*

To *Irina* for being always there for me and for her unconditional love, no matter how my strange moods were.

Abstract

The synergetic combination of inorganic and organic components on the molecular level is a challenging task in materials science and chemistry, offering a wide variety of possible properties. An important sub-class of inorganic-organic hybrid materials and nanocomposites is represented by polymers with embedded nanosized metal oxides modified with polymerizable surface groups.

In the first part of the work hybrid materials were designed through the covalent connection of metal alkoxides to a polymer backbone and subsequent hydrolysis and condensation. In a first step compounds were prepared containing both a polymerizable bond and a metal alkoxide as precursor for the sol-gel process, connected via strong chemical bonds. Hybrid materials were obtained applying both a controlled radical polymerization and the sol-gel process. Analyses of the resulting materials revealed that they were composed of monodispersed metal oxide nanoparticles incorporated inside the polymer matrices. Copolymerization with monomers resulted in materials with enhanced mechanical and thermal properties compared to organic polymers. On the other hand, elastomers in form of polysiloxanes were also used as polymer matrices. Their functionalization with similar metal alkoxide building blocks could be achieved through hydrosilation reactions. In the subsequent sol-gel process either bulk materials of polysiloxane matrices with ordered metal oxide domains inside, or hybrid core-shell nanoparticle morphologies were obtained depending on the interactions of the backbone polymers with the solvents employed.

The second part of the work was devoted to the synthesis of anisotropically surface-functionalized anatase nanoparticles and their applications as photocatalysts. The particles were produced applying the sol-gel process which allowed the control over the particle size and crystallinity. Monodispersed particles with diameters between 5 and 20 nm were obtained. These particles were anisotropically surface-functionalized with phosphonate and phosphate coupling agents containing polymerizable groups using an oil-in-water Pickering emulsion. Thus, 'Janus'-type particles were obtained that showed a good activity in photocatalysis and were able to bind to organic polymers. Using Pickering emulsions also hybrid architectures could be designed through polymerization inside the emulsion droplets. The resulting materials were hybrid polymeric spheres of 2 to 20 μm diameter which consisted of a surface that was covered by the photocatalytically active TiO_2 nanoparticles. In another approach the pristine titania nanoparticles were completely surface-modified in suspension, using the same type of organophosphorus coupling agents, and further on incorporated in polymeric matrices. The resulting hybrid materials were optical transparent and showed an increased thermal and mechanical stability.

Kurzfassung

Die synergetische Kombination von anorganischen und organischen Komponenten auf molekularer Ebene ist eine große Herausforderung in der Materialwissenschaft und Materialchemie, die zu Materialen mit einem breiten Eigenschaftsspektrum führen kann. Ein wichtiges Teilgebiet der anorganisch-organischen Hybridmaterialien und Nanokomposite stellen Polymere mit eingebetteten Metalloxid-Nanopartikeln mit polymerisierbaren Oberflächenliganden dar.

Im ersten Teil der Arbeit wurden Hybridmaterialien durch kovalente Anbindung von Metallalkoxiden an eine Polymerkette und anschließende Hydrolyse und Kondensation hergestellt. In einem ersten Schritt wurden Komponenten hergestellt, welche sowohl eine polymerisierbare Bindung, als auch Metall-Alkoxide als Vorstufe für Sol-Gel Prozesse besitzen, beide durch starke chemische Bindungen aneinander gebunden. Hybridmaterialien werden durch anschließende Durchführung einer kontrollierten radikalischen Polymerisation und des Sol-Gel-Prozesses erhalten. Die Charakterisierung der resultierenden Materialien zeigte, dass monodisperse Metalloxid-Nanopartikel mit hoher Ordnung in eine Polymermatrix eingebettet werden konnten. Durch Copolymerisation mit Monomeren konnte eine signifikante Verbesserung der mechanischen und thermischen Eigenschaften der Endprodukte erreicht werden. Weiters wurden Elastomere in Form von Polysiloxanen als polymere Matrizen verwendet, deren Funktionalisierung mit Metallalkoxiden durch Hydrosilylierung erfolgte. Im anschließenden Sol-Gel-Prozess konnten abhängig von den Wechselwirkungen der Polymerkette mit den verwendeten Lösungsmitteln entweder monolithische Materialien aus Polysiloxan-Matritzen mit geordneten Metalloxid-Domänen oder Hybrid Kern–Schale Nanopartikel erhalten werden.

Der zweite Teil der Arbeit behandelt die Synthese von anisotrop oberflächenmodifizierten Anatas-Nanopartikeln und ihre Anwendungen in der Photokatalyse. Die Nanopartikel wurden über den Sol-Gel-Prozess hergestellt, der die Kontrolle über die Partikelgröße und kristallinität erlaubte. Monodisperse Partikel mit Durchmessern zwischen 5 und 20 nm wurden erhalten. Durch die Verwendung von Öl-in-Wasser Pickering Emulsionen konnten diese Partikel mit verschiedenen Kopplungsreagenzen, wie Phosphonaten und Phosphaten mit polymerisierbaren Gruppen, anisotrop oberflächenfunktionalisiert werden. Diese ‚Janus'-Partikel zeigten eine hohe Aktivität in der Photokatalyse und konnten an organische Polymere gebunden werden. Außerdem konnten durch Polymerisation im Inneren der Emulsionströpfchen auch Hybridarchitekturen hergestellt werden. Die resultierenden sphärischen Hybridpolymere besaßen einen Durchmesser von ungefähr 2 μm, und ihre Oberfläche war mit photokatalytisch aktiven TiO_2 Nanopartikeln besetzt. In einem anderen Ansatz wurden die reinen Titandioxid Nanopartikel unter Verwendung derselben Organophosphorgruppen in Suspension oberflächenfunktionalisiert und anschließend in polymere Matrizen eingebracht. Die erhaltenen Hybridmaterialien waren optisch transparent und zeigten eine erhöhte thermische und mechanische Stabilität.

Parts of this work have been published:

1. "*Coordi nation Behavior of Acetoacetate Ligands with Attached Methacrylate Groups Containing Alkyl-Spacers of Different Length to Titanium and Zirconium Alkoxides*"; Sorin Ivanovici, Michael Puchberger, Helmut Fric, Guido Kickelbick: Monatshefte für Chemie, **138** (2007), 6; S. 529 - 539.

2. *"Hybrid Nanocomposites Based on Metal Oxides and Polysiloxanes with Controlled Morphology"*; Sorin Ivanovici, Christoph Rill, Claudia Feldgitscher, Guido Kickelbick: *Organic/Inorganic Hybrid Materials—2007*, edited by R.M. Laine, C. Sanchez, C. Barbé , U. Schubert (Mater. Res. Soc. Symp. Proc. **Volume 1007**, Warrendale, PA, 2007).

3. "*Atom Transfer Radical Polymerizations of Complexes Based on Ti and Zr Alkoxides Modified with β-Keto Ester Ligands and Transformation of the Resulting Polymers in Nanocomposites*"; Sorin Ivanovici, Herwig Peterlik, Claudia Feldgitscher, Michael Puchberger, Guido Kickelbick: Macromolecules, **41** (2008), S. 1131 – 1139

4. *"Synthesis of hybrid polysiloxane-MO_2 (M = Si, Ti, Zr) nanoparticles through a sol–gel route"*; Sorin Ivanovici, Guido Kickelbick: J Sol-Gel Sci Technol, (2008), 46(3), 273-280

5. *"Solvent effects in the formation of hybrid materials based on titanium alkoxide-polysiloxane precursors"*; Sorin Ivanovici, Christoph Rill, Thomas Koch, Michael Puchberger, Guido Kickelbick: New Journal of Chemistry, (2008), 32(7), 1243-1252

Index of Abbreviations

AAA	Allyl Acetoacetone
APA	Allyl phosphonic acid
APA-^{i}Pr	Allyl phosphonic acid, ^{i}Pr esters
AAEMA	2-(methacryloyloxy)ethyl acetoacetate (deprotonated)
AAPMA	3-(methacryloyloxy)propyl acetoacetate (deprotonated)
AABMA	4-(methacryloyloxy)butyl acetoacetate (deprotonated)
AcAc	Acetylacetonate
ATRP	Atom Transfer Radical Polymerization
BPO	Benzoyl peroxide
Bu, ^{n}Bu	Butyl
DPA	Dodecyl phosphonic acid
DPA-Et	Dodecyl phosphonic acid, Et esters
Et	Ethyl
HAAEMA	2-(methacryloyloxy)ethyl acetoacetate
HAAPMA	3-(methacryloyloxy)propyl acetoacetate
HAABMA	4-(methacryloyloxy)butyl acetoacetate
HBMA	hydroxybutyl methacrylate
HPMA	hydroxypropyl methacrylate
^{i}Pr	Isopropyl
MetC5PA-Et	2-Methyl-acrylic acid 5-(dihydroxy-phosphoryl)-pentyl ester
MetC11PA	2-Methyl-acrylic acid 11-phosphono-undecyl ester
MetC11PA-Et	2-Methyl-acrylic acid 11-(diethoxy-phosphoryl)-undecyl ester
MetC8PoA	2-Methyl-acrylic acid 8-phosphonooxy-octyl ester
MetPPOPoA	Poly(propyleneoxide)phosphate–methacrylate terminated

MMA	Methyl methacrylate
M_n	Number average molecular weight
M_w	Mass average molecular weight
MWDs	Molecular weight distributions
PDI	Polydispersity
PDMS	Polydimethylsiloxane
PDMS-co-PMHS	Polydimethylsiloxane-co-methylhydrosiloxane
PMHS	Polymethylhydrosiloxane
POSS	Polyhedral Oligomeric Silsesquioxanes
PMMA	Poly(methyl methacrylate)
PPA	Phenyl phosphonic acid
PPoA	Phenyl phosphoric acid
Pr	Propyl
PS	Polystyrene
$Ti(O^iPr)_4$	Titanium tetraisopropoxides
$Ti(OEt)_4$	Titanium tetraethoxides
$Ti(OBu)_4$	Titanium tetrabutoxides
T_g	Glass transition temperature
THF	Tetrahydrofuran
wt	weight
$Zr(O^iPr)_4$	Zirconium tetraisopropoxides
$Zr(OBu)_4$	Zirconium tetrabutoxides

Techniques

AFM	Atomic Force Microscopy
ATR	Attenuated Total Reflection
COSY	Correlated Spectroscopy
DSC	Differential Scanning Calorimetry
EDX	Energy dispersive X-ray spectroscopy
EXAFS	Extended X-Ray Absorption Fine Structure
FTIR	Fourier Transform Infrared Spectroscopy
HMBC	Heteronuclear Multiple Bond Correlation
HSQC	Heteronuclear Single Quantum Coherence

IR	Infrared Spectroscopy
NMR	Nuclear Magnetic Resonance
SAXS	Small Angle X-Ray Scattering
SEC	Size Exclusion Chromatography
SEM	Scanning Electron Microscopy
STEM	Scanning Transmission Electron Microscopy
TEM	Transmission Electron Microscopy
TGA	Thermogravimetric Analysis
TOCSY	Total Correlated Spectroscopy
XRD	X-Ray Diffraction
XPS	X-Ray Photoelectron Spectroscopy

NMR Abbreviations

δ	Chemical Shift
s	Singlet
d	Doublet
t	Triplet
q	Quartet
m	Multiplet
br	broad

Infrared Abbreviations

vs	very strong
s	strong
m	medium
w	weak
vw	very weak
sh	shoulder
br	broad

Table of Contents

1. Introduction

1.1. Inorganic – Organic Hybrid Materials

Since the beginning of civilization, materials played an essential role in the progress and development of mankind. The different stages of our history have been named after the main materials used, e. g. the Stone Age, the Bronze Age, etc.

In the last decades the technological breakthroughs generated an enormous demand for novel materials with enhanced properties than the classical materials, such as metals, ceramics or plastics[1].

Hybrid materials are not an invention of the last years. A closer look in history shows that our ancestors were often using mixtures of various materials for different applications. The most famous example is the Maya Blue (Figure 1.1.), a hybrid paint used by the Maya civilization which preserved its color for over 1300 years[2]. Recent studies showed that this dye is one of the first examples of a hybrid organic–inorganic material, in which organic dye (indigo) is protected with a complex natural clay called palygorskite. The preservation of this color for such a long time was the result of the synergistic combination of vegetal color and mineral strength[2].

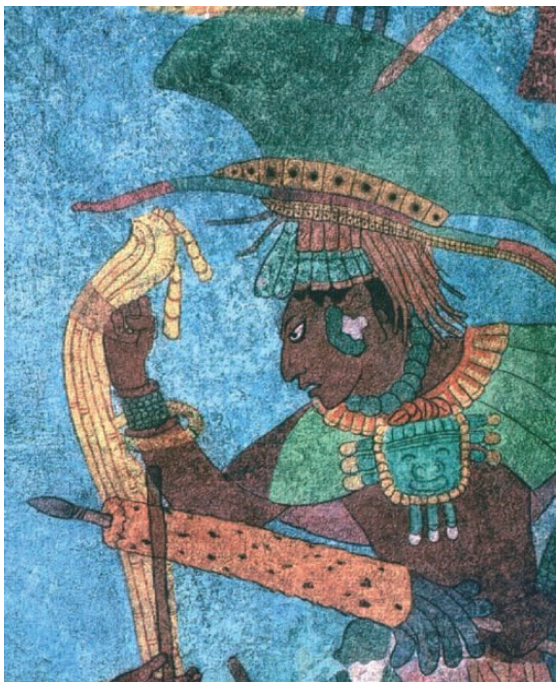

Figure 1.1. Computer-enhanced Mayan warrior from Bonampak[2]

In the last two decades, both scientists and engineers realized that mixtures of materials can show superior properties compared to their pure counterparts. Many scientists focused on the

design and development of new materials within which the characteristics of both inorganic and organic moieties would lead to enhanced properties.

Definition and Classification

Before discussing the synthetic pathways used for hybrid materials, a definition is required. A hybrid material is a material that includes two moieties blended on the molecular scale. Commonly one of these compounds is inorganic and the other one organic[1]. Thus, an inorganic–organic hybrid material is basically a material that includes two moieties, one inorganic and the other organic, blended on the molecular scale. Depending on the possible interactions between the two moieties, one can distinguish between *class I* hybrid materials and *class II* hybrid materials. *Class I* hybrid materials are those that show weak interactions between the two phases, such as van-der-Waals, hydrogen bonding or weak electrostatic interactions (Scheme 1.1).

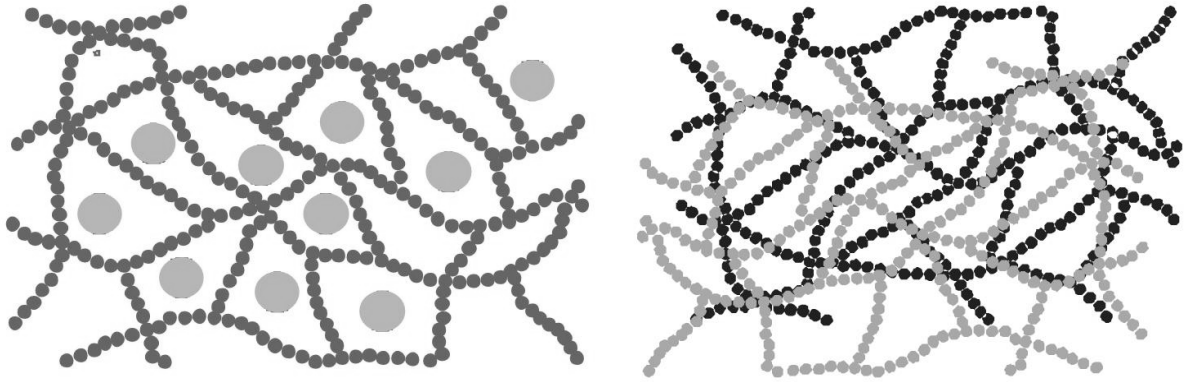

Scheme 1.1. *Class I* hybrid materials: embedded components (left) and interpenetrating networks (right)

Class II hybrid materials are those that show strong chemical interactions between the components (Scheme 1.2). The various types of interactions are presented in Table 1.1.

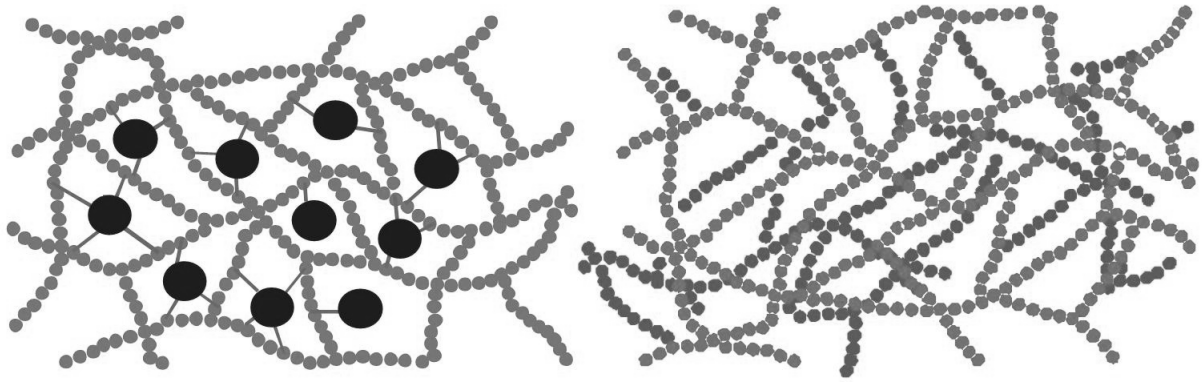

Scheme 1.2. *Class II* hybrid materials: covalently bonded particles (left) and dual networks (right)

Table 1.1. Characteristic interactions in hybrid inorganic-organic materials[1]

Type of interaction	***Strength [kJmol^{-1}]***	***Range Character***
van der Waals	ca. 50	Short nonselective, nondirectional
H-bonding	5–65	Short selective, directional
Coordination bonding	50–200	Short directional
Ionic	50–250	Long nonselective
Covalent	350	Short predominantly, irreversible

Literature reports in the last years mentioned either the term of hybrid materials or the one of nanocomposites. There is no clear borderline between these materials. Usually, the term nanocomposite is used if one of the structural units, either the organic or the inorganic, is in a defined size range of 1–100 nm. However, large molecular building blocks for hybrid materials, such as large inorganic clusters, can already be on the nanometer length scale. Commonly the term nanocomposites is used if discrete structural units in the respective size regime are used and the term hybrid materials is more often used if the inorganic units are formed *in situ* by molecular precursors, for example applying sol–gel reactions[1].

Design of Hybrid Materials and Nanocomposites

There are two main strategies widely used for the production of an inorganic-organic hybrid material or nanocomposite: i) the building block approach, where well-defined preformed building blocks are used for the formation of the final material and the precursors partially keep their original structure or ii) the *in-situ* formation of one or both structural units (organic

and inorganic) from molecular precursors[1]. In Scheme 1.3 the various pathways for the synthesis of hybrid inorganic – organic materials are summarized.

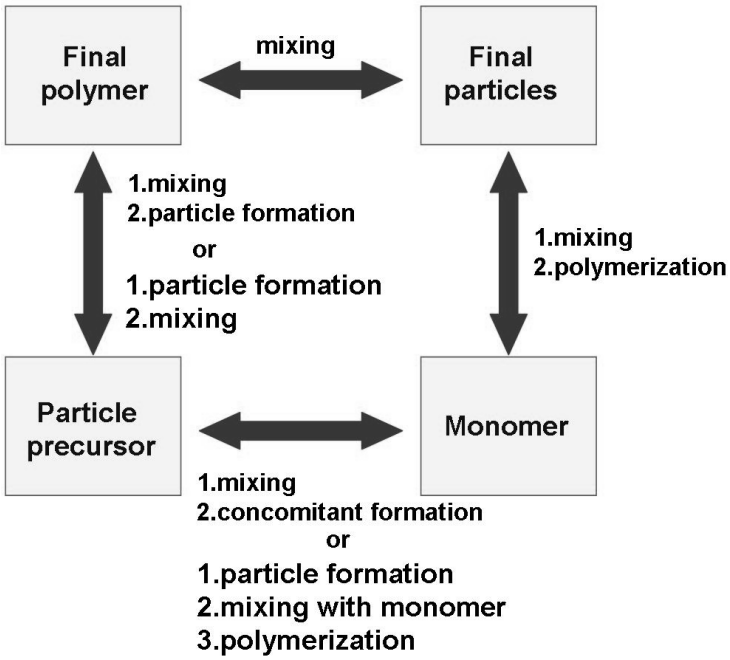

Scheme 1.3. Pathways for the synthesis of hybrid inorganic – organic materials[1]

Sol-Gel Process

One important pathway in the preparation of the inorganic component in hybrid inorganic-organic materials and nanocomposites is the sol-gel process because of its mild reaction conditions and its solvent based chemistry that opens many possibilities for the compositional and structural design of hybrid materials[3, 4]. Typical molecular precursors of this process are inorganic salts or (semi)metal alkoxides as precursors.

The sol-gel process is used for the formation of ceramic materials of high purity and homogeneity at lower temperatures than the ones used for the traditional solid-state reactions. This process is chemically very similar to an organic polycondensation reaction, in which small molecules condensate to form polymeric structures. Usually the reaction products consist of a three-dimensional (3-D) crosslinked network.

The name of the process relies on the two main stages of the reaction. Usually the hydrolysis and condensation reactions of small molecular precursors lead to the formation of a colloidal phase, which is the so-called sol, consisting of oxide nanoparticles with a size ranging from 1 to a few 10 nanometers. Further hydrolysis and condensation reactions of this

sol leads to the formation of a crosslinked network, a so-called gel. Thus, a gel can be considered a continuous network enclosing a liquid phase.

Advantages of the sol-gel process are the high control of the purity and composition of the final materials due to the small molecular educts, the use of a solvent based chemistry which offers many advantages for the processing of the materials formed, and the very mild reaction conditions, particularly the low reaction temperatures, which also allow the incorporation of quite sensitive organic moieties into the inorganic materials.

The silicon based sol–gel process is probably the process that has been most investigated and well understood[3]. A sol-gel reaction mixture regularly is formed by four components: a silicon alkoxide, water, an acidic or basic catalyst, and, optionally, a solvent to provide compatibility between the silicon alkoxide and water.

Typically, the sol-gel process of (semi)metal alkoxides takes place via hydrolysis and condensation reactions (Scheme 1.4). In a first step metal hydroxides species are formed which are not stable and further on condensed realizing water or alcohol, respectively. The mechanism of condensation is either through oxolation and alkoxolation, or hydroxo-bridges (Olation). When stoichiometric hydrolysis ratios are used, the condensation reaction producing alcohol is favored, whereas a water forming condensation is dominant for larger hydrolysis ratios[3]. Olation takes place when solvent-stabilized alkoxides are present in the solution.

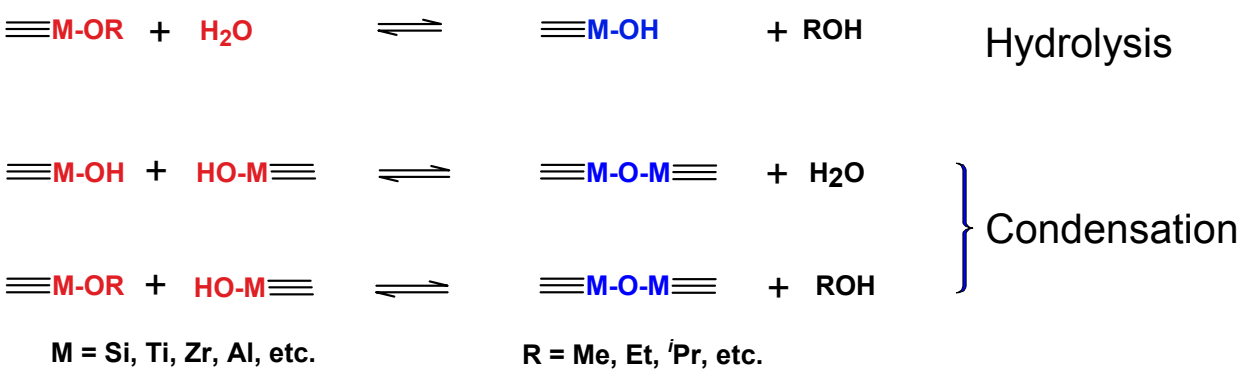

Scheme 1.4. The schematic pathway describing the hydrolysis–condensation steps during the sol–gel reaction

The chemical reactivity of (semi)metal alkoxides in hydrolysis and condensation processes depends on the electronegativity of the (semi)metal atom and its ability to increase the coordination number. The low electrophilicity of silicon together with its fully satisfied

fourfold substitution pattern leads to a rather low reactivity of $Si(OR)_4$ in hydrolysis and condensation. For this reason, acid or base catalysts have to be used in the sol-gel process of silicon alkoxides to increase the velocity of hydrolysis reactions and to obtain shorter gelation times.

While for the silicon based sol–gel process the reaction parameters are well understood and tailoring of the structure and composition of the resulting materials is nowadays state of the art, the transition-metal-based sol-gel process is much more difficult to control. The reactivity of metal alkoxides towards water is much higher. The reaction proceeds through hydroxylation that occurs upon hydrolysis[5]. The major reasons for this difference are the more electropositive character of the metals, leading to a more efficient nucleophilic attack and the larger number of coordination sites usually varying between four and nine depending on the metal[3, 6, 7].

Chemical Modification of Metal Alkoxides

Modification of metal alkoxides with organic ligands is often applied in order to reduce their reactivity by blocking coordination sites and thus decreasing their reactivity as well as to incorporate additional organic functionalizations[8].

Acetic acid or acetylacetone were mainly used for this purpose. Both act as bidentate (bridging or chelating) ligands (BL). When a metal alkoxide $M(OR)_x$ is reacted with such a ligand, part of the alkoxide groups is substituted by the ligand. A new molecular precursor $M(OR)_{x-y}(BL)_y$ is obtained with a different structure and a lower reactivity. Bidentate ligands are more strongly bonded than comparable monodentate ligands and are therefore less readily hydrolyzed than the remaining OR groups upon sol-gel processing[7].

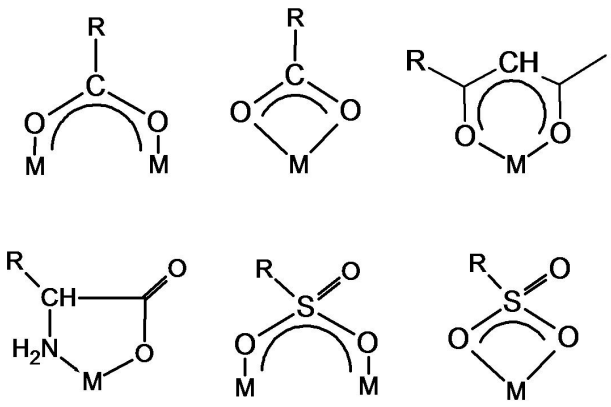

Scheme 1.5. Bonding situations of bidentate ligands in BL-substituted metal alkoxides. From upper left to lower right: bridging and chelating carboxylate, β-diketonate, α-aminocarboxylate, bridging and chelating sulfonate (R - organic substituent)[7]

In Scheme 1.6 various compounds used for the modification of metal alkoxides are presented. All of them have unsaturated bonds which can be incorporated in the sol-gel matrix due to the mild conditions of this process.

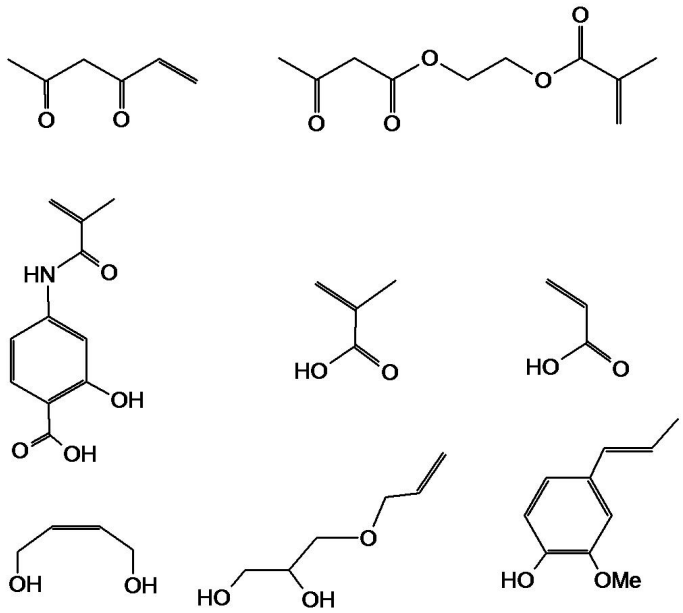

Scheme 1.6. Unsaturated organic compounds used for the modification of metal alkoxides. Upper row: β-diketonates (allylacetoacetone, 2-(methacryloyloxy)ethyl acetoacetone); middle row: carboxylic acids (methacrylamidosalicylic acid, methacrylic acid, acrylic acid, bottom row: diols (cis-but-2-ene-1, 4-diol, 3-allyloxypropane-1,2-diol) and isoeugenol[7]

When these new metal alkoxide complexes are bearing polymerizable groups, such as methacrylates (Scheme 1.6), a desired hybrid inorganic-organic material can be synthesized consisting of a metal oxide network and an organic polymer by copolymerization of the functionalized complexes followed by a sol-gel process. In the resulting materials a strong interaction between the organic polymer and the inorganic oxide network is formed via a metal-ligand coordination[7, 9, 10]. Metal alkoxides regularly used in the formation of such materials are the oxophilic early transition metals such as titanium and zirconium[11-13]. Coordinating groups used to introduce polymerizable functions in metal alkoxides derivatives or clusters are based on acids[14, 15], diols[16], or isoeugenol-type compounds[17]. β-Keto esters with attached polymerizable bonds such as 2-(methacryloyloxy)ethyl acetoacetate (HAAEMA) have only rarely been employed in the modification of metal alkoxides[16, 18-20]. *Devi et. al* showed in various papers the coordination of the bulky tert-butylacetoacetate to Hf-, Ti- and Zr-alkoxides and their thermal decomposition targeting them as precursors for

MOCVD[21-23]. In these studies bulky alkyl esters without further chemical functionalization were used. The formation of monomeric or dinuclear species was observed in dependence of the type of ligand and metal center and the ratio between metal alkoxides and acetoacetate. The studies revealed that the decomposition of the coordinating ligands under thermolytic conditions results in the formation of a variety of products.

1.2. Organic Polymerization in the Formation of Hybrid Materials

One of the most common applied polymerization techniques both in science and technological application is the free radical polymerization. Depending on the initiator type, free radical polymerization can be induced by various processes, like UV-light, temperature, etc. The initiators form radicals upon their decomposition, which afterwards can initiate the polymerization process[24]. Normally, the initial concentration of radicals is very high, which leads to various termination reactions. Thus, this type of polymerization is rather uncontrolled. Furthermore, the so called "Trommsdorf-effect" also contributes to uncontrolled growth of the polymer chains due to auto-acceleration of the ongoing polymerization through exothermic effects. Due to fast gelation, diffusion problems of the radicals appear which leads to high radical concentrations in some parts of the gel, broadening the molecular weight distribution of the resulting polymer. The usage of solvents can minimize this effect as the autoacceleration of the process can be reduced.

Hybrid inorganic-organic materials and nanocomposites can be easily synthesized from mixtures of monomers and sol-gel precursors through *in-situ* free radical polymerization and hydrolysis and condensations.

Inorganic building block like clusters and nanoparticles served as an initiator for free radical polymerization. The resulting materials showed that the organic polymer was grafted from an inorganic core[9]. Using such and approach core-shell hybrid particles were formed from metal salts and initiators followed by radical polymerization[25].

One common monomer used for hybrid materials is 2-hydroxyethyl methacrylate (HEMA). Polyacrylate-silica optically transparent hybrid materials with significantly low volume shrinkage were obtained by sol-gel reactions of tetra-Et orthosilicate and HEMA along with free-radical polymerization of the acrylate monomer[26]. PolyHEMA-silica blend hybrids 30% wt. of silica gel to the mass of polymer were also prepared through basic catalyzed sol-gel process of tetraethoxysilane (TEOS) and the alkoxysilyl unit of the hybrid monomer, followed by in situ free-radical polymerization[27]. A one-step process preparation route could also be used for the formation of hybrid materials. Free radical polymerization of

mixtures of zirconium butoxide and HEMA led to the formation of hybrid materials showing glassy behavior, remarkable thermal stability, and low shrinkage[28]. Hybrid organic-inorganic polymers have also been prepared via free radical polymerization of dimethacrylate oligomers and HEMA in the presence of different organically modified titanium-oxo-clusters[29]. A significant increase of the storage modulus was detected in these materials, while the incorporation of Ti nanoclusters in the matrix led to a significant alteration of the system's hardness. Thermogravimetric analysis also indicated a significant enhancement of the thermal stability compared to the neat matrix, probably because of the antioxidant effect of the titanium-oxo-clusters. CdS nanocrystal - polymer transparent hybrids with better thermal stability and good optical properties were also developed by free radical polymerization of MMA[30].

Radical polymerization is the most common polymerization method due to the fact that the radical process is more tolerant of functional groups and impurities and is the leading industrial method to produce polymers. However, for the synthesis of hybrid materials this technique has a great disadvantage: the lack, or the difficult control over the polymer architecture and morphology.

Atom Transfer Radical Polymerization

The recent goal of the polymer scientific and industrial world was the development of controlled radical polymerization techniques, which would allow a better design and tailoring of the polymeric materials. All of the controlled radical polymerization reactions are based on establishing a rapid dynamic equilibration between an amount of growing free radicals and a majority of dormant species. Depending on the procedure, the dormant species may be alkyl halides, as in atom transfer radical polymerization (ATRP) or degenerative transfer (DT), thioesters, as in reversible addition fragmentation chain transfer processes (RAFT), alkoxyamines, as in nitroxide mediated polymerization (NMP) or stable free radical polymerization (SFRP). Free radicals may be generated by the spontaneous thermal process (NMP, SFRP), via a catalyzed reaction (ATRP), or reversibly via the degenerative exchange process with dormant species (DT, RAFT)[31].

Among various procedures, atom transfer radical polymerization (ATRP) emerged as one of the most versatile radical polymerization method.

A general mechanism for ATRP is shown in Scheme 1.7. The radicals, which are the active species, are created through a reversible redox process which is catalyzed by a transition metal complex (Mt^nL). This metal complex undergoes a one–electron oxidation

with concomitant abstraction of a (pseudo)halogen atom (X) from a dormant species (R-X). In Scheme 1.7. the k_{activ}, respectively $k_{deactiv}$, are the rate constants of activation and deactivation. In this manner the polymer chains grow by the addition of the intermediate radicals to monomers similarly as for the conventional radical polymerization, with the rate constant of propagation k_p. Termination reactions (k_t) also occur in ATRP, mainly through radical coupling and disproportionation. However, in a well-controlled ATRP, no more than 5% of the polymer chains undergo termination. This process generates oxidized metal complexes, X-Mt^{n+1}L, as persistent radicals to reduce the stationary concentration of growing radicals and thereby minimize the contribution of termination[31, 32]. A successful ATRP has a uniform growth of all the chains, which is accomplished through fast initiation and rapid reversible deactivation, and only a small contribution of terminated chains[31].

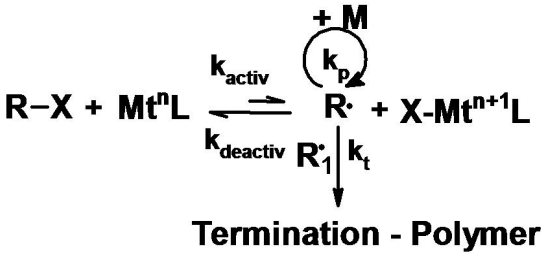

Scheme 1.7. The ATRP mechanism

In ATRP the reaction mixture is composed of the monomer, an initiator with a transferable (pseudo)halogen and a catalyst complex (transition metal species with any suitable ligand). For a successful ATRP, other factors, such as solvent, temperature, and additive have to be taken into consideration.

In the last decade a variety of monomers has been successfully used in ATRP. Typical monomers include styrenes, (meth)acrylates, (meth)acrylamides, and acrylonitrile, which contain substituents that can stabilize the propagating radicals[33-35].

The best initiators for ATRP are alkyl halides (RX) and the rate of the polymerization is first order with respect to their concentration. The main role of the initiator is to determine the number of growing polymer chains. If initiation is fast and transfer and termination negligible, then the number of growing chains is constant and equal to the initial initiator concentration of RX. To obtain well-defined polymers with narrow molecular weight distributions, the halide groups (X) must rapidly and selectively migrate between the growing chain and the transition-metal complex. Usually, when X is either bromine or chlorine, the molecular weight control is the best.

The catalyst complex consists of a transitional metal compound and a ligand. The role of the ligand in the catalytic complex is to solubilize the transition-metal salt in the organic media and to adjust the redox potential of the metal center for appropriate reactivity and dynamics for the ATRP[36]. Typical ligands used are nitrogen ligands, phosphorus ligands, etc. There are several prerequisites for an efficient transition metal catalyst

- The metal center must have at least two readily accessible oxidation states separated by one electron.
- The metal center should have reasonable affinity toward a halogen.
- The coordination sphere around the metal should be expandable upon oxidation to selectively accommodate a (pseudo)- halogen.
- The ligand should complex the metal relatively strongly.

One of the best catalytic systems is based on copper halides (bromide or chloride) and nitrogen based ligands like N, N, N', N'', N'' - pentamethyldiethylenetriamine (pmdeta), N, N, N', N'', N''', N''' -hexamethyltriethylenetetramine (hmteta), phenanthroline (Scheme 1.8).

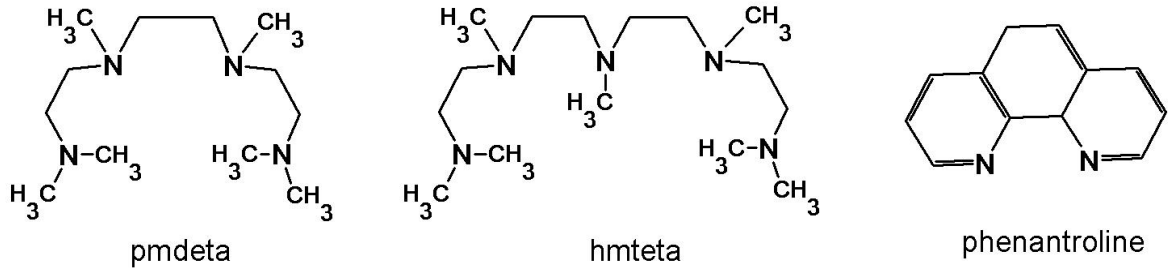

Scheme 1.8. Nitrogen based ligands used in ATRP

The recently developed controlled radical polymerization techniques allow well-controlled designs of different polymer architectures[37]. From these methods, atom transfer radical polymerization (ATRP) is most often applied due to its good control of the molecular weight and polydispersity of the resulting polymers, the possibility to use a broad variety of different monomers and the fact that a simple catalyst system can be used[31]. Various hybrid materials were already synthesized using this technique starting from inorganic building blocks such as inorganic clusters[38, 39], metal alkoxides[40], and nanoparticles[25, 41] which were modified with initiating groups active for ATRP. In other studies, such building blocks as methacryloyl-modified POSS cages were used as monomers in ATRP [42, 43]. The well-controlled manner of the polymerizations was not affected by the inclusion of all of these inorganic moieties.

Enhanced mechanical and thermal properties could be obtained by using such well-defined building blocks.

1.3. TiO_2 Nanomaterials

Titanium dioxide (TiO_2) is one of the most widely used oxide material nowadays. Since its commercial production in the early 20th century, TiO_2 has been widely used as a pigment[44], in sunscreens[45, 46], in paints[47], etc. In 1972, *Fujishima and Honda* discovered the phenomenon of photocatalytic splitting of water on a TiO_2 electrode under ultraviolet (UV) light[48-50]. These discoveries brought to a boom in the research field of titania.

Titanium dioxide appears in nature as the well-known naturally occurring minerals rutile, anatase, brookite. The most common form is rutile, which is also the most stable form. Anatase and brookite both convert to rutile upon heating. All contain 6-coordinated titanium. Additionally there are three metastable forms and five high pressure forms which were all synthetically produced.

Most synthetic methods were focused on the production of amorphous, anatase, brookite or rutile phases. Depending on the method employed, the size and shape of the materials can be designed[51]. The final properties depend on the type of crystalline phase obtained. For example, anatase has the highest photocatalytic activity while rutile is widely applied as UV absorber[51].

Synthesis of TiO_2 Nanomaterials

Semiconductor nanoparticles have been widely studied during the last decades due to their interesting electronic, optical or catalytic properties which are related to their nanometer size regime[52]. Among various colloidal systems titania nanoparticles exhibit remarkable photocatalytic properties[53] which have an enormous potential for applications such as self-cleaning materials or waste water treatment.

The size of the semiconductor particles plays a crucial role. It was observed that when the size of the materials reaches the nanometer regime, electronic changes occur, leading to the so-called quantum size effects. Furthermore, the surface to volume ratio increases dramatically, leading to an increasing importance of the surface atoms regarding the overall properties of the materials[54].

In a bulk material, the properties of the material are independent of the size and are only chemical and composition dependent. On the other hand, for nanoparticles, the size of

the particle begins to modify the properties of the material. The electronic structure is altered from the continuous electronic bands to discrete or quantized electronic levels. As a result, the continuous optical transitions between the electronic bands become discrete and the properties of the nanomaterial become size-dependent[55].

A bulk TiO_2 material posses a conduction band and a valence band, and the electron and hole experience electronic delocalization. For a TiO_2 nanomaterial, the confinement produces a quantization of discrete electronic states and increases the effective band gap of the semiconductor. Such effects can change the color of the material (due to the altered optical absorption maxima) and the photocatalytic properties[53].

TiO_2 nanostructures have been the goal of many researchers and various preparation methods were reported in the last years. For example *micelle/inverse micelle method* can be used for the synthesis of nanoparticles with a good control over the shape[56-58]. This method produces usually an amorphous structure, and calcination is necessary in order to induce high crystallinity. Another method widely used to synthesize TiO_2 nanoparticles, especially when high crystalinity is required, is the *hydrothermal method* [59-61]. The hydrothermal synthesis is normally carried out in close vessels (autoclaves) under controlled temperature and/or pressure. The reaction takes place in aqueous solutions. The temperature can be elevated above the boiling point of water, reaching the pressure of vapor saturation. A variation of the hydrothermal method is the *solvothermal method*, which is almost identical to the hydrothermal one, except that a nonaqueous solvent is used, and thus, the temperature can regulated on a broader range. The solvothermal method also has better control over the size, shape, and the crystallinity of the TiO_2 nanoparticles[62]. Another method used for the synthesis of the TiO_2 nanomaterials is the *direct oxidation* of Ti metal using oxidative reagents or electrochemical methods. For example crystalline titania nanorods were obtained by direct oxidation of a titanium metal plate with hydrogen peroxide[63]. *Chemical vapor deposition* (CVD) is a process in which materials in a vapor state are condensed to form a solid-phase material. In CVD processes, the thermal energy heats the gases in the coating chamber and drives the deposition reaction. TiO_2 nanorods[64] or thick crystalline titania films[65] can be formed through this method. When no chemical reaction occurs, the vapor deposition process is called *physical vapor deposition* (PVD). In such a way TiO_2 nanowire arrays have been obtained[66, 67]. Other methods for the preparation of TiO_2 nanomaterials are *electrodeposition[68], sonochemical methods[69], microwave methods[70],* etc.

TiO_2 by Sol-Gel Process

Among all these methods used for the production of titania, the sol-gel process is one of the most versatile, low cost routes for the preparation of such materials[51]. This method allows the design of the particle size and morphology, which is of great importance when photoactivity is targeted[71]. Due to these advantages, the sol-gel method was widely investigated in the last decade for the synthesis of TiO_2 nanomaterials. The usual precursors are titanium alkoxides or titanium chlorides, for the non-hydrolytic sol-gel method[72].

The sol-gel process of titanium alkoxides normally proceeds via an acid-catalyzed hydrolysis step followed by condensation[5, 73-80]. 3-D polymeric skeletons with close packing result from the development of Ti-O-Ti chains which are developed at low content of water, low hydrolysis rates, and excess titanium alkoxide in the reaction mixture. On the other hand, the formation of particles is favored by the presence of $Ti(OH)_4$. This is formed at high hydrolysis rates for a medium amount of water. Closely packed first order particles are yielded via a three-dimensionally developed gel skeleton[5, 51, 73, 74, 76-81].

The growth kinetics of TiO_2 nanoparticles was investigated in aqueous solution using the $Ti(O^iPr)_4$ as precursor[74]. It was found that the rate constant for coarsening increases with temperature due to the temperature dependence of the viscosity of the solution and the equilibrium solubility of TiO_2. Secondary particles are formed by the self-assembly of the primary particles at longer times and higher temperatures, and the number of primary particles per secondary particle increases with time. The average TiO_2 nanoparticle radius increases linearly with time, in agreement with the *Lifshitz-Slyozov-Wagner* model for coarsening[74]. This model provides a quantitative treatment of the time dependence of the particle size and the size distribution. It was observed that the coarsening was driven by the dependence of the solubility of a solid phase on the particle size according to the Gibbs-Thomson relation[74].

The hydrolysis–condensation reactions of the titanium alkoxides can also occur under basic conditions. For example highly crystalline anatase TiO_2 nanoparticles with various sizes and shapes were obtained in the presence of tetramethylammonium hydroxide[82, 83].

Applications of the TiO_2 Nanomaterials

One of the main applications of the TiO_2 nanomaterials in the last two decades was in the field of semiconductor photocatalysis. Due to its cheapness and availability anatase nanoparticles were used extensively in various areas as water and air purification, self-cleaning materials, decomposition of microorganisms, for the inactivation of cancer cells, for the odor control, or the photosplitting of water to produce hydrogen gas, for the fixation of

nitrogen, and for the clean up of oil spills. The reason why semiconductors such as TiO_2 can act as sensitizers for light-reduced redox processes is their electronic structure, which is typically composed by a filled valence band and an empty conduction band[84].

The mechanism of the photocatalysis has been thoroughly investigated. When a photon with an energy of ***hν*** is illuminated on the TiO_2 particles, if it matches or exceeds the band–gap energy, then an electron is promoted from the valence band (VB) into the conduction band (CB) leaving a positive hole behind (Scheme 1.10). Excited state conduction-band electrons and valence-band holes can recombine and dissipate the input energy as heat, get trapped in metastable surface states, or react with electron donors and electron acceptors adsorbed on the semiconductor surface or within the surrounding electrical double layer of the charged particles[84]. The later pathway conducts to the decomposition of organic or inorganic impurities at the surface of the photocatalyst.

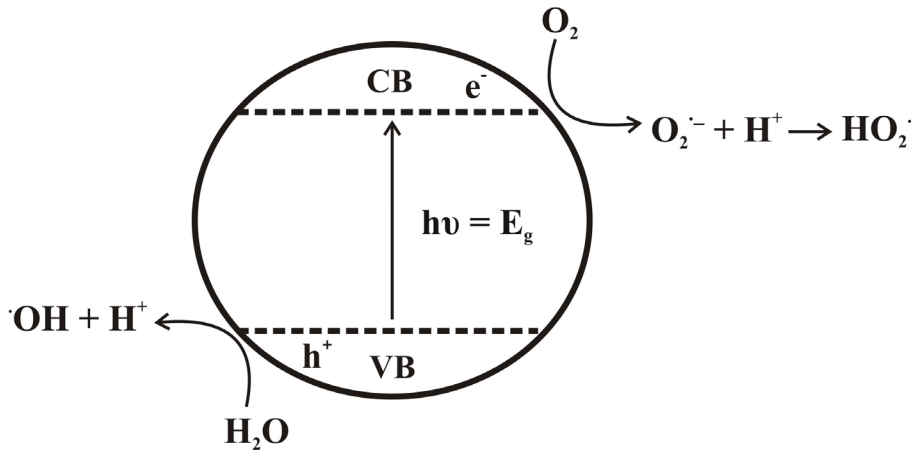

Scheme 1.10. The photochemical mechanism on the surface of semiconductors

1.4. Nanostructuring of TiO_2 - Hybrid Materials and Nanocomposites

Surface-Functionalization of TiO_2 Nanoparticles and Their Use in the Synthesis of Nanocomposites

As mentioned in the first part of the introduction, the last years showed an increasing interest in the research area of hybrid inorganic-organic nanocomposite materials. Particularly the linking of organic polymers and inorganic fillers was thoroughly investigated, due the clear advantages of combining the two opposite worlds. Nanoparticles show a large specific surface area compared to their volume, which results in the presence of many atoms located at their surface. These surface atoms show a higher energetic state because they have, compared to atoms that are located in the interior of a nanoparticle, a decreased number of neighbor atoms[52]. However, due to their high surface energy, nanoparticles tend to agglomerate rapidly. One of the challenges for preparing nanocomposite materials is the prevention of the

agglomeration of the nanofillers in the polymer matrix which leads to poor performance of the composite[85].

Nanocomposites resulting from the incorporation of nanoparticles in polymers present the advantage that the inorganic fillers have a well-defined, previously designed morphology. As mentioned, the major problems of mixing inorganic preformed nanoparticles with polymers is the fact that aggregation of the particles due to their high surface energy and diffusion phenomena in the materials can lead to changes in macroscopic properties. However, particularly optical and mechanical applications require materials with a homogeneous distribution of the nanoparticles in the polymer matrix. In most of the cases a simple blending of fillers into high molecular weight (high viscous) polymers is difficult, time-consuming and energy-intensive[86]. Hence, a chemical bottom-up route to *class II* materials is preferred due to a better control of the reaction parameters and consequently a higher homogeneity of the derived materials.

One of the methods to overcome such undesired agglomeration and to design *class II* hybrid materials is the surface functionalization of the nanofillers. This procedure has two main reasons:

- reducing the surface energy of the particles, thus decreasing their tendency to agglomerate;
- introduction of organic surface functionalization allows a compatible boundary to the organic polymer.

For this reason the various type of nanofillers used for the composite production are usually surface-functionalized with different organic groups to increase their compatibility[87].

One of the usual ways to modify the surface of colloids is through a post synthetic route, in which the particles are first synthesized and then subsequently surface modified in a second step. This can be done easily for metal oxide nanoparticles because they normally present reactive OH groups on their surface.

Applying such a surface-functionalization TiO_2 nanoparticles (4.5 nm diameter) were surface-modified with 6-palmitate ascorbic acid and then encapsulated in PMMA by *in-situ* radical polymerization, leading to materials with a significant increase in the thermal stability[88]. Methacrylic acid was also used as a surface modification agent for TiO_2 particles and thus, the nanofillers could be copolymerized with MMA. The resulting nanocomposites exhibited improved elastic properties and could be used in applications like dental and bone cements[89]. Composites with good optical absorption were based on PMMA polymers

containing oleic acid modified TiO_2. The optical absorption could be correlated to the concentration of the dispersed particles[90].

Silane coupling agents having the general formula R_nSiX_{4-n}, where X is a reactive group (i.e., halogen, amine, alkoxy, acyloxy) and R represents an organic substituent, have widely been used to alter the surface characteristics of inorganic oxides. Silane coupling agents are among the best surface modifiers for oxide surfaces[91]. Applying these silane coupling agents, the surface properties of the particles can be tailored. SiO_2 nanoparticles were widely surface modified with these types of silane coupling agents. Depending on the functional group introduced by these compounds, the surface of the particles can be tailored to be either hydrophilic or hydrophobic. Several reports were published concerning the functionalization of SiO_2 nanoparticles with modified silane alkoxides[92]. Silica particles were functionalized with commercially available silane coupling agents like 3-aminopropyltriethoxysilane or methacryloxypropyl trimethoxysilane[93]. A silica shell could also be formed on other types of nanoparticles that contain hydroxy groups like alumina[94], or Fe_3O_4[95]. Silane coupling agents were also used for the surface modification of TiO_2 nanoparticles for the formation of PMMA/TiO_2 nanocomposites. The materials showed enhanced thermal stability and higher molecular weights and MWDs compared to the pure PMMA[96].

In-situ surface functionalization of the TiO_2 could be also carried out when the particles were formed by non-hydrolytic sol-gel methods in presence of enediol ligands. Depending on the ligand employed, the surface polarity was adjusted, resulting in particles which were redispersible either in organic apolar solvents or in water[97]. The particles had diameter of about 5 nm. A single–step reaction was used for the synthesis of electronically coupled calixarenes with surfaces of anatase TiO_2 nanoparticles with primary crystallites of about 12 nm diameter. Due to the ligand–to–metal charge transfer present at the surface, these particles presented a shift of the TiO_2 absorption towards the visible region[98].

Among the usual agents used for the surface modification of oxide materials, organophosphorus coupling agents emerged as one of the most in focus modifiers nowadays, due to their huge advantages such as the stability of P-C and P-O-C bonds towards hydrolysis, their ability to introduce second organic moieties, and their relatively simple synthesis[99]. Phosphonic and phosphinic organophosphorus coupling agents were successfully used for the modification of commercially P25 TiO_2 nanoparticles with primary diameters of 21 nm. In the case of the phosphonates, quantitatively a tridentate binding mode was observed[100, 101]. Self-assembeled monolayers of dodecyl phosphate could be formed on the surface of various metal

oxide surfaces, inducing to these surfaces strong hydrophobic properties[102]. Surface-modified TiO_2-octyl phosphonic acid nanoparticles could be incorporated in polymer matrices without agglomeration, leading to a better control over the radical polymerization of MMA, suppressing the autoacceleration of the process[103].

Several studies reported the preparation of polysiloxane-metal oxide composite materials. Polysiloxanes are a class of interesting polymers due to their unique properties, such as flexibility, low T_g, biocompatibility, high oxygen compatibility, etc[104, 105]. Hybrid materials with good mechanical integrity and transparency consisting of hydrophobic and hydrophilic nanodomains have been prepared starting from dimethyldiethoxysilane and Zr alkoxides through sol-gel process[106]. Hybrid materials based on the combination of TiO_2 and polydimethylsiloxanes (PDMS) have been also reported in the last years. Polydimethylsiloxane-TiO_2 materials prepared from titanium alkoxides and end-functionalized PDMS have been synthesized and reported to show interesting optical and elastic properties[107-109]. Hybrid TiO_2-PDMS particles with controlled refractive index were synthesized by a co-precipitation method starting from titanium isopropoxides and methoxy-functionalized PDMS[109]. Applying a similar approach PDMS-metal-oxo nanocomposites constituted by metal-oxo nanodomains embedded in a PDMS matrix have been prepared as transparent monoliths from dimethyldiethoxysilane and different metal alkoxides (M = Al, Ge, Sn, Ti, Zr, Nb, and Ta). Depending on the nature of the cross-linking agent a different arrangement of the constituents of the hybrid composite has been developed[110, 111].

Janus Particles

Nanoparticles presented before are typically prepared in spherical shape and their surface chemical groups are isotropically distributed. Even if they are in the nanorange, new technological and scientific demands required more sophisticated systems. Molecular recognition and self-assembly properties require that the components have anisotropical properties.

Janus is the Roman god of gates and doors, beginnings and endings, and hence represented with a double-faced head, each looking in opposite directions. In science the concept of Janus particle describes particles which contain different surfaces from a chemical point of view[112].

Double-faced head
Roman God Janus

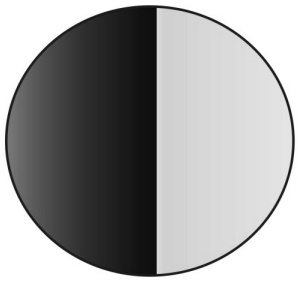

Janus Particle having
anisotropic surface

Figure1.2. Double-faced head Roman God Janus (left) and particle having two chemically different sides

Such particles attracted recently a lot of scientific attention due to their potential applications. They can be used as building blocks for supraparticular assemblies or as amphiphilic particles with one hydrophobic and one hydrophilic part, applicable in the stabilization of emulsions, for example[113]. Janus particles having positive and negative charges segregated on each half of the surface exhibit huge dipole moments[114]. They could be used for electronic displays. Other applications include bifunctional carriers for catalysis, sensing, drug delivery, etc[112].

The synthetic methods for the preparation of such anisotropically surface modified particles are usually classified in five main routes (Scheme 1.11)[115].

One of the first approaches and still used nowadays to obtain Janus particles was based on a two-dimensional approach (Scheme 1.11, a). In a first step, particles are deposited onto a substrate and then the surface lying above is coated with metals. One of pathways developed from this method was the surface functionalization of the particles positioned at the interface of two liquids. This is called the gel trapping technique method, and was based on the templating of the particles monolayer at the air-water or oil-water interfaces, followed by lifting off the particles with a PDMS stamp and their subsequent deposition on gold[116]. Even if selective, this methods has the disadvantage that it consist of only a low interface area, so only a small amount of particles can be produced.

Complex Janus micelles were developed by *Voets et al.* using the forced co-assembly of two block copolymers, each possessing an oppositely charged polyelectrolyte segment (Scheme 1.11, b)[117].

The formation of purely inorganic Janus particles (dubbell-, acorn-, snowman-shaped particles) was also carried out using the nucleation processes during the growth of the second material or the reaction-induced phase separation (Scheme 1.11, d)[112].

Another approach for the preparation of significant quantities of Janus particles was presented by *Roh et al.,* in which they employed electrohydrodynamic jetting in combination with a two-phase side-by-side spinneret tip to generate spherical and cylindrical Janus particles with submicron dimensions (Scheme 1.11, f)[118].

Photopolymerization or photolithographic polymerization within microfluidic devices lead to a novel method for the preparation of Janus particles (Scheme 1.11, e). However, this method has the disadvantage that the particles are only of micrometer dimensions[119].

An extension of the first pathway was developed by *Hong et al.*[120], who used a Pickering emulsion route to obtain larger quantities of Janus particles. The Janus particles can then be obtained after a functionalization of one side. This method has all the advantages of the 2-D method but furthermore is able to achieve higher mass fractions of Janus particles.

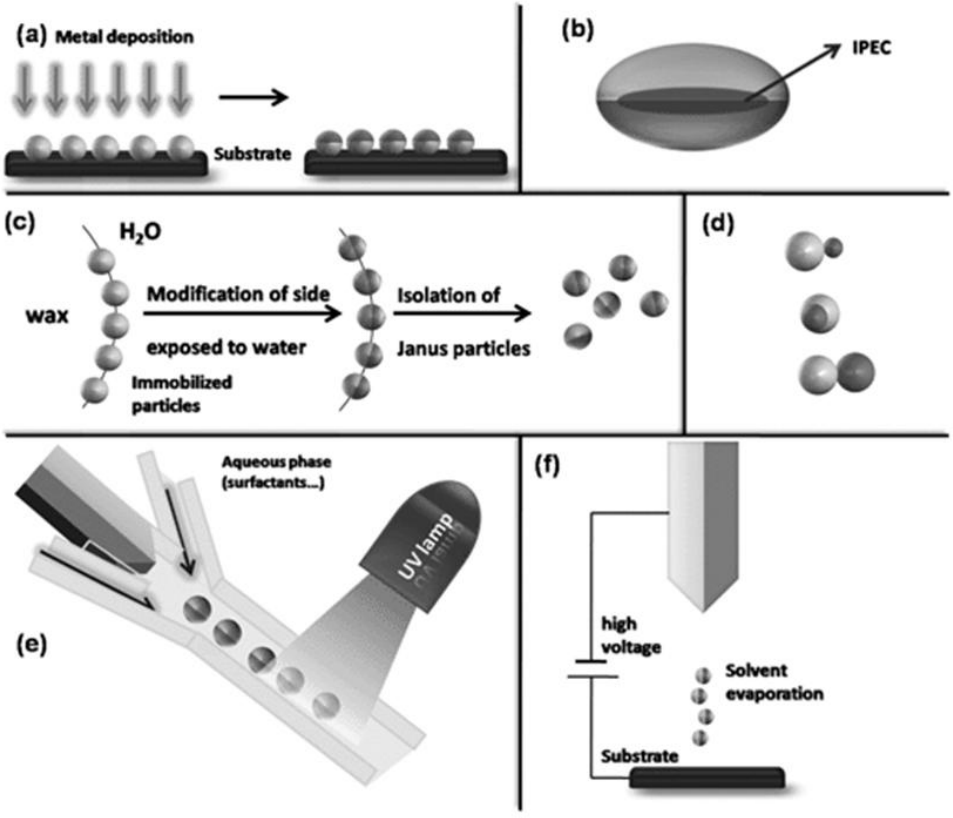

Scheme 1.11. Overview of approaches towards the preparation of Janus particles. (a) Classical two-dimensional technique involving shading of one particle side after their immobilization. (b) Ellipsoidal complex core coacervate micelle with an interpolyelectrolyte complex core (IPEC). (c) Pickering emulsion route. (d) Janus particles with two inorganic compartments, snowman-, acorn-, dumbbell-like nanoparticles (top to bottom). (e) Microfluidic photopolymerization system. (f) Electrospinning using a bi-phasic nozzle[115]

Pickering Emulsion

Colloidal particles of nanometer size are often used as stabilizers in oil-in-water or water-in-oil emulsions[121] for applications in various industries like cosmetics, food, agrochemical or paint. When an oil (solvent) is mixed to a water phase containing nanometer sized particles, these colloids will tend to create a resistant film at the interface between the two immiscible phases, namely water and oil (Scheme 1.12).

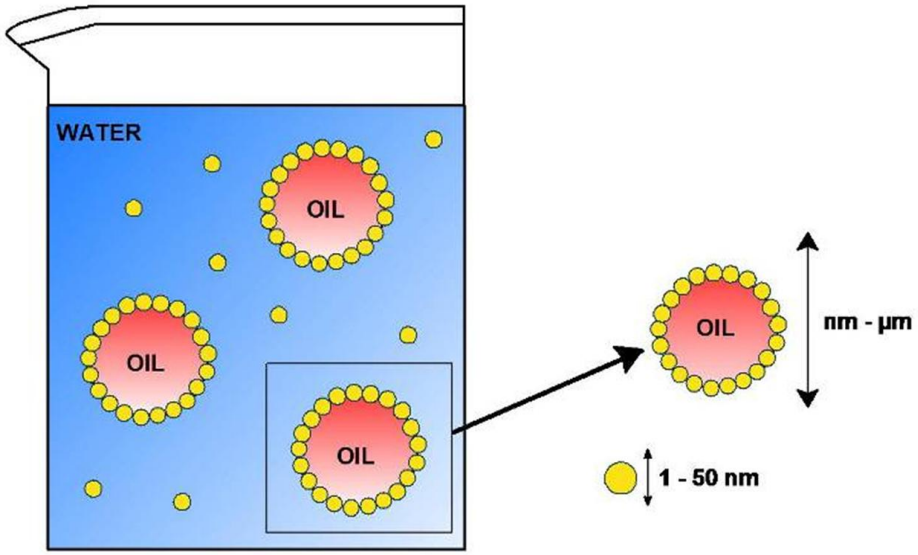

Scheme 1.12. Representation of the self-assembly of solid nanoparticles at the water – oil interface

This self-assembly of the particles at the fluid-fluid interface was first reported by *Pickering* at the beginning of the last century who investigated water – paraffin emulsions stabilized by various solid particles[122]. Only four years before *Ramsden*[123] also reported what appears to be the first example of such a Pickering emulsion, describing the formation of a membrane of solid particles evolving both air bubbles in water and oil drops in water.

The energy of attaching particles at the water – oil interface can be calculated by the following equation:

$$\Delta E = - \pi (d/2)^2 \gamma_{w/o} (1 \pm \cos\theta)^2 \qquad \text{(eq. 1)}$$

where $\gamma_{w/o}$ is the tension of the water/oil interface, d is the particle diameter, and θ is the cotact angle of the particles at the interface (Scheme 1.13)[121, 124].

It was shown that the efficiency of the colloids in stabilizing oil-water emulsions depends on factors like particle size and shape, inter-particle interactions and the wettability of the particles by both of the liquids[125, 126].

In addition to the size of the nanoparticles, the interfacial tension and, therefore, the wettability of a particle surface, also dictates the desorption energy[125.] *Finkle et al*. recognized the first time the connection between the particles wettability and the type of the emulsion formed[127]. The wettability is described by the contact angle θ between the solid and the oil/water interface. It was observed that hydrophilic particles tend to form oil-in-water (o/w) emulsions whereas hydrophobic particles form water-in-oil (w/o) emulsions[128]. In general, the less wetting liquid becomes the dispersed phase. If the contact angle θ is lower than 90°, oil-in-water emulsions are more stable; at contact angles greater than 90°, water-in-oil emulsions are favored. [129]

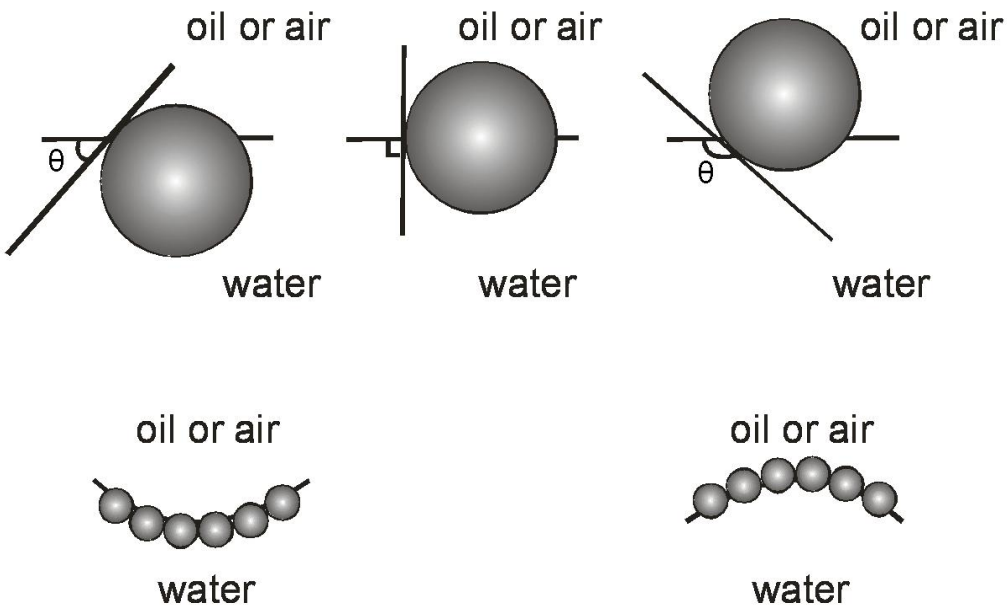

Scheme 1.13. Upper picture: Spherical nanoparticle at a planar fluid water interface for a contact angle (measured through the aqueous phase) less than 90° (left), equal to 90° (centre) and larger than 90° (right). Lower: positioning of particles at a curved fluid/water interface. For < 90° o/w emulsions may be formed (left); for > 90°, solid-stabilized w/o emulsions may be formed (right).

It is curious that not until recently such systems have drawn lots of attention due to the promising generation of novel materials which could be used in optic, acoustic, electronic or magnetic applications[129].

Stable Pickering-emulsions could be formed using TiO_2 nanoparticles. The type and stability of the prepared emulsions depended on the wettability of the stabilizing nanoparticles. The particle wettability could be tailored by the type, the amount, and the combination of inorganic and organic materials used for the surface modification of TiO_2[130].

Sacanna et al showed that it is possible to use iron-oxide, silica, or cobalt-ferrite nanoparticles to form thermodynamically stable oil-in-water emulsions with monodisperse droplet diameters in the range of 30–150 nm[131]. Stable Pickering emulsions were also prepared with paramagnetic particles (cobalt carbonyl) which could undergo macroscopic phase separation upon application of an external magnetic field[132]. Interestingly, this effect was reversible, so long-term stability were recovered by the remixing of the components with mechanical agitation. Other types of stabilizers included laponite clay particles[133] or layered double hydroxides particles[134]. Using a Pickering emulsion approach, Janus $Cu_2(OH)_2CO_3$/CuS microspheres were prepared[135]. Among other type of solid stabilizers, metal oxide nanoparticles were seldom used as stabilizers for Pickering emulsions[125, 130, 136-139].

The immobilization of such Pickering emulsion created materials with potential exciting applications as for example hollow spheres for drug delivery system. Hybrid organic-inorganic hollow microspheres composed of nanometer size metal oxide particles attracted lately much attention due to potential applications in areas such as drug release and photocatalysis[140-144]. Pickering emulsions proved to be the ideal systems for the synthesis of such elevated architectures. *Velev et al.* showed that latex particles can self-assemble into supracolloidal microstructures or multicomponent clusters. The particles were gathered, assembled, and fixed together in the restricted, colloid-size 2D or 3D space provided by the emulsion droplets[145]. *Dinsmore et al.* synthesized 'colloidosomes' structures where the particles were forming elastic shells. After that the emulsion droplets were transferred to a fresh continuous-phase fluid that was the same as that inside the droplets resulting in hollow structures whose permeability and elasticity could be controlled[146]. Using such colloidosomes *Cauvin et al.* prepared polymer-clay composites from Pickering-stabilized miniemulsion polymerization of monomer-filled clays[147]. Polystyrene-Fe_3O_4 nanocomposite spheres were prepared by the use of Fe_3O_4 nanoparticles for the stabilization of the free radical dispersion polymerizations of styrene. These composites showed magnetic properties[148]. TiO_2 particles with diameters of 200 nm were also used in the preparation of inorganic-organic hollow spheres having diameters between 10 and 50 μm[149].

2. Research Goals

The aim of the first part of the research was the well-controlled formation of hybrid materials and nanocomposites consisting of organic polymeric units and inorganic moieties. The main strategy was the development of structure-directing inorganic units as precursors for the final materials and the control over the self-assembly processes and the fixing of the final architectures. The formation of hybrid materials based on metal oxides and polymers was investigated. Several goals were targeted:

- Formation of well-defined molecular building blocks that are able to act as single-source precursors for the formation of hybrid materials.
- Application of atom transfer radical polymerization (ATRP) in the synthesis of ordered polymeric chains with pending metal alkoxides groups.
- Use of the sol-gel process for the formation of metal oxide nanoparticles inside the polymer matrix and the investigation of the hybrid materials properties.
- Modification of preformed polymeric chains containing reactive groups with sol-gel precursors based on transition metal alkoxides.
- Sol-gel reactions of such macromolecular precursors for the formation of hybrid materials.
- Investigation of the morphology of the final materials depending on the self-aggregation of the macromolecular precursors in various solvents.

A second part of the research was dealing with the formation of anisotropically surface-modified anatase nanoparticles for photocatalytic applications. Such particles should on one side be photocatalytically active and on the other side protect the organic substrates from decomposition induced by the particle catalyst. Several points were investigated in detail:

- Synthesis of size-controlled anatase nanoparticles by the sol-gel process.
- Surface-modification of the nanoparticles in suspension with organophosphorus coupling agents.
- Formation of stable Pickering emulsions based on the pristine anatase nanoparticles.
- Anisotropical surface-functionalization of the particles with organophosphorus coupling agents using Pickering emulsions and the formation of Janus particles.
- Investigation of the photocatalytic activity of the formed particles.

- Formation of transparent nanocomposites based on the surface-modified TiO_2 nanoparticles and the investigation of their properties.

Results and Discussions

3. Synthesis of Hybrid Materials from Well-Defined Single Source Precursors

3.1. Synthesis and Characterization β-keto Ester Containing a Methacrylate Group with Different Alkyl Chain Lengths

One of the research goals was the synthesis of structured inorganic-organic nanocomposites by the combination of atom transfer radical polymerization (ATRP) and sol-gel chemistry. First the synthesis and coordination behavior of β-keto esters, such as 2-(methacryloyloxy)ethyl acetoacetate (HAAEMA), ethyl acetoacetate (EAA), 3-(methacryloyloxy)propyl acetoacetate (HAAPMA) and 4-(methacryloyloxy)butyl acetoacetate (HAABMA) and their coordination behavior to titanium and zirconium alkoxides was investigated. In a second step the complexes were used as monomers in ATRP leading to well-defined metal alkoxide-containing polymers, which were further on transferred in nanocomposites by a sol-gel reaction of the alkoxide precursors.

HAAEMA is a commercial available monomer that is regularly used in the formation of metal containing polymers by either coordinating the metal first to the acetoacetate group followed by polymerization or by free radical polymerization of the methacrylate functions followed by the coordination of the metal[23, 150]. In both cases insoluble crosslinked polymers are often obtained due to several reasons: (i) the precursors contain more than one polymerizable group and therefore they act as inherent crosslinking agents, (ii) an equilibrium between compounds with different coordination patterns exists in solution, or (iii) exchange reactions occur in the final materials. Increasing the length of the alkyl spacer can have some influences on the coordination behavior, for example by inter- or intramolecular interaction of the ester functionalities of the methacrylate rest after coordination of the acetoacetate group to a metal centre. Therefore molecules were synthesized with increased alkyl chain lengths between the two functional groups, namely the molecules 3-(methacryloyloxy)-propyl acetoacetate (HAAPMA) and 4-(methacryloyloxy)-butyl acetoacetate (HAABMA). Several synthetic strategies were used for the controlled formation of these molecules. The method with the highest selectivity relating to the targeted products as well as the highest yield was the reaction of diols with methacrylic acid chlorides in a first step to form the 3-hydroxypropyl 2-methacrylate and the 3-hydroxybutyl 2-methacrylate, respectively. These

compounds were reacted with diketene, which opens to form the appropriate products in yields around 60% (Scheme 1).

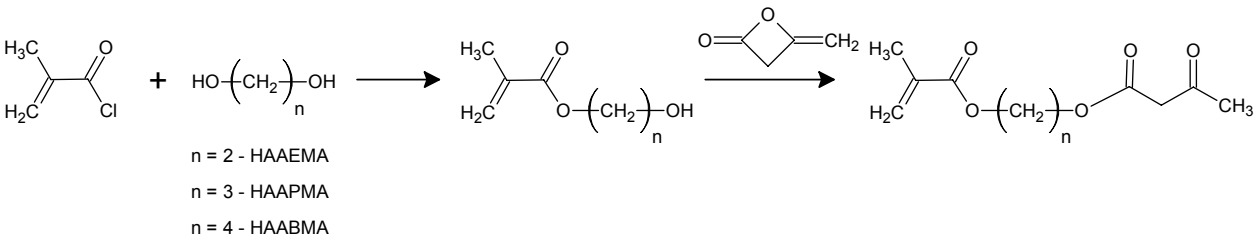

Scheme 1. The general pathway for the synthesis of β-keto esters with attached polymerizable groups

The methacryloyloxy alkyl acetoacetate derivates were obtained through the reaction of diketene with hydroxypropyl or hydroxybutyl methacrylate in dichloromethane and triethylamine. The reaction was carried out over night under vigorous stirring. The ^{1}H NMR of the 3-(methacryloyloxy propyl) acetoacetate is presented in Figure 1. The connection between the methacrylic part and the acetoacetate part was proven by the signals corresponding to the glycolic part at 1.93 ppm ($CH_2\boldsymbol{CH_2}CH_2$), 4.22 ppm ($O\boldsymbol{CH_2}$), and 4.24 ppm ($\boldsymbol{CH_2}O$). The presence of the acetoacetate moieties was shown by the signal of the methylene protons of the keto-form at 3.46 ppm. The NMR analyses were supported by the FT-IR measurements. The signals for the ester function as well as for the olefinic region are present in the region from 1716 to 1559 cm^{-1}. There is no specific signal for non reacted hydroxy propyl methacrylate. The yield for the second step was quantitative in comparison with the first step where the yield was only 60%. The overall yield of the process was about 42 %.

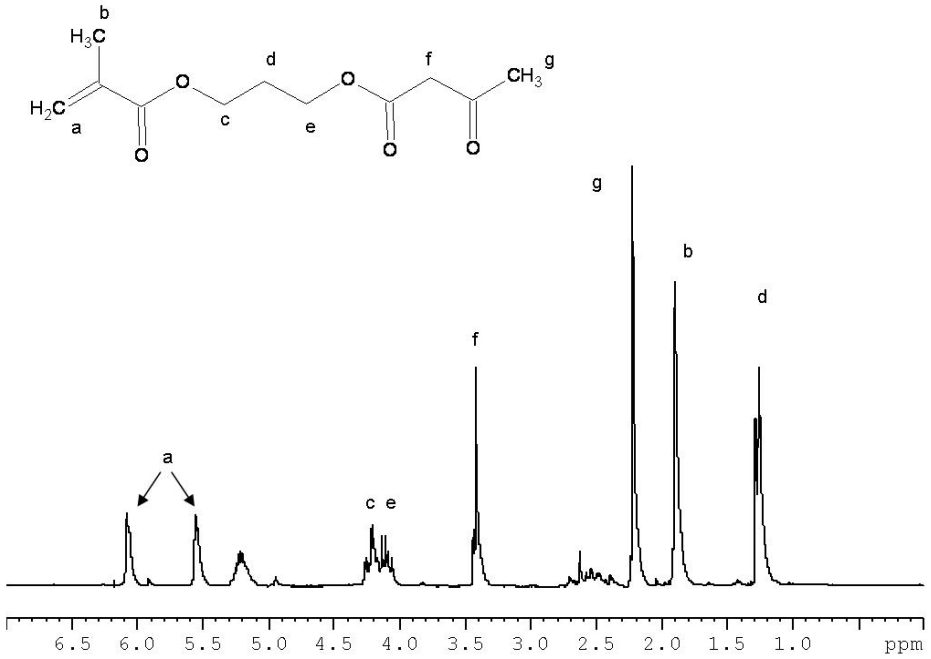

Figure 1. ^{1}H NMR analyses of the 3-(methacryloyloxy propyl) acetoacetate (HAAPMA)

Similar as for the HAAPMA synthesis, when reacting hydroxyl butyl methacrylate (synthesized from butyl diol and methacryloyl chloride) with diketene 4-(methacryloyloxy) butyl acetoacetate was obtained in similar yields. The connection between the methacrylic part and the acetoacetate part was proven by the signals corresponding to the glycolic part at 1.63-1.72 ppm (CH_2***CH_2CH_2***CH_2), 4.12 ppm (O***CH_2***), and 4.13 ppm (***CH_2***O). The ^{1}H NMR spectra of the reaction steps for the synthesis of 4-(methacryloyloxy) butyl acetoacetate are presented in Figure 2.

Figure 2. The ^{1}H-NMR spectra of the two steps for the synthesis of the HAABMA

This pathway offers the best results in the synthesis of the HAAEMA-type monomers. The FT-IR data confirmed that both steps of the synthesis were leading to the desired products.

3.2. Coordination of the Ligands to Titanium Alkoxides

The reactions between $Ti(OR)_4$ (R = Et, ^{i}Pr) and different β-keto esters (EAA, HAAEMA, HAAPMA, HAABMA) were carried out in the stoichiometric ratios 1:1 and 1:2 under variation of the solvent (toluene, n-heptane, dichloromethane, chloroform) to investigate the coordination behavior of the alkoxides and the utilized ligands. EAA was used in the studies as a model compound since it is known as a good chelating ligand[151] and the NMR spectroscopic analysis of its coordination compounds with the alkoxides are much simpler than that of the larger β-keto esters. Contrary to the ligands with longer alkyl chains a crystalline product was received reacting EAA with $Ti(OR)_4$ (R = Et, ^{i}Pr) in n-heptane in a 1:1 ratio (Scheme 2), while no crystalline product suitable for analysis was obtained under the same conditions in a 2:1 ratio.

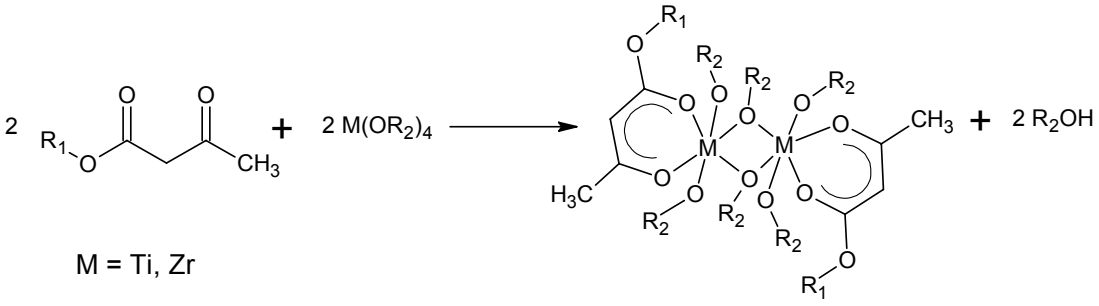

Scheme 2. Coordination of metal alkoxides with various β-keto esters

3.2.1. X-Ray Single Crystal Structures

The structure obtained from suitable crystals in the single crystal X-ray diffraction analysis revealed a binuclear centrosymmetric dimer consisting of two Ti atoms each coordinated by one chelating EAA, two terminal alkoxide ligands and two bridging alkoxides (Figure 1). Selected bond lengths and angles are presented in Table 1.

Table 1. Selected bond lengths (pm) and angles (°) for 1.

Ti(1)-O(5)	197.24(11)	O(13)-Ti(1)-O(16)	96.96(5)
Ti(1)-O(6)	213.59(11)	O(10)-Ti(1)-O(16)	102.07(5)
Ti(1)-O(10)	181.09(11)	O(5)-Ti(1)-O(16)	159.23(5)
Ti(1)-O(13)	180.90(12)	O(13)-Ti(1)-O(16)$^{\#1}$	166.24(5)
Ti(1)-O(16)	197.27(11)	O(10)-Ti(1)-O(16)$^{\#1}$	96.47(5)

Ti(1)-O(16)$^{\#1}$	207.59(11)	O(5)-Ti(1)-O(16)$^{\#1}$	88.62(5)
Ti(1)-Ti(1)$^{\#1}$	324.96(6)	O(16)-Ti(1)-O(16)$^{\#1}$	73.26(5)
C(2)-O(5)	129.65(19)	O(13)-Ti(1)-O(6)	85.25(5)
C(4)-O(6)	124.14(19)	O(10)-Ti(1)-O(6)	171.16(5)
C(4)-O(7)	134.13(19)	O(5)-Ti(1)-O(6)	81.48(5)
O(7)-C(8)	144.8(2)	O(16)-Ti(1)-O(6)	86.65(4)
		O(16)#1-Ti(1)-O(6)	84.54(4)
O(13)-Ti(1)-O(10)	95.04(6)	C(2)-O(5)-Ti(1)	135.93(11)
O(13)-Ti(1)-O(5)	98.96(6)	C(4)-O(6)-Ti(1)	130.41(11)
O(10)-Ti(1)-O(5)	89.75(5)	C(4)-O(7)-C(8)	116.30(13)

Symmetry transformations used to generate equivalent atoms: #1 -x,-y+1,-

Each Ti atom has a distorted octahedral environment where the Ti-O bond distances of the terminal alkoxides reveal similar values (180.90(12) pm and 181.09(11) pm) while the bridging alkoxides display longer Ti-O bonds (197.27(11) pm and 207.59(11) pm), as expected. These values show that the alkoxide bridge is not symmetric. The Ti-O bonds of the chelating EAA display two distinctly different values with Ti(1)-O(5) 197.24(11) pm and Ti(1)-O(6) 213.59(11) pm) leading to an asymmetric bridging mode, which most likely is based on the stronger trans influence of the terminal alkoxide compared to the β-diketonate. The structures are similar to various β-diketonate derivatives described by *Errington et al.*[152] However, the previously described structures with acetylacetonate ligands do not show a distinct difference in the Ti-O distances of the bidentate ligand. An asymmetric bonding was also observed by *Hubert-Pfalzgraf et al.* who reacted allylacetoacetate with $Ti(OEt)_4$ and obtained a similar structure[153].

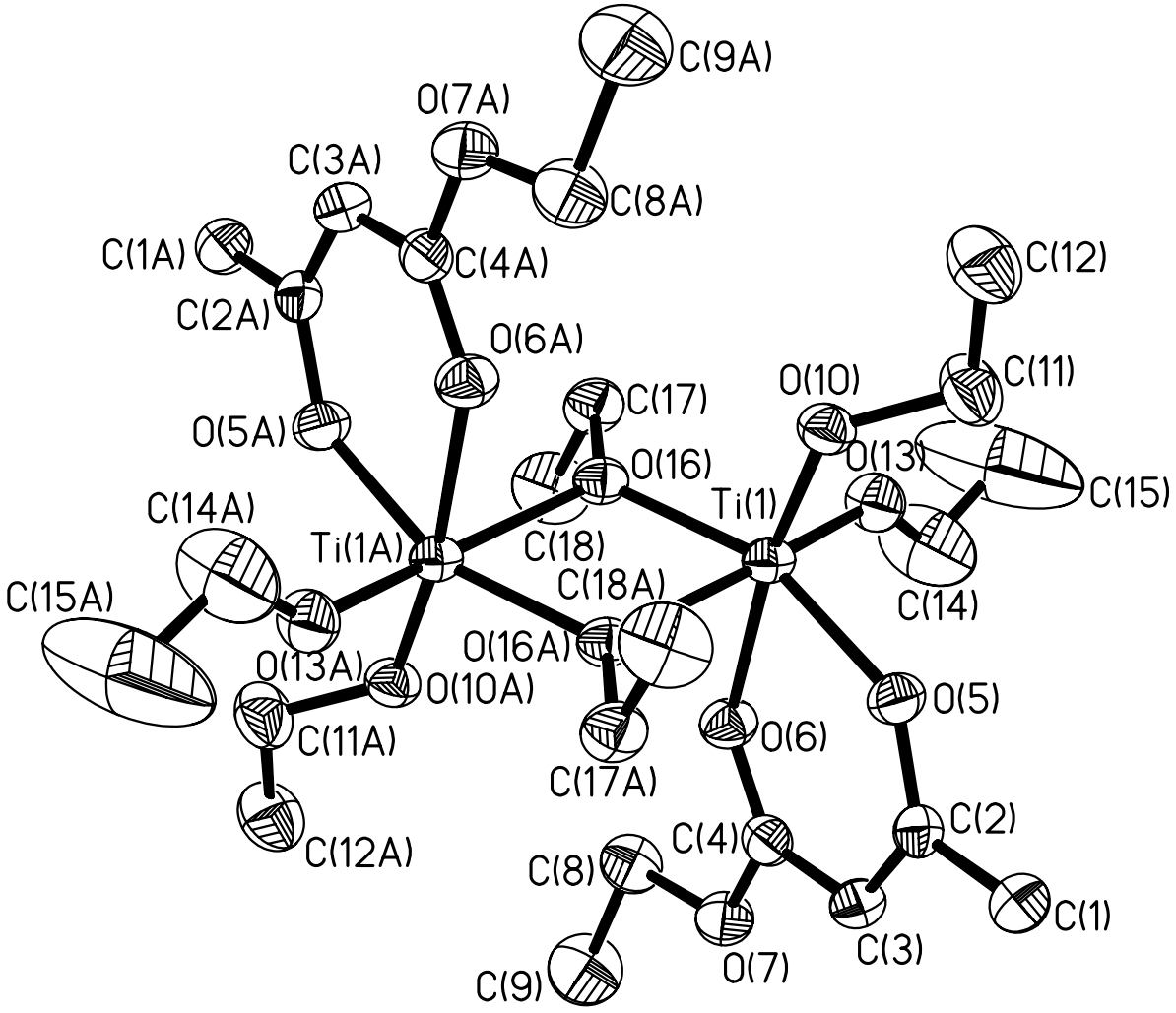

Figure 3. ORTEP plot of the structure of $Ti_2(\mu_2\text{-}OEt)(OEt)_2(EAA)_2$. Thermal ellipsoids are at a 50% probability level. H-atoms were omitted due to clarity

3.2.2. Spectroscopic Studies

The crystalline products were characterized in solution by FT-IR and NMR spectroscopy. The IR results of all coordination compounds showed the presence of the specific bands for the chelating acetoacetate ligands (C=C) and (C=O) between 1650 and 1520 cm^{-1}. In all cases complete coordination of the ligands was observed and no free ligands in solution were detected (see experimental data). ^1H NMR of $[Ti(O^iPr)_3EAA]_2$ (Figure 4) revealed clearly that coordination occurred by the disappearance of the methylene signal at 3.42 ppm corresponding to the keto form of the ethyl acetoacetate and the appearance of the methine signal of the chelating form at 4.98 ppm (Scheme 2). ^{13}C NMR spectroscopy also confirmed that no uncoordinated free ligand was present. The ^{13}C NMR signals of the carbonyl carbons of ethyl acetoacetate showed also shifts of the peaks from 200.5 ppm and 167.0 ppm in the

uncoordinated form, to 184.6 and 172.6 ppm in the coordinated species. The spectra did not allow to distinguish between an intramolecular or intermolecular coordination type.

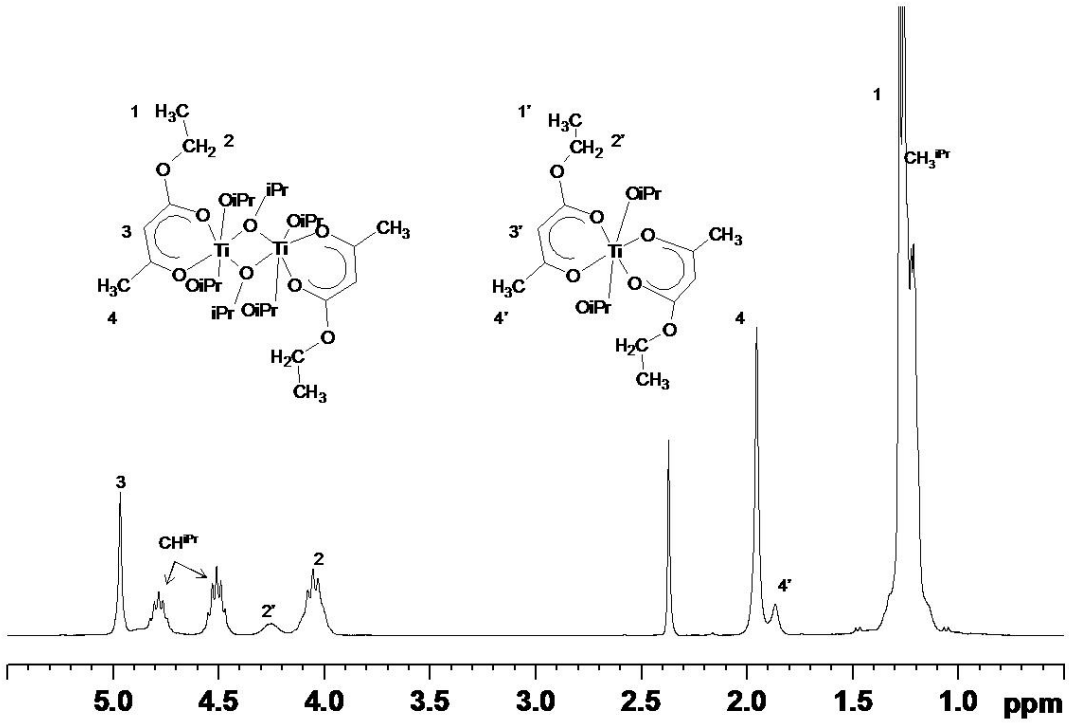

Figure 4. ^{1}H NMR spectra of Ti(O^{i}Pr)$_6$(EAA)$_2$

^{13}C-HSQC analysis (Figure 5) of the compound shows two correlations for CH (methine) protons of coordinated ligands at 4.91/88.64 ppm respective 4.97/87.15 ppm. In addition two sets of signals corresponding to two non-equivalent *iso*propoxy ligands at 4.77/79.2 and 4.5/76.2 ppm and one broad signal at 4.25/60.6 ppm are visible. The broad signal can be an indication of ligand exchange reactions which are known to take place in these types of complexes[152, 154]. We considered that these different signals are due to the different non-equivalent *iso*propoxy species. The two sets of signals derived from two non-equivalent *iso*propoxy species in a relative ratio of 2:1 are supported by the molecular structure obtained by the X-ray analyses. The signal at 4.04/60.4 was assigned to the CH_2-O group of the ester residue. Changing the ratio of EAA to Ti(O^{i}Pr)$_4$ to 2:1 provided a similar ^{1}H NMR spectrum with identical chemical shifts as in case of the 1:1 ratio, which showed that in solution an equilibrium of similar species was reached in both samples. The presence of the different signals in both cases could be explained by ligand exchange reactions that occured in the solution. This was also supported by the appearance of the broad peak in the ^{1}H NMR and the HSQC spectrum at 4.25/60.6 ppm which were assigned to the monomeric disubstituted form of the EAA-Ti complex resulting from redistribution reactions.

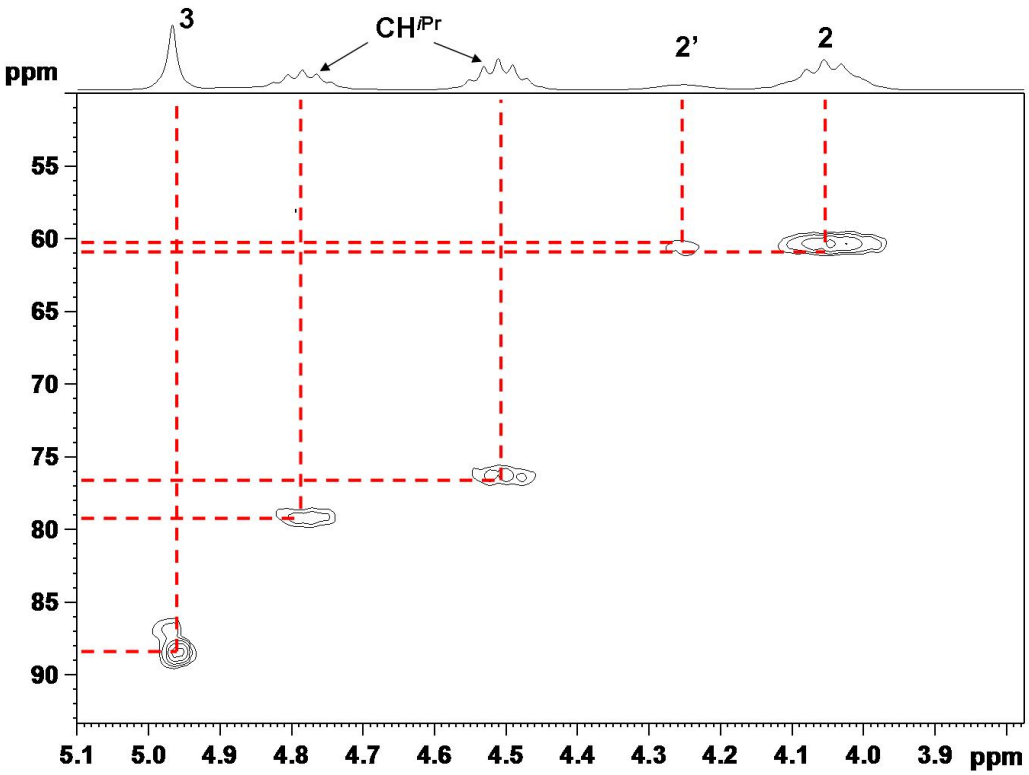

Figure 5. HSQC spectra of $[Ti(O^{i}Pr)_3EAA]_2$ in $CDCl_3$

Further confirmation was brought by the peak at 1.9 ppm which was attributed to the CH_3 protons of the EAA ligand for the monomeric form of the Ti complex, which was in agreement with previous studies where redistribution of $[Ti(OR)_3(L_b)]_2$ with R = Me, Et, ^{i}Pr, L_b = bidentate ligand (e.g. acac, thd or allyl acetoacetate) in $Ti(OR)_4$ and $Ti(OR)_2(\beta\text{-dik})_2$ was observed. Depending on the alkoxides and the ligand it was shown that a complete or partial redistribution reaction occurs. In the case of R = ^{i}Pr and L_b = acac the equilibrium was completely shifted to the monomeric compounds while for other alkoxides or bidentate ligands both species were observed in solution[152, 153].

The spectra of the coordination compounds obtained from reactions of HAAEMA and $Ti(O^{i}Pr)_4$ in 1:1 and 1:2 ratios are much more complicated in the alkyl regions of the chemical shifts due to the overlapping of many different signals (see experimental data). However, the spectra resemble those of the ethyl acetoacetate coordinated titanium alkoxides with regard to the coordination of the acetoacetoxy group. All NMR analyses showed a complete coordination of the ligands and no free acetoacetoxy derivatives were detected. Both the monomeric and dimeric species resulting from the redistribution reactions in solution could be observed similar to the case of ethyl acetoacetate ligands. Other systems which were analyzed, such as $[Ti(OEt)_3EAA]_2$ and $[Ti(OEt)_3AAEMA]_2$, $Ti(OBu)_3EAA$ and

$Ti(OBu)_3AAEMA$ showed analogous results proving the complete coordination of the acetoacetoxy group.

Coordination reactions between $Ti(O^iPr)_4$ and HAAPMA or HAABMA were carried out to study whether the alkyl part between the methacrylic moiety and the β-diketone part has an influence on the coordination process. The ^1H NMR spectra of the products between $Ti(O^iPr)_4$ and HAAPMA and HAABMA are presented in Figure 6.

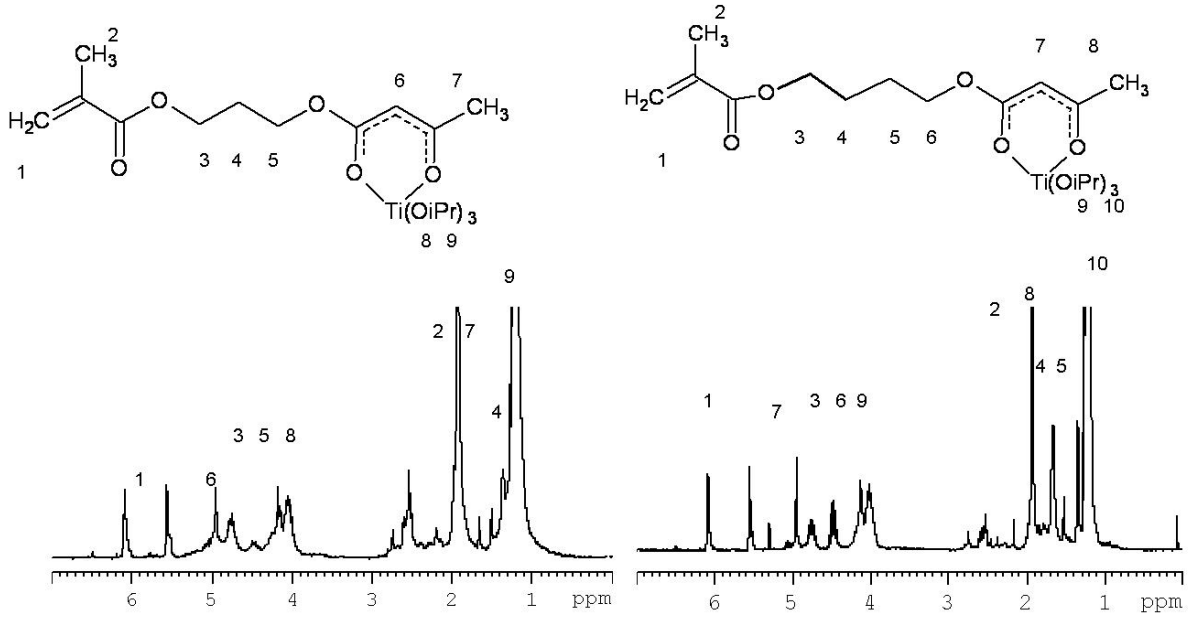

Figure 6. The ^1H NMR spectra of $[Ti(O^iPr)_3AAPMA]_2$ (left) and $[Ti(O^iPr)_3AABMA]_2$ (right)

As mentioned above the length of the alkyl chain between the polymerizable methacrylate and the coordinating acetoacetoxy group can have an influence on the coordinating behavior. For example the two oxygen atoms of the ester groups can form a reasonably unstrained intramolecular ring and thus one ligand would be able to coordinate to three coordination sites of the metal or intermolecular stabilization can occur. Thus, we investigated systematically the influence of the length of the alkyl chain on the coordination and the ligand exchange reaction. 3-Methacryloyloxy propyl acetoacetate (HAAPMA) and 4-methacryloyloxy butyl acetoacetate (HAABMA) were synthesized by the above mentioned reactions. The coordination with $Ti(O^iPr)_4$ was carried out applying the same conditions as for HAAEMA in a 1:1 ratio. The ^1H NMR spectra revealed in both cases the complete coordination of the ligands. In addition two sets of signals for the ligand and two different *iso*propoxy species were observed, confirming the dynamic equilibrium between different coordinated species. No indication for coordination of the methacrylic part of the molecule to the titanium atom was detected in solution analyses (NMR, FT-IR). This leads to the

conclusion that a stabilizing influences of the methacrylic group on the coordination by inter- or intramolecular coordination of the oxygen atoms can be neglected.

In Figure 7 the IR spectra of $[Ti(O^iPr)_3AAPMA]_2$ is presented. No signal corresponding to uncoordinated *iso*propanol was observed. The broad band between 3000 and 3600 cm^{-1} can be assigned to the coordinated *iso*propanol with the underlying C-H vibrations. The absorption bands at 1610 and 1525 cm^{-1} correspond to the C-O-Ti and C=C stretching vibration in the chelating form of HAAPMA bonded to $Ti(O^iPr)_4$. In the fingerprint area a C-O-R band is observed at 996 cm^{-1}. In the case of $Ti(O^iPr)_3AABMA$ the spectrum revealed similar characteristics.

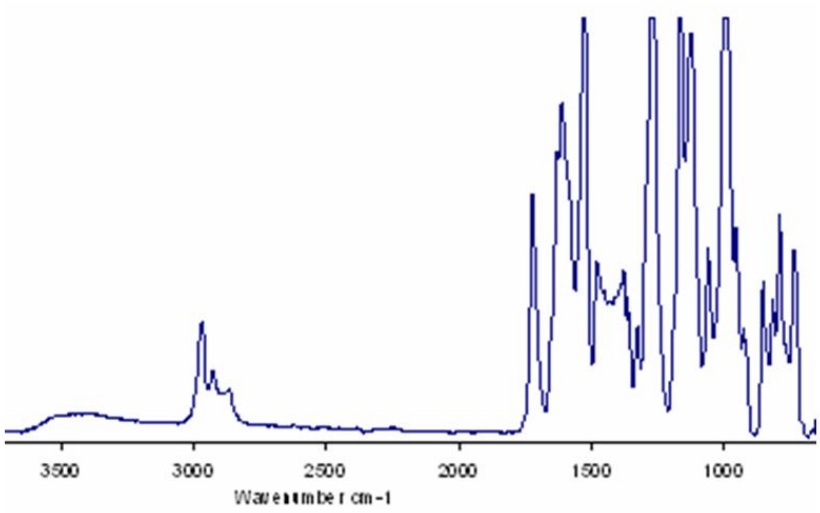

Figure 7. FT-IR spectra of $[Ti(O^iPr)_3AAPMA]_2$

3.3. Coordination of the Ligands to Zr Alkoxides

Contrary to the preferentially six coordinated Ti, Zr as its larger homologue offers an expandable coordination sphere with potential coordination numbers between 6 and 9. This can affect the coordination behavior of the bidentate ligands drastically. Therefore the coordination of the mentioned ligands to Zr alkoxides was investigated. The FT-IR spectra of the reaction product between $Zr(OBu)_4$ and EAA in a 1:1 ratio showed the typical presence of the chelating ligand bands between 1650 and 1520 cm^{-1}. ^1H NMR (Figure 8) of the same reaction supported the FT-IR results as coordination was observed from the appearance of the proton of the coordinating ligand at 5.05 ppm. However, all spectra showed broad and unresolved peaks from which further assignments were not possible.

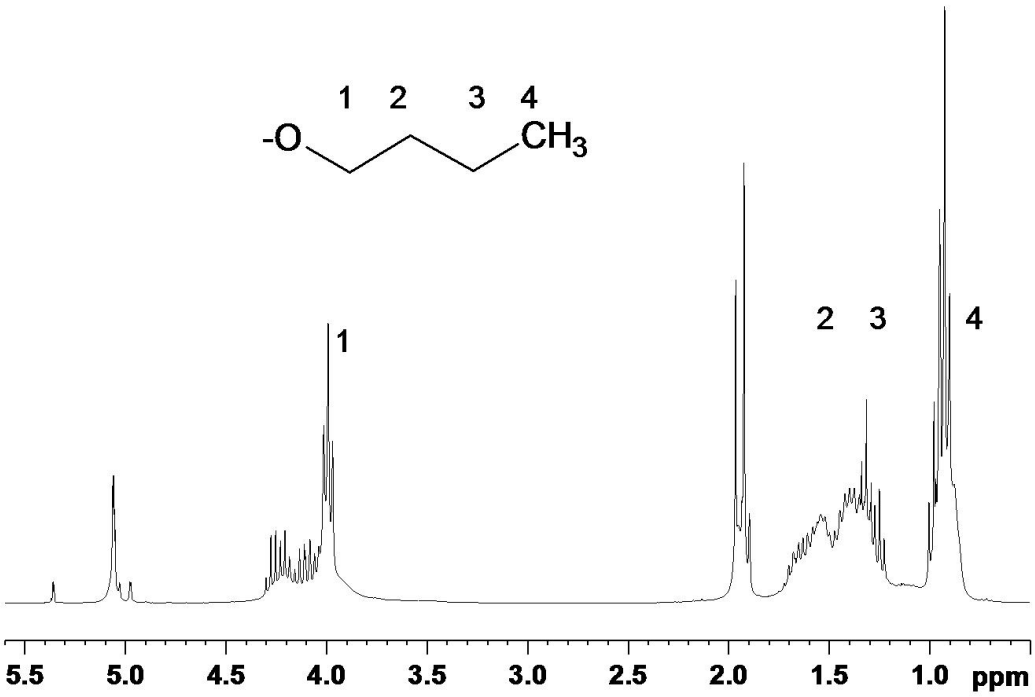

Figure 8. ^{1}H NMR spectra of the reaction product between $Zr(OBu)_4$ and EAA in 1:1 ratio

Contrary the analyses of a 1:4 mixture of $Zr(OBu)_4$ and EAA gave well resolved spectra and all signals were assigned by 2D NMR spectra. ^{13}C HMBC revealed that the methylene protons of a butoxy ligand ($-CH_2O-$) at 4.05 ppm gave a long range correlation to a carbonyl carbon at 171.9 ppm (Figure 9), which provides evidence that the butyl group is linked to a carboxylate group of the ligand. This means that even under these mild reaction conditions transesterification occurs in which a butyl acetoacetate is formed from ethyl acetoacetate under participation of the metal alkoxide (Scheme 3). In these reactions $Zr(OBu)_4$ acts as a Lewis acid. Transesterification reactions were observed at all ratios investigated (from 1:1 to 1:4) between the alkoxides and the β-keto ester ligands.

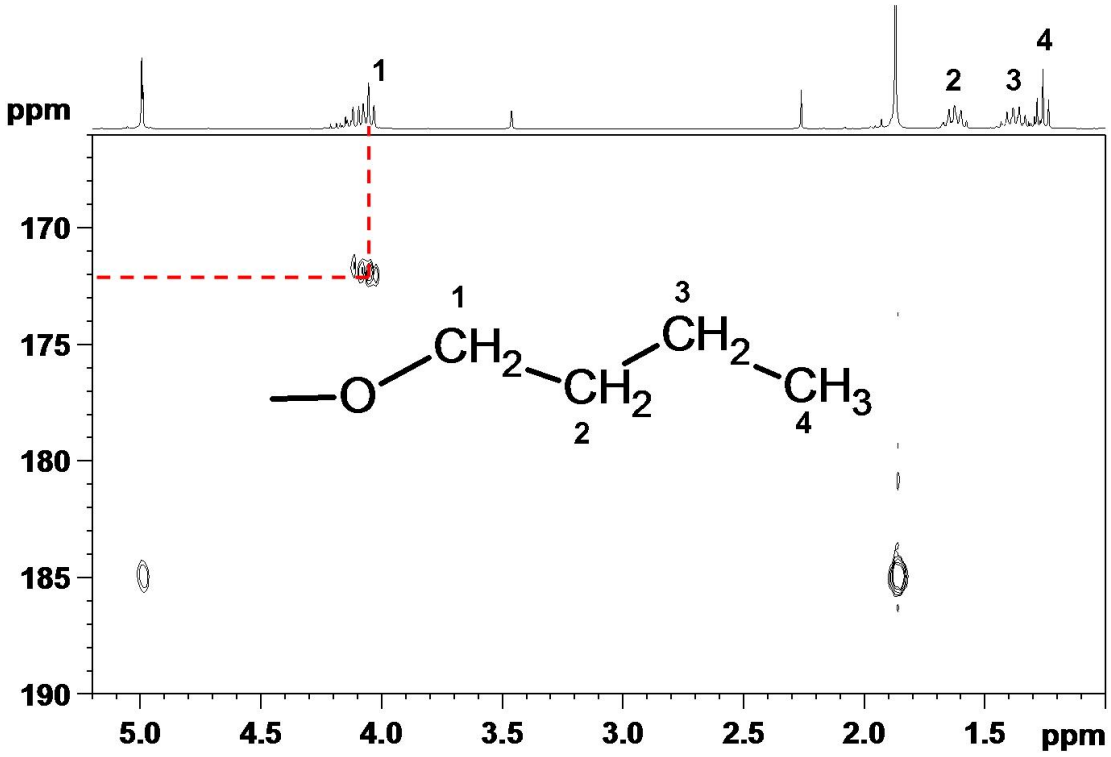

Figure 9. HMBC spectra of the reaction product between $Zr(OBu)_4$ and EAA in 1:4 ratio

The resulting ester is still coordinated to the metal center as proven by NMR which reveals only the presence of the chelating form of the ligand. The transesterification ratio could not be detected due to signal overlapping in the ^1H NMR spectra which made the integration of the signals not possible. However this reaction cannot be ignored in the formation of sol-gel materials, especially when the ligand carries a second functionality and the covalent attachment between inorganic and organic moieties is targeted. Some examples of transesterification reactions in presence of metal alkoxides were already shown in literature. *Seebach et al.* used for example, $Ti(OEt)_4$ as catalyst in the transesterification between $H_3C(O)CH_2COOR^1$ and R^2OH at elevated temperatures[155]. *Pajot et al.* synthesized $Ti_5(O^iPr)_{10}(OCH_2CH_2O)_5$ by the reaction between $Ti(O^iPr)_4$ with 2-hydroxyethyl methacrylate[156]. In this reaction the glycolate ligands were formed due to the transesterification of the 2-hydroxyethyl methacrylate mediated by the Ti alkoxide. Neither in the case of EAA nor HAAEMA a transesterification was previously reported but considering especially the fact that HAAEMA is a diester this reaction seems to be quite probable. No transesterification were observed in the cases of the Ti alkoxides under the same conditions. This behavior of the Zr butoxides can either be due to the metal center or specific for the alkoxide type.

Reacting $Zr(OBu)_4$ and HAAEMA in a 1:1 ratio the ^1H NMR reveals broad bands in the region of the methine, methylene and methylic protons from which the assignments were difficult to make, but no signal from uncoordinated ligand was observed. Again, a sharp triplet of a $-CH_2O-$ signal of a butoxy group at 4.15 ppm was observed, giving a long range correlation in the ^{13}C HMBC (Figure 10) to a carbonyl carbon at 167.6 ppm.

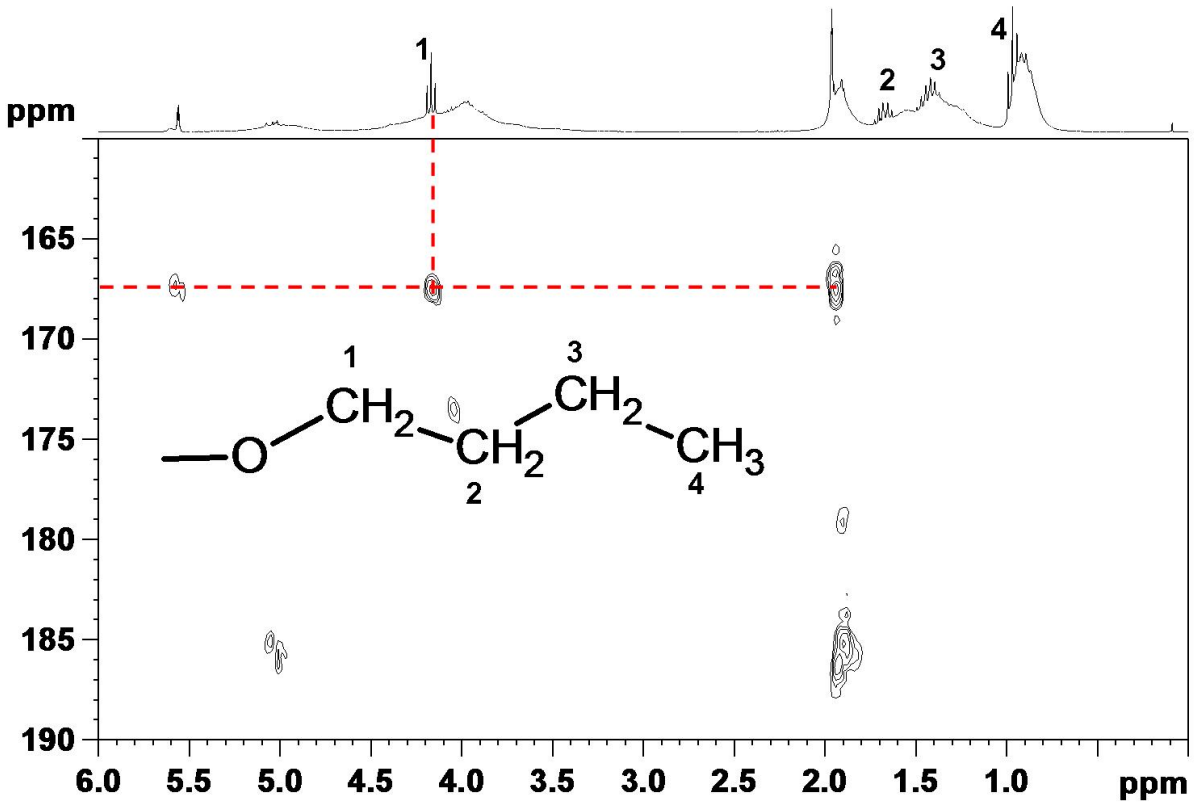

Figure 10. HMBC spectra of the products of the reaction between $Zr(OBu)_4$ and HAAEMA in 1:1 ratio

The protons of a methacrylic moiety at 6.09/5.56 ($=CH_2$) and 1.94 (CH_3) showed long range correlations to the same carbon. This means that transesterification of HAAEMA has occurred and butyl methacrylate was formed (Scheme 3).

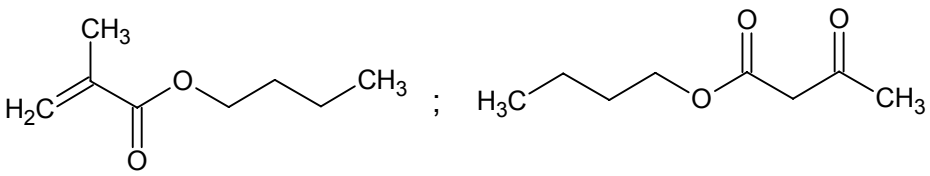

Scheme 3. Transesterification products of HAAEMA with $Zr(OBu)_4$

Although the signals in the -CH_2O- region are overlapping it was not possible to identify signals corresponding to the glycol part (-O-CH_2-CH_2-O-) of the HAAEMA ligand which is the linkage between the coordinative and polymerizable functionalities. This is a strong indication that the ligand is quantitatively decomposed and the only present species are butyl methacrylate and coordinated butyl acetoacetate, resulting from transesterification reactions. Transesterification was also detected in the analysis of the products of the reaction between $Zr(OBu)_4$ and HAAEMA in 1:2 and 1:4 ratios. These facts cannot be neglected particularly in the case of a 1:1 ratio when most of the ligand is decomposed.

Implications for materials obtained by the sol-gel process are that these materials obtained from the reactions of methacrylate-containing acetoacetoxy ligands can be mimicked by mixtures of butyl keto ester and butyl methacrylate.

The ligands showed no decomposition in the cases of Ti-alkoxides. It was important to know if the transesterification was due to the metal center or to the type of alkoxide. The commercially available $Zr(OBu)_4$ are solvated species, 80% weight solution in n-buanol. On the other hand $Ti(O^iPr)_4$ is available as pure compound (99.8%) For this reason the coordination behaviors of the two alkoxides could not be compared. Therefore the results obtained for the $Ti(O^iPr)_4$ were compared with the ones obtained when $Zr(O^iPr)_4$ was reacted with β-keto esters.

As presented in Chapter 3.2., when $Ti(O^iPr)_4$ was reacted with β-keto esters (EAA, HAAEMA) no transesterification was detected. Similar results were obtained in the reaction between $Zr(O^iPr)_4$ and EAA as well as HAAEMA in 1:1 and 1:2 ratios. Both reactions showed that full coordination occurred and no transesterification was detected, which leads to the conclusion that transesterification of HAAEMA with the alkoxides does not occur in the case with $Zr(O^iPr)_4$ but only in the reaction of HAAEMA with $Zr(OBu)_4$. Hence, a conclusion is that the transesterification is primarily based on the nature of the metal alkoxide. This means that for the solvated alkoxides the ligand is totally decomposed while in the cases of the alkoxides with an *iso*propoxy frame the transesterification does not occur. Instead the system is very complex, because of the ligand exchange reactions in solution.

In conclusion the coordination between Ti and Zr alkoxides and β-keto esters was investigated in the solid state as well as in the liquid state. X-ray single crystal diffraction analysis revealed that coordination compound obtained from Ti ethoxides or isopropoxides and EAA in 1:1 ratio appear as alkoxide-bridged dimers with chelating ethyl acetoacetate ligands, presenting a centrosymmetric structure. In these structures the metal center is six-fold coordinated. In solution ligand exchange reactions occur, which make the identification of the

chemical structures more difficult. However, the 2D NMR analyses supported a complete coordination of β-keto esters in the case of Ti-alkoxides. Comparison of molecules with various spacer length between coordinating part and polymerizable group shows that this parameter does not have an influence on the coordination. $Zr(OBu)_4$ can mediate the transesterification reaction of β-keto esters, which is probably based on the presence of free butanol in the commercially available systems. Similar reactions cannot be observed with $Zr(O^iPr)_4$. These facts make Zr butoxides not a suitable candidate for the coordination with difunctional β-keto esters if well defined materials are targeted.

3.4. Atom Transfer Radical Polymerization of β-Keto Esters with Methacrylate Bonds Attached

ATRP was used to synthesize well defined copolymers starting from the Ti and Zr complexes. First the synthesis of model HAAEMA-MMA copolymers by ATRP was carried out. The optimized process was then applied for the synthesis of $M(OR)_3$AAEMA-MMA copolymers (M = Ti, Zr and R = Et, ^{i}Pr). The obtained hybrid polymers were used as precursors for the sol-gel process. Thus, small metal oxide nanoparticles were formed inside the polymer matrix.

All the compounds which did not show metal alkoxide catalyzed transesterification reactions ($[Ti(OEt)_3AAEMA]_2$, $[Ti(O^iPr)_3AAEMA]_2$ and $[Zr(O^iPr)_3AAEMA]_2$), were used for the formation of hybrid (co)polymers by ATRP.

Lately poly(HAAEMA) homopolymers were prepared by reversible addition–fragmentation chain transfer (RAFT) radical polymerization[157] and were found to self-assemble into a hierarchical superstructure of double-stranded helical tubes with either screw sense[158]. ATRP was used as a controlled polymerization technique due to its versatility. In ATRP free growing radicals are generated via a catalyzed reaction, and they establish a rapid dynamic equilibration with majority of dormant species. This allows a good control over the polymerization process. ATRP has also the advantage that a wide range of monomers can be used. The metal alkoxide-HAAEMA monomers were used as monomers and comonomers with MMA in an ATRP process.

Possible pathways for the preparation of hybrid inorganic-organic polymers containing metal alkoxides are presented in Scheme 4, either a ligand containing a polymerizable group is coordinated to a metal alkoxide (M) and this compound is used in a

polymerization reaction, or a polymer containing the coordination ligands is formed in a first step and the coordination of the metal alkoxides is carried out subsequently. The latter pathway has the disadvantage that a control over the coordination of the metal alkoxides is not easy to obtain and that crosslinked systems are obtained immediately after mixing the ligand containing polymer and the metal alkoxides. Therefore the first pathway was chosen.

Scheme 4. Schematic representation of the two possible pathways for obtaining metal coordinating polymers

3.4.1. Spectroscopic Characterization of the (Co)Polymers

As mentioned before, model compounds based on uncoordinated HAAEMA-MMA (co)polymers in 1:1, 1:5 and 1:10 ratios between the two comonomers were prepared. The polymerizations were performed under optimized conditions. CuBr/PMDETA was used as a catalyst, 2-ethylbromoisobutyrate as initiator and the polymerization was carried out either in toluene or in bulk. The temperature of the polymerization reactions was maintained at 85ºC and the reaction time was 6 hours. For these conditions a conversion of 87% was obtained. ^{1}H NMR (Figure 12) analyses showed the presence of the methyl protons of the polymer backbone between 0.8 and 1.2 ppm while the specific signals of acetoacetoxy units were present at 2.28 ppm (***CH*$_3$**CO) and 3.55 ppm (CO***CH*$_2$**CO). These data are consistent with already reported data for poly(HAAEMAcoMMA)[159] and polyHAAEMA[158].

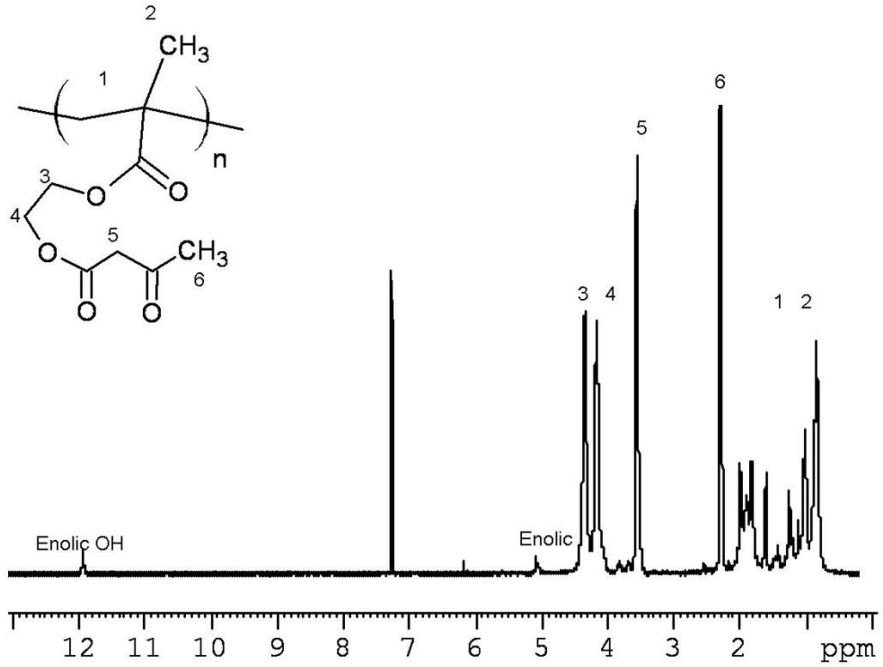

Figure 12. ^{1}H NMR of poly(HAAEMA) synthesized by ATRP and the respective assignments

A potential side reaction that could occur when HAAEMA type monomers are polymerized by ATRP is the coordination of the Cu catalyst to the acetylacetone groups of the β-kets ester ligand. However, compared to other coordinating polymers, such as amine containing systems, no coordination of the copper catalyst to the polymer by partial or full ligand exchange should occur in these systems. The reasons for this behavior lies in the higher stability of the tridentate PMDETA/copper complex compared to *β*-keto ester complexes. In addition in the cases of the polymerizations of the metal alkoxide-containing monomers, the titanium and zirconium atoms are much more oxophilic than copper. UV studies were carried out to experimentally support this theoretical prediction. These studies showed no coordination of the Cu-PMDETA complex to the HAAEMA monomer from room temperature up to the polymerization temperature of 85 °C. In this temperature range no change in the absorption band of the copper complex was detectable. Additional FT-IR investigations showed that the HAAEMA ligand was maintaining its keto form without any signs of coordination in the presence of the Cu complex.

3.4.2. Size Exclusion Chromatography Studies

SEC results of the model compounds based on uncoordinated polyHAAEMA or HAAEMA-MMA (co)polymers in 1:1, 1:5 and 1:10 revealed that the molecular weight distribution was monomodal and the theoretical and experimental molecular weights were in good agreement (Figure 13, Table 3). ^{1}H NMR analysis showed that both monomers were incorporated into the polymer backbone. Molecular weights distributions (MWDs) of the resulting polymers revealed values between 1.2 and 1.89, which were rather high for a controlled polymerization. Broad MWDs were also observed by *Krasia et al.* who investigated the ATRP of HAAEMA[157]. In the case of HAAEMA-co-MMA polymers the broad polydisperisty could be due to the different reactivity of the two monomers or due to a kind of self-organization of the copolymers. Different side groups of HAAEMA and MMA can induce different propagation rates and different reactivity of the dormant carbon-halogen terminals, which may broaden the molecular weight distribution. Such broadening phenomenon during the random copolymerization has also been observed in the cases of copolymerization of 3-(methoxysilyl)propyl methacrylate with MMA[160]. As mentioned before a coordination of the catalyst to the pendant acetylacetoxy groups can be ruled out to be responsible for the rather high MWDs. As mentioned before a coordination of the catalyst to the pendant acetyl-acetone groups was ruled out.

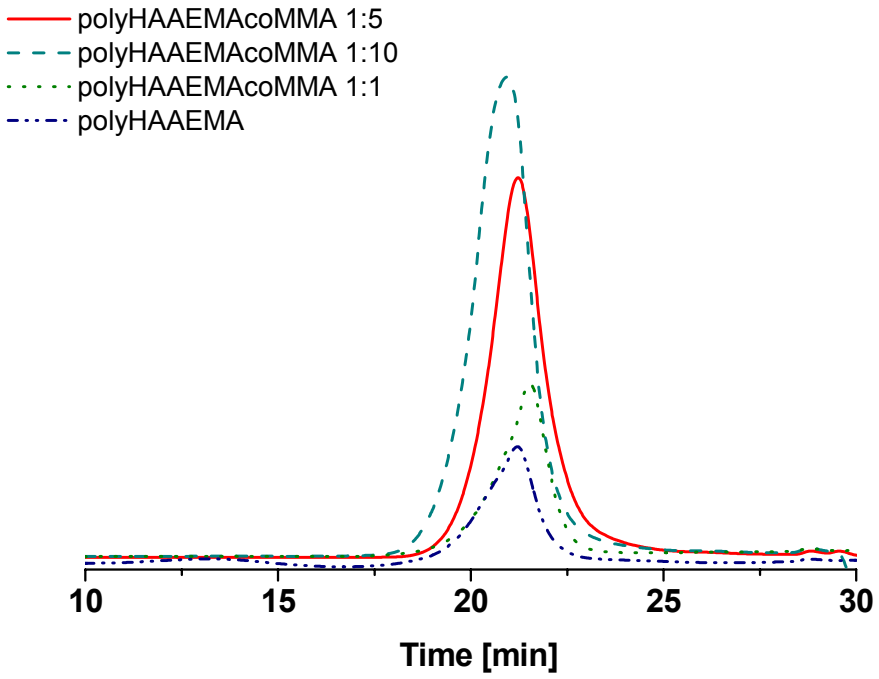

Figure 13. SEC plot of poly(AAEMA-co-MMA) in 1:1, 1:5 and 1:10 ratio between the monomers

Table 3. Size exclusion chromatography (SEC) data for the 2-(methacryloyloxy)ethyl acetoacetate – methyl methacrylate homo and copolymers obtained without metal alkoxides (M_n: numeric molecular mass; PDI: polydispersity index (M_n/M_w), DP_n: degree of polymerization)

Polymer	**Ratio between monomers**	**M_n**	**M_w/M_n**	**DP_n theoretical**	**DP_n observed from SEC**	**Yield (%)**
Poly(HAAEMA)	-	37036	1.23	200	175	68
PMMA		20395	1.18	200	203	83
Poly(HAAEMAcoMMA)	1:1	28117	1.39	100	90	74
Poly(HAAEMAcoMMA)	1:1	45261	1.70	200	144	63
Poly(HAAEMAcoMMA)	1:5	27915	1.82	200	195	71
Poly(HAAEMAcoMMA)	1:10	30572	1.58	200	275	76
Poly(HAAEMAcoMMA)	1:10	43249	1.89	400	360	69

3.4.3. Thermal Analyses of the Copolymers

The TG analyses of the copolymers in 1:5 and 1:10 ratios between HAAEMA and MMA reveal that the copolymers show an onset temperature of decomposition at 280°C for the 1:5 ratio compared to 251ºC for the 1:10 ratio (Table 4), hence the thermal stability of the copolymers decreased with an increasing MMA content. The total mass change is more than 99% proving that the polymer completely decomposes at 650ºC. The plots are presented in the next chapter.

3.5. ATRP and Sol-Gel Reactions of Ti and Zr Alkoxides-Modified β-Keto Esters

Previous studies of the metal alkoxides HAAEMA complexes showed that the coordination compounds between titanium alkoxides and β-keto esters in a 1:1 ratio appear as alkoxide-bridged dimers in solid state with chelating ethyl acetoacetate ligands, presenting a centrosymmetric structure[161]. In solution, due to ligand exchange reactions, there is an equilibrium between the dimeric species and the monomeric disubstituted species (Scheme 5). A total avoidance of crosslinking is not possible based on this equilibrium and therefore polymerization reactions should still result in at least partially crosslinked polymers.

First attempts to use coordinated Ti alkoxides with HAAEMA type ligands as monomers in ATRP were reported recently. It was shown that polymerization of pending Ti alkoxide by ATRP is possible[159].

The polymerizations were carried out under the same optimized conditions as used for the non-metal containing copolymers. CuBr/PMDETA was used as a catalyst, 2-ethylbromoisobutyrate as initiator and toluene as solvent. The temperature of the polymerization reactions was maintained at 85ºC and the reaction time was 6 hours. The sol-gel process was carried out in a desiccator under a saturated water atmosphere. The copolymers were kept inside for 7 days, either at room temperature or at 40°C. Afterwards, the polymers were dried under reduced pressure.

When homopolymerization of the metal complexes was applied, gelation occurred in minutes. This was due to the fact that the bifunctional complexes act as crosslinkers between single polymer chains[159]. Hence, the metal complexes were used in copolymerization reactions with methyl methacrylate to decrease the number of pending metal alkoxides attached to each polymer chain and thus the probability of crosslinking. However, even with a decreasing amount of metal complexes in the polymer chain reasonable crosslinking occurred. Ratios between metal containing monomers and MMA of 1:5 and 1:10 were chosen for increasing the gelation time and hence, a better control over the polymerizations. As a difference to their non-metal containing homologues, Ti- and Zr-alkoxide containing polymers could not be analyzed via SEC due to the insolubility of the crosslinked systems in common organic solvents.

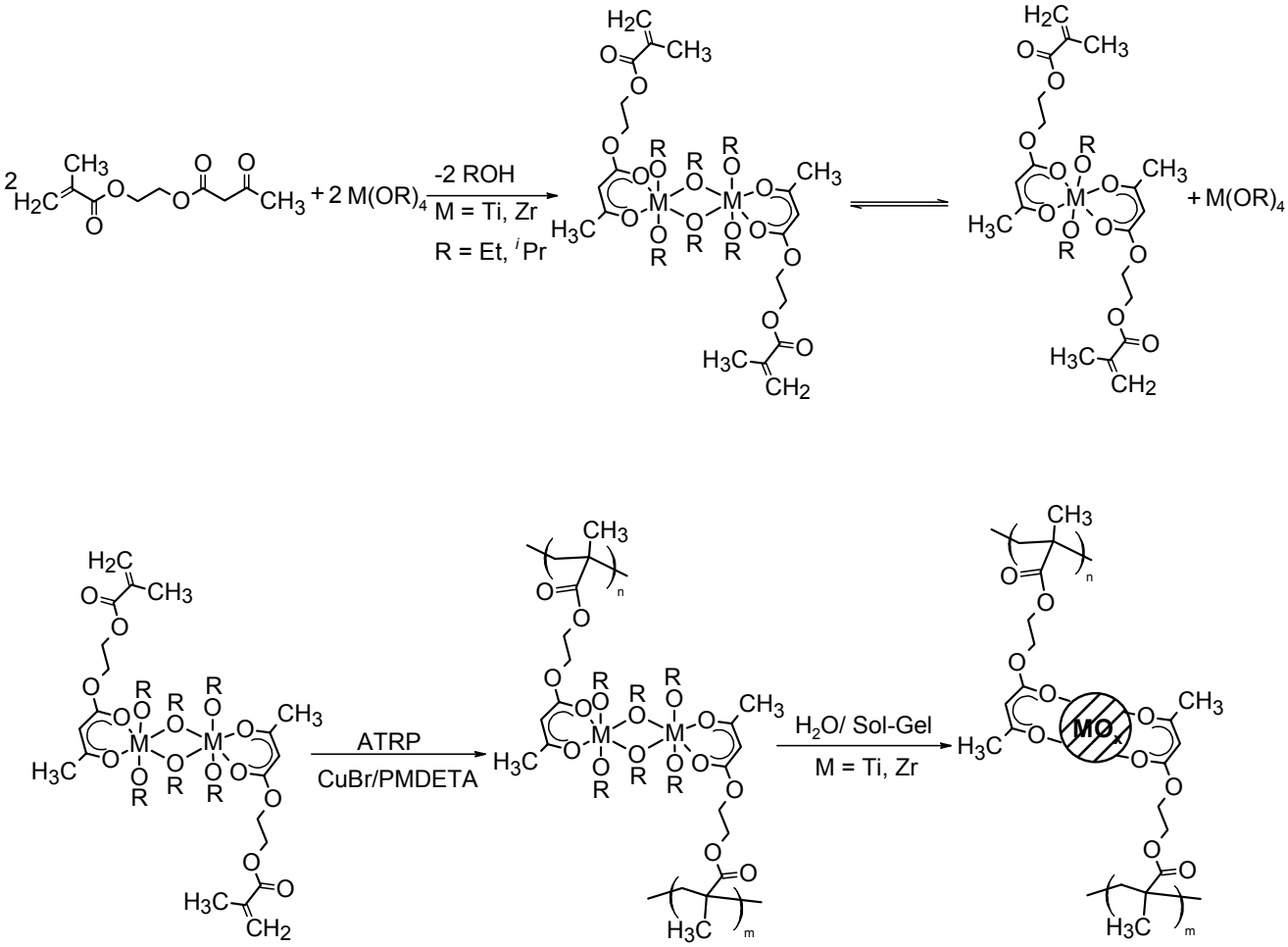

Scheme 5. Presentation of the synthetic pathway: i) coordination of Ti and Zr alkoxides with HAAEMA, ii) polymerization, iii) sol-gel process

3.5.1. Spectroscopic Analyses

The metal containing copolymers were analyzed by FT-IR and NMR spectroscopy. A ^{13}C CP/MAS spectrum of poly[Ti(O^iPr)$_3$AAEMAcoMMA] in 1:5 ratio between the two comonomers is shown in Figure 14. The resonances of the *CH_3*-groups of the *iso*propoxy unit are found at 10.0 ppm while the *CH_3* of the AAEMA ligand are located at 18.0 ppm (methacrylate part) and at 20.0 ppm (keto-ester part). Evidence for the polymerization of the AAEMA ligand is obtained by the signal at 41.0 ppm, corresponding to the quaternary carbon atoms of the polymer chains. Glycol C-atoms are observed at 57.1 ppm, and the methylene carbons *(CH)* of the *iso*propoxy groups result in a signal at 79.1 ppm.

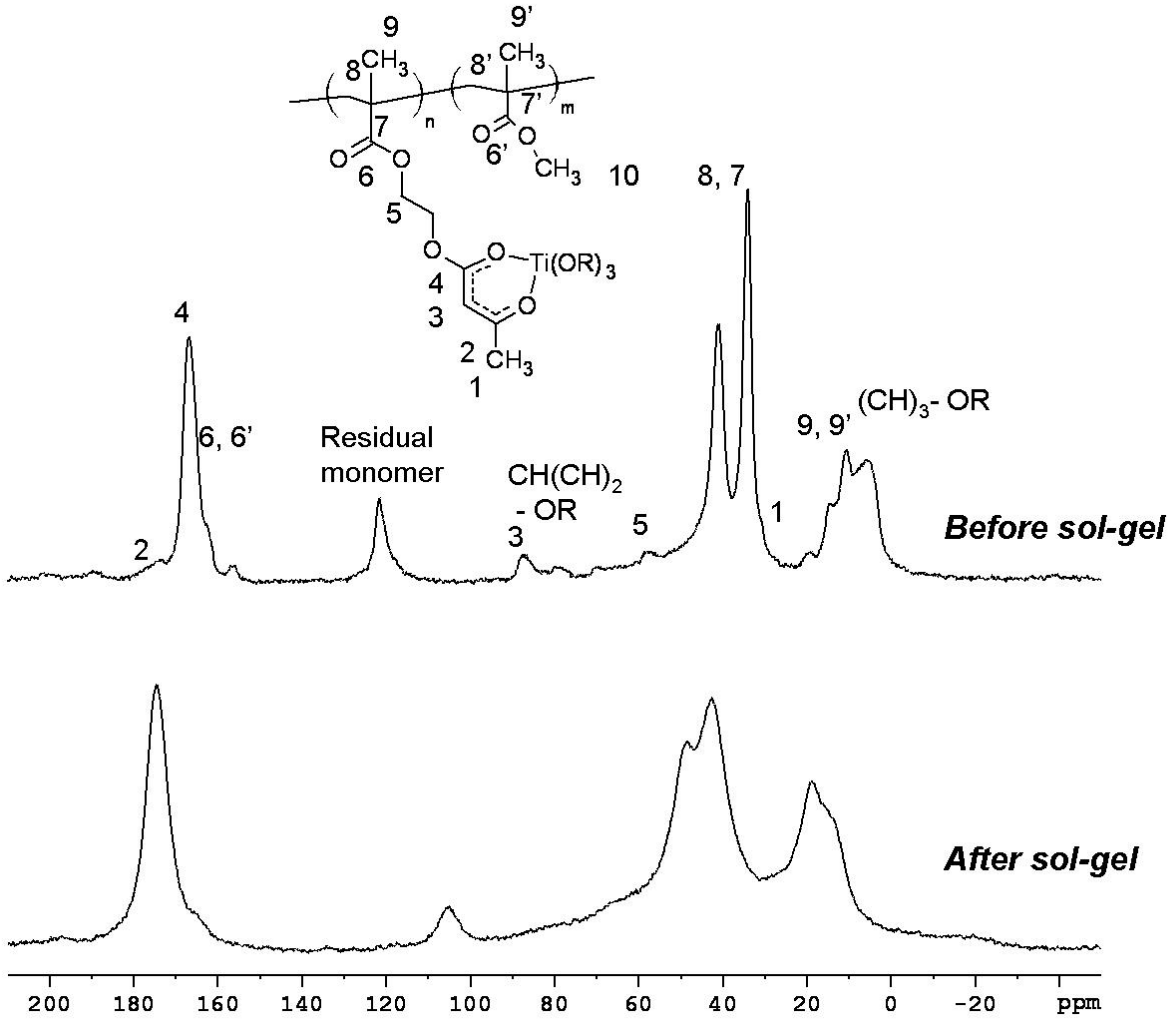

Figure 14. ^{13}C CP/MAS NMR spectra of poly[Ti(O^iPr)$_3$AAEMAcoMMA] (up) and poly(TiO_2-AAEMAcoMMA) (1:5 ratio between the two monomers) (down) and the respective assignments

The chelating form present in the final polymer was proven by the *CH* group of the coordinated ligand at 87.7 ppm which clearly revealed that coordination was still maintained after polymerization. In the copolymerization of metal-free HAAEMA no free monomers were detected after polymerization at 85°C for 6 hours. The optimized conditions were also used for the monomers coordinated on the metal alkoxides. However, due to crosslinking, the hybrid materials still showed a signal at 121.6 ppm which can be assigned to residual olefinic carbons of the monomers[162]. Hence a full conversion of the double bonds was not achieved during the 6 hours of the polymerization. The carbonyl region showed resonances for the chelating form at 166.8 ppm and 189.7 ppm. There are no signals corresponding to uncoordinated ligand, which proves that coordination is maintained during the polymerization

process. It is important for further sol-gel reactions applying the obtained polymers that the alkoxides are still bound to the metal centers and that a good linkage between the inorganic and organic phase is achieved.

After the sol-gel reaction a broadening of the peaks in the ^{13}C NMR spectrum was observed. The carbons of the polymer chains still give the same signals (42.6 ppm and 48.5 ppm). There is no signal detected for the *CH* carbon of the *iso*propoxy moieties at 79 ppm. However, due to the broadening of the bands no statement could be given whether all of the *iso*propoxy groups have been hydrolyzed or not. Also only a small shoulder around 13 ppm was observed which could be due to the CH_3 of the *iso*propoxy groups. The *CH* groups of the coordinated ligand formerly present at 87.7 ppm are not visible anymore. The carbonyl region presented almost the same shifts as before the sol-gel reaction (165 ppm, 174.5 ppm, and 197 ppm). Due to these spectroscopic results it was difficult to make a statement whether the AAEMA ligand was still coordinated. Most likely parts of the ligand were hydrolyzed. *Hoebbel et al.* investigated the hydrolysis behavior of different complexes of β-keto ester ligands and Ti or Zr alkoxides[151] and showed that even at small water to metal ratios some of the methacryloyloxy ethyl acetoacetate ligands were hydrolyzed.

The FT-IR data of the samples with the metal alkoxides also proved that the linkage between the inorganic and the organic part still exists after the polymerization. The typical bands at 1626 cm^{-1}, 1611 cm^{-1} and 1527 cm^{-1}, (C=C) and (C-O) stretching of the chelating form of the ligand are still present. The frequencies are characteristic for coordinated diketones and keto esters[163]. In addition these results were supported by the data obtained in the cases of HAAEMA ATRP systems[161]. After the sol-gel process the disappearance of the characteristic bands of the coordinated ligand at 1626 cm^{-1}, 1611 cm^{-1}, and 1527 cm^{-1} (Figure 15) was observed and the appearance of a broad band between 1650 cm^{-1} and 1700 cm^{-1} was detected. These facts suggest that most of the chelating ligands were hydrolyzed and the keto form of the ligands was present instead of the chelating form. These results were consistent with the NMR data.

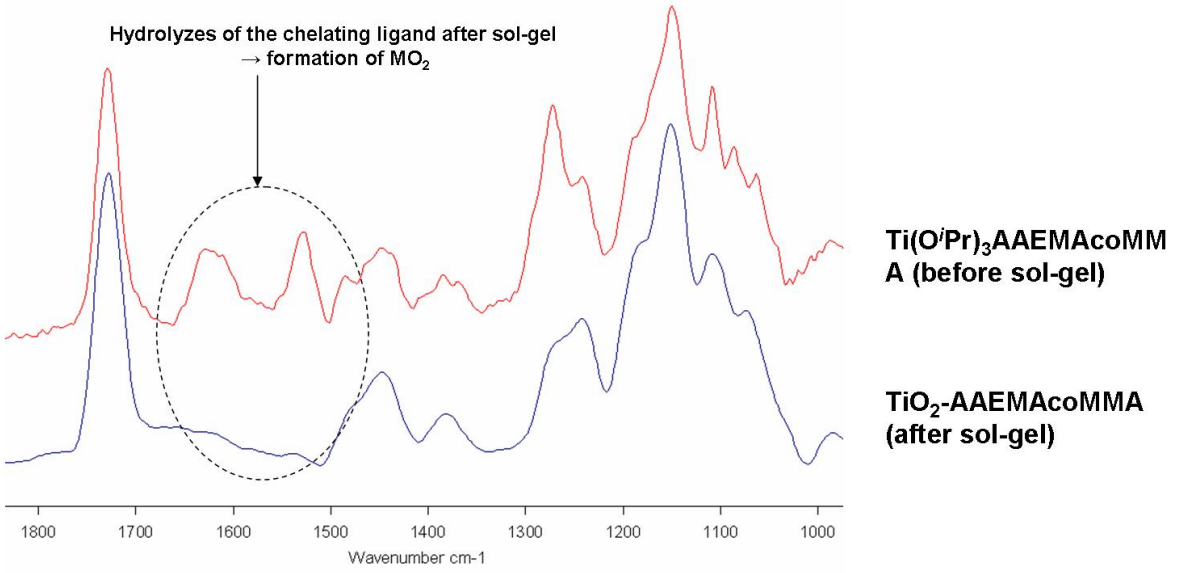

Figure 15. FT-IR spectra of the poly[Ti(O^iPr)$_3$AAEMA-co-MMA] and poly(TiO_2AAEMA-co-MMA) 1:5 ratio

3.5.2. Thermal Analyses of the Materials

Thermogravimetric Analyses

TG analysis for both 1:5 and 1:10 copolymers with and without metal alkoxides were carried out. As mentioned before the analyses of the copolymers in 1:10 ratios reveal that the copolymers without metal alkoxides (HAAEMA: MMA 1:10) show an onset temperature of decomposition at 251ºC (Table 4). The total mass change is more than 99% proving that the polymer completely decomposes at 650ºC. Contrary, the metal containing copolymers showed two onset temperatures (Figure 16). The first one around 85ºC is most likely due to the evaporation of the volatiles (alcohols) as well as to the cleavage of alkoxide ligands and the decomposition of the Ti and Zr β keto ester complexes[164]. The mass loss for this first event which takes place below 200ºC is around 13%. The second onset temperature for decomposition was detected at 266ºC for Ti *iso*propoxides and at 260ºC for Ti ethoxides, which is most likely due to the decomposition of the polymer main chain. A slight increase in the onset temperature in the cases of the copolymers containing metal alkoxides compared with the ones without metals was observed, which was most likely due to crosslinking which blocks depolymerization mechanisms. However, these results are not very accurate because the onset temperatures used for this comparison are strongly influenced by the slopes of the tangents before and after the event. The mass loss due to the more volatile alkoxides falsifies the real value of the degradation of the main polymer chain. The residual mass at 650ºC is

5.1% for polymers containing Ti *iso*propoxides. The mass of the residues can be attributed to the formation of TiO_2. This seems very realistic after the analyses of the copolymers with 1:5 ratio between HAAEMA [or $Ti(OR)_3$AAEMA] and MMA. In this case the mass of the final residual was higher (around 13%) corresponding to the higher quantity of metal oxide in the copolymer. The residual mass was similar to the calculated metal content. However, without a clear information about the molecular mass a strict calculation cannot be made. This is in accordance with the data reported by *Chang et al.* for the PMMA-$M(OBu)_2EAA_2$ nanocomposites (M=Ti, Zr)[164].

Table 4. TGA results of some copolymers obtained from monomers containing Ti and Zr alkoxides as well as their homologues after sol-gel process (Td_1-1st onset temperature; Td_2-2nd onset temperature).

Copolymer	Ratio between monomers	Td_1, ºC	Td_2, ºC	Mass loss (1), %	Mass loss (2), %	Residual mass, %
Poly(HAAEMAcoMMA)	1:5	-	280	-	100	0
Poly[Ti(O^iPr)$_3$AAEMAcoMMA]	1:5	84	290	14.6	72.7	12.7
TiO_2-Poly(AAEMAcoMMA)	1:5		290		87.3	12.7
Poly(HAAEMAcoMMA)	1:10	-	251	-	100	0
Poly[Ti(O^iPr)$_3$AAEMAcoMMA]	1:10	87	266	13.8	81.2	5.1
TiO_2-Poly(AAEMAcoMMA)	1:10	-	273	-	93.1	6.9
Poly[Zr(O^iPr)$_3$AAEMAcoMMA]	1:5		271	6.27	78.2	14.3
ZrO_2-Poly(AAEMAcoMMA)	1:5	-	270	-	83.9	16.1
Poly[Zr(O^iPr)$_3$AAEMAcoMMA]	1:10	52	251	10.4	78.3	11.3
ZrO_2-Poly(AAEMAcoMMA)	1:10	130	269	8	81	11

An increase of the thermal stability is expected when transferring the alkoxides into a sol-gel network. Comparing the copolymers without metals in 1:5 and 1:10 ratio between HAAEMA and MMA it is clear that the onset temperature corresponding to the degradation of the main polymer chains is decreasing with increasing MMA content, so the thermal stability is lower for higher MMA content. Decreasing the MMA content accelerates the gelation due to the higher number of crosslinking sites. Hence, the degree of polymerization and the conversion of the monomer decrease, resulting in less controlled over the molecular

weights and MWDs. Therefore an optimum has to be found between a good thermal stability and a convenient gelation time. The copolymers containing *iso*propoxy groups show an increase in the thermal stability compared to the copolymers without metals.

These results provided prove that the metal alkoxide monomers are incorporated into the copolymer chains. The obtained structure of the metal containing polymers is consistent with the one predicted and allows further reaction via the sol-gel process.

As mentioned before, the sol-gel process was applied to the metal alkoxide moieties by storing the samples for 7 days in a desiccator in a water saturated atmosphere. The excess of volatiles and water was removed in vacuum. The conversion of the alkoxides to the respective metal oxides was analyzed by TGA (Table 4, Figure 16).

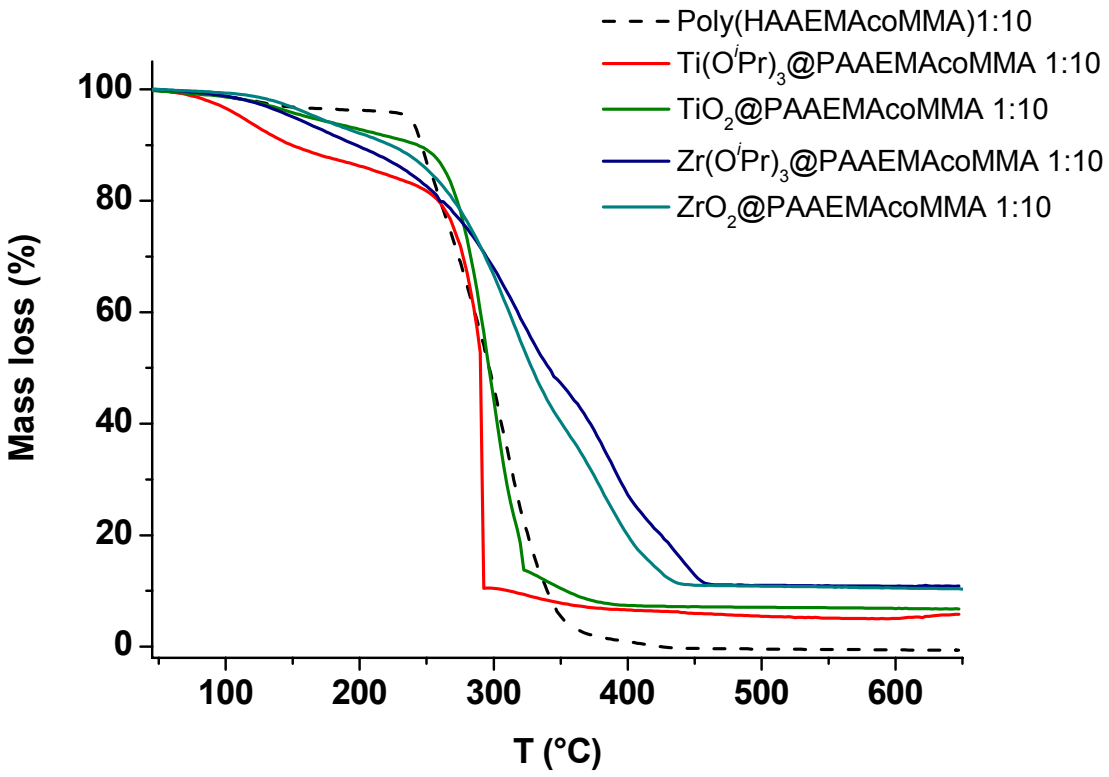

Figure 16. TGA of poly(AEEMAcoMMA) 1:10; poly[Ti(O^{i}Pr)$_3$AAEMAcoMMA] and poly[Zr(O^{i}Pr)$_3$AAEMAcoMMA]1:10; poly(TiO$_2$-AAEMAcoMMA) and poly(ZrO$_2$-AAEMAcoMMA) (after sol-gel)

It is obvious for all samples (Ti and Zr modified alkoxides) that the first decomposition step (before 200°C) almost disappeared, the mass loss in this region being below 2%. These volatiles are most likely non-hydrolyzed alkoxide groups and water. The second stage (decomposition of the polymer main chain) shows an increase in the

decomposition temperature of the material (273°C for the 1:10 ratio, TiO_2 sample). The final residual percentage is exactly the same for both alkoxide containing samples and the sol-gel samples.

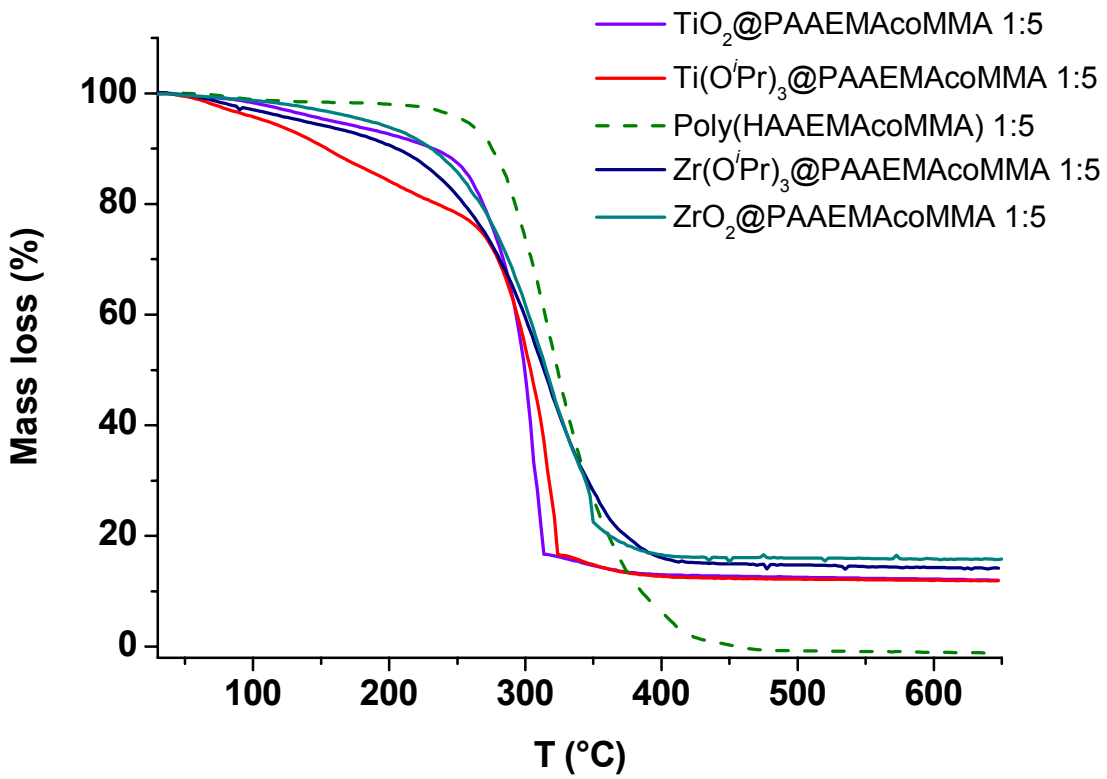

Figure 17. TGA of poly(AEEMAcoMMA) 1:5; poly[Ti(O^iPr)$_3$AAEMAcoMMA] and poly[Zr(O^iPr)$_3$AAEMAcoMMA] 1:5; poly(TiO_2-AAEMAcoMMA) and poly(ZrO_2-AAEMAcoMMA) (after sol-gel)

Differential Scanning Calorimetry

DSC measurements of the hybrid polymers were conducted under a nitrogen atmosphere in aluminum pans. The sample mass was kept between 4 and 8 mg. Glass transition temperatures (T_g) were determined by first removing thermal history of the samples in a heating run with a ramp of 10 °C/min. After cooling the samples, they were heated again with a ramp of 10 °C/min. In Figure 18 the thermographs of the hybrid polymers for the Ti and Zr series with HAAEMA : MMA = 1:5 (simple copolymers, copolymers containing metal alkoxides and copolymers containing TiO_2 and ZrO_2 nanoparticles) are presented.

Homopolymers of HAAEMA have a T_g of around 2°C as reported before in literature from *Krasia et al.*[157]. On the other hand, PMMA has a T_g situated above 100°C. In Figure 18

it could be observed that the simple polymers without any metals show one second order phase transition with a decrease of the heat capacity, of a value of 90°C, which we assigned to a glass transition point. This is consistent with the T_g of a PMMA based copolymer.

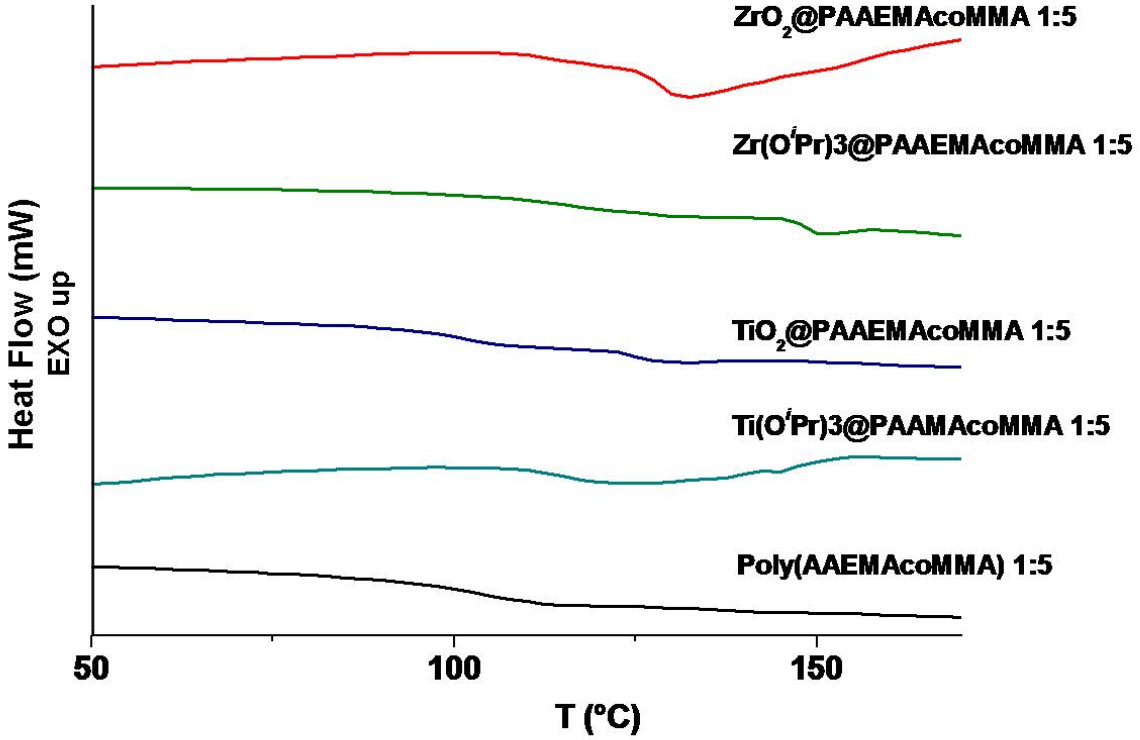

Figure 18. DSC analysis of poly(AEEMAcoMMA) 1:5; poly[Ti(O^iPr)$_3$AAEMAcoMMA] and poly[Zr(O^iPr)$_3$AAEMAcoMMA] 1:5; poly(TiO_2-AAEMAcoMMA) and poly(ZrO_2-AAEMAcoMMA) (after sol-gel)

Tabel 5. T_g data of poly(AEEMAcoMMA) 1:5; poly[Ti(O^iPr)$_3$AAEMAcoMMA] and poly[Zr(O^iPr)$_3$AAEMAcoMMA] 1:5; poly(TiO_2-AAEMAcoMMA) and poly(ZrO_2-AAEMAcoMMA) (after sol-gel)

Sample	T_g (°C)
PolyHAAEMAcoMMA 1:5	90
Ti(O^iPr)$_3$AAEMAcoMMA 1:5	98
TiO_2AAEMAcoMMA 1:5	96
Zr(O^iPr)$_3$AAEMAcoMMA 1:5	107
ZrO_2AAEMAcoMMA 1:5	126

Comparing the obtained results with those of copolymers containing Ti alkoxides the situation differs to some extent. At 107°C a second order phase transition was observed with a decrease of the heat capacity which was assigned to a glass transition point (Table 5). This is similar to the one observed in the pristine polymers, showing a small increase for the hybrid samples. The increase of the T_g is due to the decrease of the mobility of the polymer chains due to crosslinking of the network through the metal complexes. Strong interfacial bonding between the cluster and polymer matrix leads to an increase of the T_g by impeding chain flexibility[89].

Interestingly another endothermic transition at 176°C was observed which is assigned to a decomposition of the Ti alkoxide complex[164]. This is sustained also by the fact that after the sol-gel process the later effect is strongly reduced, being not visible anymore in most of the samples. In the sample containing TiO_2 nanoparticles a second order thermal transition assigned to the T_g is present at 96°C proving that the alkoxide moieties were hydrolyzed and transformed into the respective oxides. The formation of the TiO_2 particles and the hydrolysis of the β-keto ester ligand led probably to the destruction of the alkoxide crosslinking sites. Thus, without crosslinking site the chain flexibility is increasing which results in a decrease of the T_g compared to the crosslinked polymers.

The Zr-series shows an even larger increase in the glass transition temperature compared to their Ti homologues. The polymers containing Zr alkoxide clusters show a T_g at 107°C which is almost 20°C higher than in the case of the copolymers without metal alkoxides and 10°C higher than their Ti alkoxide homologues. This leads to the conclusion that the mobility of the chains in the polymer crosslinked by the Zr clusters is reduced compared to the Ti homologues, due to a more efficient crosslinking of the Zr complexes. Decomposition of the clusters appears around 175°C as in the case of the Ti-series.

When changing the ratio between the metal-HAAEMA complex and the MMA to 1:10 a small increase in the T_g was observed in the cases of the pure copolymers of HAAEMA and MMA. This is understandable by the fact that a higher amount of PMMA in the copolymer would lead to a higher glass transition temperature. T_g's in the temperature region of about 100 °C were visible for all the copolymer systems. Due to crosslinking, this effect was less pronounced for the hybrid polymers bearing higher cluster loadings. This was consistent with

the hypothesis that by increasing the ratio of PMMA in the copolymer the T_g of the materials will increase.

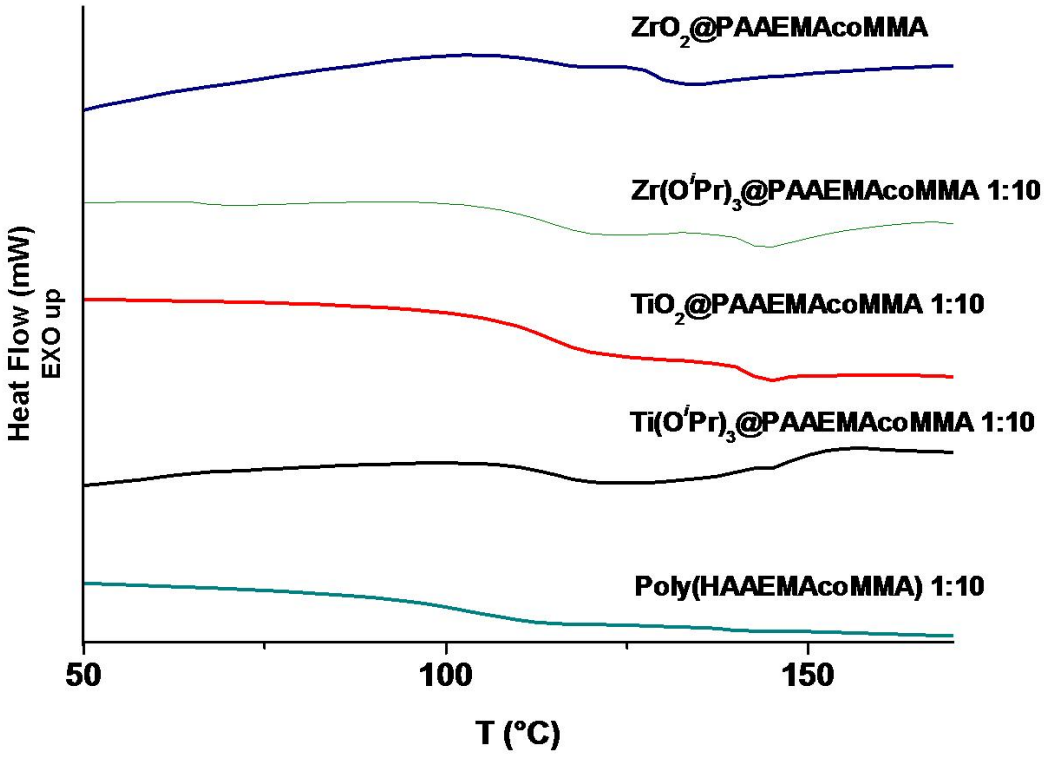

Figure 19. DSC analyses of poly(AEEMAcoMMA) 1:10; poly[Ti(O^iPr)$_3$AAEMAcoMMA] and poly[Zr(O^iPr)$_3$AAEMAcoMMA]1:10; poly(TiO_2-AAEMAcoMMA) and poly(ZrO_2-AAEMAcoMMA) (after sol-gel)

Similar as discussed in the 1:5 series, the copolymers containing Ti and Zr alkoxides showed second order phase transitions with a decrease of the heat capacity between 106 and 111°C which was assigned to glass transition points (Tabel 6). The increase of the T_g is due to the decrease of the mobility of the polymer chains based on the crosslinking of the network as mentioned before. The differences in the T_g temperatures compared to the simple copolymer were up to 10°C. However in this later case the amount of cluster which acts as crosslinker is less, which results in relative smaller T_g differences compared to the simple copolymer as in the case of 1:5 ratio, when increases up to 20°C in the T_g temperatures of the hybrid copolymers compared with the pristine copolymers were observed.

Tabel 6. T_g determined from DSC for poly(AEEMAcoMMA) 1:10; poly[Ti(O^iPr)$_3$AAEMA-coMMA] and poly[Zr(O^iPr)$_3$AAEMAcoMMA]1:10; poly(TiO_2-AAEMAcoMMA) and poly(ZrO_2-AAEMAcoMMA) (after sol-gel)

Sample	T_g (°C)
PolyHAAEMAcoMMA 1:10	92
Ti(O^iPr)3AAEMAcoMMA 1:10	109
TiO_2AAEMAcoMMA 1:10	106
Zr(O^iPr)$_3$AAEMAcoMMA 1:10	106
ZrO_2AAEMAcoMMA 1:10	111

3.5.3. Transmission Electron Microscopy

The polymers containing metal alkoxides as well as the polymers containing metal oxides (after sol-gel) were analyzed by transmission electron microscopy (TEM). TEM micrographs of the polymers before and after the sol-gel process (Figure 20) of Ti alkoxides containing polymers showed a uniform distribution of the inorganic phase in the polymer matrix. Agglomerates or particles were not detected. The darker regions presented in the samples are based on a different thickness of the samples and not due to a different material.

The morphology of the hybrid material changes drastically after the sol-gel process was applied (Figure 20, bottom). Small particles are observed uniformly distributed in the polymer matrix. The different contrast suggests that the particles are formed from a heavier element, in this case titanium. It is important to remark that all sample regions analyzed were similar, for both of the TiAAEMA-complex: MMA ratios used. The diameter of the particles was ranging from a few nanometers up to 20 nm.

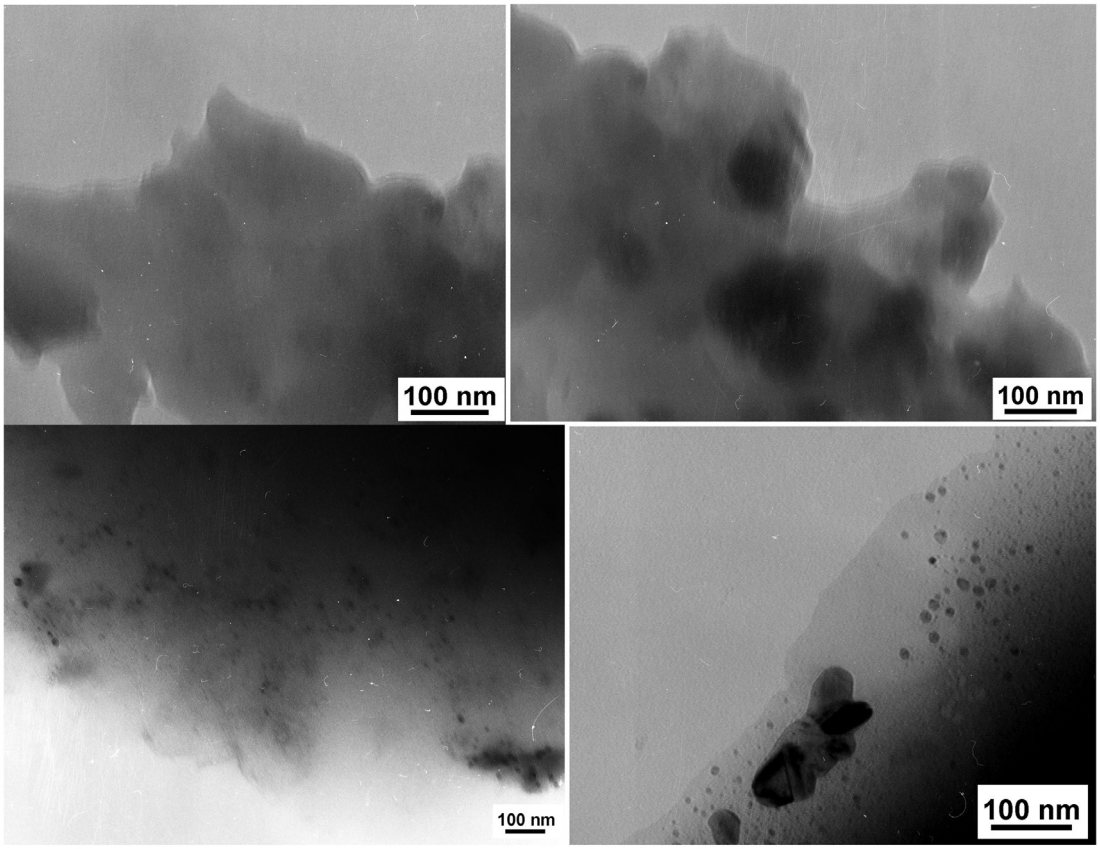

Figure 20. TEM micrographs of the poly[$Ti(OR)_3$AAEMAcoMMA] (top, 1:5 and 1:10) and TiO_2-polyAAEMAcoMMA (bottom, 1:5 and 1:10)

The same trend was observed in the cases of copolymers containing Zr alkoxides and ZrO_2. No agglomerates or particles were detected in the cases of copolymers containing Zr *iso*propoxides. However, after the sol-gel process, small nanoparticles were detected in all measured samples (Figure 21). These were most likely the result of the hydrolysis of the zirconium alkoxides and the formation of the respective oxides. The diameter of the particles was ranging from a few nanometers up to around 20 nm.

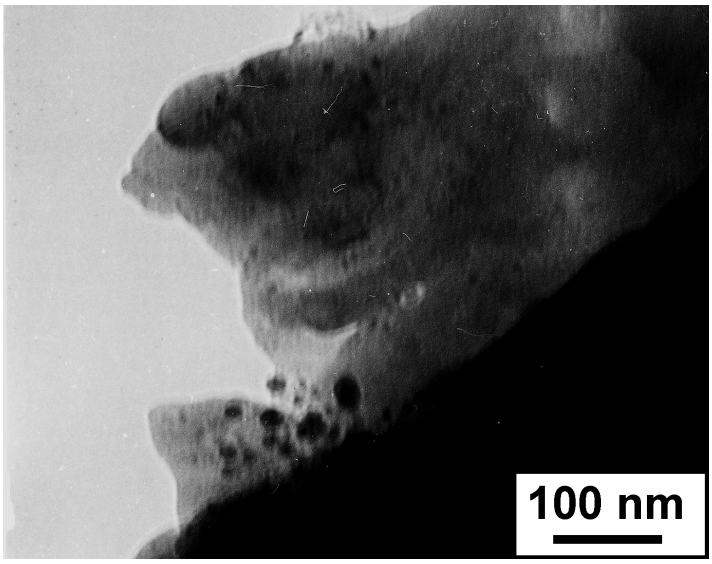

Figure 21. TEM micrographs of the ZrO_2-polyAAEMAcoMMA (1:5)

3.5.4. Small Angle X-Ray Scattering Investigations

SAXS measurements were carried out for the three systems investigated, the simple copolymers, the copolymers containing metal alkoxides (Ti and Zr *iso*propoxides) and the copolymers with metal oxides (after sol-gel).The copolymer without any metal alkoxides showed just a q^{-4} scattering from larger units within the polymer, and a broad and weak peak between q=8 and q=12 nm^{-1} (Figure 22) assigned to the polymers.

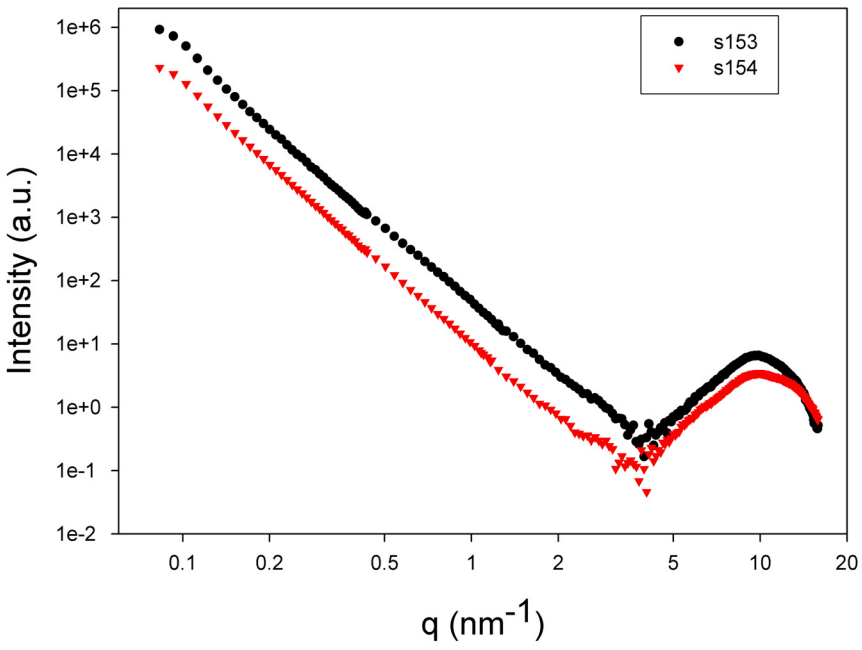

Figure 22. SAXS intensities of the HAAEMAcoMMA copolymers in 1:5 and 1:10 ratios between the two monomers. The curves are vertically shifted for better visibility.

The polymers containing Ti alkoxides (Figure 23), before carrying out the sol-gel process, exhibit a strong order (peak at q=10.1 nm^{-1}), corresponding to a repeating distance of 0.62 nm in real space. This strong order is probably due to a regular alignment of the Ti alkoxide clusters in a one-dimensional chain. The weak and broad peak at q=4.3 nm^{-1} (1.5 nm in real space) is only visible in the polymer containing a higher amount of metal alkoxides and is attributed to a short range order of the chains, i.e. a typical chain-to-chain distance.

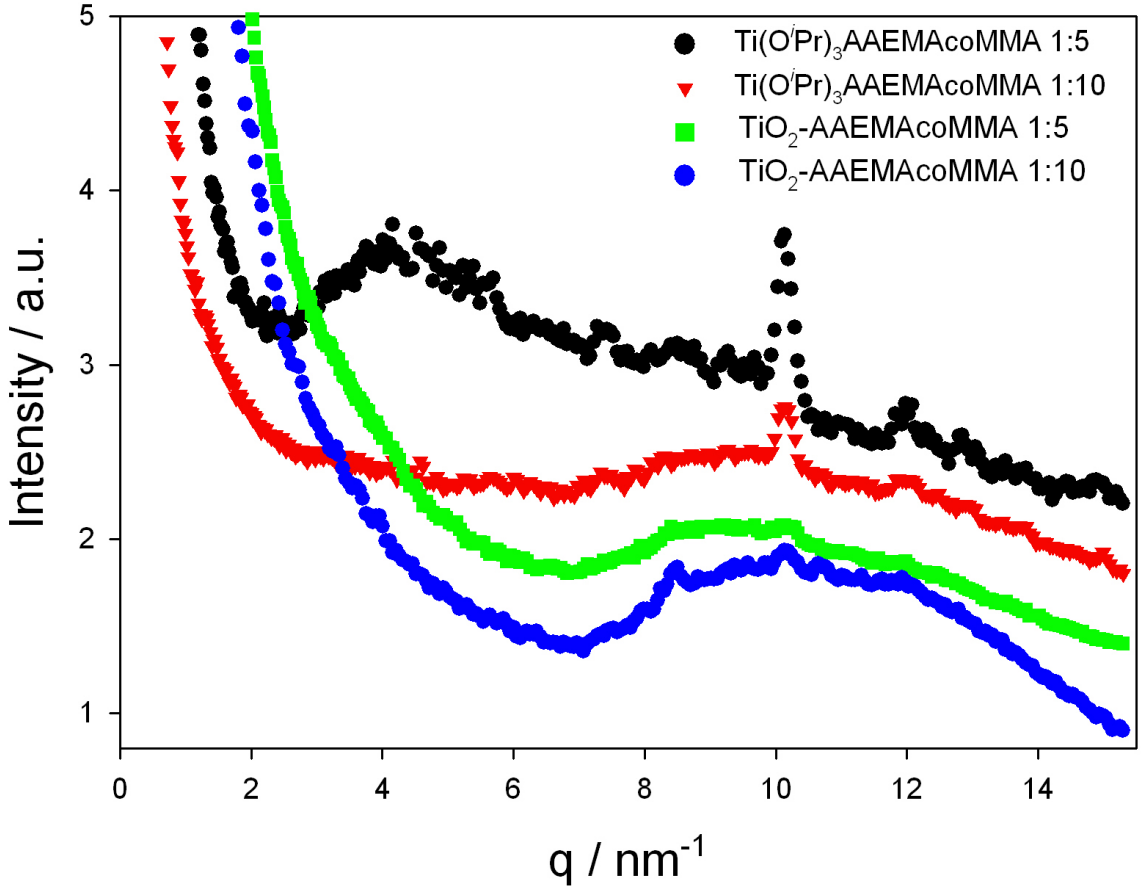

Figure 23. SAXS intensities of the copolymers containing Ti alkoxides and TiO_2 particles in 1:5 and 1:10 ratios between the two monomers. The curves are vertically shifted for better visibility.

This order is not visible any more after the sol-gel process and only a broad peak around q=10 nm^{-1} remains, which could either be due to a short range order of the particles or the original copolymer. It is suggested that this dissolution can be attributed to the hydrolysis of the well defined coordination compounds and the probable formation of metal oxides, which do not exhibit a well defined order.

The interpretation of the zirconium series (Figure 24) differs in some aspects. In the materials before gelation, there is a weak short range order in the range of 1.6 nm (peak at q=4.0 nm^{-1}), which is more pronounced for the material with a higher amount of zirconium alkoxides. This weak order is similar to the polymer with the higher amount of Ti alkoxides, but for Zr it was visible in both concentrations. This ordered was assigned to chain-to-chain distances. Similar with the results for the Ti containing material, this order is also nearly completely dissolved after the sol-gel process. Only a shoulder in the scattering intensity remains, which shows just a random distribution of particles.

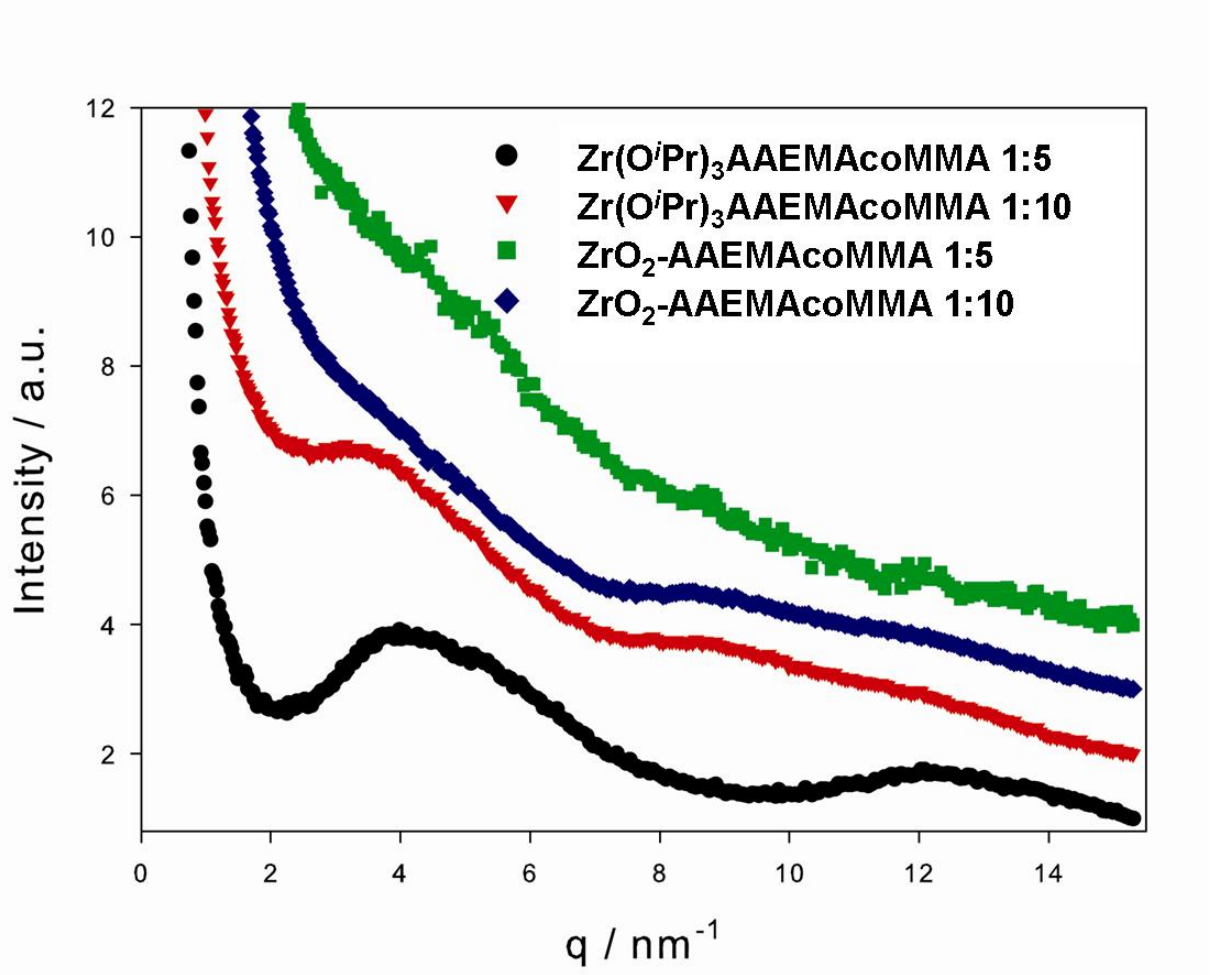

Figure 24. SAXS intensities of the copolymers containing Zr alkoxides and ZrO_2 particles in 1:5 and 1:10 ratios between the two monomers. The curves are vertically shifted for better visibility.

Contrary, the scattering intensity towards very low q-values follows, for the Zr samples with a 1:10 ratio between the alkoxides and the MMA series, a power law decrease with q^{-3} instead of q^{-4} as for all other samples, which could be a possible indication for the dissolution of the Zr particles or some extensive clustering.

The absence of distinct ordering phenomena of the Zr *iso*propoxides copolymers compared to the Ti-alkoxide copolymers before the sol-gel reaction can be also explained with the differences in the coordination behaviour of the two metals. Contrary to the preferentially six coordinated Ti, Zr as its larger homologue offers an expandable coordination sphere with potential coordination numbers between 6 and 9. This can restrict the formation of well-defined clusters with a restricted order, leading rather to multiple species (mono – and di-substituted, mono-, di-, oligo-meric). This can explain the absence of an intense ordering in the samples containing Zr *iso*propoxides.

3.5.5. General Remarks

Coordination between Ti and Zr alkoxides and β-keto esters affords well defined complexes as shown by the investigations in both solid state as well as in liquid state. Single crystal X-ray diffraction analysis shows that coordination compounds obtained from Ti- ethoxides or *iso*propoxides and EAA in 1:1 ratio appear as alkoxide-bridged dimers with chelating ethyl acetoacetate ligands, presenting a centrosymmetric structure. In these structures the metal center is six-fold coordinated. In solution the picture is different. ^{1}H NMR analysis does not allow a complete analysis of the structure due to ligand exchange reactions which do not permit clear assignments. However, 2D-NMR analyses supported a full coordination of β-keto esters in the case of Ti alkoxides. Investigation of the spacer length between coordinating part and polymerizable group shows that this parameter does not have an influence on the coordination behavior. However a careful choice of the metal alkoxide precursor has to be made because some compounds (e,g. $Zr(OBu)_4$) can mediate the transesterification reaction of β-keto esters leading to the decomposition of the desired hybrid material precursor.

ATRP can be applied to these well-defined coordination compounds resulting in hybrid homo- or copolymers. Spectroscopic methods such as NMR or FT-IR provided proof of the successful incorporation of the complexes in the polymers while SEC shows that the polymerization can be controlled. The metal atoms are evenly distributed in the polymer after polymerization as shown by electron microscopy. The thus prepared metal alkoxides containing polymers can be used further on as precursors in an aqueous sol-gel process. In such a way, the formation of nanosize particles with diameters between 3 and 20 nm inside the polymer matrix can be achieved.

3.6. Synthesis of Hybrid Materials by Post Modification of Polysiloxanes

Sometimes the *in-situ* approach towards the formation of both the inorganic and the organic components of the hybrid material is difficult for example if certain properties of one of the components are required which have to be previously designed. Furthermore, there are various classes of polymers which are prepared by other polymerization techniques than radical polymerization (e.g. polycondensation, anionic polymerization) and in which the sol-gel process can change the conditions of their preparation and hence their final properties. In this case for obtaining structured inorganic-organic hybrid materials and nanocomposites a different approach would be more preferable, namely either: i) an approach in which the polymer is synthesized in a first step with the targeted structure and properties, and after that modified with active groups for the formation of the inorganic part, or ii) an approach in which preformed inorganic particles and organic polymers are mixed together without any covalent interaction.

The first approach was used to synthesize hybrid materials based on siloxane polymers applying polysiloxanes containing functional groups that allowed further modification with precursors for the sol-gel process. A control over the morphology and the structure of the final material was carried out during the oxide matrix formation adjusting several parameters like concentration, pH, or interaction of the macromolecular precursors with the solvent.

3.6.1. Synthesis of $Si(OEt)_3$@PDMS-co-PMHS

SiO_2 modified polysiloxanes nanoparticles were obtained through the hydrosilation reaction of vinyltriethoxysilane with PDMS-co-PMHS, followed by their transformation in oxide particles via the sol-gel process (Scheme 6). The modification of the polysiloxanes was carried out in toluene by hydrosilation, using a Pt(0) catalyst. The mixture was stirred over a period of 12 hours and the solvent was removed in vacuum.

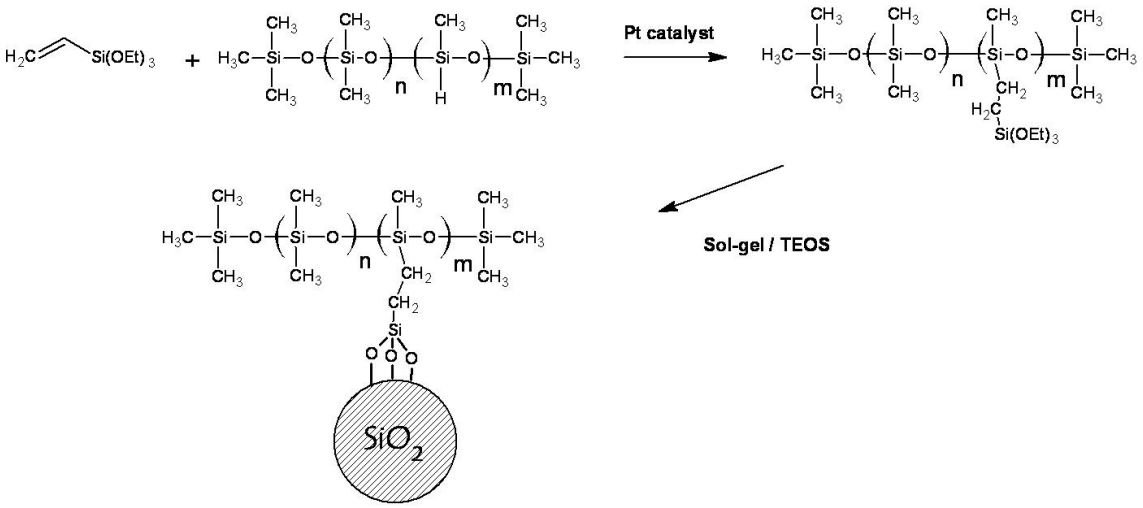

Scheme 6. The synthesis of hybrid SiO_2-polysiloxane nanoparticles through hydrosilation followed by sol-gel process

The complete conversion of the Si-H moieties was proven by NMR and FT-IR spectroscopy. ^{1}H NMR analyses showed the disappearance of the olefin proton peaks of the vinyl triethoxysilane and of the Si-H peak at 4.7 ppm (Figure 21). Furthermore the signals of the new formed Si-CH_2 bond were detected at 0.6 ppm. The presence of the ethoxy groups is evidenced by the peaks at 3.8 respectively at 1.2 ppm. ^{13}C and ^{29}Si NMR analyses confirmed these results.

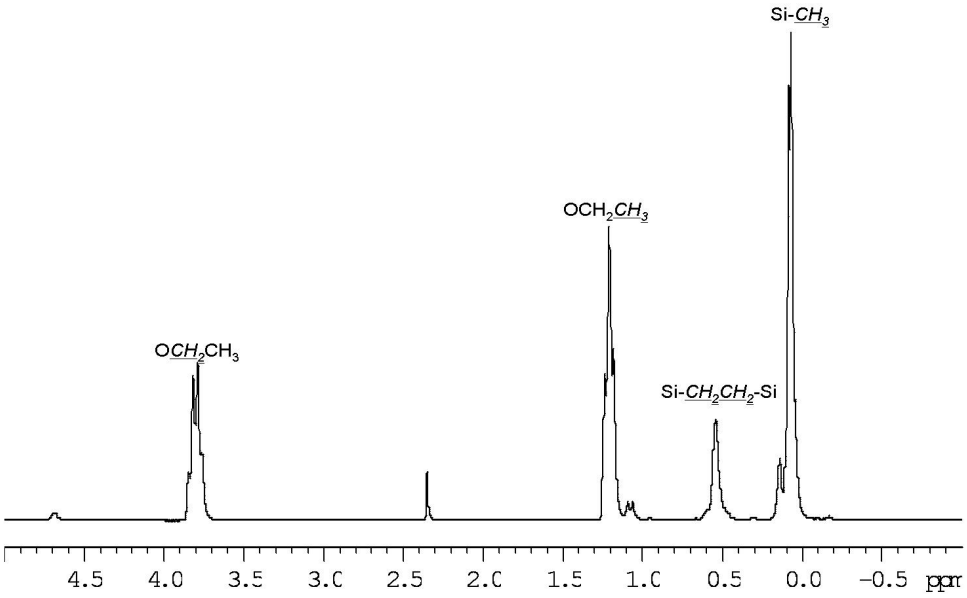

Figure 21. ^{1}H NMR spectrum of the triethoxysilane modified polysiloxanes

FT-IR analyses (Figure 22) showed the disappearance of the Si-H band at 2160 cm^{-1}. The specific bands of the polysiloxanes were still present at 1025 cm^{-1} and 1259 cm^{-1} after the reaction.

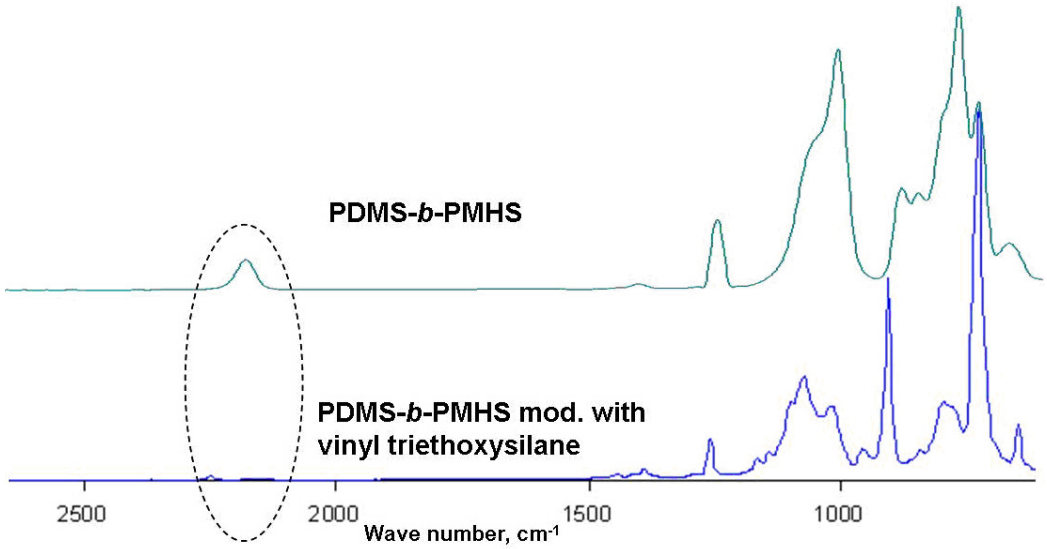

Figure22. FT-IR spectra of the unmodified and modified polysiloxanes

3.6.2. Sol-Gel Process of $Si(OEt)_3$@PDMS-co-PMHS

Sol-gel was applied to the modified polysiloxanes following a general Stöber procedure[165]. Two main ratios were used between water, NH_3 and the amount of precursor. Also copolymerization with TEOS was carried out under the same conditions.

3.6.3. Characterization

The ^{29}Si CP/MAS NMR spectrum of the hybrid nanoparticles prepared only from the polysiloxane precursor (s108_1) is presented in Figure 23. The analysis confirms the existence of both D and T units in the hybrid particles, as well as the presence of the end-groups of the polysiloxane chains. These data were supported by the FT-IR analyses which showed the presence of the polysiloxane typical frequencies. The spectroscopic data were in concordance with the literature data reported for SiO_2-PDMS hybrid gels[166].

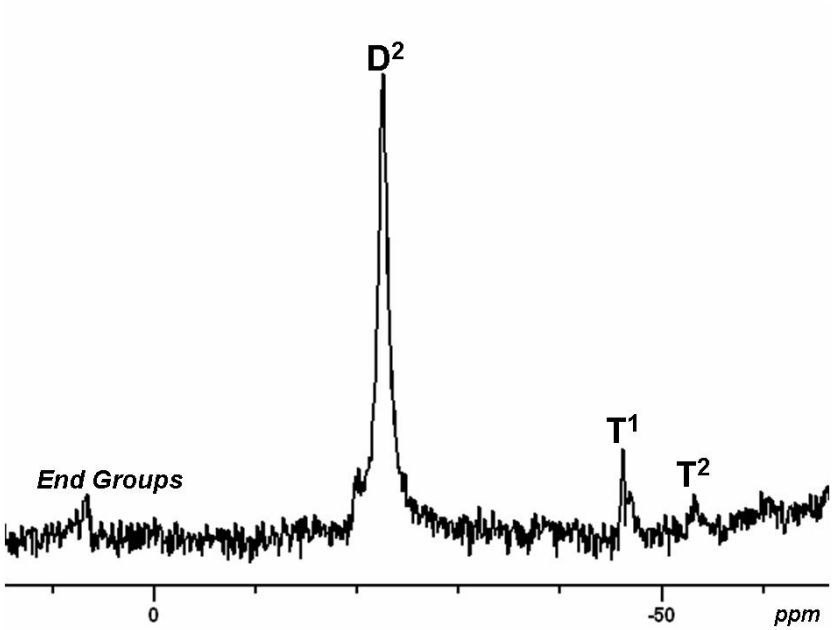

Figure 23. ^{29}Si CP/MAS NMR analysis of SiO_2@PDMS-co-PMHS hybrid nanoparticles

The size as well as the size distribution of the obtained particles was analyzed by dynamic light scattering in ethanol as solvent. The mass weighted analysis of the obtained correlation function revealed a monomodal narrow distribution for the NH_3: H_2O: precursor ratio of 5.2: 10.5: 1 (sample 1) with an average particle radius of 3.9 nm (+/- 0.2) (Figure 24). This radius decreased reaching 1.77 nm (+/- 0.31) with an increasing amount of ammonia and water in the sol-gel reaction (NH_3: H_2O: precursor = 12.43: 77.6: 1, sample 2). Two different distribution functions were obtained if TEOS was added to the reaction mixture using a ratio NH_3 : H_2O: Si-modified polysiloxane : TEOS of 5.2: 10.5: 0.5: 0.5 equivalents (sample 3). The first signal in the DLS revealed an average radius of 2.5 nm (+/- 0.12) representing 88% of the total amount of the particles applying a mass weighted analysis. The second signal shows an average radius of 8 nm (+/- 1.6) representing 12% of the total particle mass. The distribution in this case was very broad, suggesting either agglomeration or most likely homocondensation of the tetraethoxysilane producing pure SiO_2 particles. This is also supported by the fact that the second signal has approximately the same size as the one obtained in the case of production of pure Stöber particles.

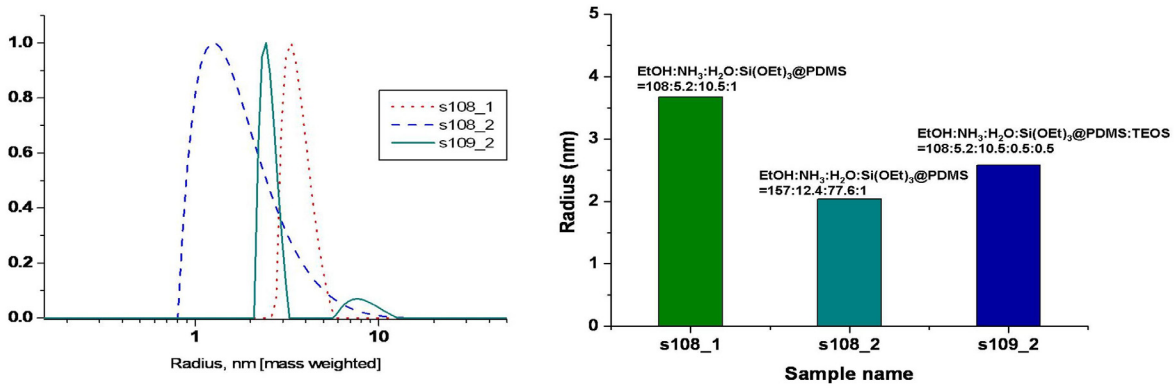

Figure 24. DLS analyses of the SiO_2@PDMS-co-PMHS hybrid nanoparticles

TEM analyses confirmed the presence of nanoparticles in the samples. In Figure 25 small nanoparticles with diameters of approximately 10 nm are present together with larger agglomerates. The later ones are most likely formed due to the drying of the sample on the TEM grid.

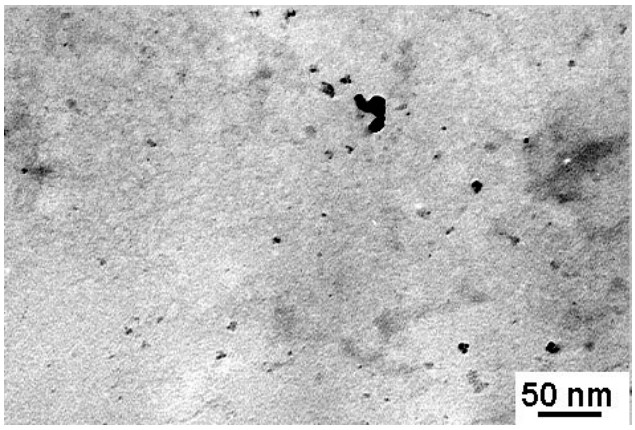

Figure 25. TEM analyses of the SiO_2@PDMS-co-PMHS hybrid nanoparticles

3.6.4. Coordination of Ti and Zr Complexes with β-Keto Esters Containing an Unsaturated Group for Hydrosilation

This pathway was also used for the synthesis of other polydimethylsiloxane-MO_2 particles. These types of materials have been recently synthesized and reported to show interesting optical and elastic properties[107-109]. Applying similar procedures as used for SiO_2-polysiloxane materials we developed a novel approach for the synthesis of well-defined nanometer sized MO_2-polysiloxanes hybrid nanoparticles (M = Ti, Zr). Also one of the main issues was to maintain a chemical bond between the polymer and the oxide matrix in the final

material. The general pathway for obtaining MO_2-modified polysiloxane hybrid materials is presented in Scheme 7.

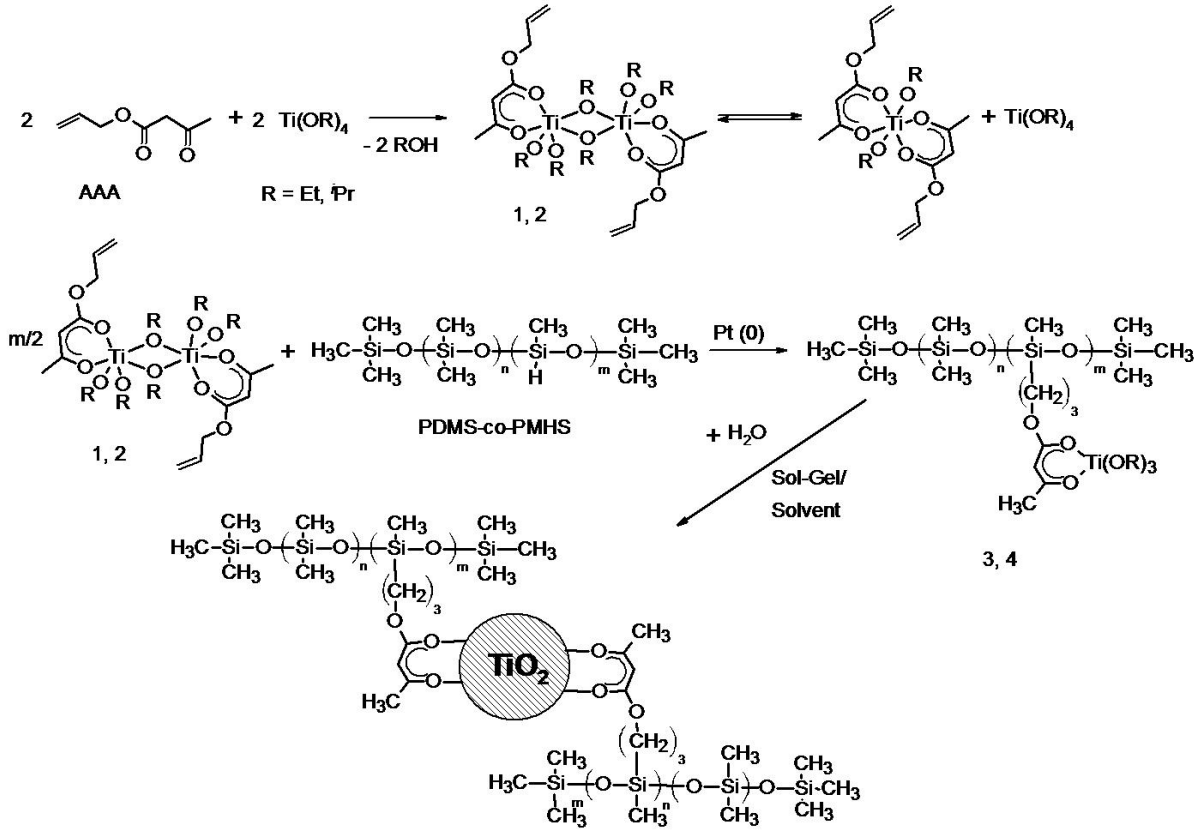

Scheme 7. General pathway for obtaining TiO_2-polysiloxanes hybrid materials (similar for ZrO_2-polysiloxanes): first coordination and then hydrosilation

The first step in the formation of these materials was the coordination of the Ti or Zr alkoxides with allyl acetoacetate and the hydrosilation reaction with PDMS-co-PMHS. The reaction products between titanium alkoxides and allyl acetoacetate were investigated by means of NMR and FT-IR spectroscopy. The ^{1}H NMR spectroscopy (Figure 26) showed the presence of the methine protons of the chelating ligand at 4.98 ppm in the case of the Ti *iso*propoxides. No signals of the uncoordinated form of the ligand were detected proving the full coordination of the allyl acetoacetate. The ^{13}C NMR shifts of the carbonyl atoms from the values of uncoordinated ligand (around 201 ppm/165.6 ppm) to the one of the chelating ligand (184 ppm/173.4 ppm) confirmed the ^{1}H NMR results. These data correlates very well with the ones reported before in literature[153].

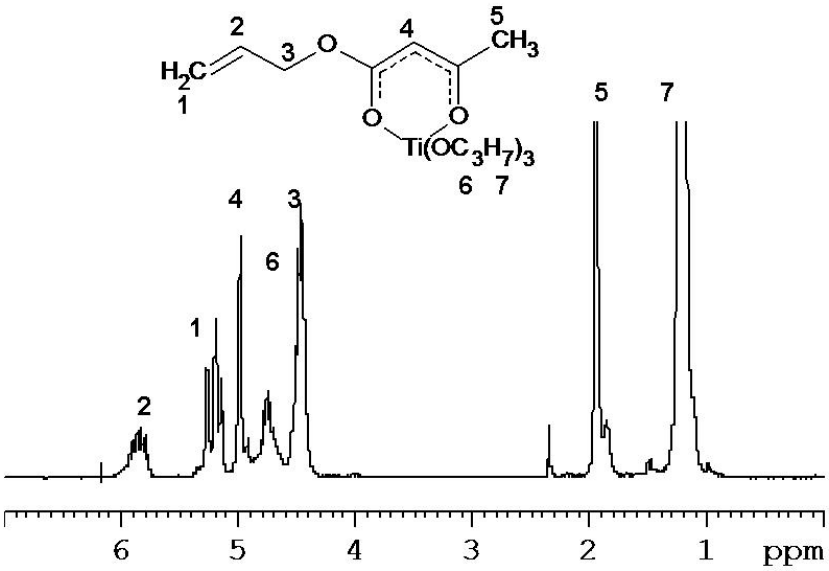

Figure 26. ^{1}H NMR spectrum of Ti(O^{i}Pr)$_3$AAA

While in the solid state the compounds are binuclear centrosymmetric dimers consisting of two Ti atoms each coordinated by one chelating AAA and two terminal alkoxo ligands (Figure 27[153]) in solution it has been reported that an equilibrium between dimeric and monomeric, monosubstituted and disubstituted species resulted from redistribution reactions[153].

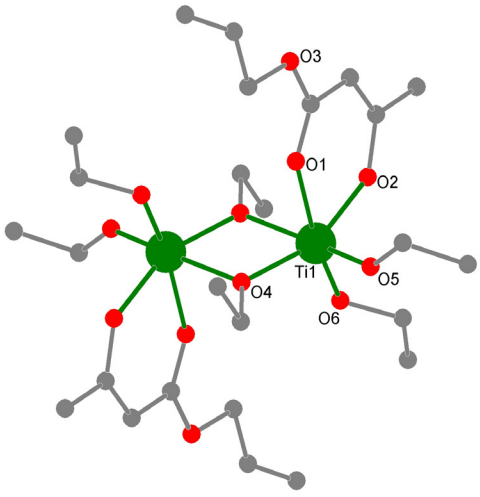

Figure 27. XRD structure of the structure of $Ti_2(\mu_2OEt)\ (OEt)_2\ (AAA)_2$[153]

Figure 28 presents the IR spectra of the synthesis of the Ti alkoxides modified with polysiloxanes. The coordination was proven by the presence of the chelating ligand absorption bands at 1633/1610 cm^{-1}(νC=C) and 1574/1524 cm^{-1} (νC=O). No bands of the free ligand were detected. Also the νTi-OR absorption bands are present between 620 cm^{-1} and 500 cm^{-1} showing that the alkoxide moieties are still available for further reactions.

3.6.5. Hydrosilation Reaction with PDMS-co-PMHS

Two pathways were used for the preparation of Ti alkoxide modified polysiloxane chains: coordination of Ti alkoxides with allyl acetoacetate and then hydrosilation with different polysiloxanes containing Si-H bonds or first hydrosilation followed by coordination of Ti alkoxides. The hydrosilation reaction of $[Ti(OR)_3AAA]_2$ with polydimethylsiloxane-co-methylhydrosiloxane (PDMS-co-PMHS) was carried out over night resulting in the complete conversion of the Si-H moieties using a Pt(0) Karstedt catalyst. The reaction progress was monitored by FT-IR and NMR spectroscopy. It was obvious from the IR spectra displayed in Figure 28 that the coordination between the titanium and the β-keto ester was maintained after the hydrosilation by the presence of the specific bands of the chelating ligand (νC=C: 1633/1610 cm^{-1}, νC=O: 1574/1524 cm^{-1}) and as well as of the appearance of the absorption bands of Ti-OR moieties (620-500 cm^{-1}).

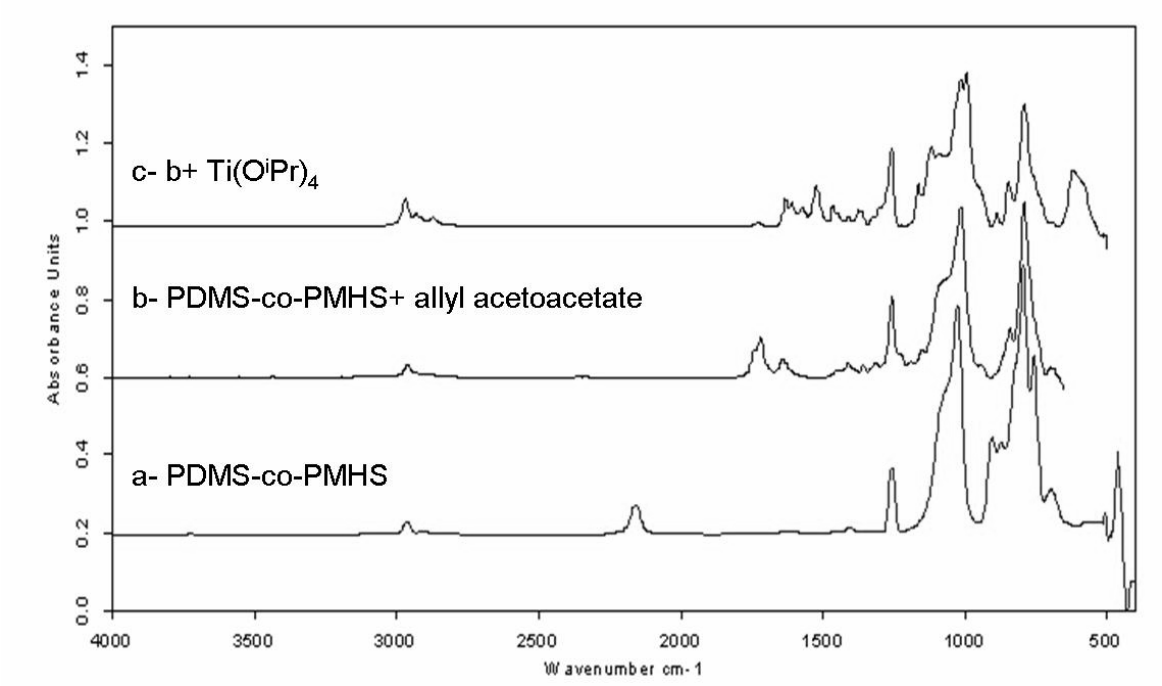

Figure 28. The FT-IR analyses for the synthesis of the Ti alkoxides modified with polysiloxanes

Additionally, the complete hydrosilation was proven by the disappearance of the Si-H band at around 2160 cm^{-1}. From the ^1H NMR the disappearance of the peak corresponding to the Si-H protons at 4.72 ppm and the disappearance of the olefin protons of the allyl acetoacetate ligand (5.86/5.19 ppm) showed the successful hydrosilation reaction. The coordination between the metal and the β-keto ester was maintained after the hydrosilation as revealed by the presence of the chelating ligand bands (νC=C: 1633/1610 cm^{-1}, νC=O: 1574/1524 cm^{-1}) in the FT-IR spectra. The second pathway (Scheme 8) gave similar results.

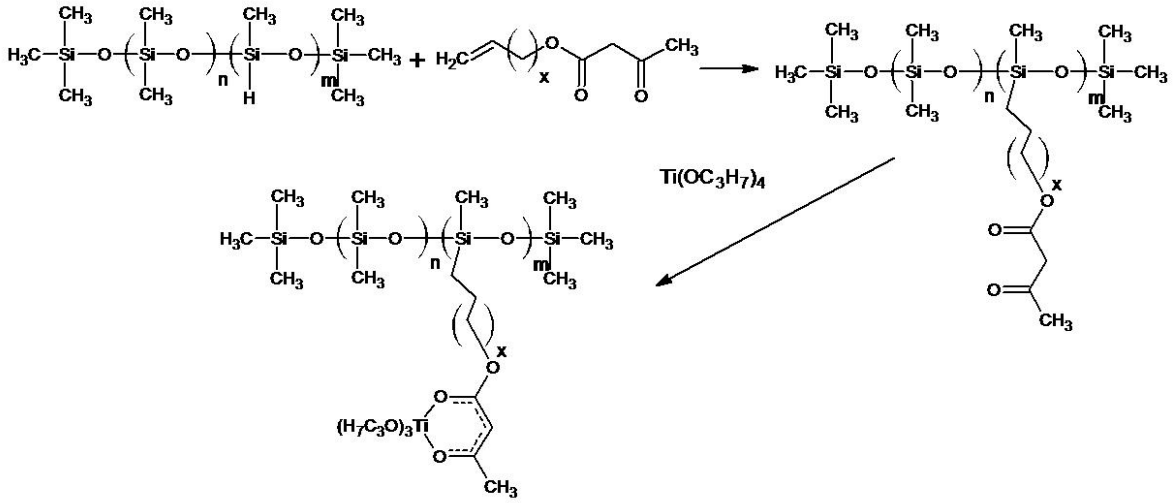

Scheme 8. The second pathway: hydrosilation followed by coordination of $Ti(O^iPr)_4$

First the hydrosilation between the AAA and the PDMS-co-PMHS was evidenced in the ^1H NMR spectrum by the disappearance of the Si-H peak at 4.7 ppm and of the olefinic signals of the AAA (Figure 29).

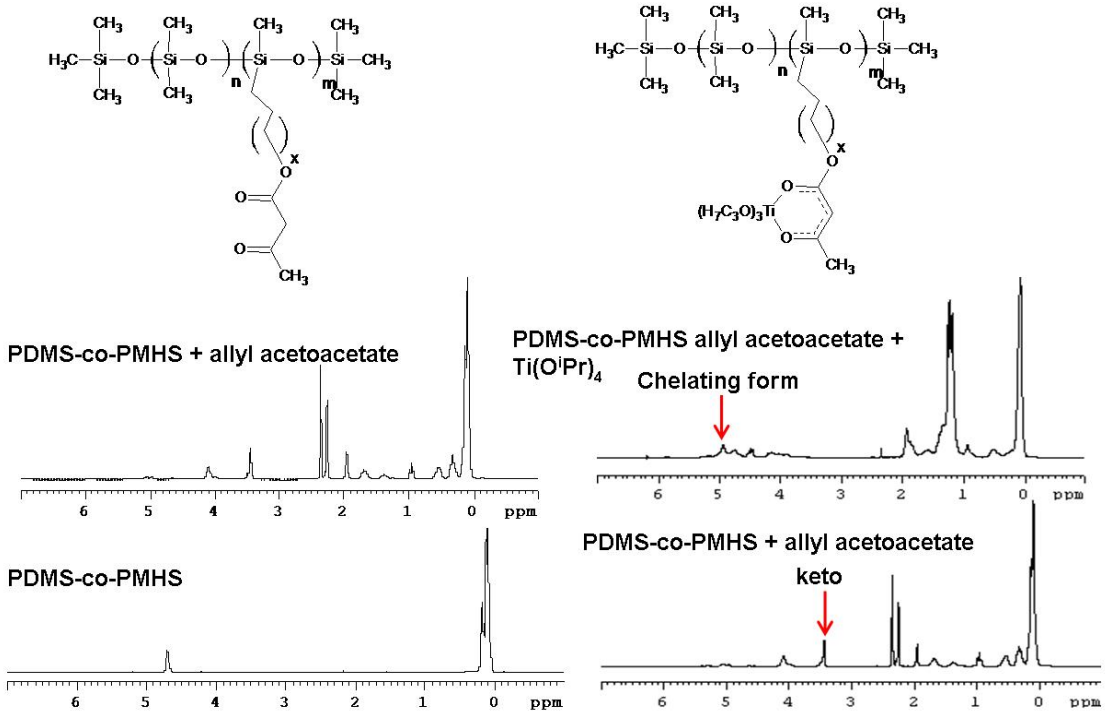

Figure 29. ^1H NMR spectra of the products obtained through the second pathway

The $^1H/^{13}C$ HMBC and $^1H/^{29}Si$ HMBC analyses (Figure 30) showed as well the complete disappearance of the signals corresponding to the allyl moieties complemented by the

appearance of two new methylene signals corresponding to the newly formed -Si-CH_2-CH_2-CH_2O chain (13.3, 22.6 ppm).

The coordination of the Ti alkoxides was evidenced in the ^1H NMR by the appearance of the chelating form of the ligand at 4.9 ppm. Furthermore the 2D NMR showed a correlation between the methane protons and the carbonyl atoms (Figure 30). No trace of uncoordinated ligand was observed. The $^1H/^{29}Si$ HMBC showed correlation between two type of protons and Si atoms.

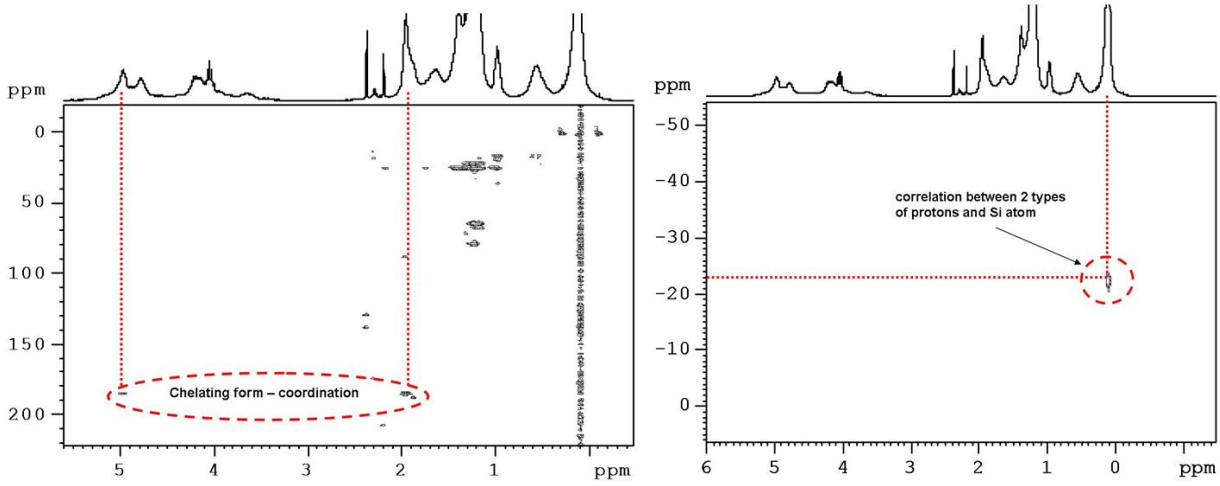

Figure 30. $^1H/^{13}C$ HMBC (left side) and $^1H/^{29}Si$ HMBC (right side) analyses of Ti(O^iPr)$_3$AAA@PDMS-co-PMHS

The FT-IR spectra also confirmed that the hydrosilation reaction between PDMS-co-PMHS and allyl acetoacetate followed by coordination of Ti alkoxides could be accomplished. However the first pathway has proven to have a better reproducibility of the results. Therefore it was chosen for further investigations.

3.6.6. Synthesis of MO_2-Polysiloxane Hybrid Core-Shell Nanoparticles

3.6.6.1. Spectroscopic Studies

Hybrid nanoparticles were obtained by applying a sol-gel process to the titanium or zirconium alkoxides modified polysiloxanes in the corresponding alcohol as solvent over night. The ratio between the metal atoms and water was varied from 1:1 to 1:3. Co-condensation with pure alkoxides was investigated as well. The particles were centrifuged and dried under vacuum and their chemical structure was investigated by NMR and FT-IR spectroscopy. FT-IR analyses clearly revealed that the characteristic bands of the chelating ligand between 1640

cm^{-1} and 1525 cm^{-1} were present, which proved that the linkage between the Ti or Zr atoms and the polysiloxanes was maintained after the hydrolysis of the modified alkoxides. The specific absorption bands of the polysiloxanes were found at 1024 cm^{-1} and 791 cm^{-1}. The ^{13}C CP/MAS and ^{29}Si RAMP CP/MAS spectra of the same sample are presented in Figure 31 and Figure 32.

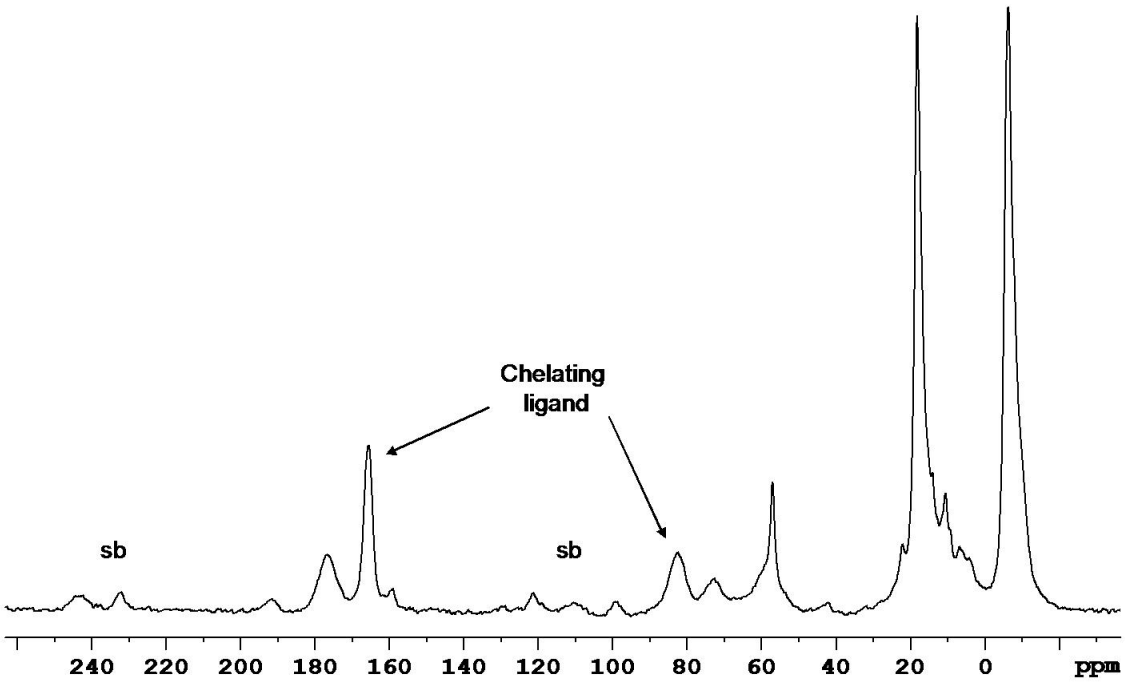

Figure 31. The ^{13}C CP MAS NMR of the TiO_2-polysiloxane nanoparticles (sb-sidebands)

The ^{13}C CP/MAS spectra for the TiO_2-polysiloxane nanoparticles showed the presence of the two carbonyl atoms of the chelating form of the allyl acetoacetate ligand at 177.2 ppm and 165.7 ppm and the presence of the methine (CH) carbons of the chelating ligand at 81.8 ppm. These values correspond well to the ones of the chelating ligand measured in liquid state proving that coordination was maintained after the sol-gel process. The presence of the polysiloxanes in the final nanoparticles was demonstrated by the peak at -6.4 ppm corresponding to the methyl carbon atoms from the main polymer chain. The connection between the polysiloxane chain and the chelating part of the ligand was proven by the presence of the methylene atoms at 14.1 ppm.

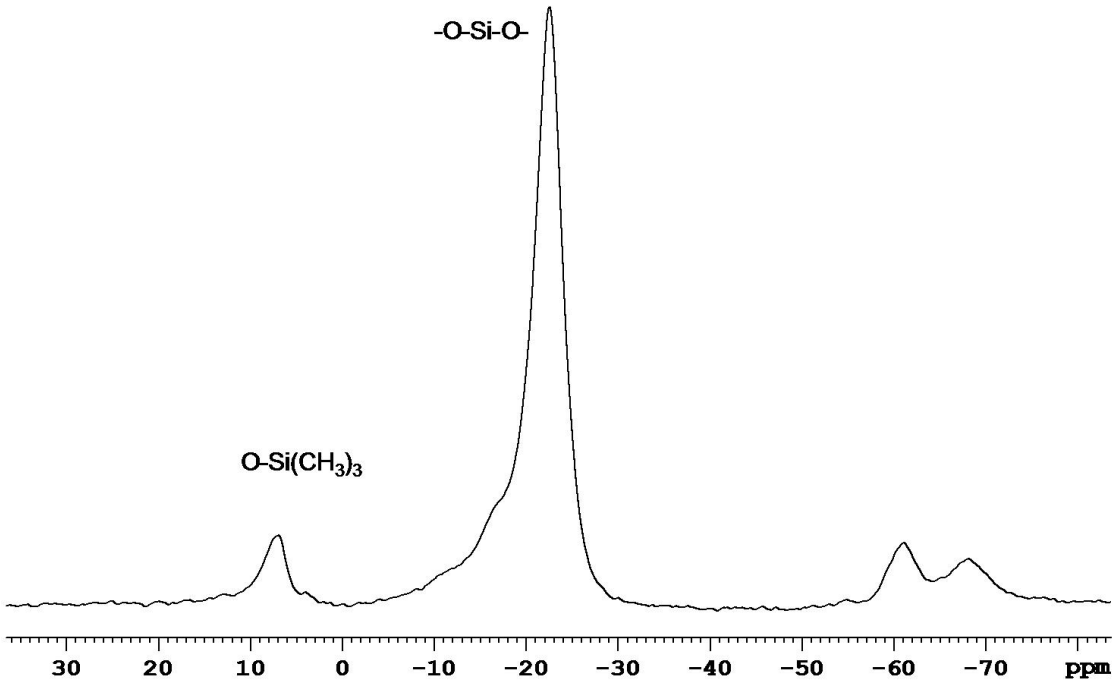

Figure 32. ^{29}Si CP MAS NMR of the Ti-polysiloxanes hybrid nanoparticles

The ^{29}Si CP/MAS spectra revealed the presence of the end-groups in the M region (6.7 ppm). The Si atoms from the main chain gave a signal in the **D** region (-22.51 ppm). The signals between -62 and -68 ppm may be due to some **T** type Si atoms which are resulting from a side-reaction of the hydrosilation process[167, 168].

3.6.6.2. Dynamic Light Scattering Studies

The DLS analyses showed that most of the samples present an unweighted bimodal distribution function with sizes between 3-15 nm (1st mode) and 70-100 nm (2nd mode) (Figure 33). The larger particle sizes can be explained by an agglomeration process. However, after the weighting of the peaks (number and mass weight) it was obvious that the majority was represented by the small sizes with the large-sized species less than 25% of the total amount. In the cases of polysiloxanes modified with Ti *iso*propoxides it was observed that the ratio between the two distributions were dependent on the concentration of the precursor (modified polysiloxanes). The quantifications were carried out by the mass weighting of the distribution functions obtained by DLS. Different measurements were carried out in a concentration range between 0.01 and 0.0275 mol/L precursor concentration. For a concentration of 0.018 mol/l modified polysiloxane in ethanol the percentage of particles with radius of 2.72 nm (the 1st distribution function) was approximately 100% while for a

precursor concentration of 0.0275 mol/l the percentage of particles with 11.3 nm radius (1st distribution function) was only 76%. For high concentrations of modified polysiloxanes (>0.04 mol/l) no nanoparticles were obtained. The increase of the particle size with the increase of the alkoxide concentration is most likely based on the probability of two centers growing together which is higher than in the cases of more diluted solutions. Hence, agglomeration occurs in very early stages of the sol-gel process.

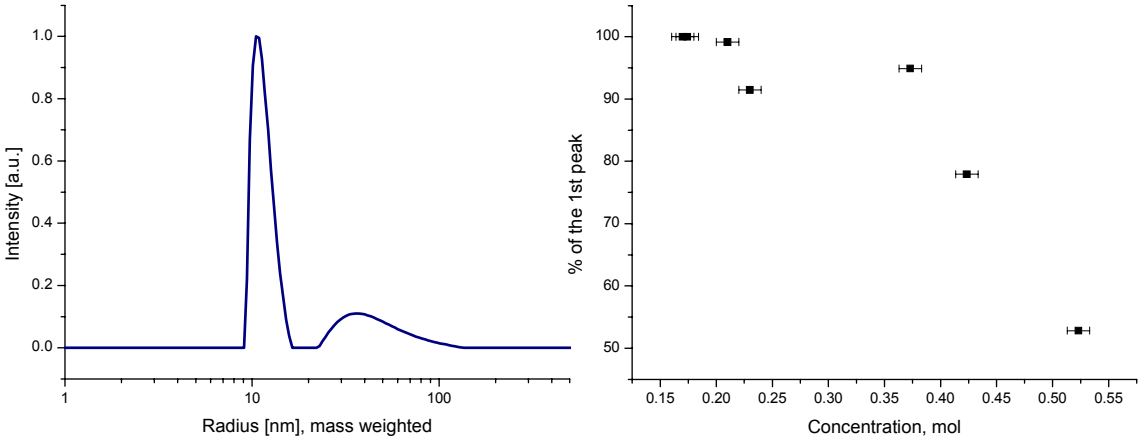

Figure 33. The DLS distribution functions unweighted and mass weighted (left) and the concentration dependence of the ratio between the two particle sizes

With the increase of the water content the nanoparticles size distribution function broadens significantly. The determination of the particle radius with DLS analysis was not possible anymore. Very likely this is due to the hydrolysis of the β-keto esters moieties which increase the reactivity of the titanium alkoxides. *Hoebbel et al.* investigated the hydrolysis behavior of the complex between allyl acetoacetate ligands and $Ti(OBu)_4$. For a ratio between H_2O and OR of 1 ($Ti:H_2O$ = 1:3) 15% of the AAA ligand was dissociated from the complex[151]. A chemical bond should be maintained between the polysiloxane and the oxide matrix. Thus, ratios higher than 3 between Ti and H_2O which were not investigated. Also by copolymerizing Ti-modified polysiloxanes with $Ti(O^iPr)_4$ in a 1:1 ratio with regard to the Ti content two types of sizes were obtained, 138.5 nm and 1.618 µm radii. Both of the distribution functions were broad. In this case, the increase in the particle size is due to the high reactivity of the Ti alkoxides in the sol-gel reaction. Smaller radii were obtained for $Ti(O^iPr)_4$ than for $Ti(OEt)_4$. This can be due to either a sterical effect of the bulky *iso*propoxy groups hindering the growth of the particles, or due to the different equilibrium between monomeric and dimeric species[153].

It is well-known that contrary to homopolymers like PDMS, block copolymers can show thermo- or lyotropic self-assembly[169, 170] and the resulting aggregates have been successfully used as templates for the preparation of mesostructured materials[171]. Mesoporous silica structures and mesostructured silica and titania films can nowadays be synthesized using commercially available block copolymers as structure-directing agents[172-174]. Furthermore, the direct linkage of block copolymers to alkoxysilane groups can result in the formation of organic-inorganic nanohybrids when gelation occurred inside the alkoxysilane aggregates[175]. The idea of using the self-assembly of diblock copolymers led to the formation of highly ordered arrays of TiO_2 nanoparticles in a block copolymer matrix[176]. In such a way the design of new morphologically controlled architectures could be realized.

It was expected that the formation of the nanoparticles is strongly influenced by the interactions of the PDMS chains with the solvent. The PDMS chains have a low solubility in ethanol[177] causing the PDMS-PHMS copolymers to form 'micelle-type' moieties. This was observed by DLS measurements of the polysiloxanes in ethanol before the modification and sol-gel process (Figure 34).

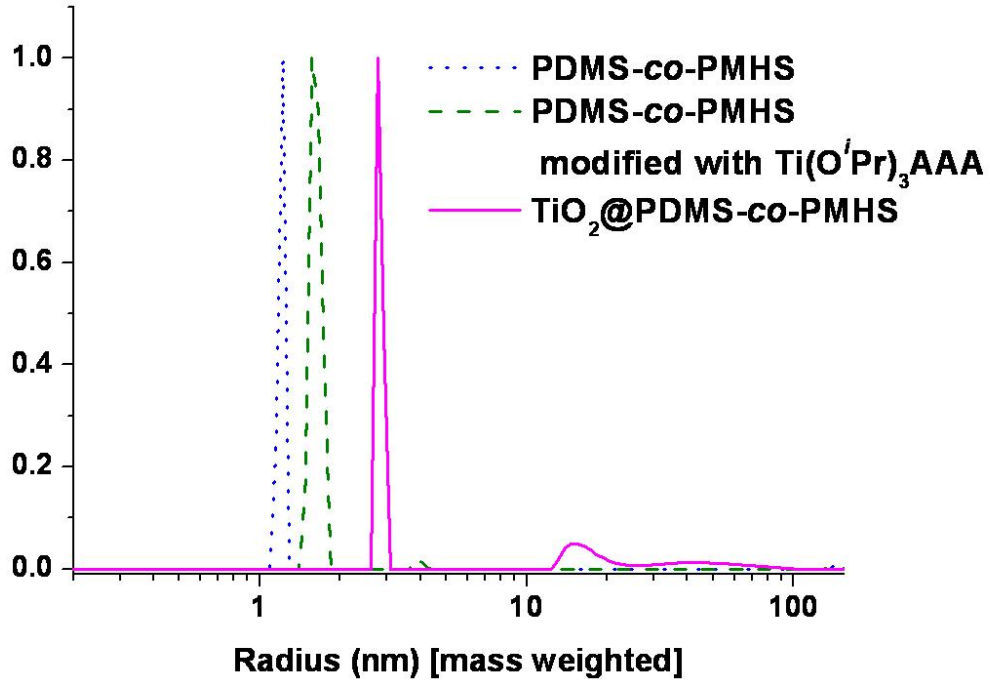

Figure 34. DLS distribution function of PDMS-co-PMHS (dot), PDMS-co-PMHS modified with $[Ti(O^iPr)_3AAA]_2$ (dashed) and TiO_2-polysiloxanes hybrid nanoparticles (line) in ethanol

It appears that when dissolved in alcohols, the PDMS chains form stable coil-like structures with a size less than 2 nm. After modification and sol-gel process this architecture is frozen by the condensation of the Ti alkoxides. The growth of the nucleation centers is hindered by the PDMS chains.

DLS results of Ti alkoxide-modified polysiloxanes in ethanol before the sol-gel process revealed colloids with diameters of 2 nm. After the sol-gel process the diameter of the particles is doubled (~ 6 nm ± 1). The dispersions are stable and no agglomeration or precipitation was observed. DLS is not able to give a hint on the morphology of the particles, because the theory assumes a spherical nature of the particles. As mentioned above the nanoparticles were stable after purification for several weeks when dispersed in solvent but they precipitate after a few days when left in the reaction mixture. This can be due to the further condensation of the not reacted alkoxides as well as to the hydrolysis of the ligands, leading to agglomeration and precipitation.

3.6.6.3.Transmission Electron Microscopy

TEM analyses confirmed the formation of the nanoparticles. Figure 35 presents a characteristic TEM picture of the hybrid nanoparticles and the size distribution calculated from the same picture by counting and measuring 50 particles.

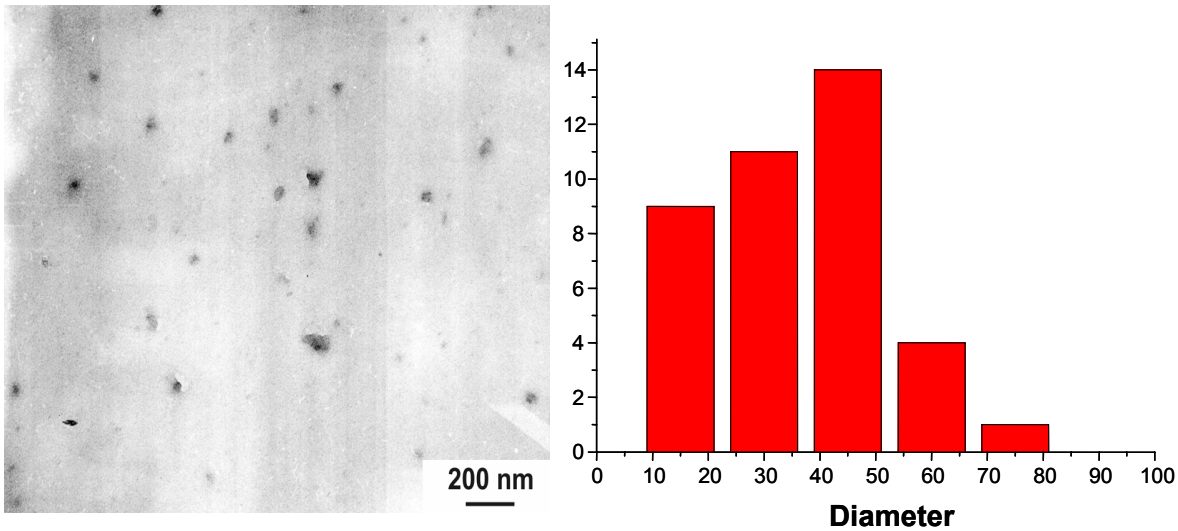

Figure 35. TEM pictures of the Ti-polysiloxanes hybrid nanoparticles and the size distribution calculated from the picture

TEM showed the presence of particles and agglomerates with diameters ranging from 10 up to 80 nm with a main distribution at around 45 nm. This confirmed the DLS measurements if it is also considered the fact that the larger structures were probably due to agglomeration after the evaporation of the solvent. What was interesting to notice was the fact that the particles appeared to have a 'core-shell'-like morphology, which was confirmed by further measurements (Figure 36).

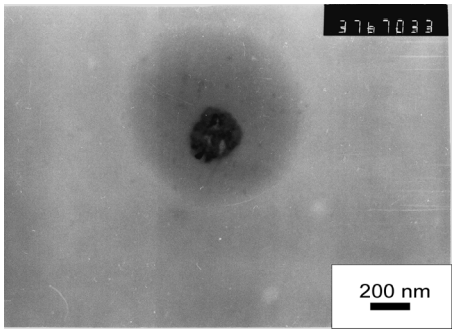

Figure 36. TEM image of the TiO_2-polysiloxane core-shell particles

The core has a higher contrast so it corresponds to a heavier element, in this case TiO_2. The shell with a lower contrast is mainly composed of the polymer. When looking closely at the core it can be seen that this is actually an agglomeration of smaller particles. This explains the larger sizes compared with those obtained from DLS. The shell is mainly composed of the polymer. Small particles with higher contrast are also dispersed in the shell. These are most likely TiO_2 particles which are not agglomerated, with diameters of only a few nanometers. This 'core-shell' morphology was observed also for other samples in which the particles had a small diameter. The same morphology was observed when SiO_2-polysiloxane nanoparticles were synthesized after the same procedures starting from vinyl triethoxysilane and the PDMS-co-PMHS. Such morphology sustains the theory that the formation of the hybrid particles is due to the stabilizing effect of the polysiloxane chains.

A similar behavior was observed in the case of $Zr(O^iPr)_4$ modified polysiloxanes (Figure 37). The polymers modified with $Zr(O^iPr)_4$ presented however a large distribution function with a mean diameter of 50 nm. This is probably due to the fact that Zr can increase its coordination sphere from 6 to 9, and so an agglomeration could occur. Also here, after the sol-gel process most of the samples present a bimodal distribution function with one narrow distribution function having a radius of about 70 nm and a very broad second distribution with radii between 200 nm and 500 nm. However the big particles represented less than 15% of the total amount after mass weighting.

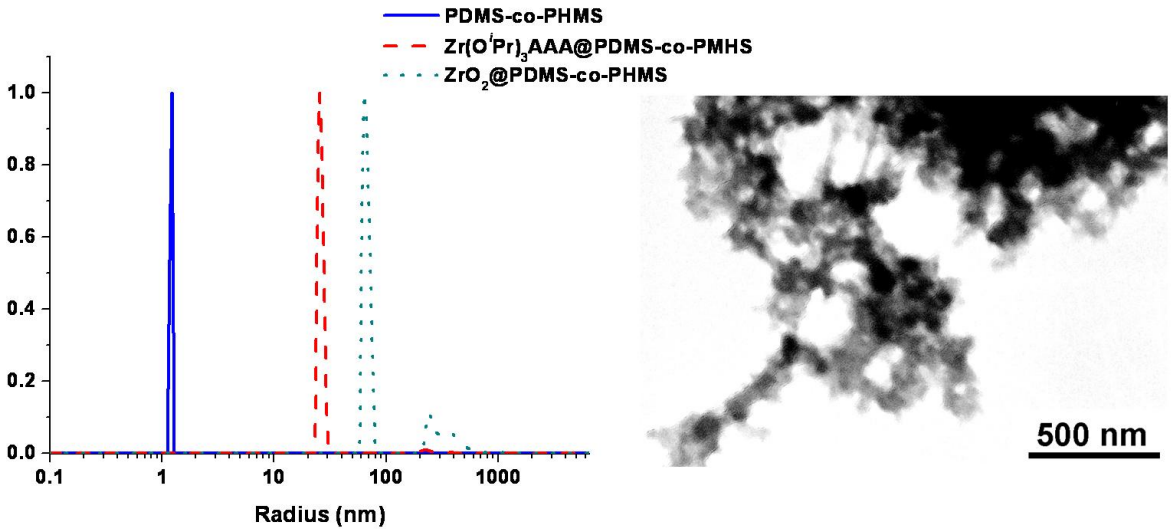

Figure 37. Left: DLS distribution function of PDMS-co-PMHS (dot), Zr(O^{i}Pr)$_3$AAA@PDMS-co-PMHS (dashed) and ZrO_2@PDMS-co-PMHS (line) in ethanol. Right: TEM image of ZrO_2@PDMS-co-PHMS hybrid nanoparticles

3.6.6.4. Scanning Electron Microscopy

SEM also showed the presence of agglomerates of small particles with diameters of about 30 nm. Further EDX measurements displayed that these nanoparticles were containing both Ti and Si elements. This fact proved the hybrid nature of the nanoparticles (Figure 38).

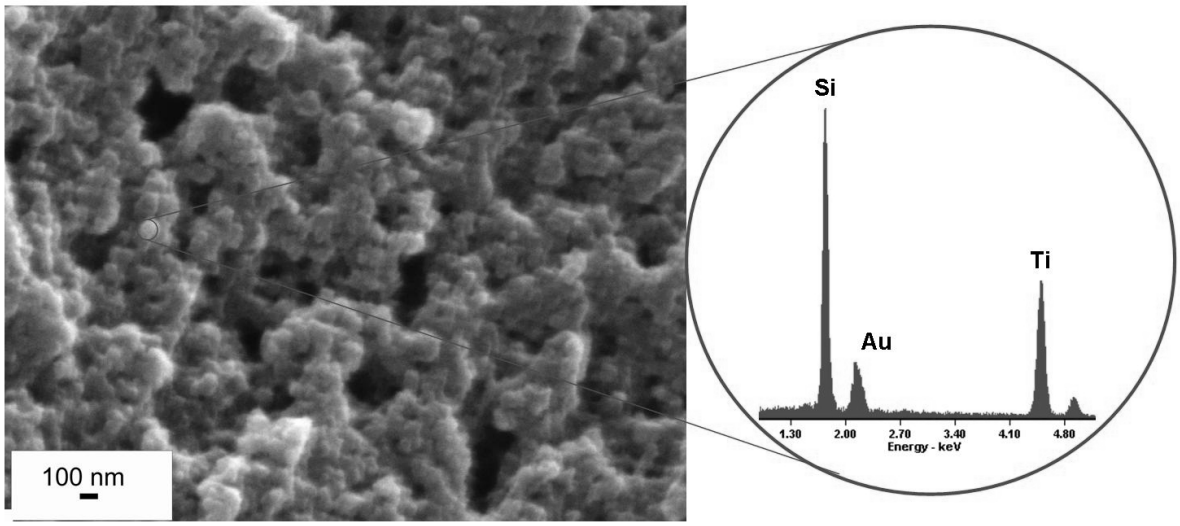

Figure 38. SEM image and EDX analyses of the TiO_2-polysiloxane hybrid nanoparticles

3.6.6.5. Atomic Force Microscopy

Atomic force microscopy was used to further characterize particles after deposition on a clean mica surface. Use of the dynamic (or tapping) mode allowed the acquisition of phase images which – containing some chemical information – nicely complements the high resolution topographical information obtained by classical contact mode. Figure 39 presents a representative AFM image containing both the topographic and the phase information. The clear phase contrast between the particle center and the edge further supports the core-shell morphology already detected by TEM. The topographic analysis shows that the core of the larger particles clearly consists of agglomerates of many small-sized particles. The line scans through the core and the shell of the particles show that while the polysiloxane shell forms a thin layer with a thickness of roughly 2 nm on the mica surface, the agglomerated core has a relatively irregular morphology with sample height ranging from 10 to 18 nm. The large height difference results from the fact that the particles are deposited and dried on a surface. This leads to a collapse of the polysiloxane shell which is expected to extend homogenously and spherically around the TiO_2 core when dispersed in a solvent.

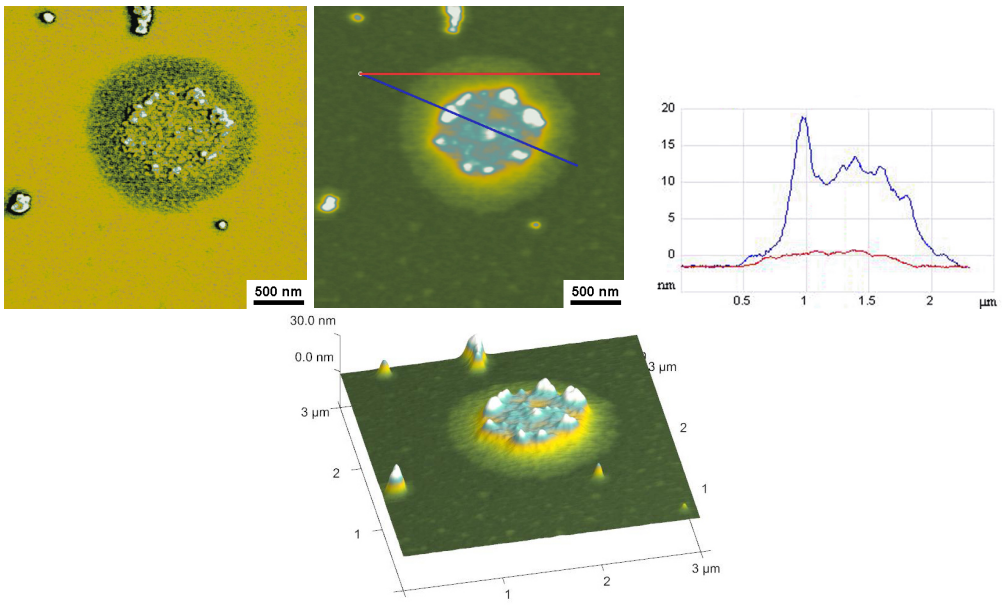

Figure 39. TiO_2-polysiloxane core shell particles; top: phase image (left); topographic image (center) with the lines indicating the sections through the image (right); bottom: 3D topographic representation of the particle.

On the other hand, the core, predominately composed of the oxide, remains virtually unaffected by the drying process. As seen in Figure 40, in addition to the large particles many smaller particles were encountered in the same sample substrate surface showing very similar

core-shell morphology. Throughout the prepared samples this shell exhibits a phase contrast to the particle core representing the chemical difference between the TiO_2 core and the polysiloxane shell.

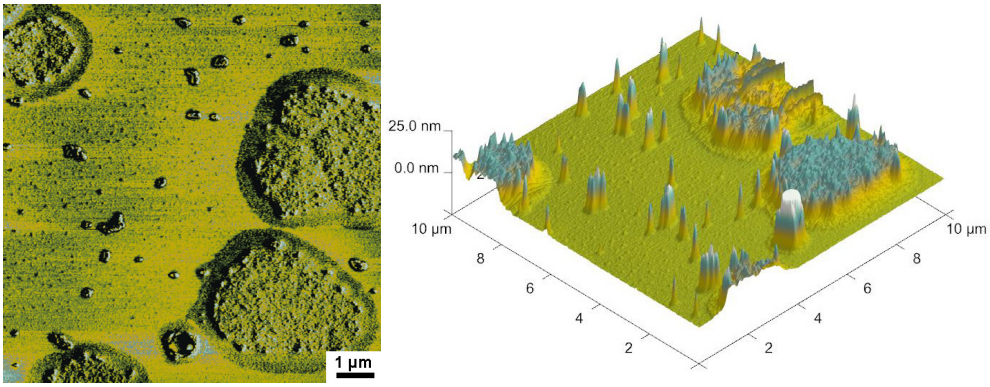

Figure 40. AFM phase image (left), and the corresponding 3D topographic image of the TiO_2-polysiloxane nanoparticles

3.6.6.6. Thermal Analyses

The thermal stability of the hybrid metal oxide – polysiloxane nanoparticles was investigated by TGA (Figure 41). Amounts of sample around 10 mg were placed inside an open Pt pan and heated up with 10°C per minute in an air flow. The conversion process of the PDMS-co-PMHS polysiloxanes into the respective inorganic moieties (SiO_2 under air) is divided into several stages from 100°C up to 500°C. These thermal effects are due to weight losses corresponding to the evolution of various silanes and siloxanes from the polymer back-bone[178-180]. At 600°C there is about 40% residual mass which is assigned to the remaining SiO_2.

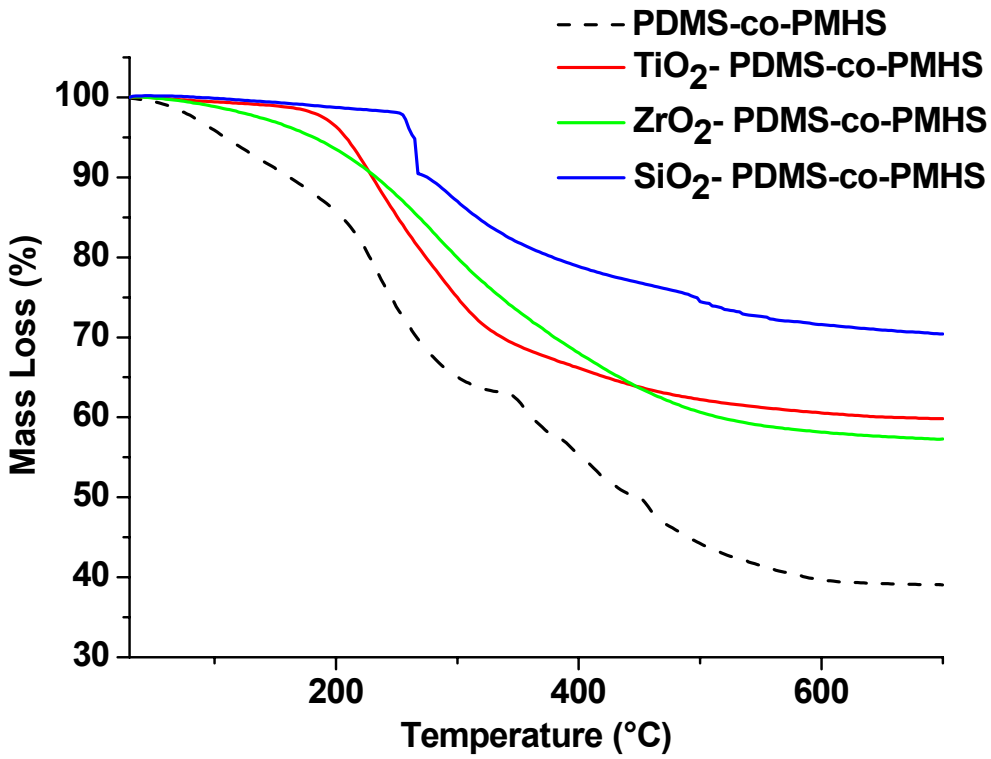

Figure 41. TGA curves of MO_2-polysiloxane nanoparticles (M = Ti, Zr, Si)

In the case of the hybrid metal oxide-polysiloxane nanoparticles the picture differs to some extend. For the TiO_2 systems it was observed the presence of only one onset decomposition temperature starting at 200°C. This can be assigned to the decomposition of the main polymer backbone. Another conclusion that can be drawn from here is that there are no reactive alkoxide moieties which would show an earlier decomposition onset. A similar behavior is observed in the case of the ZrO_2-polysiloxane hybrid particles. The only remark here is that the decomposition starts at 100°C and takes places in a large temperature range. No real onset can be determined in this case due to the fact that the slopes are flat.

An initial small weight loss (1-2 %) can be detected up to 300 °C with evolution of water which indicates a dehydration of the product, resulting probably from the condensation of the remaining hydroxyl groups[179]. The second weight loss between 300 °C and 600°C is more important (~ 25%), involving a loss of volatiles as different fragments similar to the ones reported in the literature in the cases of SiO_2-siloxane hybrids[181]. These fragments are usually assigned to cyclic siloxanes of various formula derived from different fragments.

3.6.7. Synthesis of TiO_2-Polysiloxane Bulk Gels

The hypothesis that the solubility of the PDMS chains in ethanol is the main driving force in the formation of the hybrid nanoparticles was sustained by the synthesis of Ti-polysiloxane gels. Applying the sol-gel process to the Ti alkoxides modified polysiloxanes and changing the solvent to toluene, no nanoparticles but bulk gels were obtained after one night. The water to titanium ratio was 1:1.5 as in the case of the synthesis of the nanoparticles in alcohols as solvents.

The coordination between the titanium and the acetoacetate ligand is still maintained, as confirmed by the presence of the chelating bands of the ligand at 1610 cm^{-1} (νC=C) and 1528 cm^{-1} in the FT-IR spectrum. Also the incorporation of the polysiloxanes in the final gel is sustained by the presence of specific absorption bands of the polysiloxanes at 1024 cm^{-1} and 792 cm^{-1}. The ^{29}Si CP/MAS spectra revealed the presence of the end groups in the **M** region (6.7 ppm) and the Si atoms from the main chain gave a signal in the **D** region (-22.75 ppm). Also all the characteristic signals of the chelating ligand were present in the ^{13}C CP/MAS spectra and no trace of residual alkoxides was identified. The gelation occurred over night. The wet-gels were stabile for months when kept in toluene or ethanol. Even if in the first hours of the sol-gel reaction the presence of nanoparticles was observed by DLS, the TEM analysis showed that the gels were uniform and no presence of separate domains was observed, proving that the polysiloxanes were uniformly included in the titanium oxide matrix.

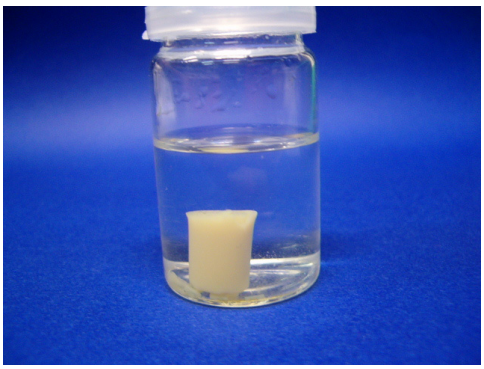

Figure 42. TiO_2-polysiloxanes hybrid gels photo

Xerogels were prepared from the TiO_2-polysiloxane hybrid gels by drying at room temperature for several days. XRD measurements showed that the gels were amorphous. The crystalline phases of TiO_2 (anatase, brookite and rutile) appear usually at higher temperatures.

To demonstrate the presence of TiO_2 in the composition of the gels a sample was calcinated at 800 °C for several hours and analyzed again with XRD (Figure 43). The XRD analysis showed the presence of both crystalline anatase and rutile phases of TiO_2. The patterns were rather broad, suggesting small sizes of the primary crystallites domains.

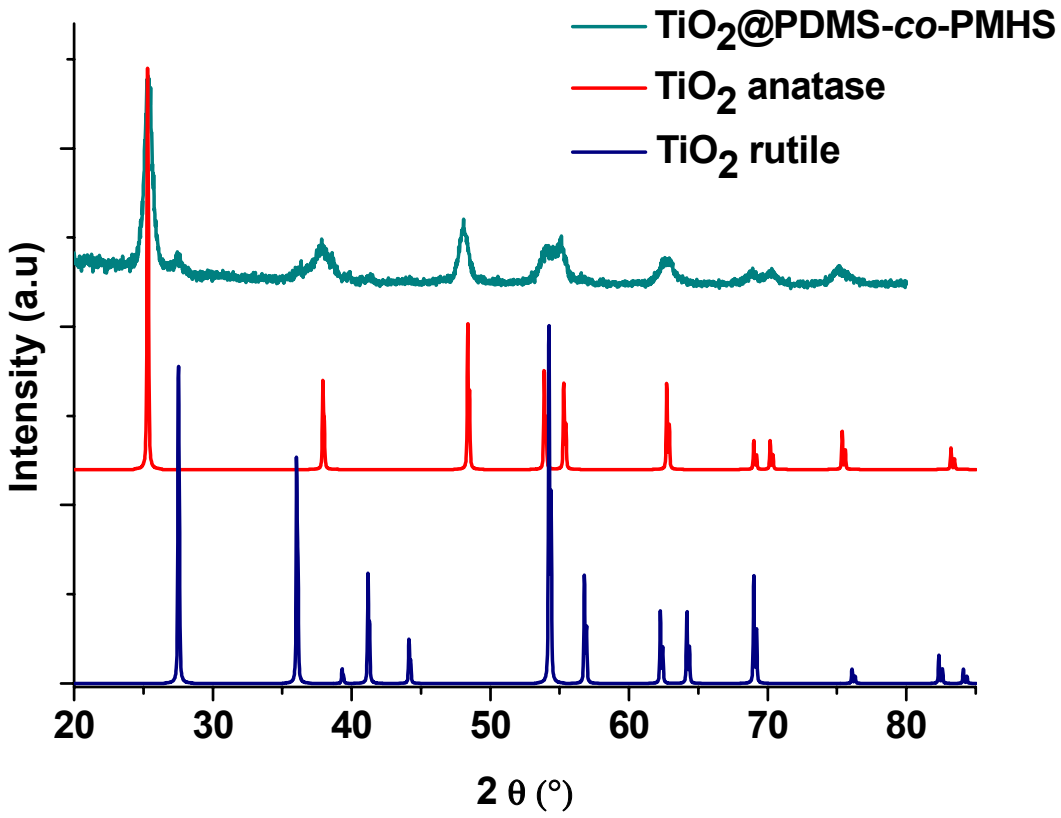

Figure 43. X-ray powder diffraction of the TiO_2-polysiloxanes hybrid xerogels

The TiO_2-polysiloxanes gels were also investigated by AFM. In contrast to the nanoparticles samples only very large particles which showed no evidence of a core shell morphology were detected. This is in accordance with the fact that in this case the particle growth is not restricted, thus leading to the formation homogenous gels.

The SEM analyses showed no presence of ordered pore structures. However, SEM images displayed round equal domains present on the surface of the hybrid xerogels. The surface between the domains showed an interesting rippled texture. EDX was conducted on the same sample in order to establish the composition of the xerogels and also to see if the observed dimples are metal oxide agglomerates or are just due to the evaporation of the

solvent. Figure 44 presents the SEM images and the EDX results. The interesting fact to find out was if the surface domains (which were perfectly symmetric to each other and showed the same diameters, with a star-like shape) are a defect of the surface or if they are formed regularly during the sol-gel process. Because the samples were sputtered with a thin gold layer for better conductivity the EDX results could not be quantified. Also the analysis of light elements (carbon, oxygen) is problematic in EDX. However the results were well reproducible so that some general statements can be given. From the analyses it can be seen that the main matrix is basically composed from Si, Ti, O and C. In the case of the 'star-shape domains' the ratio between Si and Ti was similar to the one from the matrix. The only difference was an increased concentration of carbon in the centered round 'domain' compared to the surrounding matrix. This could be due to the solvent drying or to some kind of higher agglomeration of the PDMS chains in that region. However these results show that a hybrid xerogel is formed, containing both the metal oxide and the polymer highly dispersed into each other.

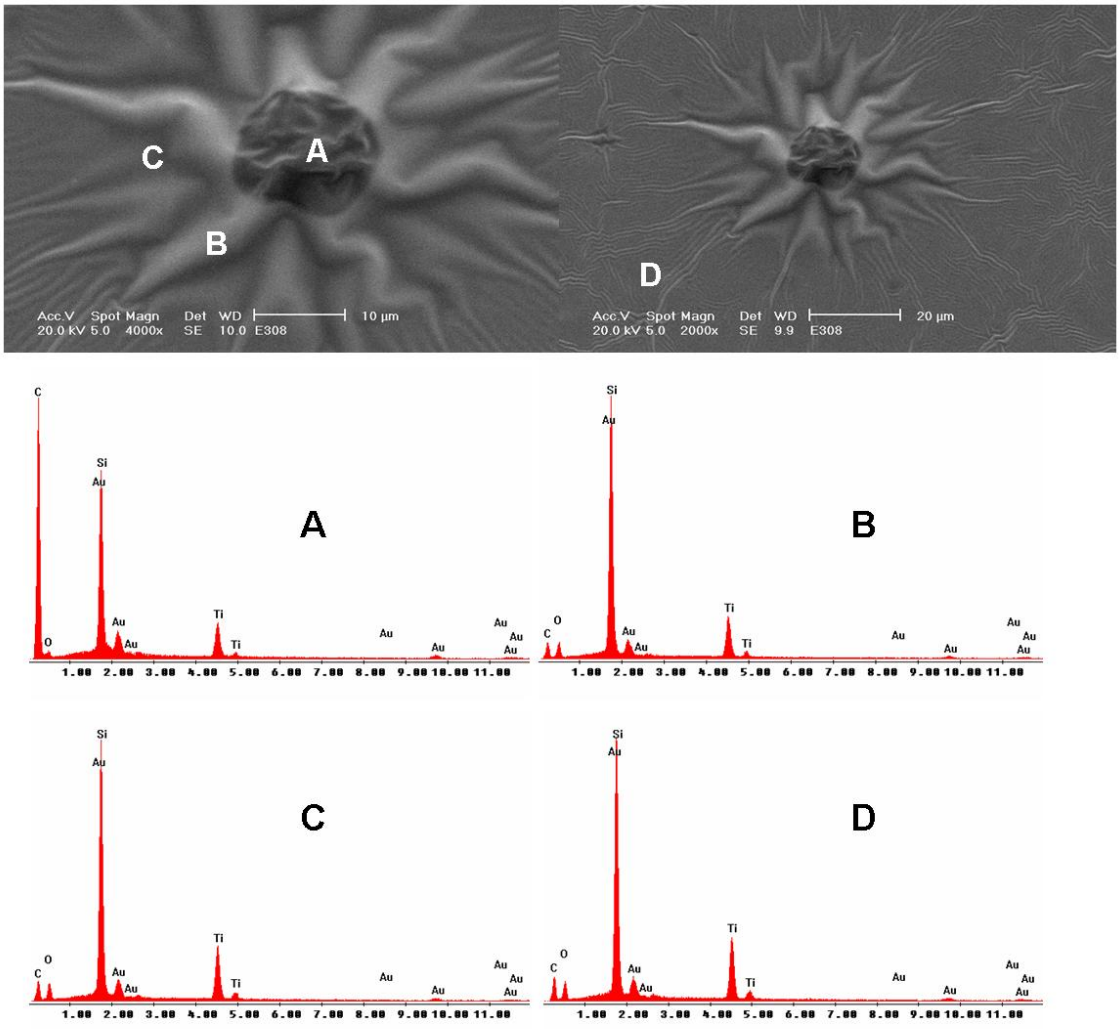

Figure 44. SEM images and EDX analyses of the TiO_2-polysiloxanes hybrid xerogels

3.7. General Remarks

A new pathway for the formation of composite materials based on different polysiloxanes and metal oxides was investigated, starting from preformed copolymers containing reactive groups and metal alkoxides modified with ligands containing coupling units. The coordination between allyl acetoacetate and different metal alkoxides affords well defined compounds which can be linked to a polymer chain via the hydrosilation reaction when Si-H bonds are available in the (co)polymer. Important to mention is the fact that spectroscopic investigations (e.g. NMR, FT-IR) showed that the coordination between the β-keto esters and the Ti alkoxides is not disturbed by the hydrosilation reaction, so this copolymer can still be used as a macromolecular precursor in the sol-gel process.

A proposed mechanism can be proposed for the two possible pathways for the synthesis of polysiloxanes modified with metal oxides, from the results obtained for the differently prepared samples (Scheme 9). As shown by DLS investigations of the unmodified block copolymers, the PDMS chains are not well soluble in alcohol forming some aggregate moieties. This architecture can be fixed by the sol-gel reaction of the Ti alkoxide-modified polysiloxanes as proven by DLS, TEM and AFM. Toluene is a good solvent for the PDMS chains and the sol-gel process is not hindered by the incompatibility between the polymer and the solvent. The nucleation centers can now evolve, forming a metal oxide network by the condensation of the metal alkoxides. From the NMR, FT-IR, and EDX investigations we could see that the polysiloxanes are indeed incorporated into the metal oxide matrix.

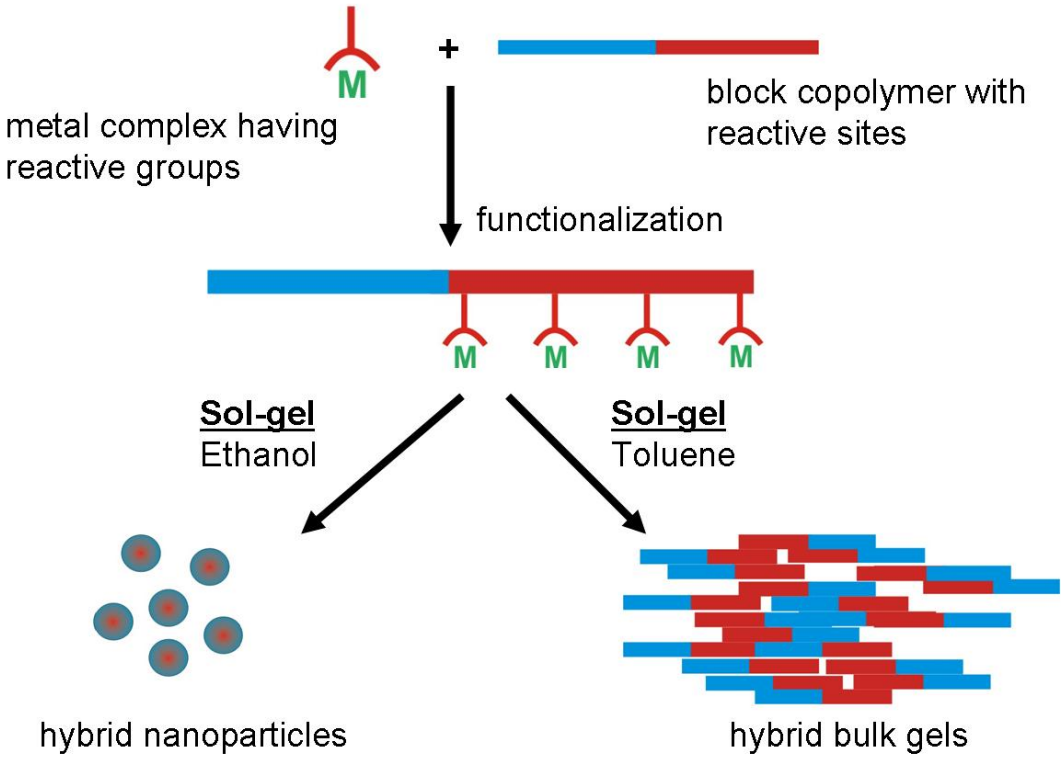

Scheme 9. The possible mechanism in the synthesis of metal oxide modified with polysiloxane nanoparticles and gels

4. Synthesis of Anisotropically Surface-Modified TiO_2 Nanoparticles

As presented in the *Introduction*, TiO_2 nanomaterials were extensively studied for their photocatalytic properties which led to many applications such as self-cleaning materials or for waste water treatment. The attachment of such catalysts to inorganic surfaces was widely investigated and is nowadays state of the art. However, if organic substrates are targeted, it has to be avoided that the particles induce as well the decomposition of the organic substrate under the exposure of light. The surface modification of the particles for protection fails because a plain titania surface is required for photocatalytic activity. An other possibility is the coverage of the organic substrate with an intermediate layer, e.g. silica[182], which protects it from photocatalytic decomposition.

An ideal system would be formed from TiO_2 nanoparticles having a bare surface, active for photocatalysis, and a second surface covered by a protective group, which could hinder the decomposition of the organic substrate. Such anisotropical surface-modified nanoparticles are called Janus particles, after the roman god with the two faces.

The goal of this research was the synthesis of TiO_2 nanoparticles active for photocatalysis and their anisotropically functionalization with organophosphorus coupling agents. The organophosphorus coupling agents bind well to oxide surfaces and they also show good stability against photocatalytic decomposition[100]. Such Janus particles could be incorporated on organic substrates. The bare TiO_2 surface would be available for photocatalysis, while the organophosphorus coupling agents should protect the organic substrate from decomposition.

4.1. Synthesis of TiO_2 Anatase Nanoparticles

4.1.1 Hydrothermal and Solvothermal Methods

The solvothermal methods are based on a simple pathway: mixtures are placed in a sealed vessel (autoclave, bomb), and the solvents are heated to temperatures well above their boiling points by the increase of the autogenous pressures in the autoclave. When a chemical reaction takes place under such conditions it is referred to as a solvothermal process or, in the case of water as solvent, hydrothermal process. The advantage of solvothermal processes is the possibility of the preparation of inorganic materials with good control over the crystallinity and morphology at reasonable temperatures, substantially below those required by traditional solid-state reactions. Unlike the cases of co-precipitation and sol-gel methods, which also allow for substantially reduced reaction temperatures, the products of solvothermal reactions are usually crystalline and do not require postannealing treatments. The synthesis of TiO_2

nanoparticles is one of the most thoroughly investigated solvothermal/hydrothermal reactions. *Oguri et al.* reported in 1988 the preparation of monodispersed anatase by hydrothermally processing[183]. Many extensions of this method have been reported[184-186].

Based on these literature-known procedures various hydrothermal methods were used in the preparation of anatase TiO_2 nanoparticles (S161_1 and S161_2). Typical 5 mL of $Ti(O^iPr)_4$ were slowly added to a mixture $EtOH/H_2O$ previously acidified with HNO_3 (pH = 0.7)[60]. The reaction mixture was stirred over night and then introduced into a teflon capped autoclave. The autoclave was heated at 200°C for 4 hours. The particles were isolated by centrifugation, dried under vacuum, and redispersed in water. In Figure 45 the DLS analysis of the particles dispersed in water (both of the analyses were prepared from the same reaction batch) is presented revealing the size distribution obtained before and after the hydrothermal treatment from the measurements.

The DLS analysis showed the presence of small particles before the hydrothermal treatment with a mean radius of about 5.5 nm ± 0.05 and a very narrow distribution. Also a small amount of particles presented higher radii (between 50-300 nm, ± 0.74) which were probably due to agglomeration during the hydrolyses-condensation reactions. After the hydrothermal treatment DLS revealed an increase in the particle size distribution. The analyses showed in this case the presence of particles having a mean radius of about 60 nm ± 0.12. This means that a growth of the particles occurs, which can be expected when using elevated temperatures. Similar as in the case of the untreated particles a small amount of particles showed higher radii (200 - 300 nm) which were probably due to, as mentioned before, agglomeration during the sol-gel or the hydrothermal process. TEM analysis showed only the presence of larger aggregates.

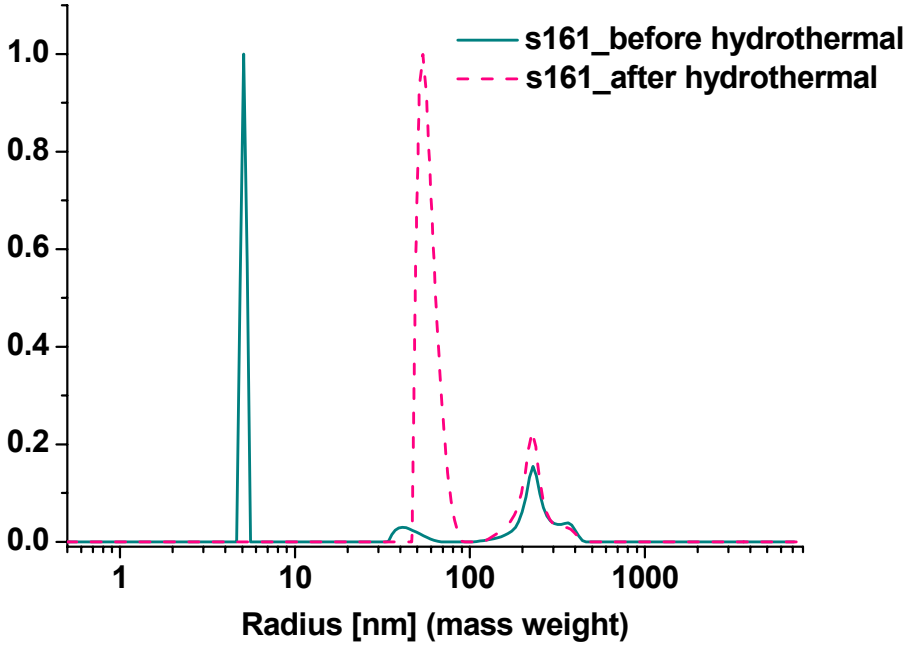

Figure 45. DLS analysis showing the distributions of the TiO_2 nanoparticles before and after the hydrothermal treatment (H_20, 25°C)

XRD analyses were carried out in order to determine the crystallinity of the particles before and after the hydrothermal process (Figure 46). As expected, the simple room temperature hydrolysis-condensation reactions afforded no crystallinity to the titania sol, as can be seen in Figure 46. After the hydrothermal process the situation changes drastically. The XRD analysis of the dried powder showed the exclusive presence of anatase with a crystallite size of about 7.4 nm. At this point it is important to differentiate between the primary crystallite size, obtained from the XRD analysis, which gives the smallest crystalline particle, and the size obtained from the DLS analysis, which gives the size of the smallest redispersible particle. One such nanoparticles can contain one or more crystallites. Obviously, in this case, the particles (120 nm diameter) contained more crystallites (XRD ~ 7.4 nm diameter). Also some impurities could be observed which were in low percentage.

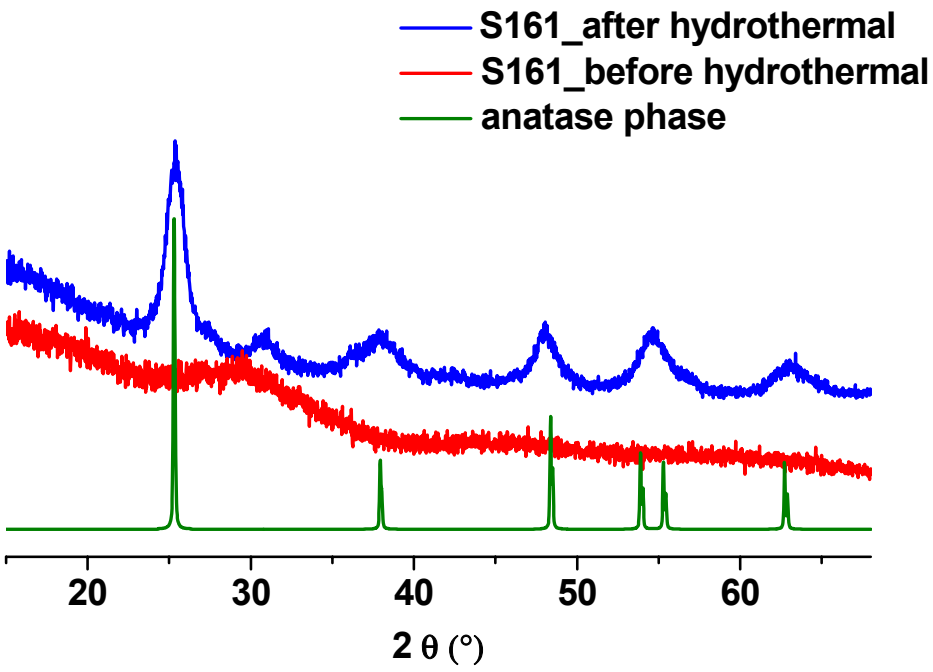

Figure 46. XRD analysis showing the pattern of the TiO_2 nanoparticles before and after the hydrothermal treatment

However, this method did not allow a well controlled tailoring of the particle size as observed from the light scattering investigations. Further variations in precursor concentration, pH and reaction temperature led to similar results. A large amount of the particles were agglomerates. Another disadvantage of this method was the poor dispersibility of the dried nanoparticles. One of the main requirements for the further use of such particles in the preparation of Pickering emulsions is their good dispersibility in solvents such as water or organic solvents (hexane, cyclohexane, toluene, etc).

Solvothermal Methods

Based on a reported literature procedure a different method was used for the synthesis of size controlled TiO_2 nanoparticles. Various amounts of $Ti(O^iPr)_4$ were mixed with toluene as the organic solvent under argon atmosphere. Different weight ratios between the alkoxide and toluene were used (between 10:100 and 30:100). The mixture was stirred for 3 h and transferred into a stainless steel teflon capped autoclave and subsequently heated at 200°C for 3 h. During thermal treatment, $Ti(O^iPr)_4$ is decomposed by the thermal energy of the solvent

and finally crystallization of the TiO_2 occurs.[187-189] After cooling gradually to room temperature, the precipitates were separated by centrifugation and dried. The DLS analysis showing the size distribution of the TiO_2 particles dispersed in toluene is presented in Figure 47.

DLS analysis showed the presence of small particles after the solvothermal treatment with a mean diameter of about 9 nm ± 0.07, having a very narrow distribution (25%, after mass weighting) and of agglomerates of particles (between 20- 200 nm diameter) with a very broad distribution (75%, after mass weighting). This analysis revealed that the synthesized particles have a relatively broad size distribution. Literature reports suggest that as the concentration of the $Ti(O^iPr)_4$ in the solution increases, the particle size of TiO_2 should as well increase.[187, 188] In our cases the size distribution was not dependent on the $Ti(O^iPr)_4$ concentration and agglomeration after the solvothermal process could not be avoided.

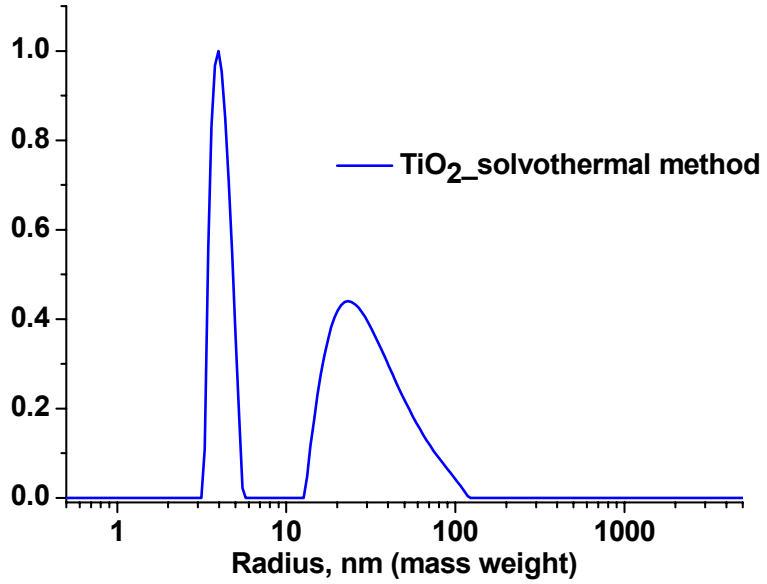

Figure 47. DLS distribution of the TiO_2 nanoparticles synthesized by the solvothermal method (25°C, toluene)

4.1.2. Sol-Gel Methods

Disadvantages of the solvo/hydrothermal methods are that they usually require extra-time, heating (energy) and that the amounts produced by this method depend on the technological equipment which is available (e.g. autoclave). For this reason the goal was to find an easier, cheaper and quantitative method, which can produce TiO_2 anatase nanoparticles.

After literature search and preliminary experiments a simple synthesis was developed based on the method reported by *W. Choi et al.*[190] In this procedure 1.25 mL of $Ti(O^iPr)_4$ were dissolved in 25 mL of dry ethanol and then added dropwise under vigorous stirring to 250 mL of distilled water (4 °C) adjusted to pH 1.5 with nitric acid. The resulting transparent colloidal suspension (containing 1.34 g particles /L) was stirred overnight. The solution was evaporated (40°C) using a rotavapor and dried under vacuum to obtain a crystalline powder sample. The dried sample contained still some HNO_3 as seen from the FT-IR analysis, confirming earlier reports that suggested that the powders still contain about 30 weight % HNO_3[190]. The method does not require any harsh conditions. The biggest advantage of this method was the fact that the particles were very good redispersible in water, leading to a clear solution with a pH ~ 2. The good redispersibility can be explained by the fact that the pH of the sol is far from the point of zero charge (pH = 5.9 for TiO_2), so the electrostatic repulsive forces due to charged surface sites lead to a good redispersion of the particles. DLS showed the presence of nanoparticles having a mean radius of 3 nm ± 0.18 in 100% proportion (after mass weighting) (Figure 48). As mentioned earlier, after drying the particles could be easily redispersed in water. The DLS measurement showed again the presence of s particles with a mean hydrodynamic radius of 3 nm ± 0.15 (95% after mass weighted). The presence of particles having larger sizes (between 100 and 1000 nm) was also observed. This is most likely due to some content of agglomeration which occurs after drying or to impurities.

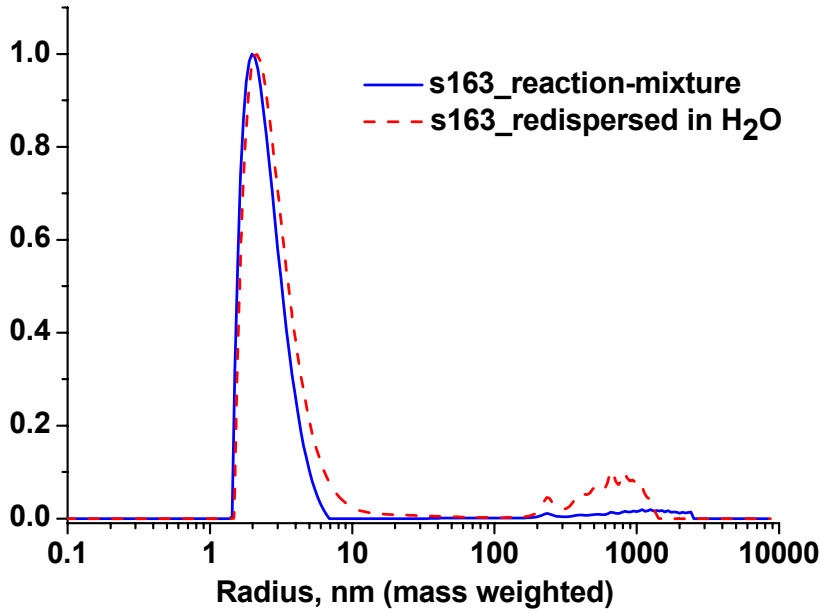

Figure 48. DLS analysis of the size distribution obtained for the sol-gel TiO_2 nanoparticles in the mother sol (S163) and after their drying and redispersion (H_2O, 25°C)

XRD analyses were carried out in order to determine the crystallinity of the resulting sol before and after the water evaporation of the mother sol at 40°C using the rotavapor. The analysis of the simple sol-gel room temperature process showed no presence of crystalline phases, suggesting that the sample is quantitatively amorphous. For this reason the water was slowly evaporated under reduced pressure, concomitant with heating it to 40°C. The XRD patterns of the sample dried in this manner (Figure 49) showed that the particles were composed of 100% anatase phase, with a crystallite size of 3.4 nm. No further impurities were observed.

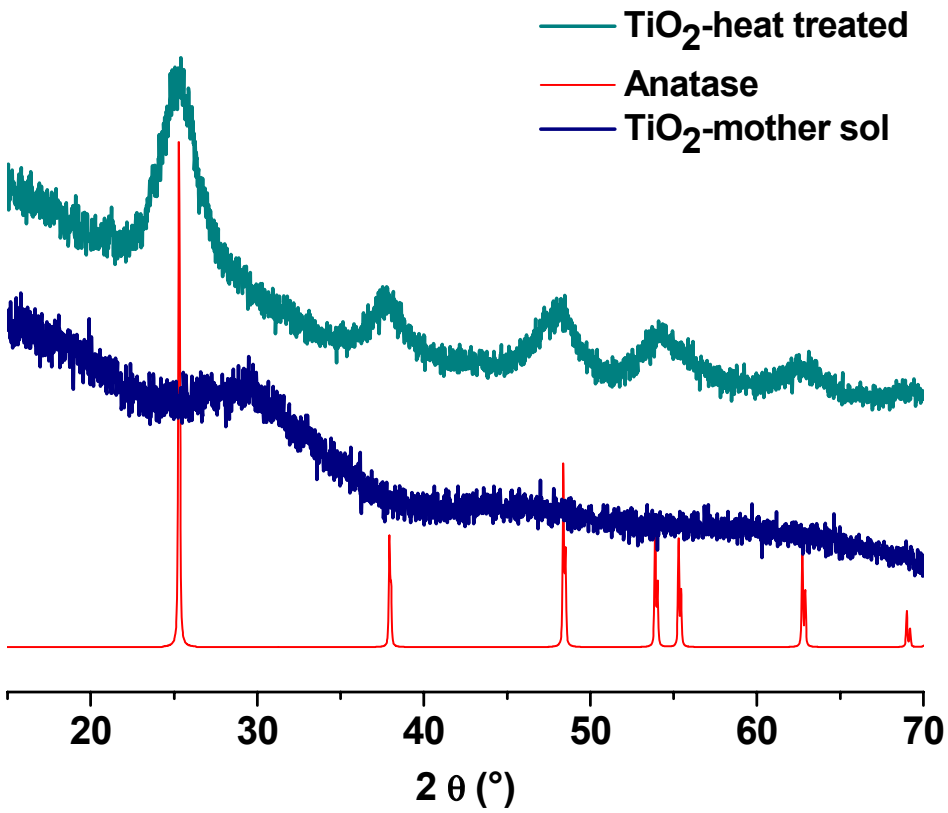

Figure 49. XRD pattern of the sol-gel TiO_2 nanoparticles after the evaporation of the H_2O and heat treatment using a rotavapor at 40°C (S163)

Transmission electron microscopy (TEM) confirmed both the presence of small nanoparticles, and the fact that the nanoparticles were crystalline. In Figure 50 some characteristic TEM micrographs (bright field, dark field) as well as a typical diffraction pattern are presented. The sample measured in TEM was prepared after the drying of the particles and redispersion in ethanol. The TEM micrographs revealed that the particles have

diameters with a mean of about 7 nm, with a very narrow size distribution. This result fits perfectly with the one obtained from the light scattering analysis. Furthermore, from the dark filed image (Figure 50, B) it can be noticed that all of the particles are crystalline. This is also proven by the electron diffraction patterns (Figure 50, D). The presence of the continuous rings is a hint that the sample shows some nanocrystallinity, with small crystallites sizes.

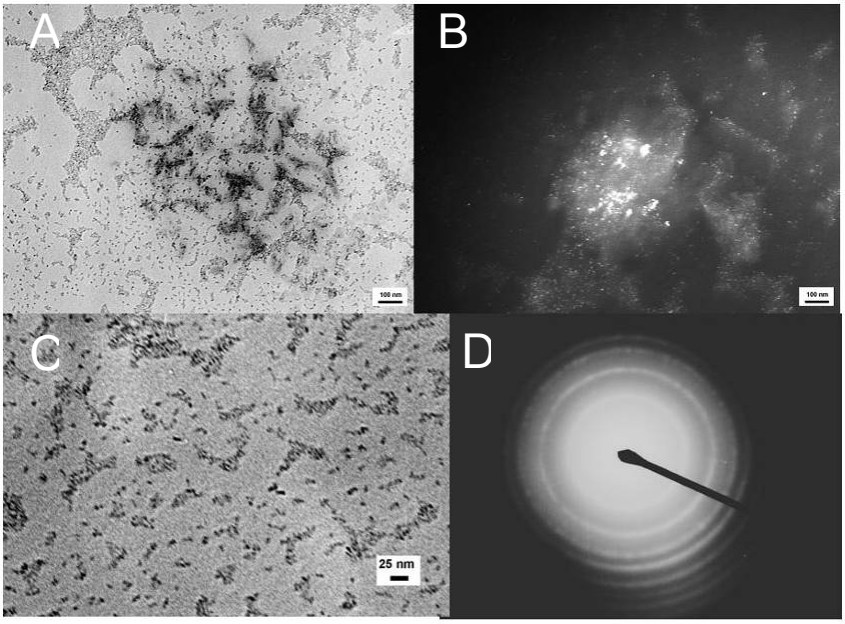

Figure 50. A) Characteristic TEM bright field micrograph of the TiO_2 nanoparticles; B) characteristic TEM dark field micrograph of the TiO_2 nanoparticles; C) higher resolution TEM bright field micrograph of the TiO_2 nanoparticles; D) Characteristic electron diffraction pattern of the TiO_2 nanoparticles

a. Variation of the Precursor Concentration

The next step in the synthesis of the nanoparticles was the investigation of the reaction parameters on the size and morphology of the obtained TiO_2 materials. Based on the reported procedure for synthesizing well-defined redispersible nanoparticles the variation of some of the reaction parameters was tried, like the amount of precursor or the reaction time to study if we can control the particle size.

In a first step the amount of precursor used was increased to detect if it could be obtained larger particles. The concentration of the $Ti(O^iPr)_4$ was increased in the fllowing order: 1.25 mL (0.17 mol/L), 2.5 mL (0.34 mol/L), 3.75 mL (0.51 mol/L) of $Ti(O^iPr)_4$ were dissolved in 25 mL of dry ethanol and then added to 250 mL of distilled water (pH = 1.5).

The obtained sol was stirred over night and the water was evaporated at 40°C under reduced pressure to assure the formation of anatase phase.

DLS analysis of the particles obtained from the three specific precursor concentrations are presented in Figure 51. The DLS measurements show the presence of nanoparticles having a mean diameter of 5 nm ± 0.18 (0.17 mol/L), 8 nm ± 0.20 (0.34 mol/L), and respectively 12 nm ± 0.18 (0.51 mol/L) in 100% proportion (after mass weighting). This shows that by increasing the precursor concentration the mean radius slightly increases, still having narrow distributions. This fact is not unexpected. Considering that all of the other parameters (temperature, pH, time) of the sol-gel process were kept constant, the growing of the particles was only due to the higher amount of precursor species present in the reaction mixture.

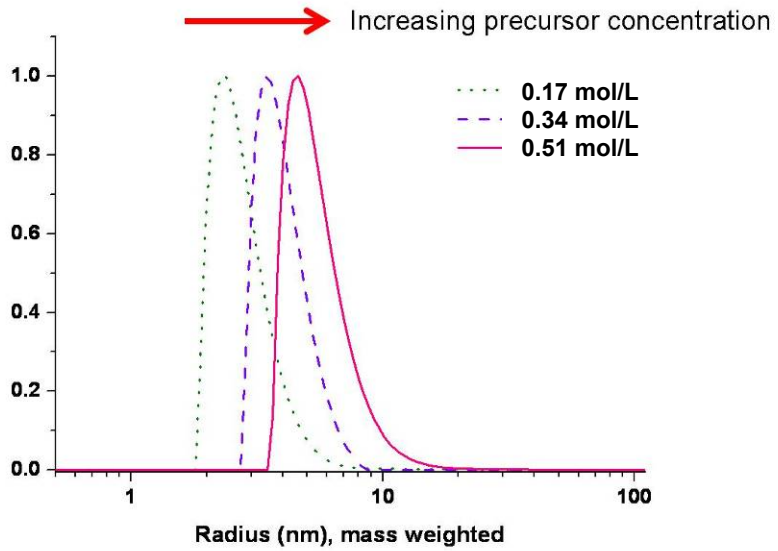

Figure 51. Dependence of the TiO_2 nanoparticle sizes on the $Ti(O^iPr)_4$ concentration (H_2O, 25°C)

The formation of the particles was additionally investigated by electron microscopy. TEM and HRTEM images revealed the presence of particles with 5 nm diameters for the sample with a precursor concentration of 0.17 mol/L, which confirmed the DLS analysis (Figure 52). Furthermore, the HRTEM image showed that the particles were fully crystalline. The image even reveals the crystal lattices, no trace of amorphous regions being detectable on the photograph. The crystallinity is also supported by the electron diffraction patterns.

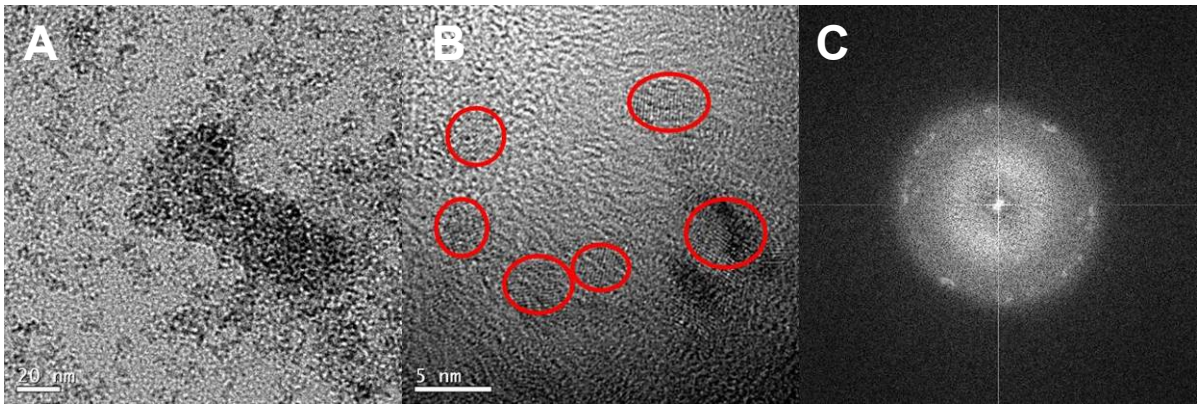

Figure 52. A) Characteristic TEM bright field micrograph of the TiO_2 nanoparticles prepared with 0.17 mol/L $Ti(O^iPr)_4$; B) characteristic HRTEM micrograph; C) Characteristic electron diffraction pattern of the nanoparticles

b. Variation of the Aging Times

Beside the precursor concentration, the reaction time can also play an important role in the growth behaviour of the nanoparticles. DLS analysis (Figure 53) presents the effect of the reaction time on the size of the nanoparticles. After 1 day of reaction the DLS measurements showed the presence of 3 nm ± 0.22 diameter particles. An increase in the diameter, of about 3 nm (d = 6 nm ± 0.17), was observed, when the particles were left in the suspension for additional 24 hours. This is probably due to further condensation reaction of the unreacted alkoxides which are still present in the suspension on the surface of the particles, leading to an increase in their size. However, after one more day, we could not observe any significant change in the particle radius. This can be explained by the total consummation of the alkoxide precursors. In liquid state the particle surface is stabilized by the presence of the nitric acid, which lowers the pH of the solution. Due to this low pH the particles are far from the point of zero charge (5.9 for TiO_2) and the surface of the particles is charged creating electrostatic repulsive forces which hinder the agglomeration of the particles, as presented before.

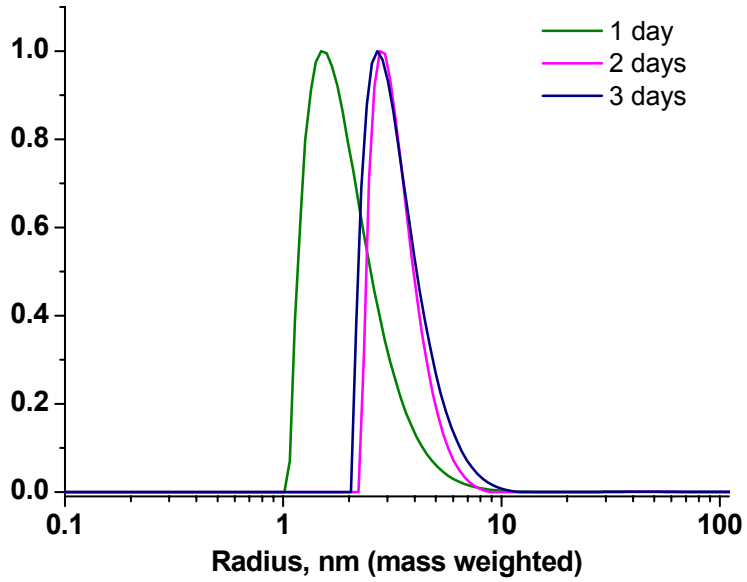

Figure 53. Dependence of the TiO_2 nanoparticle sizes on the reaction time (H_2O, 25°C)

4.2. Surface-Modification of Commercially Available TiO_2 Nanoparticles Using Organophosphorus Coupling Agents

Before investigating different Pickering emulsions, it was necessary to investigate the surface modification of TiO_2 nanoparticles with various phosphonates in solution.

Phosphonic acids can be easily synthesized through the Arbuzov reaction[191], which is based on the reaction of an alkyl halide with a trialkyl phosphite, yielding a dialkylphosphonate. Thus, during the transformation, a trivalent phosphorus is converted into a pentavalent phosphorus (Scheme 10). In general, the alkyl group of the halide attaches to the phosphorus, and one alkyl from phosphorus combines with a halogen to form a new alkyl halide. Applying this method a broad variety of phosphonates can be prepared in high yields (e.g. dodecylphosphonic acid, allyl phosphonic acid). The pathway is quite simple, being carried out just by heating the phosphite and alkyl halide to the required temperature until the reaction is complete. Sometimes temperatures above 150 °C are required for the reaction completion. After that the reaction mixture is then fractionally distilled[191].

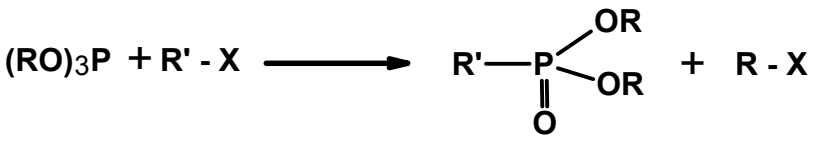

Scheme 10. The Arbuzov reaction for the synthesis of phosphonates (X = halogen)

The synthesis of organophosphorus compounds with polymerizable double bonds cannot be carried out using an Arbuzov reaction due to the high temperatures required, because this would lead to the thermal polymerization of the double bonds.

Another method to generate an organophosphorus compound is the radical addition of a diethyl phosphate to an unsaturated bond. When organophosphorus compounds with polymerizable double bonds are targeted, allyl alkyl alcohols together with diethyl phosphate can be used as precursors (Scheme 11). The first step is generally the protection of the OH alkyl chain end, in order to avoid the production of undesired by-products during the second step. The next step is the radical addition of the diethyl phosphate to an unsaturated bond, followed by the deprotection of the OH group and reaction with methacryloyl chloride.[192] In such a way various methacrylic functionalized organophosphorus coupling agents were synthesized.

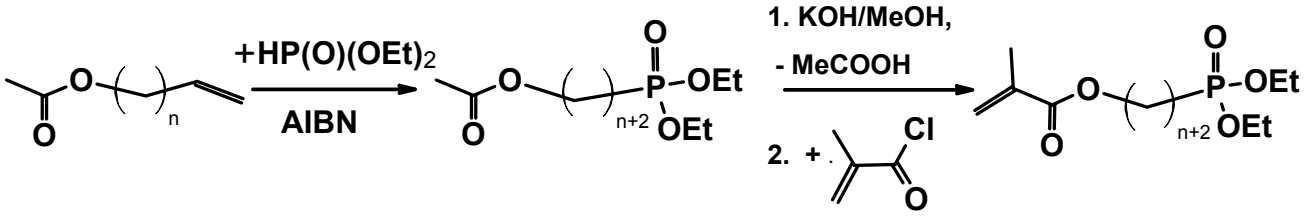

Scheme 11. General pathway for the synthesis of methyl-acrylic acid (diethoxy-phosphoryl)-alkyl esters

In case that bromo-alcohols or bromoalkyl-acetates are available, it is possible to replace the above mentioned addition of diethyl phosphite on the alkenyl acetate by Arbuzov reaction of triethyl phosphite with bromoalkyl acetate.

The surface functionalization of the TiO_2 particles with various organophosphorus coupling agents was investigated. Various phosphonic and phosphoric acids (phenyl phosphonic acid, allyl phosphonic acid, methacryloylox undecyl phosphonic acid, phenyl phosphoric acid, methacryloyl octyl phosphoric acid) were dissolved in different amounts in a 3:1 mixture of methanol and water (500 mL) as solvent. The mixture was used to assure that both the phosphonic acids will dissolve and the nanoparticles will be dispersed. A suspension of 1 g TiO_2 in 100 mL of water was added to the acid solution (Scheme 12) and the resulted suspension was stirred at room temperature for 3 days. In the literature, the surface-modification of TiO_2 with phosphonic acids is usually carried out in aqueous media at 100

°C.[193, 194] Depending on the reaction time and the phosphonic acid concentration, significant amounts of bulk titanium phosphonate may be formed. For this reason we carried out all the reactions at room temperature. In the reaction the pH was varying between 2 and 3.5, depending on the type of particles used (sol-gel particles had a pH around 2, while commercially available P25 were further acidified to pH 3.5 for better redispersibility). The obtained modified particles were isolated via centrifugation, washed several times with ethanol, and dried at temperature between 40 and 120°C in vacuum. The phosphonates and phosphates with attached polymerizable bonds were dried at lower temperatures (40°C) to avoid the thermal polymerization.

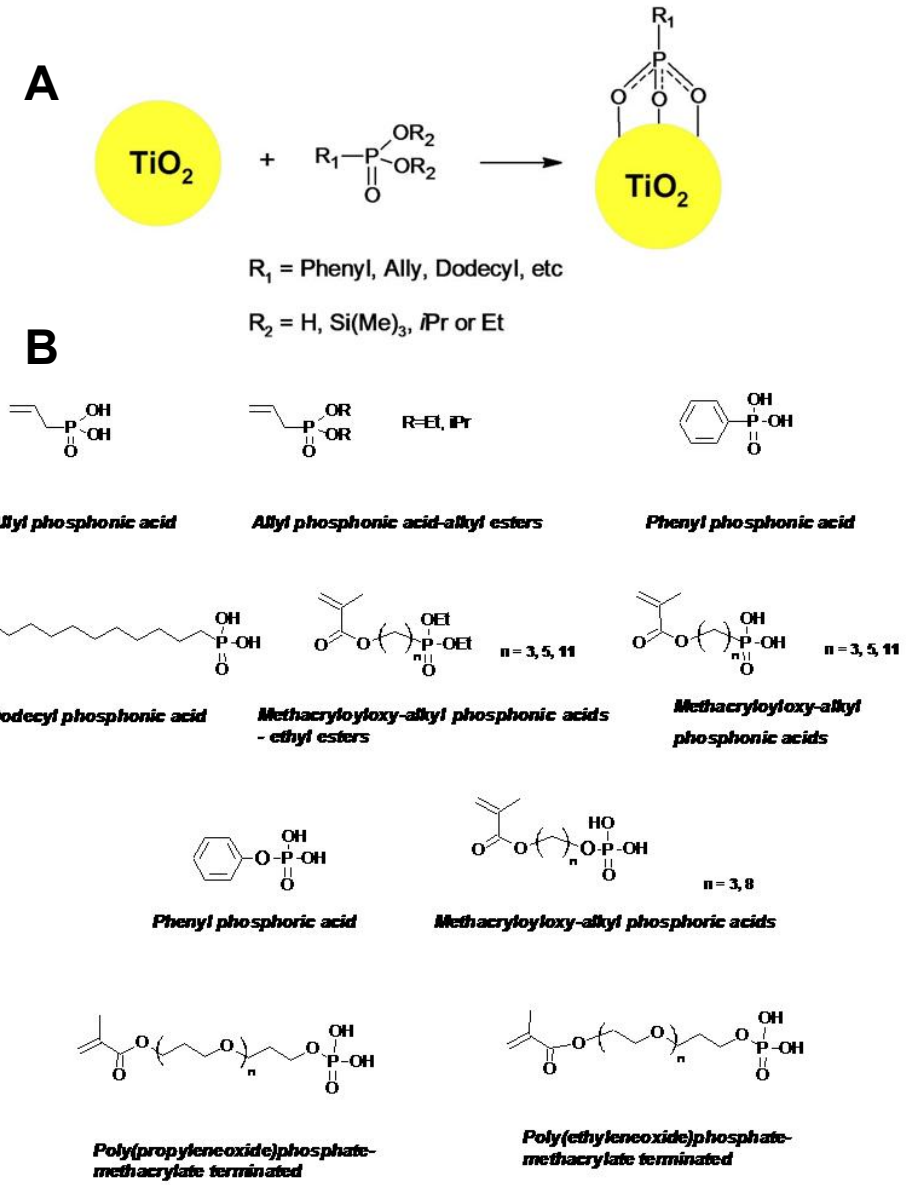

Scheme 12. A) Surface-functionalization of TiO_2 nanoparticles with organophosphorus ligands; B) Different phosphonates and phosphates used for the surface modification

The commercially available Degussa TiO_2 P25 nanoparticles are used as standards when titania materials are applied for photocatalysis. The particles have both anatase and rutile phases in a ratio of 3:1 (Figure 54 – XRD and DLS picture). The percentage of anatase phase is in the range of 75 – 80 wt. %. The primary particles reported by Degussa have 21 nm diameters, while the crystallite size shows an average of 30 nm for anatase and 55 nm for rutile as calculated from the XRD data. The P25 particles have a surface area of 51 m^2/g, as determined by the nitrogen sorbtion measurements.

The P25 particles were dispersed in water at a pH of about 3.5. The DLS measurements of this dispersion proved the presence of the particles with 21 nm diameters (10.5 nm ± 0.05 radii, Figure 54, left side). However there is a considerable amount of agglomerates (87 % analyzed by mass weight) which could not be broken down to primary particles, even when using an ultrasonic finger.

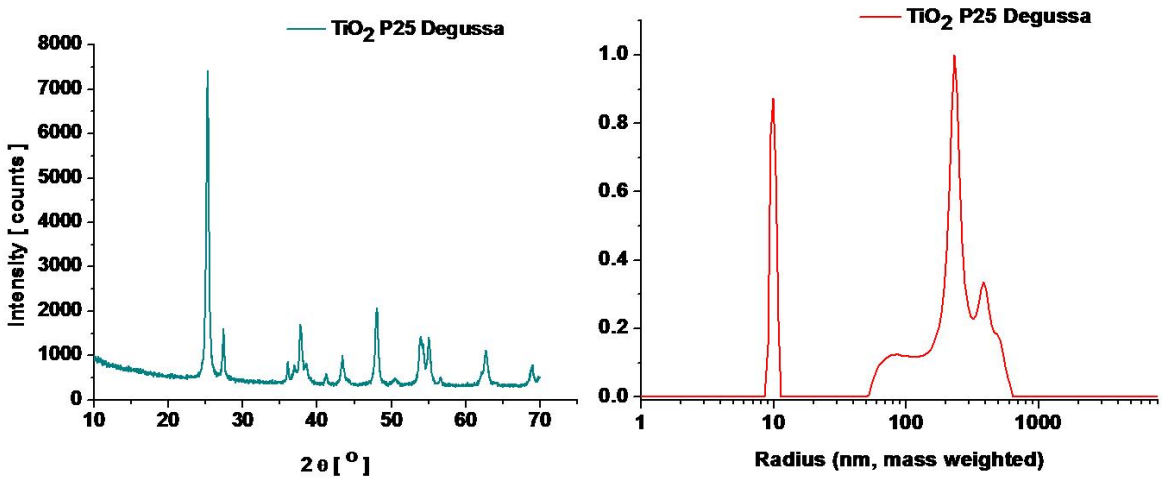

Figure 54. XRD (left side) and DLS (right side) of the commercially available TiO_2 P25 nanoparticles

In a first step, the binding of the phosphonates on the surface of these particles was investigated in order to compare their reactivity with the sol-gel materials.

As mentioned, before the surface-modification the pH of the particle dispersions was adjusted to 3.5 with HCl to be far from the point of zero charge (pH = 5.9 for TiO_2). Hence, the electrostatic repulsive forces due to charged surface sites can break up the particles' aggregates. The surface of the TiO_2 particles was modified by treatment with a solution of the phosphonate molecules in different amounts (excess relative to the amount required for a full surface coverage on the particles, based on the surface calculation for particles having diameters of 21 nm). Stable suspensions were obtained with all the organophosphorus

coupling agents used. For the cases of the alkyl ester derivates of the phosphonic acids the particles were dispersed either in mixtures H_2O/MeOH or in pure MeOH. After the surface modification, the suspensions were centrifuged and the powders were thoroughly washed with EtOH to remove unreacted and physisorbed species and then dried before analysis.

4.2.1. Spectroscopic Studies

Literature reports suggested that the anchoring of organophosphorus derivatives on a titania or another metal oxide surface is expected to involve both coordination of the phosphoryl oxygen to Lewis acid sites as well as condensation reactions between the surface hydroxyl groups Ti-OH and the P-OH groups[100, 193]. The organophosphonates can have mono-, bi-, or tridentate bonding modes (Scheme 13).

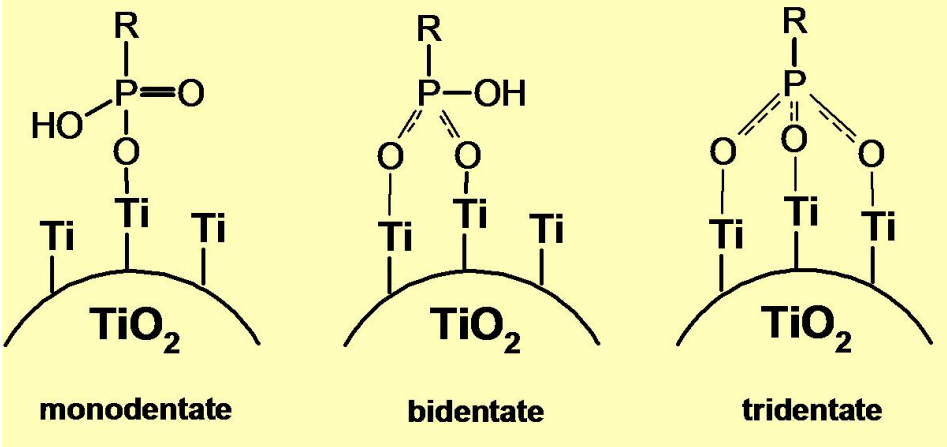

Scheme 13. Different bonding modes of a phosphonate to a TiO_2 surface

The first attempts to identify the bonding modes for each coupling molecule were carried out by FT-IR and ^{31}P NMR spectroscopy. The FT-IR analyses of the commercially available TiO_2 P25 Degussa nanoparticles modified with phenyl phosphonic acid (PPA) are presented in Figure 55. For the modified particles a strong band at 1147 cm^{-1} was observed, which is characteristic for the P-phenyl groups[100]. The broad band between 1000 and 1200 cm^{-1} corresponds to the P-O-(Ti) stretching vibration, proving the condensation of the ligand's OH-groups with residual Ti-OH at the particle surfaces. The disappearance of the P=O signal of the phosphonic acid (1190 - 1210 cm^{-1}) shows that the phosphonate acts as a tridentate ligand. These results are consistent with the ones reported by *Guerrero et al* who investigated the surface-functionalization of TiO_2-P25 (Degussa) with phenyl phosphonic acid and esters[100].

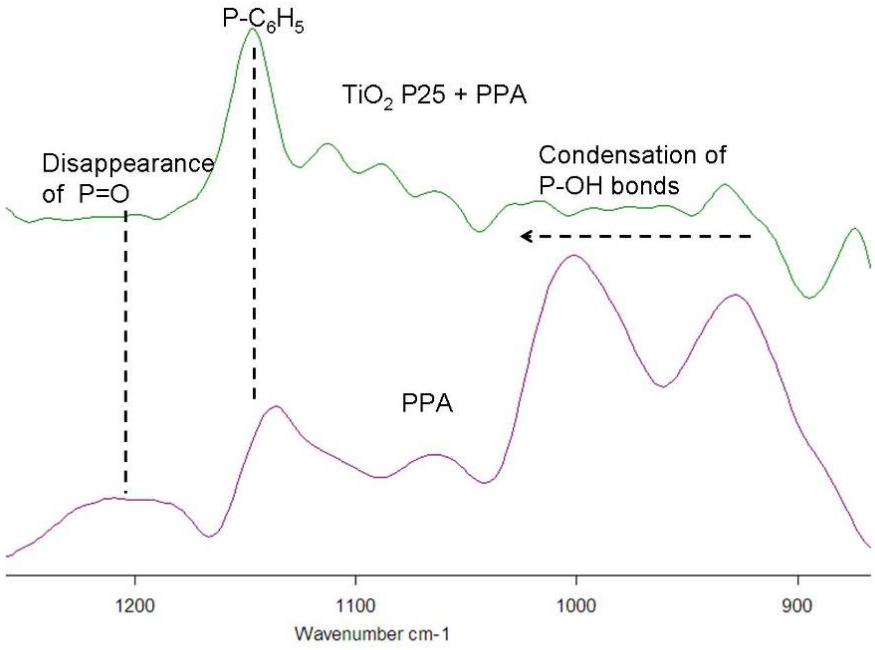

Figure 55. FT-IR spectra of TiO_2 P25 Degussa particles modified with PPA

Applying the same approach the P25 particles were also modified with the phosphoric homologue of the PPA, namely the phenyl phosphoric acid (PPoA). The spectrum of the modified particles presents similar features. The disappearance of the P-O-H vibration bands at around 1000 cm^{-1} and the formation of a new broad band between 1000 and 1200 cm^{-1} which corresponds to the P-O-(Ti) stretching vibration proves the condensation of the ligand OH-groups with the residual Ti-OH from the particle surfaces. Similar as in the case of the phosphonates the disappearance of the P=O signal of the phosphonic acid (at 1230 cm^{-1}) supports a tridentate binding mode of the organophosphate ligands.

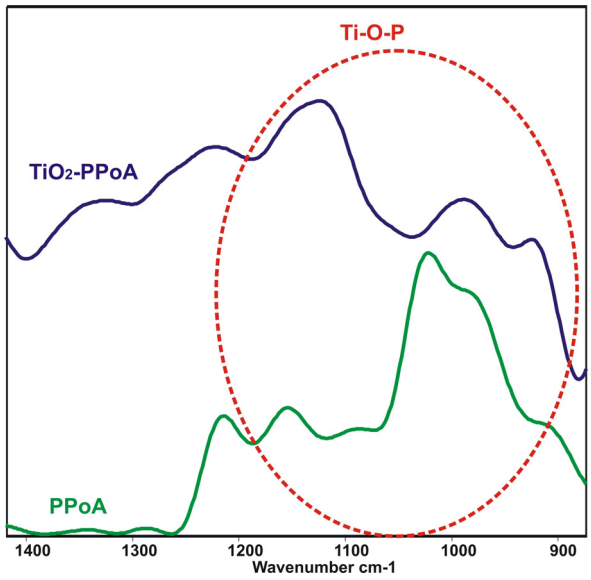

Figure 56. FT-IR spectra of the pure PPoA and of TiO_2 Degussa P25 particles modified with PPoA

FT-IR spectra of the nanoparticles modified with long chain phosphonates and phosphates (MetC11PA, MetC8PoA) (Figure 57) show the presence of organics on the particle surfaces. The bands presented at 1725 cm^{-1} were assigned to the C=O vibration of the methacrylic groups. This demonstrates that the double bonds are present of the surface of the TiO_2 nanoparticles. The residual broad pattern between 1000 and 1200 cm^{-1} corresponds to various P-O-Ti vibrations. The FT-IR spectra indicate tridentate binding modes for both the phosphonate and phosphate modified particles.

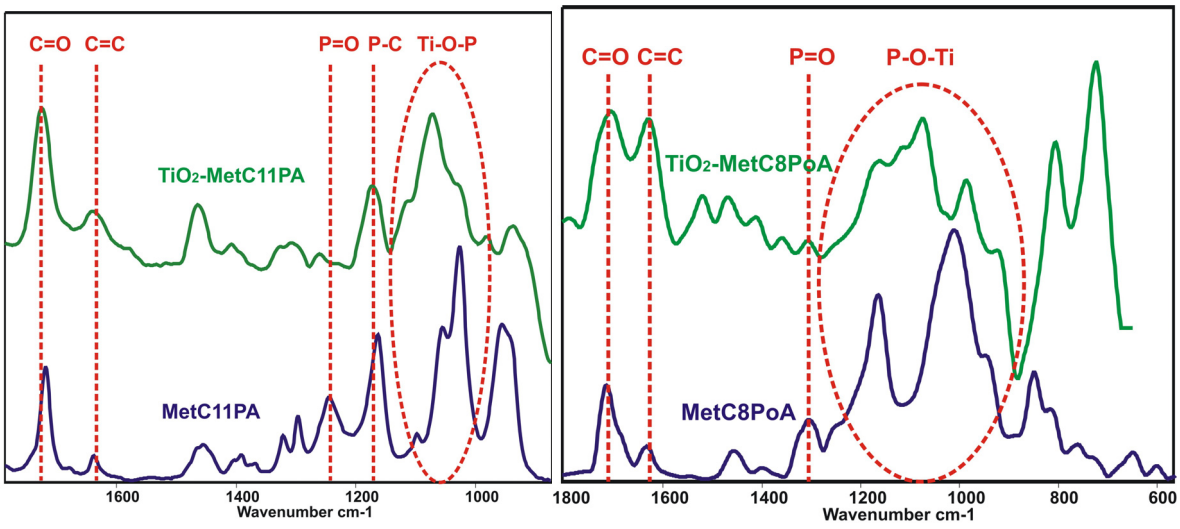

Figure 57. FT-IR spectra of the pristine organophosphorus coupling agents and of the TiO_2 P25 Degussa particles modified with MetC11PA (left) and MetC8PoA (right)

NMR

All of the ^{31}P MAS NMR spectra of the TiO_2 P25 particles modified with various phosphonates are similar regardless of the coupling molecule. For the case of PPA, as mentioned already, the disappearance of the P=O in the FT-IR results led to the conclusion that the major resonance at 16 ppm is due to the tridentate phosphonate sites $PhP(OTi)_3$[100]. This chemical shift is also close to those found for phenylphosphonate/TiO_2 hybrids prepared by a sol-gel method[195].

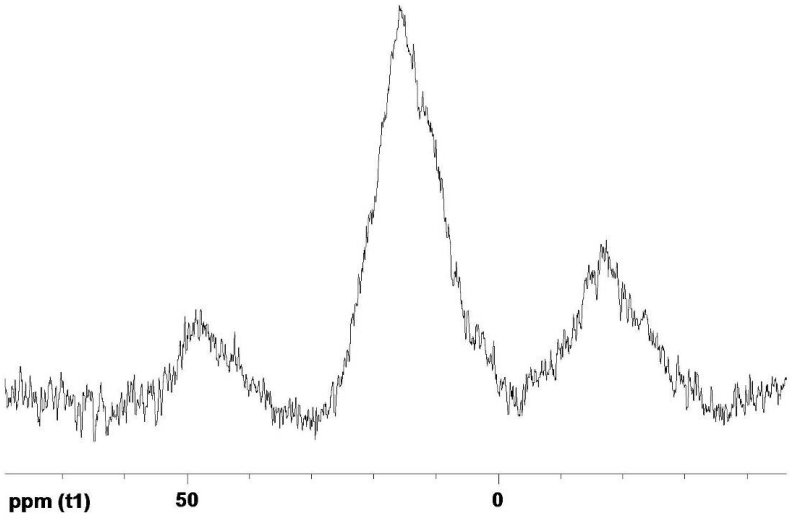

Figure 58. ^{31}P MAS NMR of TiO_2 P25 particles modified with PPA

Similar ^{31}P MAS NMR spectra were obtained for the cases of the methacryloyloxy alkyl phosphonic acids and alkyl esters. The presence of an additional resonance near 19 ppm for the MetC11PA points to another binding mode of the phosphonate groups, which is likely to be bidentate (-P- $(OTi)_2OH$ sites) (Figure 59).

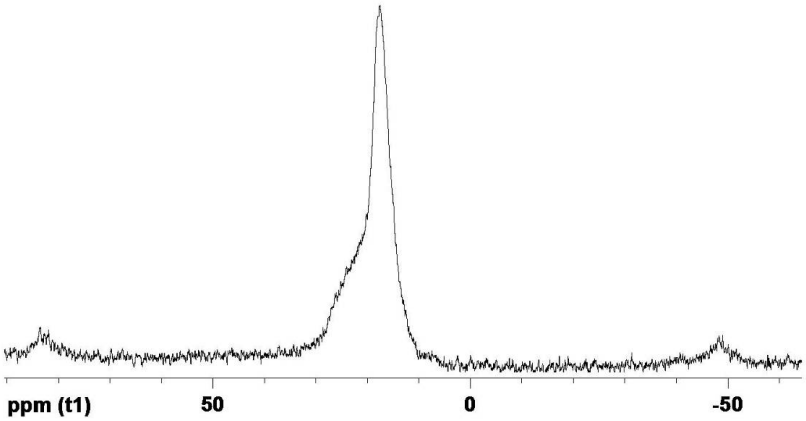

Figure 59. ^{31}P MAS NMR of TiO_2 P25 particles modified with MetC11PA

Phosphates

^{31}P NMR can also be used to study the surface-functionalization with phosphates. Phenyl phosphoric acid was used for comparison with its phosphonate homologue, phenyl phosphonic acid. The ^{31}P MAS NMR spectra of the PPoA (Figure 60) present only one resonance at -3.5 ppm, which is characteristic for phosphates. After the particles modification, this resonance is shifted downfield. The new resonance at 1.2 ppm was assigned to bonded phosphates on the particles surfaces. The modification is also proven by the broadening of the resonance, similar as observed for the phosphonates. Residues of physically adsorbed PPoA were also detected at - 3.5 ppm.

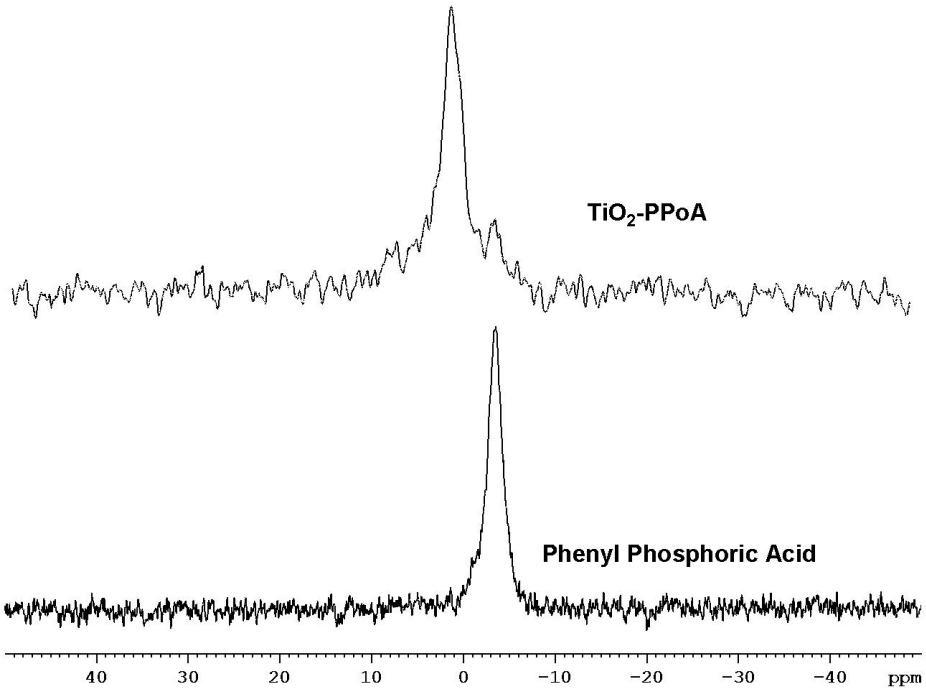

Figure 60. ^{31}P MAS NMR of the free PPoA and of the TiO_2 P25 particles modified with PPA

4.2.2. Thermal Analyses

The TiO_2 P25 Degussa nanoparticles were functionalized with short long chain phosphonates and phosphates (phenyl, C11-phosphonate, C8-phosphate) and analyzed by thermal analysis (Figure 61). The TG analyses were used to determine the amount of organophosphorus coupling agents attached to the surface of the particles and their thermal stability.

The TGA in air of the TiO_2 P25 nanoparticles showed a small mass loss starting with 100°C of about 1% which was due to adsorbed water. In contrast, the thermal analysis of the modified TiO_2 particles displayed all mass losses between 200 °C and 400°C. The weight loss was calculated between 200 °C and 600 °C, to exclude the mass loss due to volatiles, and was

assigned to the oxidative degradation of the organic ligand. For all of the cases, the weight loss due to the organophosphorus ligands was between 2 and 7 %.

The small amount of mass loss can be explained by two factors:

- The particles are highly agglomerated, as seen from DLS studies. This means that the real surface area available for functionalization is much smaller than the theoretical one, based on the particles primary diameter (21 nm as reported by Degussa). The smaller surface area leads to a decreased amount of coupling agents bonded to the surface.
- There are less active Ti-OH species on the surface of the particles, due to their calcination. For this reason the surface is not very reactive in the binding of the coupling agents.

The amount of ligand bonded to the surface of the particles appeared to be dependent on the type of organophosphorus coupling agent used. The highest mass loss was observed for the modifications with MetC11PA. Between 200 °C and 600 °C about 7 % mass loss was observed, attributed to the phosphonate. The MetC8PoA has a lower mass loss (3.8 %) in the same temperature range.

The particles modified with organophosphorus ligands having phenyl groups, PPA and PPoA, revealed even smaller weight losses due to the functionalization. The particles modified with PPA presented an onset temperature due to the oxidative degradation of the phenyl rings at about 400 °C, with a mass loss between 200 °C and 600 °C of about 2 %. The particles modified with PPoA presented a very similar onset temperature due to the oxidative degradation of the phenyl rings at (350 °C), with a mass loss between 200 °C and 600 °C of about 3 %.

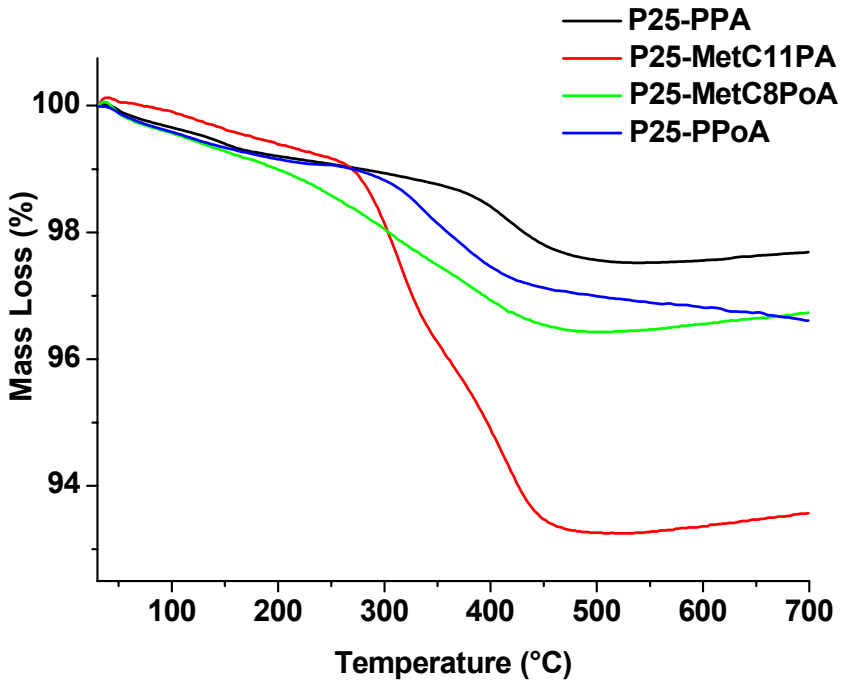

Figure 61. TiO_2 P25 nanoparticles functionalized with PPA, PPoA. MetC11PA and MetC8PoA

4.2.3. Dynamic Light Scattering Studies

Dynamic light scattering was used to investigate the behavior of the particles in liquid state as well as the evolution of their hydrodynamic radius upon surface-modification. In Figure 62 the size distributions of various modified TiO_2 Degussa P25 particles with organophosphorus ligands are presented. As mentioned before, the commercially available P25 particles have a particle size of about 21 nm diameter. When suspended in water the white powder turns into a milky suspension. The DLS distribution of the particles dispersed in water showed the presence of agglomerates having very broad size distributions. These agglomerates can be partially broken by the use of a digital sonifier for 4 min at 70% amplitude and with a 30 sec pause every minute. Indeed, after redispersion, the DLS analysis presented a distribution corresponding to particles with a diameter of 21 nm. A second distribution was obtained corresponding to agglomerates ranging from 0.1 to 1.6 µm. In the case of PPA modified TiO_2 particles, after drying and redispersion, only the presence of one size distribution (100%, mass weighted) was observed corresponding to particles displaying a diameter of about 786 nm. This was probably due to agglomeration upon functionalization of the dispersed particles, leading to larger but still uniform aggregates. Similar DLS results were received in the case of the P25 nanoparticles modified with the methacryloyloxy undecyl phosphonic acids.

However, here two distribution functions were observed which correspond to two different sizes of particles. Apparently there is a distribution with a mean of 60 nm radii corresponding to about 25 % of the total particles (mass weight), while the rest is represented by agglomerates between 100 and 1000 nm. The agglomerates have approximately the same shape as the agglomerates observed in the case of the P25 unmodified particles, so it is reasonable to sustain that they are not due to further condensation of the particles.

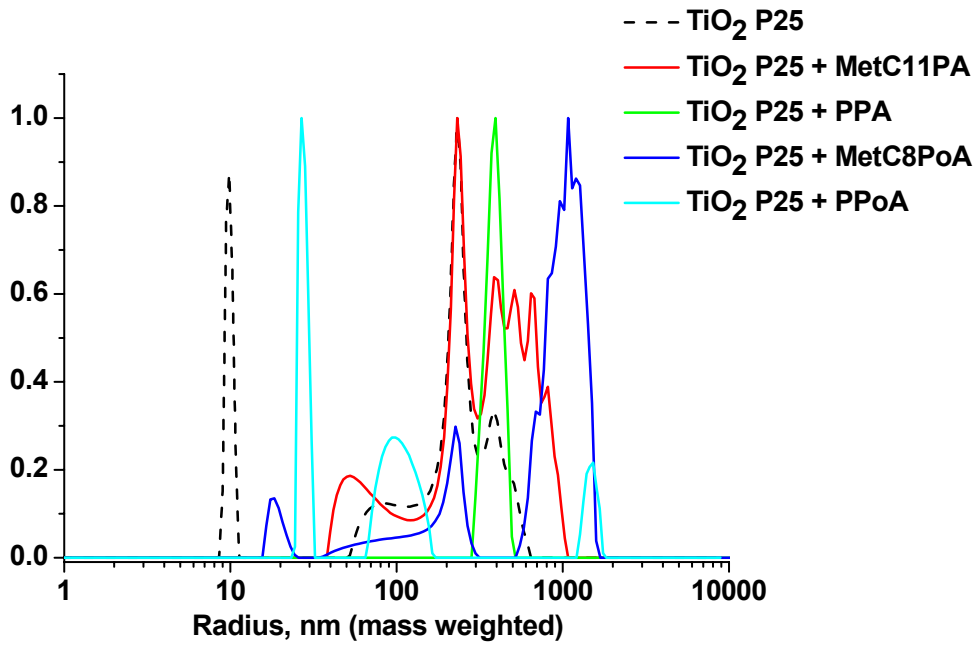

Figure 62. DLS of TiO_2 P25 modified particles (25°C, H_2O)

The situation changed to some extent when the organophosphates were used. In the case of the PPA homologues, the phenyl phosphoric acid, we can detect that 44% of the total particles (mass weighted) posses radii of about 21 nm. A second distribution is observed with radii of about 106 nm (46 % after mass weighting), while some agglomerates with radii of 1200 nm were also detected representing 9% of the total amount of particles present in the dispersion. The small particles are most likely derived from the surface modification of the P25 particles. The larger one instead can be residual aggregates of P25 not completely dispersed in the water phase. The long chain phosphates (MetC8PoA) have a similar size distribution, with small particles having radii of 16 nm diameter (44%) and agglomerates and aggregates between 40 and 1000 nm.

4.2.4. Morphological Investigations

TEM

Transmission electron microscopy (TEM) was used to investigate the morphology of the modified nanoparticles. The samples measured in TEM were prepared after drying of the particles in vacuum and redispersion in ethanol. In Figure 63 are presented some characteristic TEM micrographs of the particles modified with phosphonates (short and long chain).

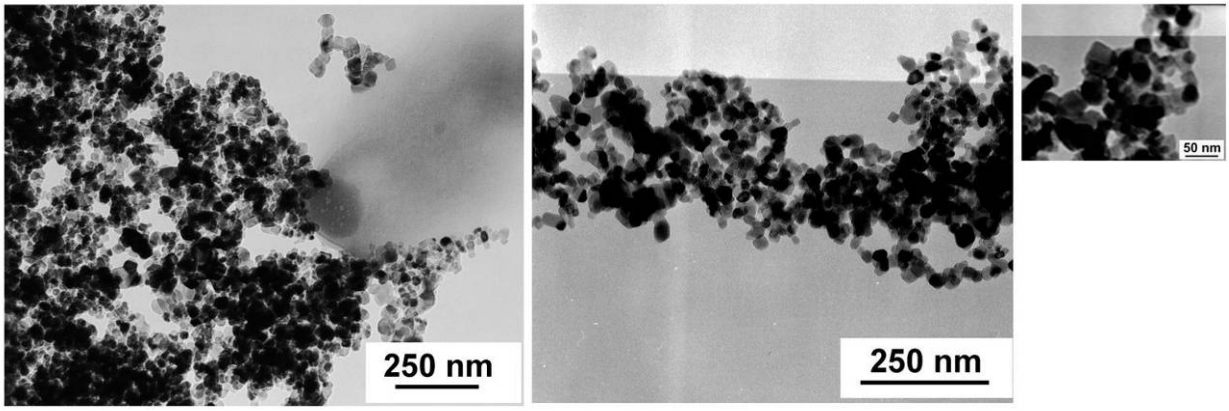

Figure 63. TEM micrograph of TiO_2 P25 nanoparticles modified with MetC11PA (left) and PPA (right and inset)

In the case of PPA modified particles the TEM measurements showed the presence of particles having a mean diameter of about 30 to 40 nm, with narrow distribution. The dark field image and the diffraction patterns have proven that all of the particles were crystalline. The presence of agglomerates was also noticed, which most likely are due to the drying of the sample on the TEM grid. However, these measurements could not confirm the presence of the organophosphorus ligands on the surface of the particles.

SEM and EDX

Due to the low resolution of the TEM and to the lack of chemical information regarding the composition, SEM and EDX measurements were carried out to elucidate the chemical nature of the particles and to prove the presence of the organophosphorus ligands. The dried powders were deposited on a sample holder and sputtered with gold for better conductivity. The SEM images revealed the presence of spherical shape nanoparticles confirming the TEM analysis. Also in this case the particles had a rough diameter of around 40 nm, with narrow polydispersity. No larger particles were detected. In Figure 64 one example of the P25 particles modified with MetC11PA is given. EDX analysis of the particles presented on the

SEM image confirmed the chemical nature of the modified particles. As it can be seen, the presence of Ti and O is evidenced by their specific bands. Furthermore, a band of P was also detected, confirming the presence of the organophosphorus coupling agents. Due to the presence of the gold on the surface of the particles no quantification could be made, the peaks of P and gold interfering with each other. However the simple qualitative information has proven the presence of the ligands at the surface of the nanoparticles, supporting the TG analyses.

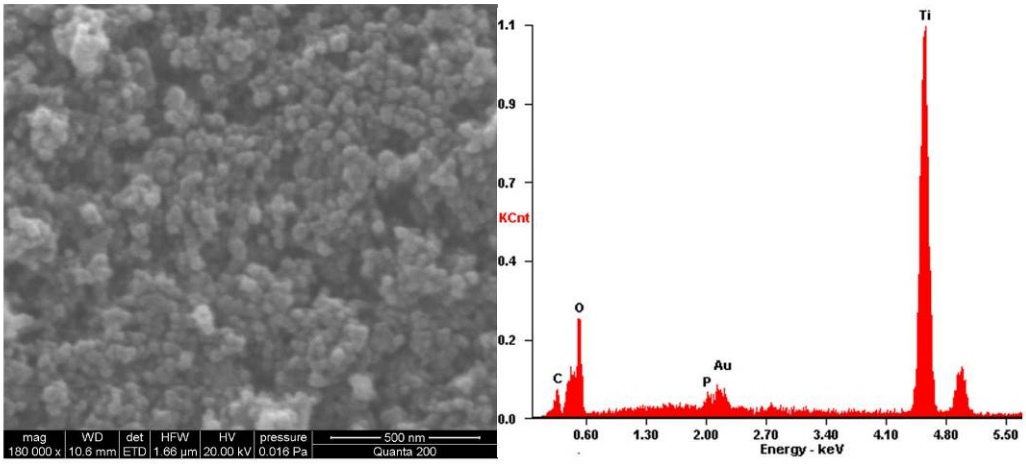

Figure 64. SEM and EDX analyses of TiO_2 P25 nanoparticles modified with MetC11PA

4.2.5. Photocatalytic Activity of the Modified Particles

The decomposition of methylene blue (MB) was used for quantifying the photocatalytic activity of the various TiO_2 nanoparticles. Figure 65 presents the chemical structure of the MB dye. When dissolved in an aqueous solution, the MB dye adopts a cationic configuration. This helps its adsorption on the surface of TiO_2 nanoparticles through the Coulombic interaction with the OH^- ions present on the surface.[196]

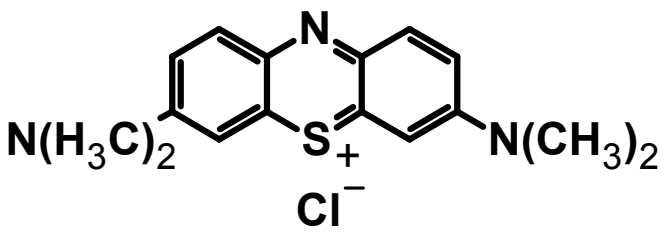

Figure 65. Chemical structure of methylene blue

Figure 66 presents the absorption spectrum of MB which was measured between 200 and 800 nm. The absorbance band of MB is situated at 665 nm and can be taken as a measure of the residual concentration of the MB dye.

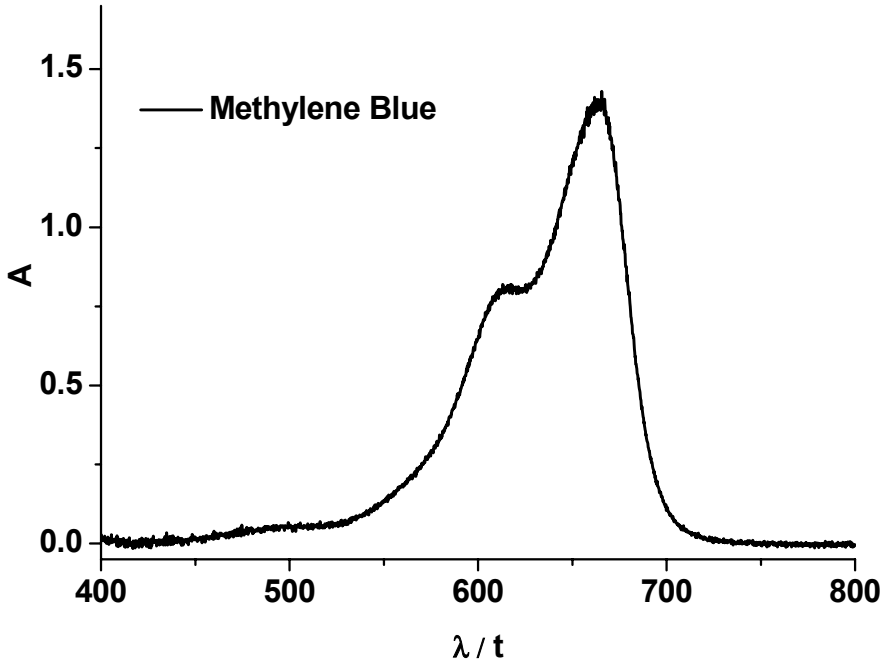

Figure 66. UV-Vis absorption spectra of methylene blue in water

When TiO_2 nanoparticles are irradiated with UV radiation ($h\upsilon$), e^-/h^+ pairs are created inside, due to excitation of an electron from the valence band into the conduction band (charge-carrier generation).

$$TiO_2 + h\upsilon \rightarrow TiO_2 + e^- + h^+ \qquad (1)$$

If OH^- ions are adsorbed at the surface of the particles they can react with the positive holes leading to the formation of $OH^\cdot$ radicals.

$$OH^- + h^+ \rightarrow OH^\cdot \qquad (2)$$

In a similar manner, if O_2 is present at the surface of the particles, it can react with the formed electrons leading to O_2^- species. These react in a further step with protons forming the hydrogen peroxide (H_2O_2) as an intermediate product, which subsequently gets decomposed

to the OH radical by releasing the OH^- ions into the aqueous solution. The overall reaction steps are presented in equations 1 – 6[196, 197].

$$O_2 + e^- \rightarrow O_2^- \quad (3)$$

$$O_2^- + H^+ \rightarrow HO_2 \quad (4)$$

$$2HO_2 \rightarrow H_2O_2 + O_2 \quad (5)$$

$$H_2O_2 + e^- \rightarrow HO^\cdot + HO^- \quad (6)$$

When MB is adsorbed on the surface of TiO_2 nanoparticles, the $HO^\cdot$ radicals are the ones responsible for the degradation of the dye through successive reactions. As mentioned in literature[196, 198], the degradation of the MB starts with the cleavage of the $C\text{-}S^+\text{=}C$ functionality, which is the group of the dye that binds to the surface of the TiO_2 nanoparticles. The decomposition products resulting after the decomposition of the dye are mainly CO_2 gases, NO_3^- iones, SO_4^- ions, H^+, and water, according to the following equation:

$$C_{16}H_{18}N_3S^+ + 102\ HO^\cdot \rightarrow 16\ CO_2 + 3\ NO_3^- + SO_4^- + 6\ H^+ + 57\ H_2O$$

First, the commercially available TiO_2 Degussa P25 particles were evaluated. In a standard experiment, 200 mL water solution of MB (20 μM concentration) and 0.05 g particles were used. The pH was 4 and the suspension was mixed in the dark for 20 minutes to assure a full adsorption of the dye on the surface of the photocatalyst. The solutions were irradiated with a UVA black light (wavelength 350 – 400 nm). After various reaction times, the solution was filtrated and analyzed using an UV-Vis spectroscopy. The absorption spectrum of MB was measured between 200 and 800 nm. The intensity of the absorbance band of MB at 665 nm was taken as a measure of the residual concentration of the MB dye. In Figure 67 the decrease of the MB concentration measured by the absorbance of the specific MB band is presented.

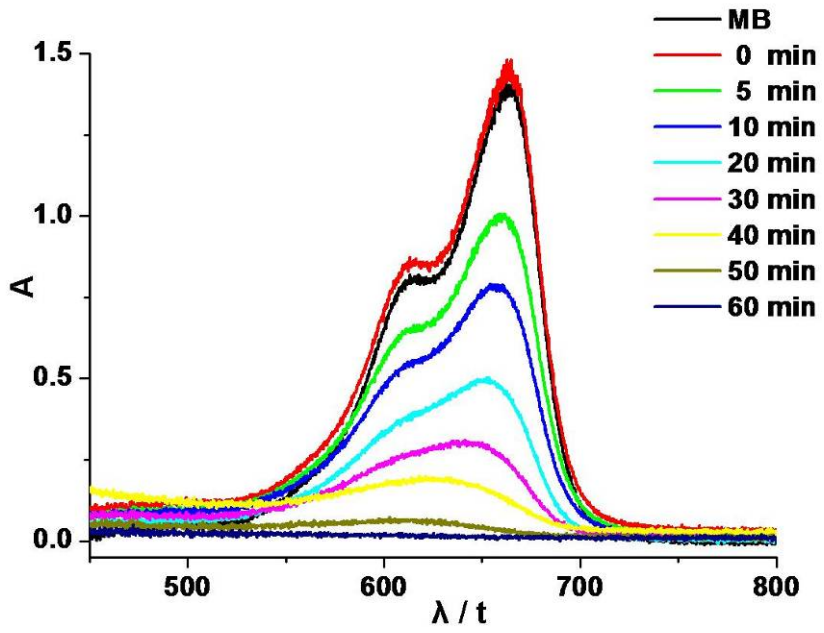

Figure 67. UV-Vis absorption spectra of methylene blue adsorbed on TiO_2 P25 Degussa nanoparticles in suspension after different UV exposure times

The absorbance band of MB at 665 nm decreased with increasing exposure time to UV light. One can easily see that after 1 hour of irradiation practically the whole amount of MB dye is decomposed.

The photocatalytic decomposition of the organic molecules follows the Langmuir – Hinshelwood kinetics (equation 7)[196, 198, 199].

$$dC/dt = k_{app} \cdot C \quad (7)$$

where: dC/dt represents the change in the MB concentration, t is the UV irradiation time, k_{app} is the apparent first-order reaction rate constant, and C is the concentration of the MB.
The solution of the equation (7) is presented in equation (8):

$$\ln(C_0/C) = k_{app} \cdot t \quad (8)$$

In conclusion the photocatalytic activity can be plotted as $\ln(C_0/C) = f(t)$. Figure 68 shows the plots of the photocatalytic measurements of different P25 phosphonate and phosphate surface-modified particles.

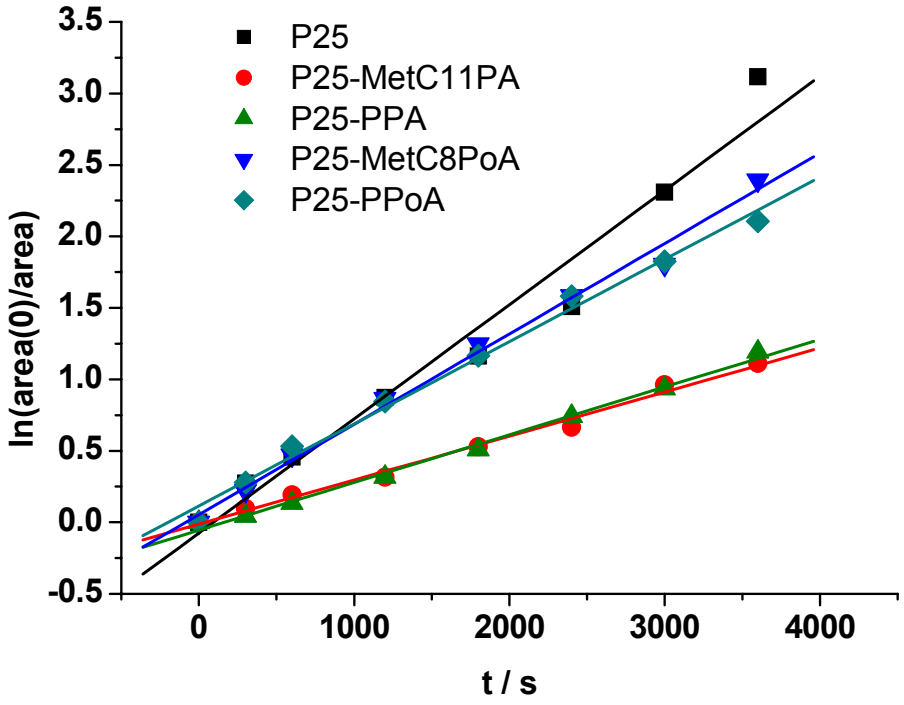

Figure 68. The photocatalytic activity of TiO_2 P25 and various TiO_2 P25 surface modified nanoparticles as a function of the concentration of methylene blue

All of the plots presented followed first-order kinetics. As expected, when modifying the surface of the particles with phosphonates, a decrease in the photocatalytic activity was observed. The largest decrease was observed when using the MetC11PA, probably due to the incompatibility of the long alkyl chains with the MB dye. Also the surface-coverage obtained when using the MetC11PA was the highest (7 % mass loss as calculated from the TGA data). A higher surface-coverage will lead to a decrease in the amount of adsorbed dye on the particles surface, which explains the lower photocatalytic activity. The hydrophobicity of the ligand can also influence the dispersibility of the particles in water, considering that the measurements were carried out in aqueous phase. A smaller decrease was observed when the particles were modified with PPA. This is also consistent with the smaller amount of surface-coverage observed in the TGA analysis. On the other hand, when using phosphates, almost no change in the photocatalytic activity of the modified particles was observed. This is rather curious considering that the degree of surface-coverage is very similar as in the phosphonate cases, so a lower amount of phosphate bonded to the P25 surface can be excluded. The low dispersibility of the modified particles in water solution could explain the results obtained for the phosphonates.

4.3. Surface-Modification of Sol-Gel TiO_2 Nanoparticles

4.3.1. Spectroscopic Studies

FT-IR Investigations

The TiO_2 nanoparticles synthesized by the sol-gel method were also modified by phosphonates and phosphates according to the procedure used in the case of the commercially available TiO_2 P25.

The FT-IR analyses for TiO_2 nanoparticles modified with phenyl phosphonic acid using an excess of the acid (1.56 * 10^{-3} mol / g particles) are presented in Figure 69. For the modified particles a strong band at 1138 cm^{-1} was detected which is characteristic for the P-C groups. The broad band between 930 and 1200 cm^{-1} corresponds to the P-O-(Ti) stretching vibration, proving the condensation of the ligand's OH-groups with some of the Ti-OH from the particles' surface. The disappearance of the P=O signal of the phosphonic acid (1194 cm^{-1}) shows that the phosphonates act as tridentate ligands. These results are consistent with the ones obtained in the cases of the P25 surface-modification and are also consistent with earlier literature reports.[100]

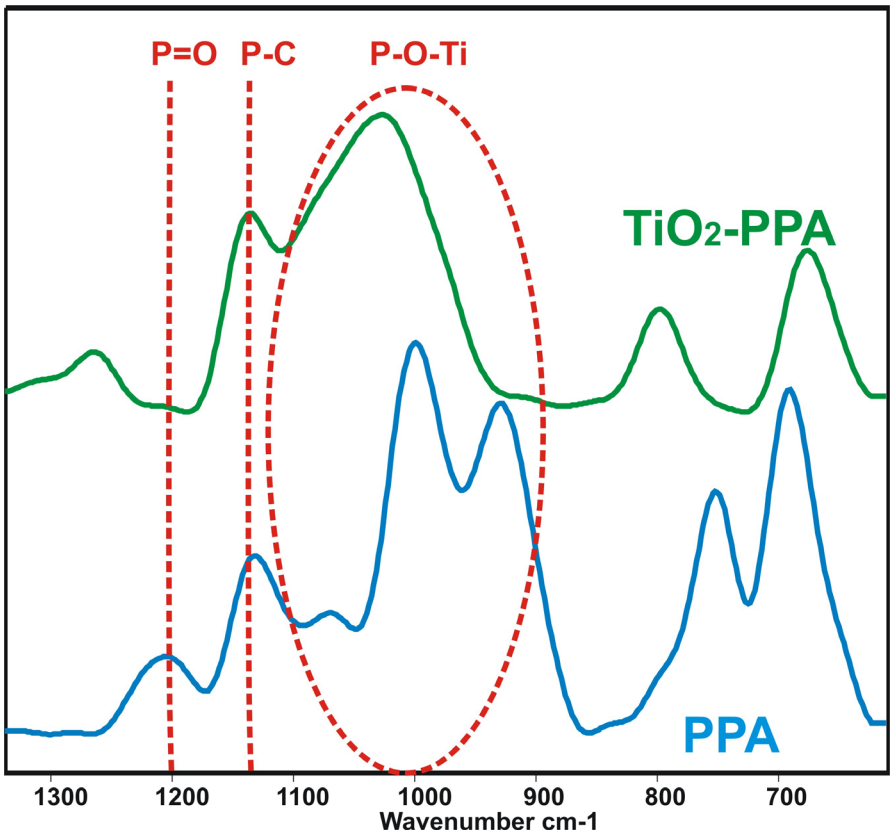

Figure 69. FT-IR analyses of TiO_2 nanoparticles (S163) modified with PPA

The FT-IR analyses for the modification with methacryloyloxy undecyl phosphonic ethyl esters are presented in Figure 70. It is known from literature that the alkyl esters of the

phosphonic acids are much less reactive. The cleavage of P-OEt bonds on oxide surfaces has already been reported, for instance, in the case of dimethyl methylphosphonate on different metal oxides substrates[200]. Usually P-OEt groups are quite stable toward hydrolysis. Therefore typical hydrolysis conditions of these groups involve refluxing overnight in 6 N HCl. Literature studies sustained that it is very unlikely that the hydrolysis of these P-OEt groups is due to the adsorbed surface water prior to the interaction with the surface. Most probably, coordination of the phosphoryl oxygen to an acidic surface site assists the condensation by increasing the electrophilicity of the P atom, thus facilitating the condensation of P–O–R groups with surface OH-groups[100].

For the modified particles a strong band at 1164 cm^{-1} was observed which is characteristic for the P-C groups. The broad band between 930 and 1100 cm^{-1} corresponds to the P-O-(Ti) stretching vibration, proving the condensation of the OH-groups of the ligand with the Ti-OH groups from the particles' surface. However, this band is not as broadened and shifted as in the cases of the phenyl phosphonic acid. It is possible that not all the ethyl esters are hydrolyzed. The disappearance of the P=O signal of the phosphonic acid (1245 cm^{-1}) shows the coordination of the P-O, showing that probably most of the phosphonates act as tridentate ligands. These results are consistent with the ones reported by *Guerrero et al*[100]. who investigated the surface functionalization of TiO_2 Degussa P25 with phenyl phosphonic acid.

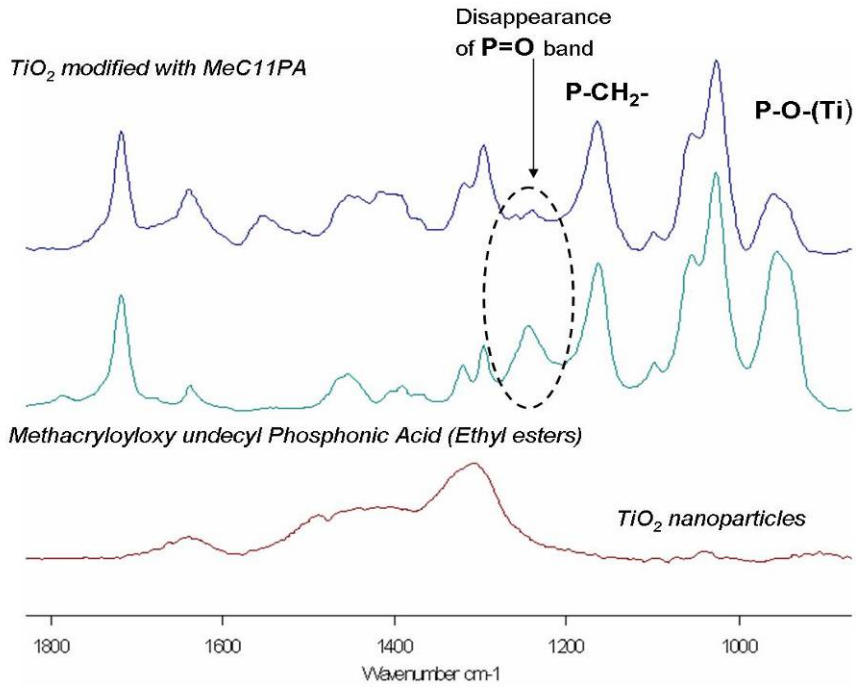

Figure 70. FT-IR spectra of surface-functionalized TiO_2 nanoparticles with MetC11PA-Et

A similar behavior was observed in the case of the methacryloyloxy pentyl phosphonates ethyl ester (Figure 71). Again the disappearance of the P=O signal of the phosphonic acid (1234 cm^{-1}) is already observed, proving the tridentate binding mode of the organophosphorus coupling agents on the particles' surface. The broad band between 960 and 1080 cm^{-1} corresponds to the P-O-(Ti) stretching vibration. Finally, the presence of the P-C vibration is evidenced by the band at 1171 cm^{-1}.

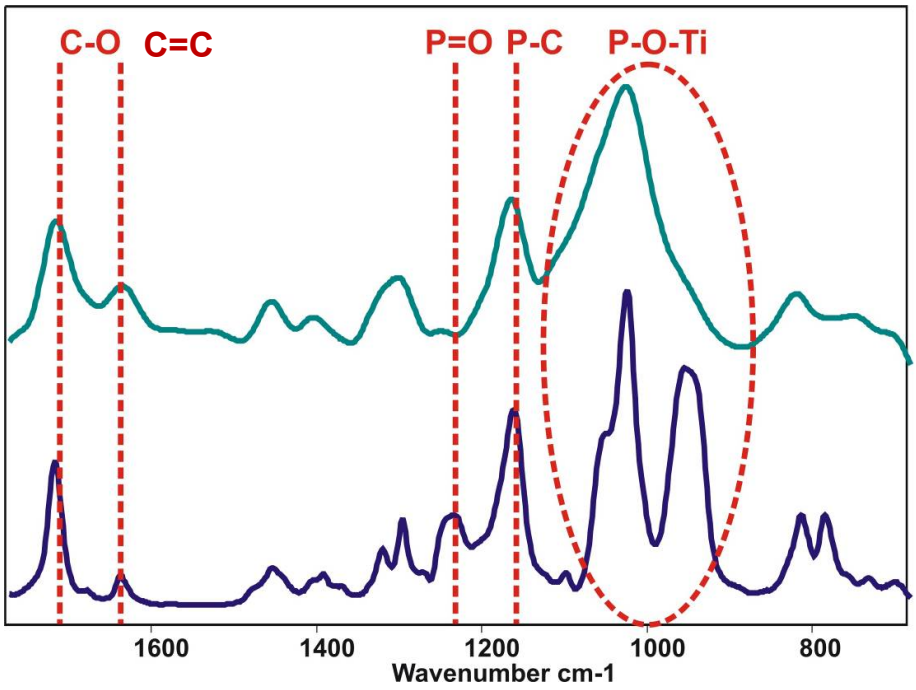

Figure 71. FT-IR spectra of surface-functionalized TiO_2 nanoparticles with MetC5PA-Et

NMR

The reported FT-IR results have proven the successful surface-modification of TiO_2 nanoparticles using phosphonic acids. In all of the cases the phosphonates were acting as tridentate ligands by the condensation of the P-OH bonds and the disappearance of the P=O bond. In Figure 72 is presented the ^{31}P SP MAS NMR spectra of the phenyl phosphonic acid and of the modified TiO_2 nanoparticles.

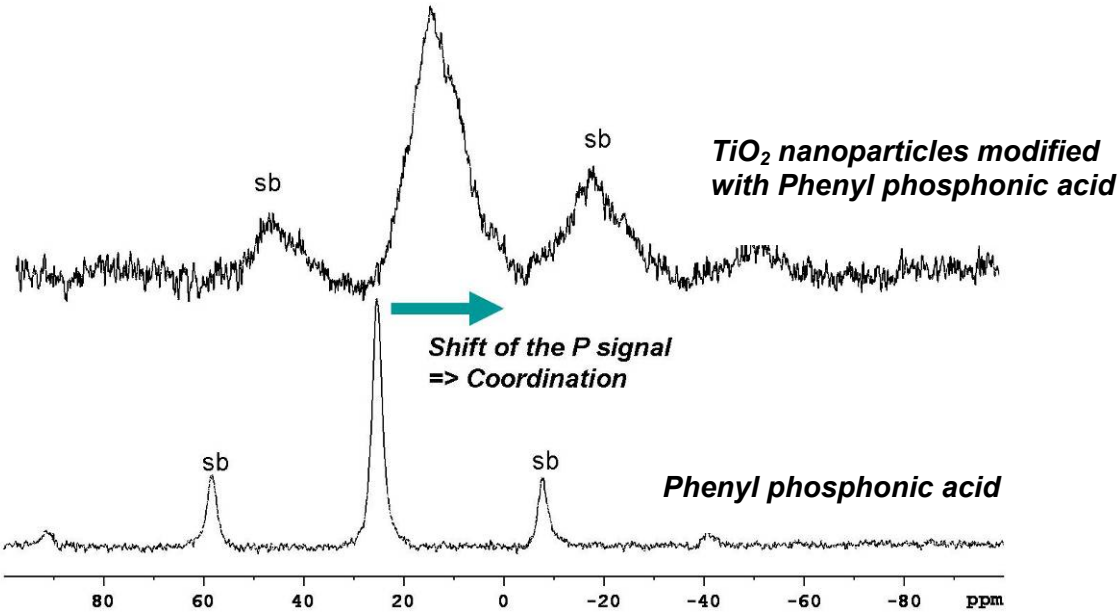

Figure 72. ^{31}P SP MAS NMR spectra of PPA and TiO_2 nanoparticles modified with PPA

In the case of PPA one resonance at 25.4 ppm was observed. This was shifted highfield to around 15.9 ppm for the modified particles. According to literature the resonance at 15 ppm is ascribed to tridentate phosphonate sites $PhP(OTi)_3$. This chemical shift is also found for phenylphosphonate/TiO_2 hybrids prepared by a sol-gel method.

Similar shifts were recorded in the cases of the organophosphorus coupling agents containing alkyl chains of various lengths terminated with methacrylate groups. Figure 73 shows such an example, when TiO_2 sol-gel nanoparticles were modified with MetC5PA-Et. The main resonance present at 37 ppm is very broad, similar as observed for PPA-modified TiO_2 nanoparticles, and can be assigned to tridentate phosphonates on the surface of the oxide particles. An additional shoulder can be observed at about 35 ppm which can be due to free ligand or to another bonding mode of the phosphonate groups, which is likely to be bidentate (PhP- $(OTi)_2OH$ sites) (Figure 73).

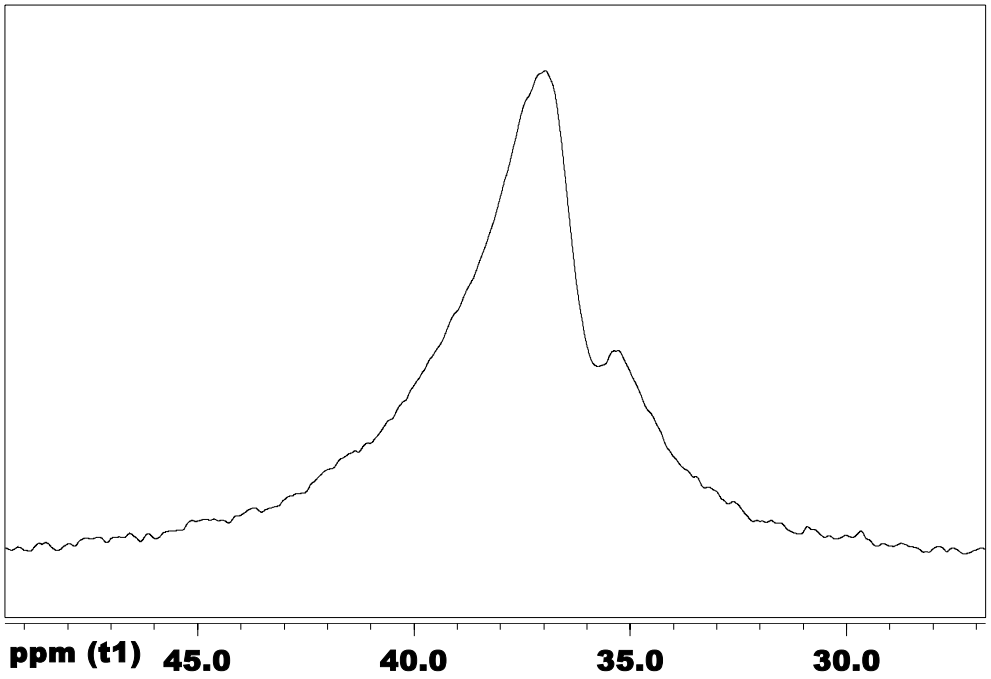

Figure 73. ^{31}P SP MAS NMR spectrum of the TiO_2@MetC5PA-Et modified nanoparticles

4.3.2 Thermogravimetric Analyses

Variation of the ligand concentration

The TG analyses in air of phenyl phosphonic acid–modified nanoparticles showed clearly that the surface-modification with phosphonates was successful. The TG analyses presented different curves for the modified particles compared with the unmodified TiO_2 particles (Figure 74). The unmodified sol-gel particles presented a main decomposition starting from 100°C with an onset temperature at around 150°C. This is assigned to adsorbed water and nitric acid on the particle surface, as well as to residual alkoxy groups that remained after the hydrolysis-condensation reactions. On the other hand, the modified particles present two decomposition steps. The first one is similar to the one observed in the cases of the pristine particles, with a main onset around 150°C due to the residues on the surface. The second decomposition step presents an onset temperature around 400° C and is due to the decomposition of the phenyl phosphonic acid groups bonded to the surface of the particles. This was revealed by TGA-MS measurements and corresponds to earlier literature reports[100]. Depending on the amount of ligand employed in the surface-modification reaction, the ratio between the first and the second onset varies. This results from the fact that a higher surface coverage with organophosphorus coupling agents will result in the removal of more nitrates or adsorbed water from the surface of the pristine particles, though in a decrease of the mass

loss due to their decomposition. Figure 74 and Table 7 show the dependence of the surface-coverage on the phenyl phosphonic acid concentration.

Table 7. Mass loss of different TiO_2 modified particles (0.2 g particles)

Sample	**Concentration of PPA for 0.2g TiO_2 (mol*10^{-3})**	**Amount of mass loss (310 - 600°C) (%)**
S212	0.312	10.2
S213	0.156	7.7
S214	0.0624	4.2
s221	0.624	13.77
S271	2	18.30

When looking at the TG plots, at a first sight one could say that by decreasing the concentration of the PPA the mass loss increases. The increase in the mass loss means a higher surface coverage with the PPA. But the overall mass loss is falsified by the fact that the particles have residual organics on their surface (residual alkoxides, adsorbed water and nitric acid on the surface). For this reason, the amount of phosphonate coupling agents covering the surface of the particles was calculated taking into account only the mass losses between 300 and 600 °C.

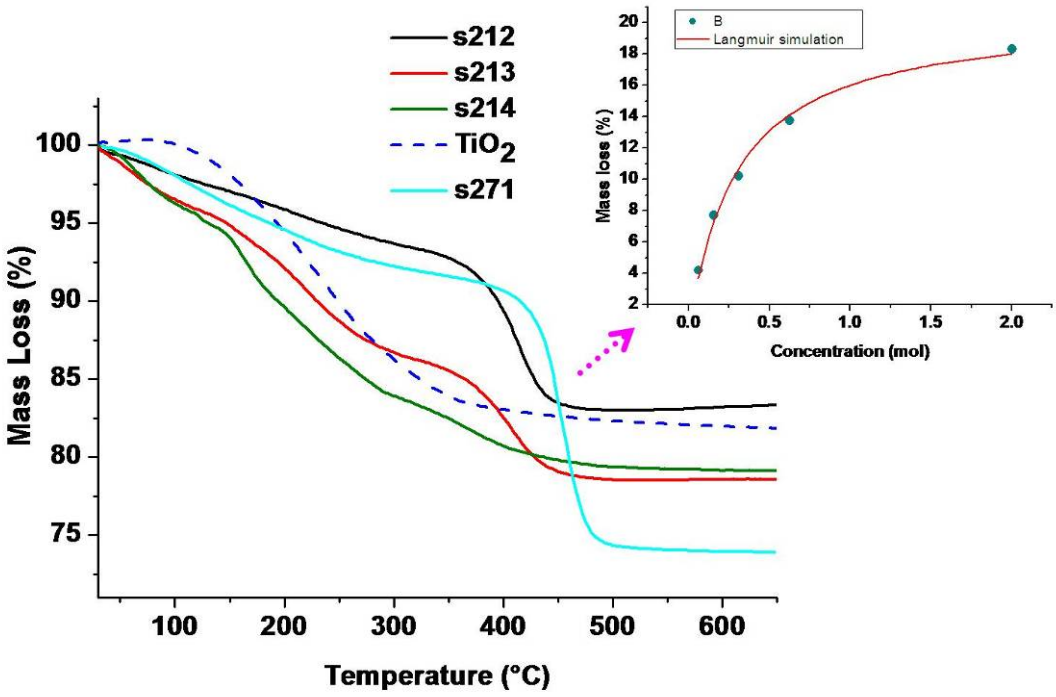

Figure 74. TGA plots of TiO_2 nanoparticles modified with different amounts of PPA (see Table 7). Inset: dependence of the amount of surface functionalization on the concentration of PPA

A result revealed by TGA measurements is that the amount of mass loss between 310 and 650 °C decreases with the decrease of the concentration of the phenyl phosphonic acids. When plotting the amount of mass loss against concentration of the organophosphorus coupling agent in the reaction mixture the dependence of the surface coverage amount to the phosphonate concentration used in the reaction is obtained. For concentrations of PPA up to 0.5 mol the surface coverage increases approximately linear with the increase of the concentration until a concentration of 2 mols PPA, where a kind of saturation is reached. Up to this concentrations the mass loss (surface coverage) can be also fitted to a Langmuir simulation[201]. Physically this means the formation of a complete monolayer at concentrations of about 2 mols PPA in the reaction mixture. However these results are more qualitatively and are not very accurate because the onset temperatures used for this comparison are strongly influenced by the slopes of the tangents before and after the event. Also for a real Langmuir fit equilibrium data have to be considered, which was not the case for the presented example. What it can definitely be detected is that by the increase of the ligand concentration the surface coverage increases up to a concentration where it reaches a saturation sate, most likely

due to complete monolayer coverage. The mass loss due to the more volatile residues (up to 200 °C) falsifies the real value of the degradation of the main effect due to the decomposition of PPA. Hence, by controlling the phosphonates concentration in the reaction mixture, the amount of surface coverage can be tailored, up to a saturation value.

Variation of the Particle Size

The amount of surface-coverage depends as well on the size of the particles. In this study TGA was used to investigate the dependence of the surface-coverage to the size of the particles. In this model studies a PPA solution was used with a constant concentration (0.624 mmol/L). The amount of surface coverage was calculated from the mass loss between 310 and 650 °C, on the same basis as before. Two types of sol-gel particles were used, showing diameters of 7 respectively 12 nm, and the commercially P25, with diameters of 21 nm (Figure 75 and Table 8). When particles with different sizes were compared small differences in the amount of surface-functionalization were observed.

Table 8. Variation of the amount of surface functionalization with the particle size (same concentration of the PPA)

Sample	**Diameter (nm)**	**Mass loss (310 – 600°C) (%)**
TiO_2	7 nm	10.2
TiO_2	12 nm	7.7
TiO_2 – P25	21 nm	4.2

When using TiO_2 P25 a mass loss of only around 4% was observed. As mentioned before, the particles are highly aggregated in solution and difficult to disperse. Higher amounts of surface-coverage were obtained with the sol-gel particles.

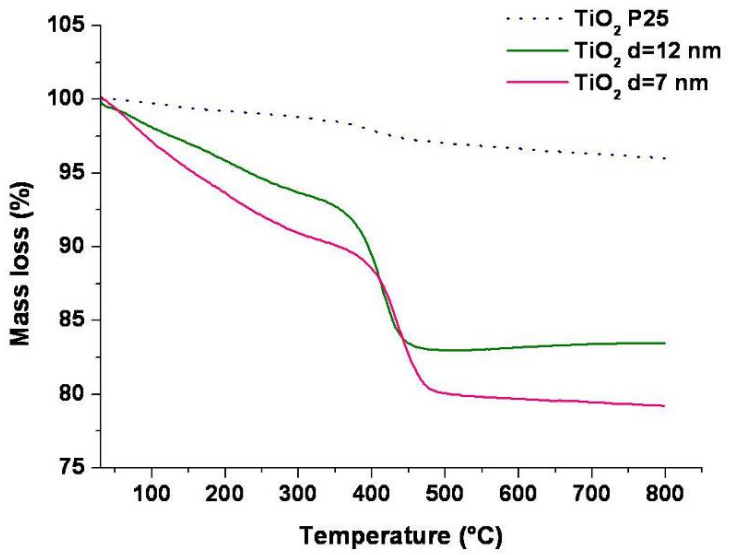

Figure 75. TGA plots of different TiO_2 nanoparticles modified with PPA

A small difference was detected between the two sol-gel nanoparticle samples. Expectably, the mass loss decreases with increasing particle sizes. This is due to the fact that small particles have a higher surface area than larger particles, so higher amount of the ligand can be bonded on the surface.

4.3.3. Dynamic Light Scattering Studies

Similar to the cases of the surface-modification of the P25 particles, light scattering techniques were used to investigate the behavior upon surface modification of the sol-gel particles in liquid state as well as the evolution of their hydrodynamic radius. In Figure 76 there are presented the size distributions of various modified sol-gel TiO_2 nanoparticles having a diameter of 5 nm ± 0.18 with organophosphorus ligands.

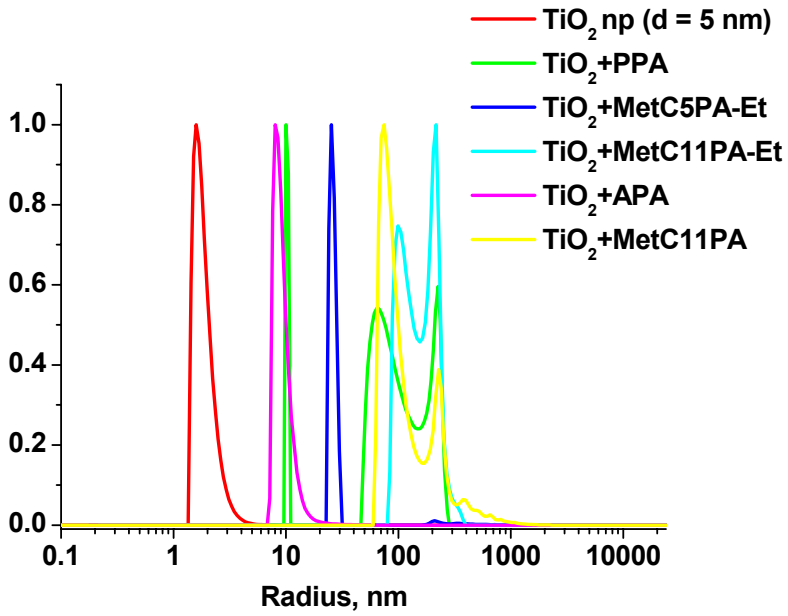

Figure 76. DLS distribution of various organophosphorus surface-modified TiO_2 nanoparticles

The DLS showed two distributions after the particles redispersion for the case of PPA modified TiO_2 particles. After the mass weighting of the particles 12% presented small radii (11 nm ± 0.12) while the rest was represented by larger particles due to agglomeration (between 48 nm and 270 nm). Allyl phosphonic acid modified TiO_2 presented only particles having radii of 9.4 nm ± 0.20 with a large distribution. Also the MetC5PA-Et modified particles had small radii, of about 28 nm ± 0.28 with narrow polydispersity. The situation changed drastically when longer alkyl chain phosphonates were used for the modification of the sol-gel TiO_2 nanoparticles. DLS results showed that in the case of the particles modified with MetC11PA-Et only one broad distribution function could be observed, having two corresponding peaks. The particles modified with the corresponding acids (MetC1PA) showed a similar behavior. One explanation of this behavior is that longer chain phosphonates induce a higher agglomeration of the particles rather than their small chain homologues which can be based on some self-aggregation phenomena comparable with the formation of self-assembly monolayers[193]. It was also shown that densely packed monolayers of single-chain surfactants often tend to form crystalline domains. The chains' conformational freedom is greatly restricted within the compact monolayer, with site densities nearly equal to their molecular cross section. The surfactant layers thus behave as if exposed to poor solvent conditions, and experience little or no loss of entropy when approached by another surface[202].

4.3.4. Morphological Investigations

TEM

TEM was used to investigate the morphology of the modified nanoparticles. The samples measured in TEM were prepared after the drying of the particles and redispersion in ethanol. When using an excess of PPA (0.312 mmol / 0.2 g particles), the TEM micrograph of the obtained modified particles showed the presence of small spherical nanoparticles together with larger aggregates (Figure 77). However the latter also consisted of small nanoparticles. Most likely these aggregates were formed during the solvent evaporation from the TEM grid. The measurement of the particles present on the TEM micrographs demonstrated that they have mean diameters of about 10 nm, with a very narrow distribution which fits perfectly with the results obtained from the DLS studies. The surface modification did not disturb the crystallinity of the particles. The dark field images recorded in TEM showed that the particles were still crystalline (Figure 77).

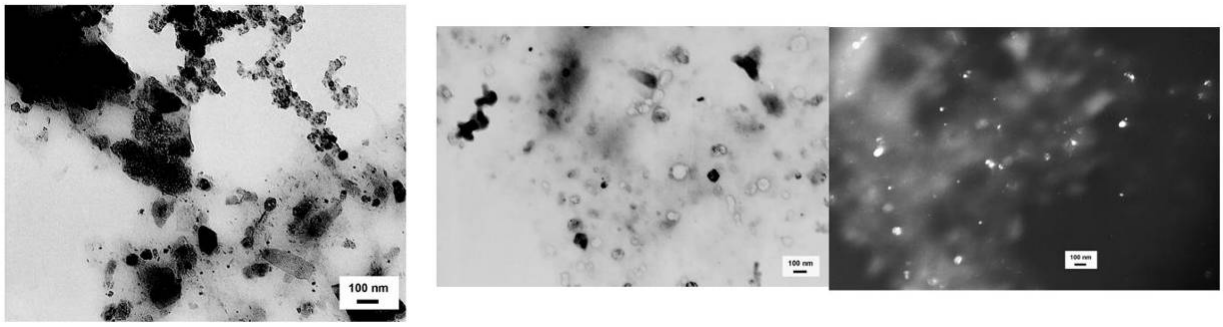

Figure 77. TEM analyses of PPA-modified TiO_2 nanoparticles

A similar situation was observed even when a higher excess of PPA was used (2 mmol/ 0.2 g particles). The TEM micrographs have proven the presence of small monodisperse nanoparticles showing a mean diameter of about 10 nm, either as separate entities or agglomerates (Figure 78). Again the dark field images have proven the crystallinity of the particles.

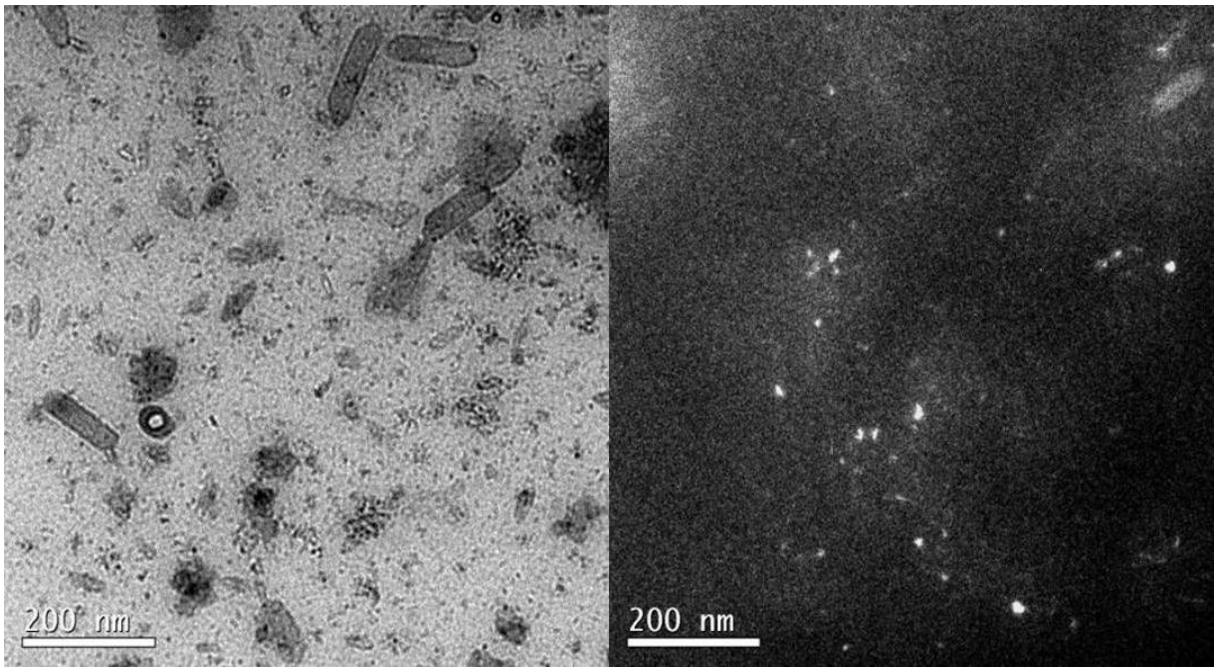

Figure 78. TEM analyses of PPA-modified TiO_2 nanoparticles

SEM

Further information about the surface modification of the sol-gel nanoparticles with organophosphorus ligands was provided by the SEM and EDX measurements. The dried powders were deposited on a sample holder and sputtered with gold for better conductivity. In Figure 79 one example of the TiO_2 sol-gel particles modified with MetC11PA is given. In this case the SEM images clearly revealed the presence of spherical nanoparticles confirming the TEM analysis. The approximate diameter of the particles was around 10-20 nm, with a narrow size distribution. No larger particles were detected. The EDX analyses revealed the presence of the Ti and O specific bands. Also the specific band of P was detected. Due to the presence of gold on the surface of the particles no quantification could be carried out because the peak of P and gold interfering with each other. It is important to mention that the relative intensity of the P band in the case of the modified sol-gel anatase particles was five times higher than for the same system using the commercially available Degussa P25 particles. This confirms the TG analysis and can be explained by the following two aspects:

- the sol-gel particles have smaller sizes than their commercially available homologues, Degussa P25, which implies a higher surface area and thus, a higher amount of ligands can be attached to the surface of the particles;
- the surface of the sol-gel particles has much more residual OH and O^{i}Pr groups from the sol-gel process which can further condensate with the P-OH and P-OEt groups of the phosphonates.

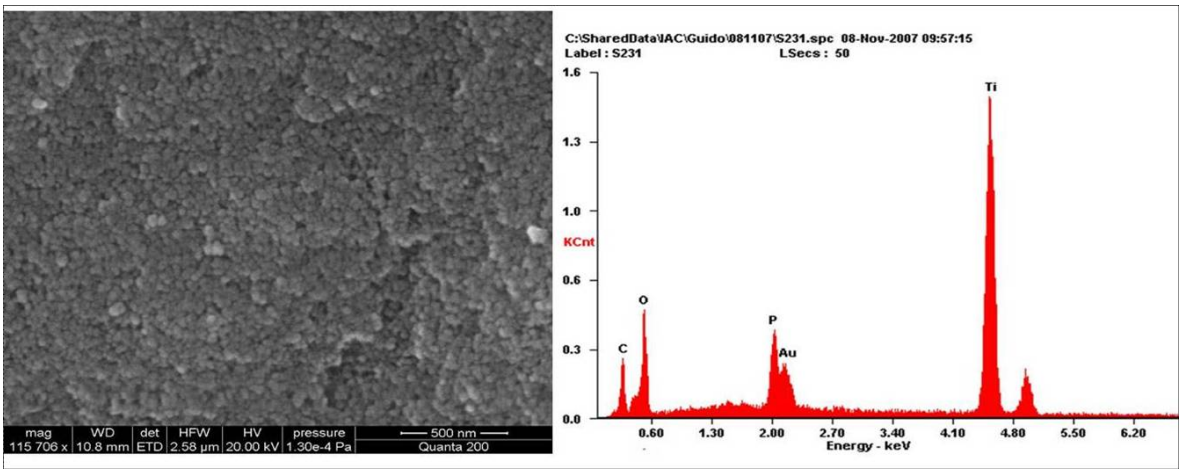

Figure 79. SEM and EDX analysis of TiO_2 sol-gel nanoparticles modified with MetC11PA-Et

4.3.5. Photocatalytic Activity of the Sol-Gel TiO_2 Nanoparticles

The photocatalytic activity of the sol-gel synthesized TiO_2 nanoparticles was evaluated by the decomposition of MB in water solutions (20 μM), similar as reported for the P25 particles. Again, the intensity of the absorbance band of MB at 665 nm was taken as a measure of the residual concentration of the MB dye. In Figure 80 the decrease of the MB concentration measured by UV/Vis absorbance of the specific MB band is presented.

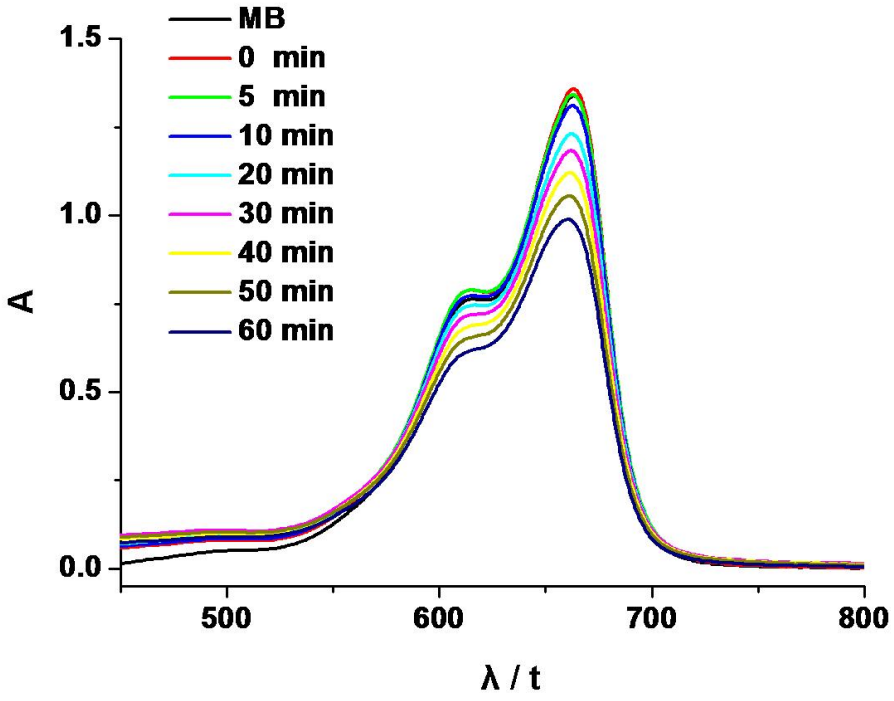

Figure 80. UV-Vis absorption spectra of the MB solution at different time intervals after the filtration of the heterogeneous solution

The photocatalytic studies showed that there is a decrease in the main absorbance band of the MB (665 nm) after irradiation with UV light. However, the efficiency of the sol-gel particles (decrease of the MB absorption band after 60 min) in the photocatalytic decomposition of the MB is considerably lower compared the Degussa P25 particles (Chapter 4.2.5.).

The reason of this behavior can be due to the difference in the absorbance of the MB on the particles surface compared to the Degussa P25 particles. As shown before, the surface of the sol-gel particles is covered with residual alkoxides and adsorbed water and nitric acid, which can hinder the adsorption of the dye on the particle surface. For this reason the particles were calcined at different temperatures and their photocatalytic activity was compared (Figure 81). Comparing the reactivity of the sol-gel particles it can be observed that by increasing the calcination temperature the photocatalytic activity increases. The maximum is reached for a calcination temperature of 400°C. Above this temperature, the activity shows no further enhancement, reaching saturation. The increase in the photocatalytic activity can be explained by the releasing of the adsorbed species on the particles surface. This leaves a larger area for the adsorption of the dye, which explains the increase in the photocatalytic activity.

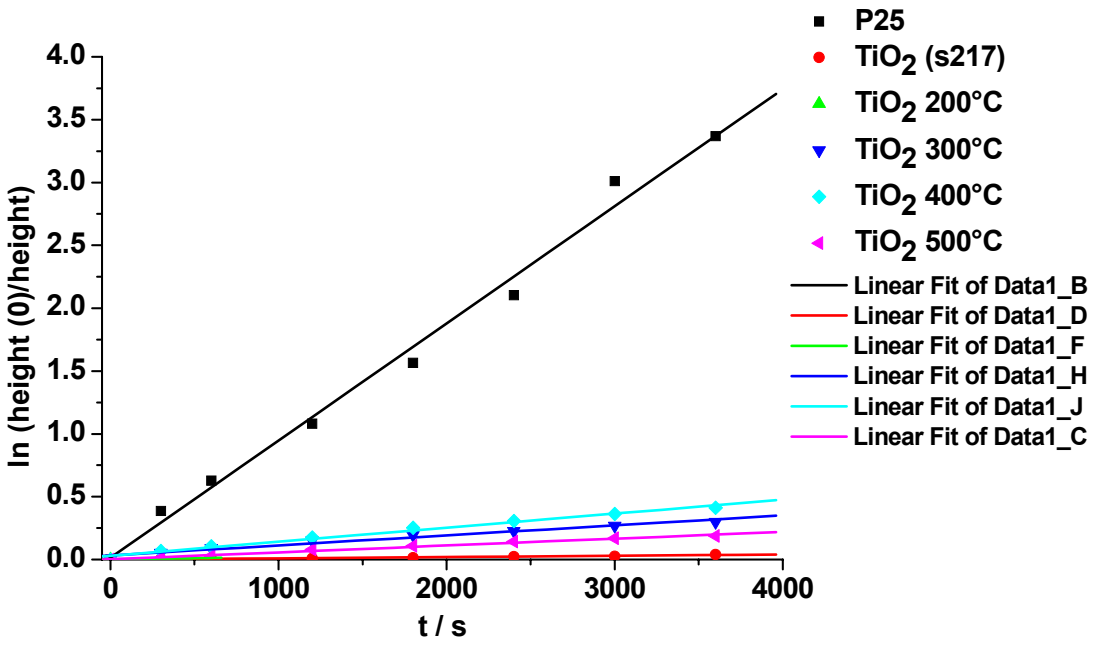

Figure 81. The photocatalytic activity of various TiO_2 (sol-gel) nanoparticles calcined at various temperatures as a function of the concentration of methylene blue

The surface-modified nanoparticles were also investigated in the photocatalytic decomposition of the methylene blue, similar as reported for the modified Degussa P25. The plots could still be fitted to first-order kinetics (Figure 82). Contrary to the Degussa P25 cases, when modifying the surface of the sol-gel TiO_2 nanoparticles with phosphonates, an increase in the photocatalytic activity was observed. As shown before, the surface of the sol-gel particles is covered with residual alkoxides, adsorbed water and nitric acid, which can hinder the adsorption of the dye on the particle surface. This leads to lower yields of the photocatalytic degradation of the MB. However, by the modification with phosphonates there is a release of the nitrates and adsorbed water, which allows a better adsorption of the dye, in spite of the surface-modification with phosphonates, which should decrease the available pristine surface of the particles. This was also proven by comparing the two samples modified with PPA, s213 and s214. The only difference between the two of them is the concentration of the ligand used for the surface-modification, $0.156*10^{-3}$ mol/0.2 g particles in the case of s213 and $0.062*10^{-3}$ mol/0.2 g particles for s214. There is a considerable increase in the photocatalytic degradation of methylene blue with increasing the amount of phosphonates bonded to the particles' surface (s213 compared to s214).

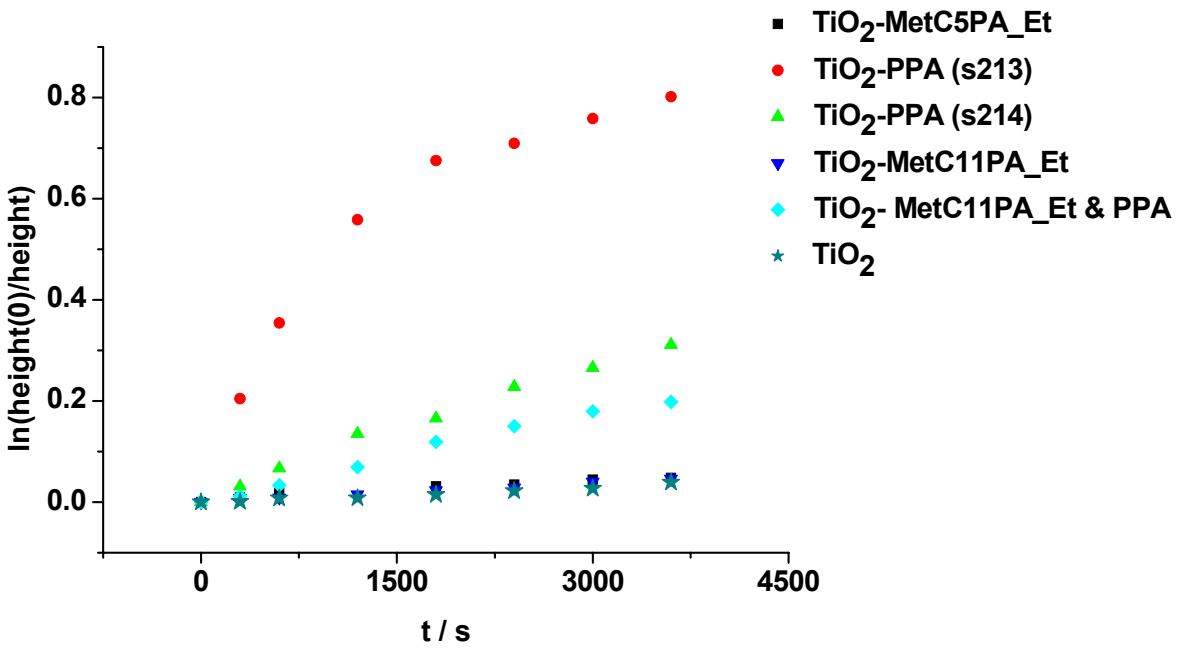

Figure 82. The photocatalytic activity of various TiO_2 (sol-gel) surface modified nanoparticles as a function of the concentration of methylene blue

Another reason for the lower photocatalytic activity of the sol-gel particles compared to the commercially available P25 could be linked to the different crystallinity of the two types of

particles. As mentioned, the Degussa P25 consists of a mixture of about 87 % anatase and 13 % rutile. The combination of the two crystalline phases offers them a synergetic effect which is responsible for the enhanced photoactivity. On the other hand the sol-gel particles consist of only anatase phase which can explain the lower activity in the degradation of methylene blue.

4.4. Synthesis of Janus Nanoparticles

One of the main goals of the research carried out was the anisotropical surface-functionalization of TiO_2 nanoparticles. However, this is impossible when the surface-functionalization is carried out in an usual suspension because no differentiation between different parts of the particle surface is obtained. Oil-in-water or water-in-oil emulsions offer the possibility of having two phases in one.

Colloidal particles are often used as stabilizers in oil-in-water or water-in-oil emulsions[121] for applications in various industries like cosmetics, food, agrochemical or paint. As presented in the Introduction part, when an oil (solvent) is mixed with a water phase containing nanometer sized particles, these colloids will tend to create a stabilizing layer at the interface between the two immiscible phases, namely water and oil. Among other types of solid stabilizers, metal oxide nanoparticles were seldom used as stabilizers for Pickering emulsions[125, 136-139].

A TiO_2-stabilized Pickering emulsion containing the organophosphorus ligand in one of the two phases, e.g. the oil or the water phase, would represent the ideal environment for the formation of the anisotropically surface modified TiO_2 nanoparticles. Such a stable emulsion would allow the attachment of the ligand on only one side of the anatase particles, protecting the other side from photocatalytic decomposition.

4.4.1. Formation of Stable Pickering Emulsions

As mentioned before, Pickering emulsions are o/w or w/o emulsions stabilized by solid particles. The formation of the Pickering emulsions can be represented by Scheme 14. When the oil solvent is mixed with the water phase containing TiO_2 nanoparticles, the colloids form a layer at the interface between the two immiscible phases. It was shown that the efficiency of the colloids in stabilizing oil-water emulsions depends on factors like particle size and shape, inter-particle interactions and the wettability of the particles by both of the liquids.[125, 126]

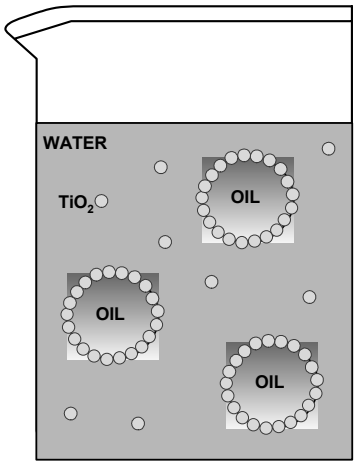

Scheme 14. Representation of the self-assembly of solid nanoparticles at the water – oil interface

4.4.1.1 Synthesis of TiO_2-Stabilized Pickering Emulsions

The self-synthesized sol-gel TiO_2 or the commercially available TiO_2 P25 Degussa nanoparticles were applied as stabilizers for the preparation of o/w emulsions. The organophospourus coupling agents are soluble in apolar organic solvents like hexane, cyclohexane, toluene, so it would stay in the oil phase of an emulsion. Furthermore, the methacrylic double bonds could be copolymerized inside the emulsion droplet while the phosphonate functionality would coordinate to the TiO_2 stabilizing particles, fixing this Pickering architecture.

Typical Pickering emulsions were prepared from cyclohexane, hexane or toluene with the organophosphorus molecules in the oil phase and H_2O dispersions of TiO_2 nanoparticles as the water phase (Figure 3). The metal oxides were acting as surfactants for these emulsions. The emulsions were generally formed from volume fractions of 20% oil and 80% aqueous sol of particles and contained between 0.125 and 2 wt.% TiO_2 nanoparticles. The emulsions were prepared by dropwise addition of the oil phase to an aqueous sol containing the particles under vigorous stirring using an UltraTurrax at 20000 rpm for 20 minutes. The pH was varied between 1 and 6.

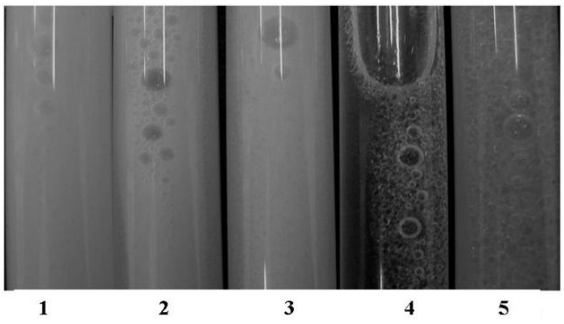

Sample	pH	Conductivity	Remarks
1	5.5	4.48 µS/cm	TiO_2 21 nm water/toluene
2	5.21	2.44 µS/cm	TiO_2 21 nm Water/Cyclohexane
3	5.83	57 mS/cm	1 with 1M NaCl
4	2.37	667 µS/cm	TiO_2 8 nm
5	3.12	248 µS/cm	TiO_2 42 nm

Figure 83. Series of various Pickering emulsions stabilized by TiO_2 nanoparticles (Degussa P25 or sol-gel synthesized)

An image and a microscope image of a Pickering emulsion stabilized by TiO_2 P25 particles are presented in Figure 84. One can see clearly that the oil droplets were separated and that they exhibit diameters ranging from 50 to 500 µm.

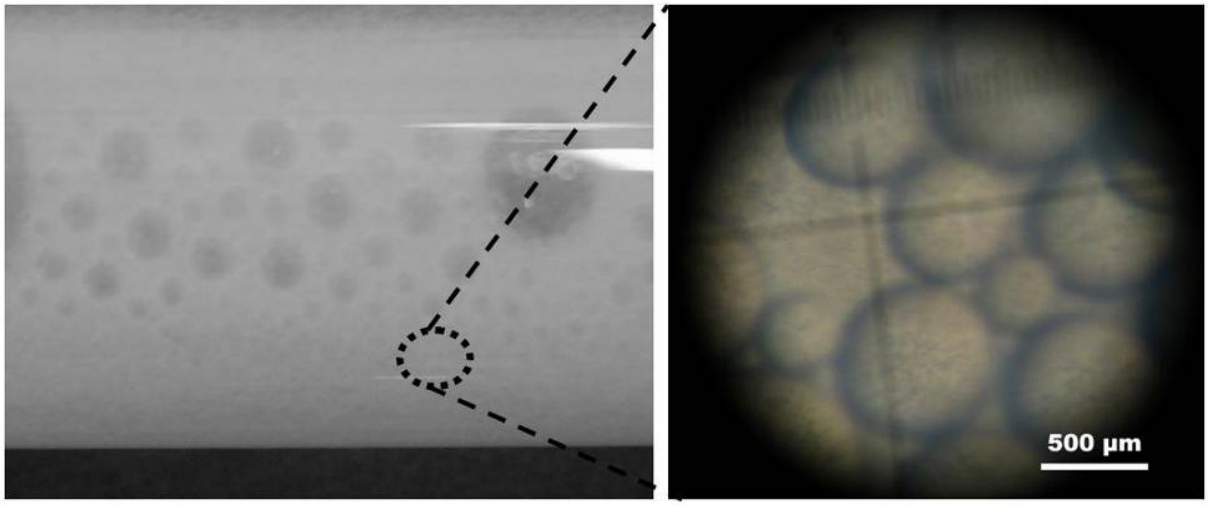

Figure 84. Characteristic photograph and microscope photograph of a Pickering emulsion stabilized by 0.5 wt% TiO_2 P25

4.4.1.2. Influence of the NaCl Concentration and of the pH on the Emulsion Stability

As reported in literature, the addition of a salt can have an important influence on the type of the emulsion (w/o or o/w) formed, the flocculation of the particles, the stability of the emulsion, and the inversion of the emulsion. *Allen and Matijevic*[203] analyzed emulsions stabilized by SiO_2 Ludox® sols with diameters of 15 nm. The isoelectric point and the point of zero charge of silica are both at pH 2, i.e. above this pH the silica particles are negatively charged. When NaCl was used as an electrolyte, the emulsions remained stable up to the

solubility limit of NaCl (around 5 M) at pH values between 2 and 5. Above pH 6, the so-called 'critical coagulation concentration' decreased with increasing pH.

Binks et al.[138] reported that the stability of the oil-in-water emulsions stabilized by fumed silica oxide particles can be controlled by the pH or by the addition of simple electrolytes. The stability of emulsions containing NaCl decreased once the particles were flocculated by the salt.

In this study various emulsions (cyclohexane/water in 20:80 vol. %) were prepared with TiO_2 (P25) nanoparticles as stabilizer. NaCl was used in concentrations of 0.5, 1, 1.5, 2 M to investigate the stability of the emulsions. The pH was kept constant at 3.5. The isoelectric point of Degussa P25 is around 6 while the determined experimental point of zero charge of P25 is 6.25[84, 204]. Conductivity can be employed to determine the type of the emulsion. In all cases, the conductivities of the emulsions are high, indicating that the emulsions are of the o/w type and no inversion to w/o was observed with increasing the salt concentration (Figure 85, left). As expected, by the addition of an electrolyte, the conductivity was increasing. The dependence of conductivity to the amount of NaCl used follows a linear function. In the first stages no flocculation occurred and the emulsions were stable even at high salt content (2M). After 24 hours however some extent of flocculation was detected but no precipitation of the particles was observed.

The pH was varied from 1.25 to 5.5 (Figure 85, right) to examine the emulsion stability considering that a better dispersion of the particles should be possible beneath or above the isoelectric point of TiO_2. The influence of the pH on the emulsion stability was done by keeping the salt concentration constant at 0.5 M and varying the pH. We observed that at low pH values the conductivity was high, dropping fast with increasing pH. No flocculation was observed but partial precipitation of particles was detected after a few days. This can be the result of further condensation of active Ti-OH groups on the particle surfaces, considering that the particles are close to the point of zero charge and agglomeration can occur. However, 20% of the volume remained as stable Pickering emulsion.

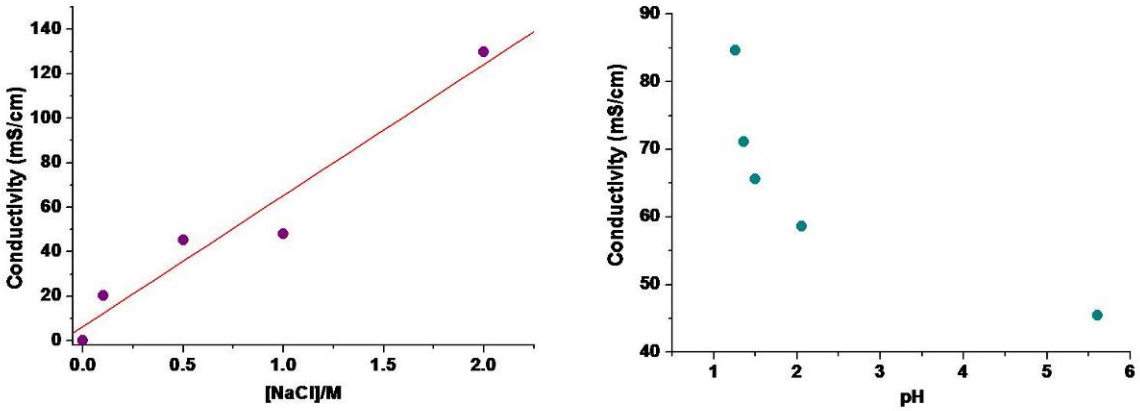

Figure 85. Conductivity of the emulsions depending of the salt concentration (left) and the conductivity of the emulsions depending on the pH (right)

4.4.2. Synthesis of Pickering Emulsions Having an Organophosphorus Coupling Agent in the Oil Phase

Pickering emulsions containing in the oil phase an additional organophosphorus ligand were prepared based on oil/H_2O mixtures (Scheme 15). The Pickering emulsions contained 1 wt % TiO_2 (self-synthesized or Degussa P25). The pH was maintained around 3 to be far from the point of zero charge and the isoelectric point of titania. The emulsions were formed from 10 ml H_2O sol of particles and various amounts of cyclohexane or toluene as the oil phase. Different phosphonates were used as additives, either as pure acids or as the alkyl esters.

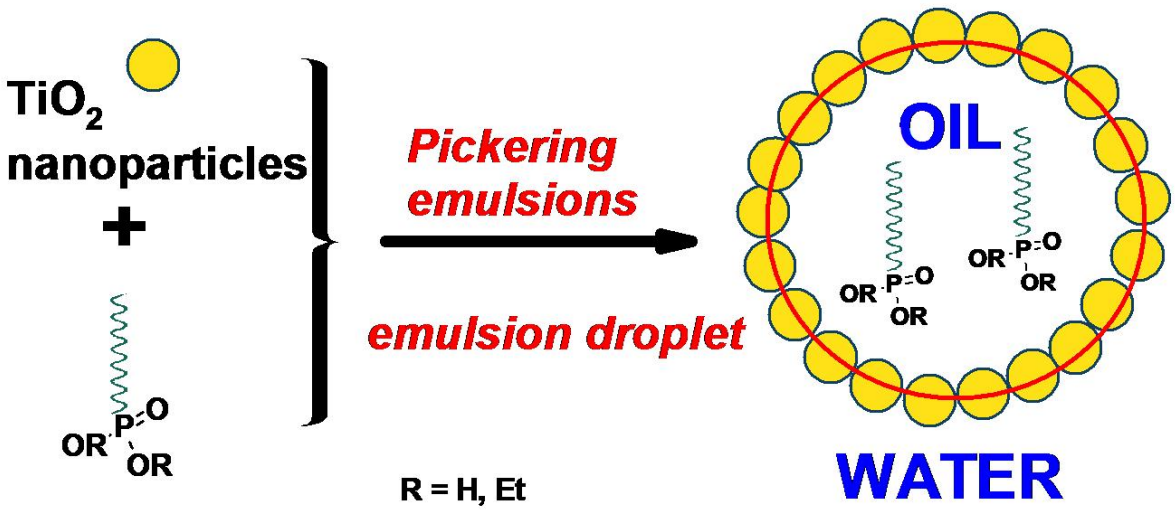

Scheme 15. Formation of Pickering emulsions containing an organophosphorus compound inside the emulsion droplet

The concentration of the ligand in the oil phase was the same used for the surface-functionalization in suspension ($1.5*10^{-3}$ mol/L). The emulsions were formed using an Ultraturrax at 20000 rpm for 15 min. The oil phase was added to the water sol during mixing. The particles were separated by centrifugation, dried and analyzed. For DLS measurements a few drops of the emulsion were further on diluted with water and then analyzed. Typical Pickering emulsions are presented in Table 9.

Sample	***TiO_2 H_2O 10 mL***	***Ligand (1.5*10^{-3} mol/L)***	***Oil (mL)***
Se234	**P25 – 21 nm**	**APA (iPr esters)**	**2.5 - cyclohexane**
Se235	**P25 – 21 nm**	**APA (iPr esters)**	**1 - cyclohexane**
Se236	**P25 – 21 nm**	**MetC5PA (Et esters)**	**2.5 - cyclohexane**
Se237	**P25 – 21 nm**	**MetC5PA (Et esters)**	**1 - cyclohexane**
Se241	**s227 – 5 nm**	**MetC5PA (Et esters)**	**2.5 - cyclohexane**
Se242	**s217 – 5 nm**	**MetC5PA (Et esters)**	**1 - cyclohexane**
Se243	**s227 – 5 nm**	**APA (iPr esters)**	**2.5 - cyclohexane**
Se244	**s217 – 5 nm**	**APA (iPr esters)**	**1 - cyclohexane**
Se245	**s225 – 8 nm**	**MetC5PA (Et esters)**	**2.5 - cyclohexane**
Se246	**s225 – 8 nm**	**MetC5PA (Et esters)**	**1.5 - cyclohexane**
Se247	**s225 – 8 nm**	**PyrenePA**	**3 - cyclohexane**
Se248	**s225 – 8 nm**	**DPA (Et esters)**	**2 - cyclohexane**
Se250	**s249 – 5.6 nm**	**MetC11PA (Et esters)**	**2.5 - toluene**
Se251	**s249 – 5.6 nm**	**MetC11PA (Et esters)**	**2.5 - toluene**
Se252	**s249 – 5.6 nm**	**DPA**	**2 - cyclohexane**
Se253	**s249 – 5.6 nm**	**DPA**	**2 - toluene**
Se254	**s249 – 5.6 nm**	**DPA**	**1 - toluene**
Se255	**s249 – 5.6 nm**	**DPA**	**1.5 - toluene**
Se256	**s249 – 5.6 nm**	**DPA (Et esters)**	**1.5 - cyclohexane**
Se257	**s249 – 5.6 nm**	**DPA (Et esters)**	**1 - cyclohexane**
Se258	**s249 – 5.6 nm**	**DPA (Et esters)**	**2.5 - cyclohexane**
Se259	**s249 – 5.6 nm**	**MetC5PA (Et esters)**	**2.5 - cyclohexane**

Tabel 9. Typical Pickering emulsions prepared from H_2O sol (10 ml, 1 wt.% TiO_2 nanoparticles) and various amounts of oil (cyclohexane or toluene)

4.4.3. Spectroscopic Studies of the Janus Particles

FT-IR

MetC5PA-Et was used for the anisotropic-surface-modification of TiO_2 nanoparticles. First question to be answered was if the phosphonates and phosphates attached to the surface similar as in the cases of modifications in typical suspensions. Different sol-gel TiO_2 nanoparticles and the commercially available Degussa P25 were used to stabilize Pickering emulsions having the MetC5PA-Et in the oil phase, and subsequently to result in anisotropically modified TiO_2 particles. The resulting emulsions containing the phosphonates in the oil phase were broken by dilution with water and centrifugation of the resulting suspension in order to separate the anisotropically surfaced-modified particles. The particles were dried and analyzed by FT-IR and solid state NMR. The FT-IR spectra obtained are presented in Figure 86.

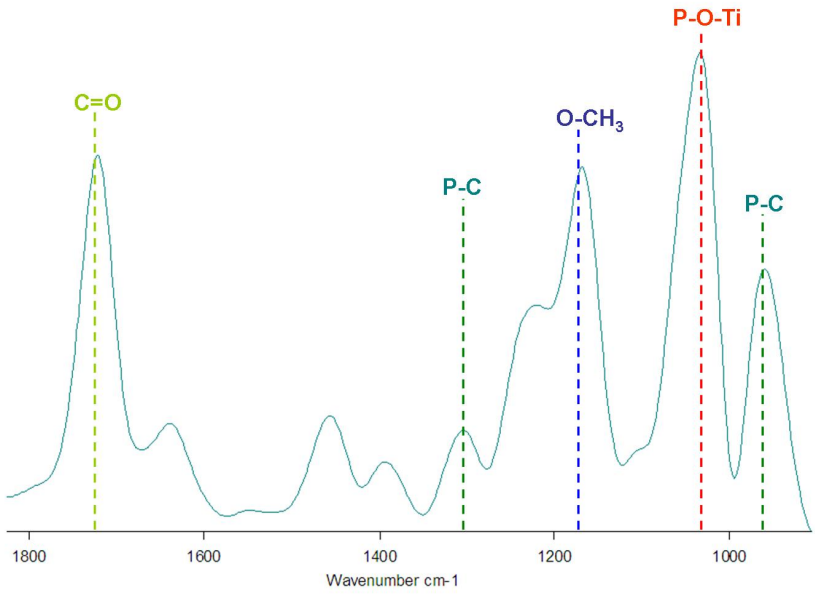

Figure 86. FT-IR analyses of TiO_2 nanoparticles (P25 - 21 nm) functionalized in a Pickering emulsion with MetC5PA-Et

The first important observation that can be drawn from the spectra is the fact that organic groups are present on the surface of the modified particles. The main characteristic of the surface modified particles, the presence of P-O-Ti is evidenced by the band between 1000 and 1100 cm^{-1}. This vibration is also observed in the similar cases when the particles were modified in solution using the same ligand. Another proof for the presence of organics on the surface of this particles is the presence of the C=O bands resulting from the methacrylic moieties of the ligands (1725 cm^{-1}). These facts are clear indications of the attachment of the

phosphonates on the nanoparticle surfaces. A second observation is that the P-C bond is present in all of the cases, proving that the phosphonate ligand was not decomposed.

Better FT-IR analyses were obtained using phosphonic acids instead of their alkyl esters, due to their higher reactivity. The FT-IR analysis obtained using DPA as organophosphorus coupling agent both in Pickering emulsion as well as in solution are presented in Figure 87.

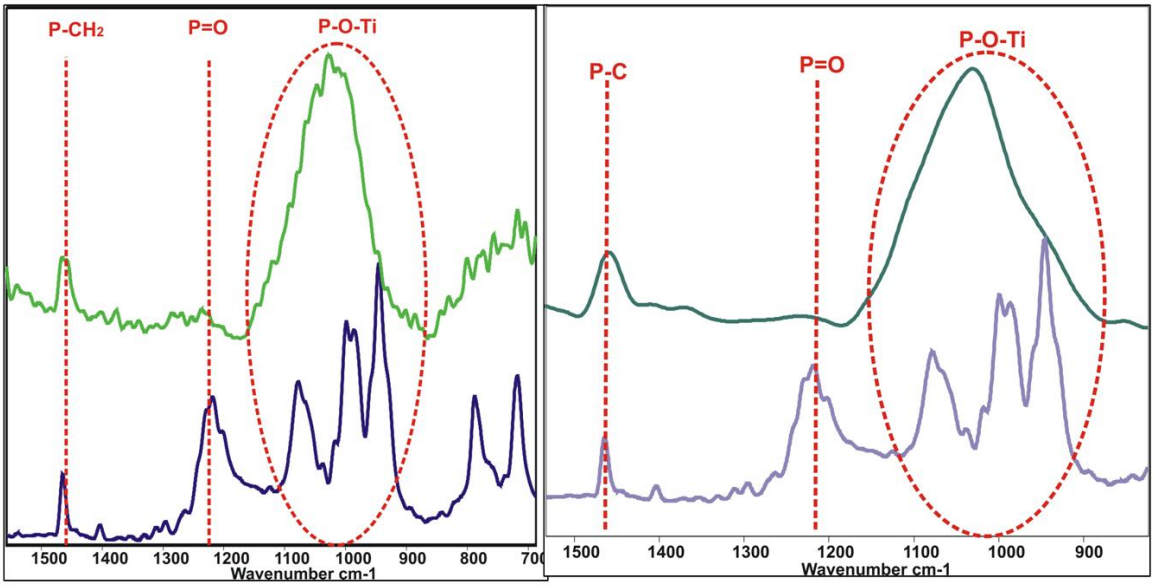

Figure 87. Left side. Top: TiO_2-DPA functionalized in Pickering emulsion, bottom: DPA. Right side. Top: TiO_2-DPA functionalized in solution, bottom: DPA

In both cases, the main characteristic of the surface modified particles, the presence of P-O-Ti is evidenced by the broad intense band between 900 and 1100 cm^{-1}. Similar for both spectra, the disappearance of the P=O band at 1218 cm^{-1} proves that the phosphonates act as tridentate ligands, in the same manner presented for the functionalization in suspension and in accordance with earlier literature reports[100]. Finally, the presence of the P-CH_2 bonds is evidenced by the band at 1465 cm^{-1}, proving that the phosphonate-carbon bond is not decomposed during the modification. The two cases are identical, which led to the conclusion that the coordination of the organophosphorus coupling agents to the TiO_2 surface in Pickering emulsion does not differ at all from the coordination in solution of the same ligands.

NMR

The ^{31}P MAS NMR spectra of both the free DPA and the Janus TiO_2-DPA are presented in Figure 88. In the case of DPA only one resonance is detected at 34.8 ppm. After the separation of the Pickering emulsion and isolation of the particles modified in the Pickering

emulsion, the signal is broadened and shifted highfield to 30 ppm, very similar as for the modification of the particle in suspension. Considering the disappearance of the P=O band in the FT-IR analysis, this resonance was ascribed this to tridentate phosphonate sites $C_{12}H_{25} - P(OTi)_3$.

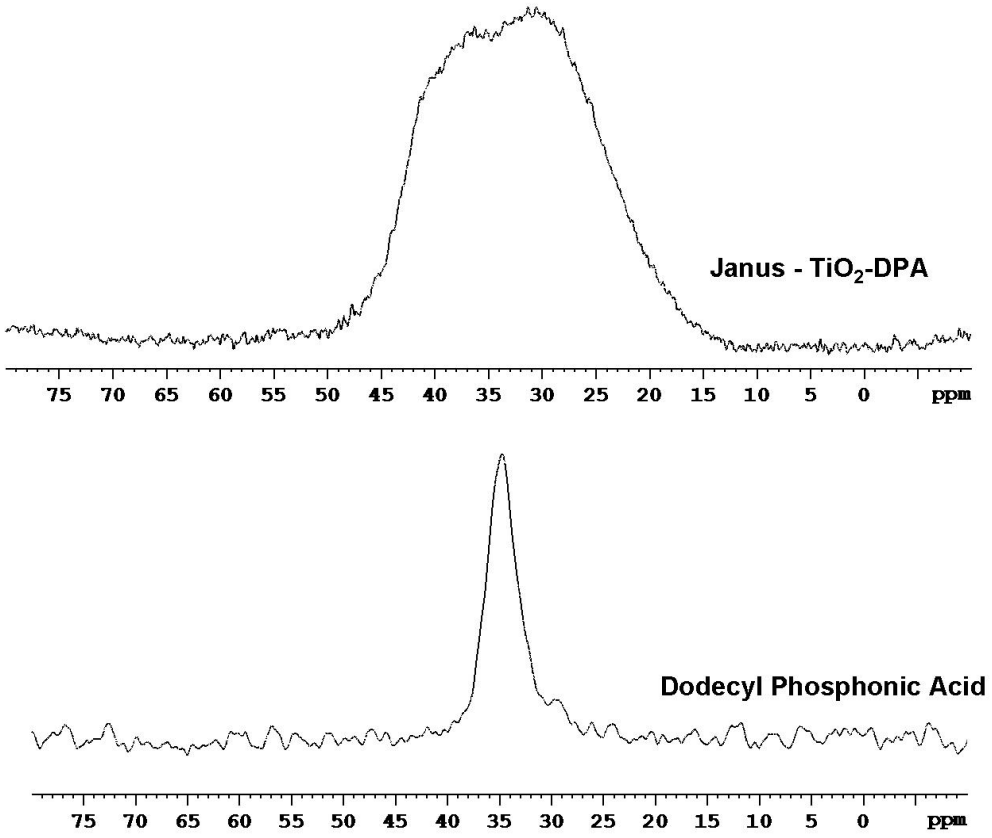

Figure 88. ^{31}P MAS NMR of the Janus TiO_2@DPA nanoparticles

4.4.4. Thermal Analyses

The TG analyses as the next logic step confirmed the presence of organic groups on the particles surfaces. In Figure 89 the results obtained for different particles modified in Pickering emulsion using MetC5PA-Et are presented (s237: TiO_2 P25 d = 21; s241, s242: d = 5 nm).

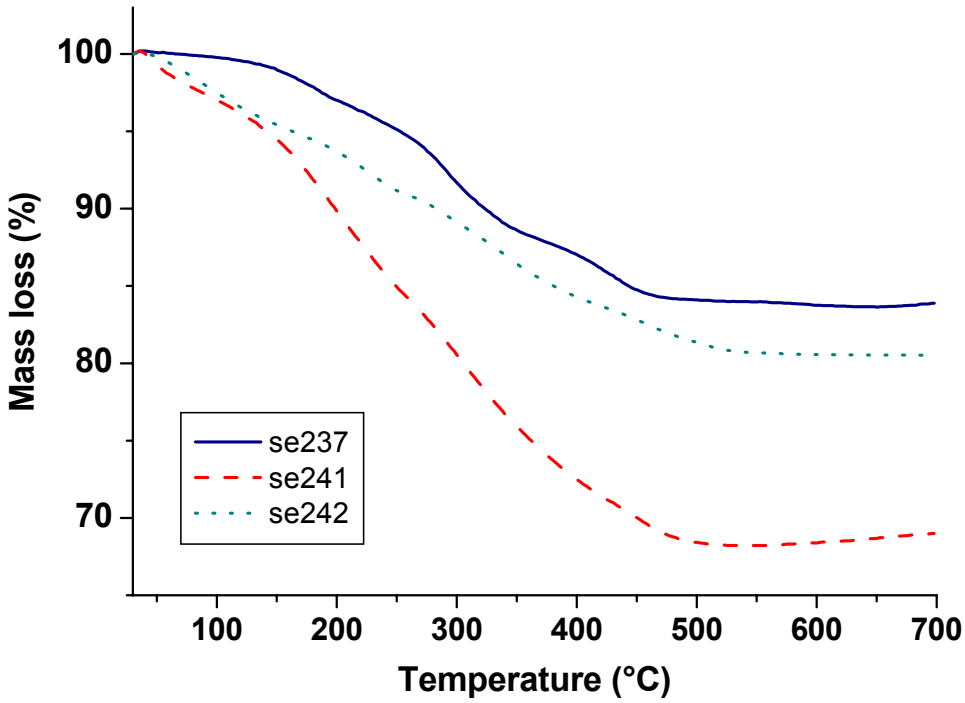

Figure 89. TG analyses of the TiO_2 nanoparticles functionalized in Pickering emulsions with MetC5PA-Et

The first observation is that there are three main onset temperatures, no matter which sample is discussed. The first one is located at around 150°C and is most likely due to adsorbed water that desorbs from the surface of the particles at elevated temperatures. The second one shows an onset at around 280°C and appears also in theTGA of the pure ligand. This is most likely due to the decomposition of the alkyl moieties of the ligand. The third onset shows a temperature of about 410°C (also present in the pure ligand) that can be assigned to the decomposition of the phosphonates and the formation of PO_x species on the surface of the particles. Another important observation is that there is a significant increase in the amount of organics from TiO_2 P25 to the sol-gel particles (s237 compared to s241, s242). This cannot be totally quantified due to the falsifying induced by the amounts of volatiles (H_2O adsorbed on the particles' surface). The increase in the amount of the phosphonate bonded to the TiO_2 surface is due to smaller particle size of the sol-gel particles (5 - 6 nm diameter compared to 21 nm diameter for the Degussa P25) which induces a higher surface area. By decreasing the amount of the oil phase apparently the amount of surface coverage decreases as well (s241 compared to s242).

The amounts of surface coverage calculated from the TGA of the particles modified in Pickering emulsions were compared with the ones obtained when the modification was employed in suspension. Figure 90 presents the results obtained when MetC5PA-Et was used for the modification of sol-gel TiO_2 nanoparticles with approximately 8 nm ± 0.20 diameters, both in Pickering emulsion and in suspension. Between 30 °C and 170 °C both of the curves have a similar shape, due to the decomposition of volatiles. As mentioned before, the onset between 200 and 420 °C can be assigned to the decomposition of the phosphonate and appears well resolved for both of the samples. However, there is a clear decrease of the particles coverage when the modification is carried out in Pickering emulsion compared to the samples modified in usual suspension (about 18% mass loss). The smaller amount of phosphonate presented in the case of the Pickering emulsion modification is an indirect indication that the particles could be anisotropically surface modified.

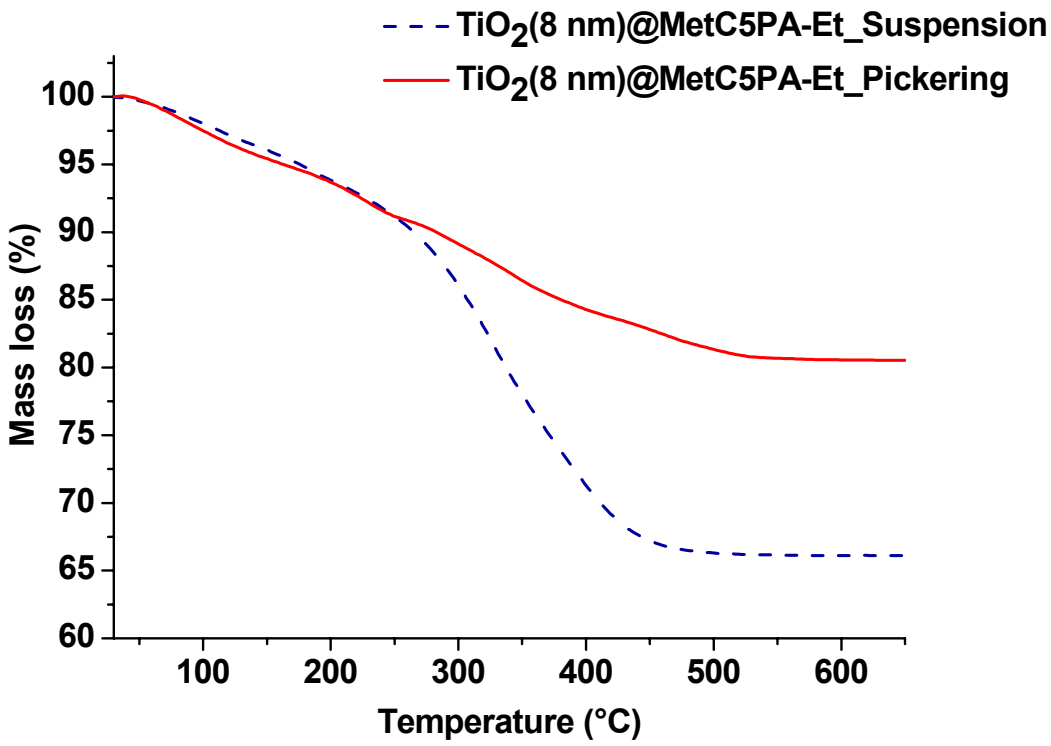

Figure 90. TG analysis of the TiO_2 nanoparticles functionalized in Pickering emulsions and in suspension with MetC5PA-Et

Similar results were obtained with phosphonic acids. Figure 91 presents the results obtained when DPA was used for the modification of sol-gel TiO_2 nanoparticles with 8 nm diameters, both in Pickering emulsion and in suspension. Both of the curves presented one onset between 30 °C and 150 °C which is most likely due to the decomposition of volatiles. A second onset

at 280 °C was again presented in both of the cases. This can be assigned to the decomposition of the phosphonate and has the same shape for both of the samples. However, there is a clear decrease of the particles coverage when the modification is carried out in Pickering emulsion compared to the samples modified in usual suspension. For the sample modified in suspension the residual mass at 700 °C after the decomposition of the organics is about 65 %, while for the sample modified using a Pickering emulsion the residual mass is about 72.5 %.

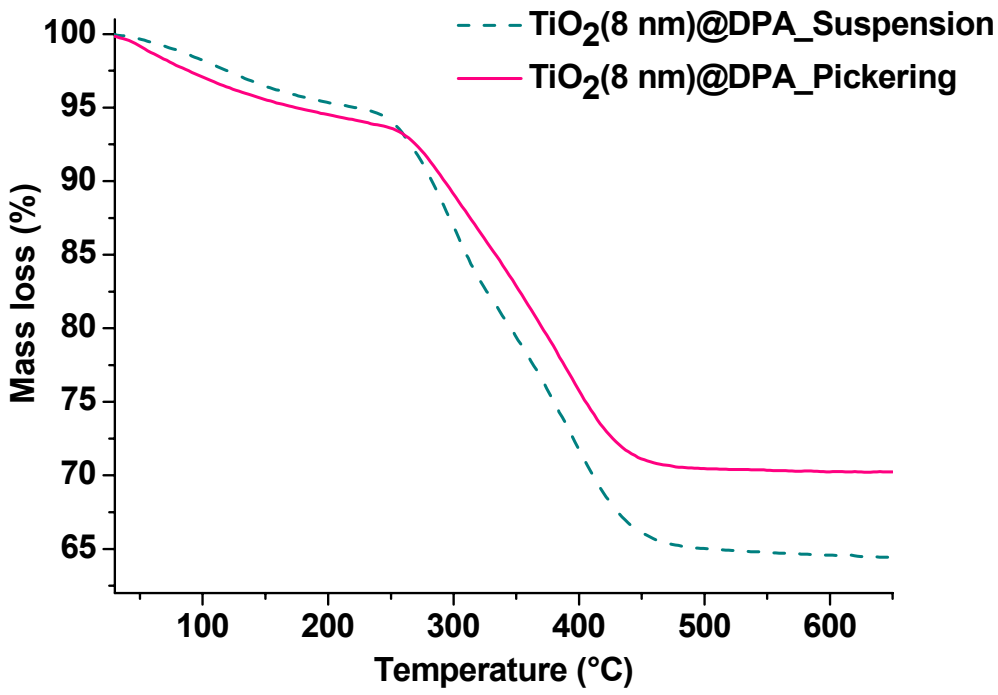

Figure 91. TG analysis of the TiO_2 nanoparticles functionalized in Pickering emulsions and in suspension with DPA

These results showed that the surface-modification of the particles using Pickering emulsions leads to lower amounts of organophosphorus coupling agents attached to the surface. This could be a first indirect proof of the formation of the desired Janus morphologies.

4.4.5. Dynamic Light Scattering Studies

Further characterization of the Pickering emulsions was carried out using light scattering techniques. Two drops of the emulsion were diluted with 2 mL of water (the continuous phase) and then analyzed by DLS. The investigations of the Pickering emulsion immediately after the dilution with the continuous phase showed the presence of a new monomodal narrow

distribution with a diameter of 3 µm ± 0.16. This new distribution has a completely different radius than the sol-gel synthesized TiO_2 nanoparticles, where a size distribution of about 5 nm ± 0.18 diameter was observed. The formed emulsion was stable up to three days and then the turbid emulsion became a clear suspension proving the dissolution of the oil droplets. When measuring again this solution by light scattering, the presence of a narrow size distribution corresponding to nanoparticles displacing a diameter of 18.5 nm ± 0.06 in a weight ratio of 62 % (after mass weight analysis) was observed. Agglomerates were also detected in small amounts (28 % after mass weight analysis). However, no trace of the initial distribution at 3 µm (Figure 92) corresponding to the signal obtained by measuring the initial Pickering emulsion could be detected. This leads to the conclusion that the emulsion is broken and the solution contains a new type of particles formed by the surface modification of the initial particles with phosphonates. Most likely these particles are formed by the anisotropical surface-functionalization of the TiO_2 stabilizers with the organophosphorus ligands contained in the oil droplet.

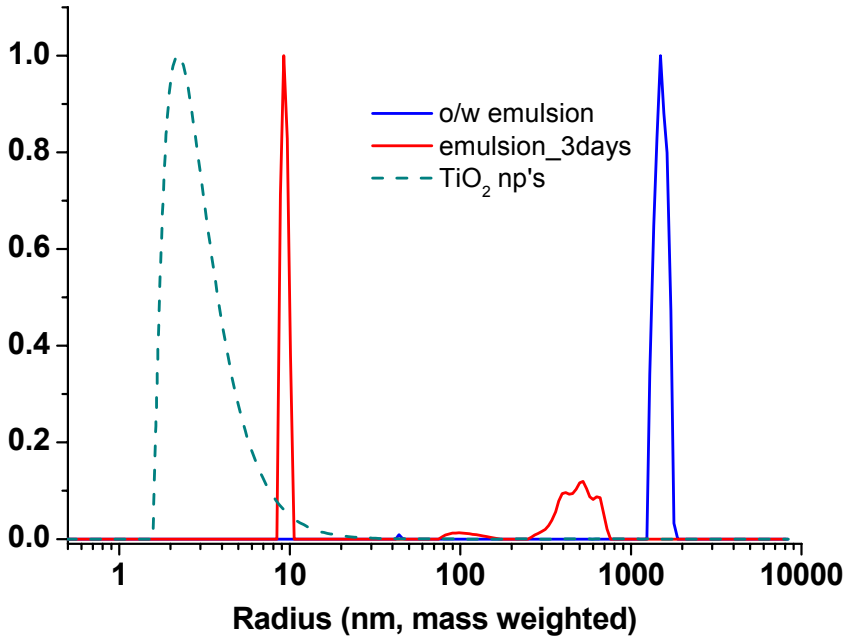

Figure 92. DLS analyses of a Pickering emulsion after formation (blue) and after 3 days (red). The particles were functionalized with MetC5PA-Et. Details of the emulsion: 0.1 g TiO_2 sol-gel particles with 5 nm diameters; cyclohexane: 2 mL; water: 10 mL.

When using the same solvent (cyclohexane) as the oil phase and the same amount of particles the type of the phosphonate ligand contained in the oil phase could be varied (Figure 93). In all of the cases (short chain phosphonates – APA-^{i}Pr, long alkyl chain phosphonates – DPA-

Et, methacrylic functionalized phosphonates – MetC5PA-Et, aromatic ring phosphonates – PyrPA) stable emulsion were obtained.

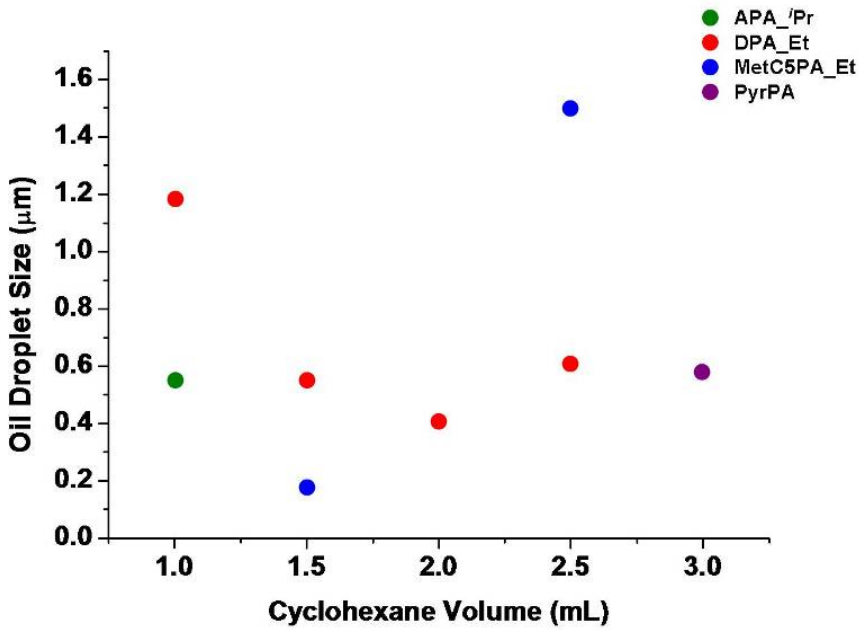

Figure 93. Qualitative image of the oil droplet size depending on the oil volume and type of phosphonate employed

However, due to the fact that the light scattering intensity is strongly influenced by the turbidity of the sample, the measurements were not used for quantifying the dependence of the emulsion droplet to the particle size or oil amount.

After the Pickering emulsions were destroyed the resulting particles could be redispersed in various solvents and analyzed by DLS. Figure 94 presents the distribution function resulted from the redispersion of Janus TiO_2@MetC5PA-Et nanoparticles obtained from sol-gel TiO_2 particles with 8 nm ± 0.20 diameters (Pickering emulsion formed from 0.1 g particles, 10 mL H_2O, 1 mL cyclohexane).

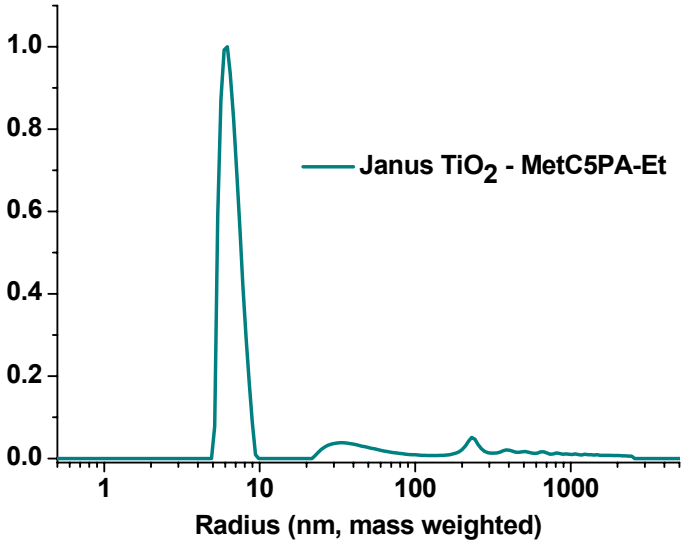

Figure 94. DLS analyses of TiO_2@MetC5PA-Et nanoparticles (25 °C, H_2O). Details of the emulsion: 0.4 g TiO_2 sol-gel particles with 8 nm diameters; cyclohexane: 8 mL; water: 40 mL; MetC5PA-Et: 0.24 g.

The DLS measurements revealed the presence of nanoparticles having a narrow mean distribution of 13 ± 1.6 nm diameter in 82 % after mass weighting. Some agglomerates were also present. This proves that the formed particles have different sizes than the pristine TiO_2 used for the stabilization of the Pickering emulsion.

4.4.6 Morphological Analysis

SEM

The morphology of the formed Janus particles was investigated with SEM and EDX analysis. The dried powders were deposited on a sample holder and sputtered with gold for better conductivity. Figure 95 presents two typical examples of the TiO_2 sol-gel particles modified with MetC5PA-Et and MetC11PA-Et. In both cases the SEM images revealed the presence of nanoparticles with different morphologies than the ones observed for the TiO_2 particles modified with phosphonates in suspension (full surface modification). Among small spherical particles the pictures revealed the presence of some aggregates. EDX analysis for the Janus TiO_2@MetC5PA-Et obtained from sol-gel TiO_2 particles with 8 nm diameter (Pickering emulsion formed from 0.1 g particles, 10 mL H_2O, 1 mL cyclohexane) revealed the presence of both Ti- and O- atoms. Phosphorus is also present in the spectra. What is interesting here is the fact that the P signal is much smaller than in the homologue sample prepared in solution (See chapter 4.3.4). This can be closely connected to the synthetic pathway. The sol-gel

particles used for the stabilization of the Pickering emulsion are hydrophilic, more than half of their volume being immersed in the water face. This means that less than half of the surface is immersed in the oil phase, which can explain the smaller amount of ligand bonded to the overall surface of the particles. Due to the presence of gold on the surface of the particles no quantification could be made, the peak of phosphorus and gold interfering with each other. However, it is obviously that the amount of phosphorus in the case of the TiO_2@MetC5PA-Et prepared in the Pickering emulsion is drastically reduced compared to the particles with a full surface coverage synthesized in emulsion.

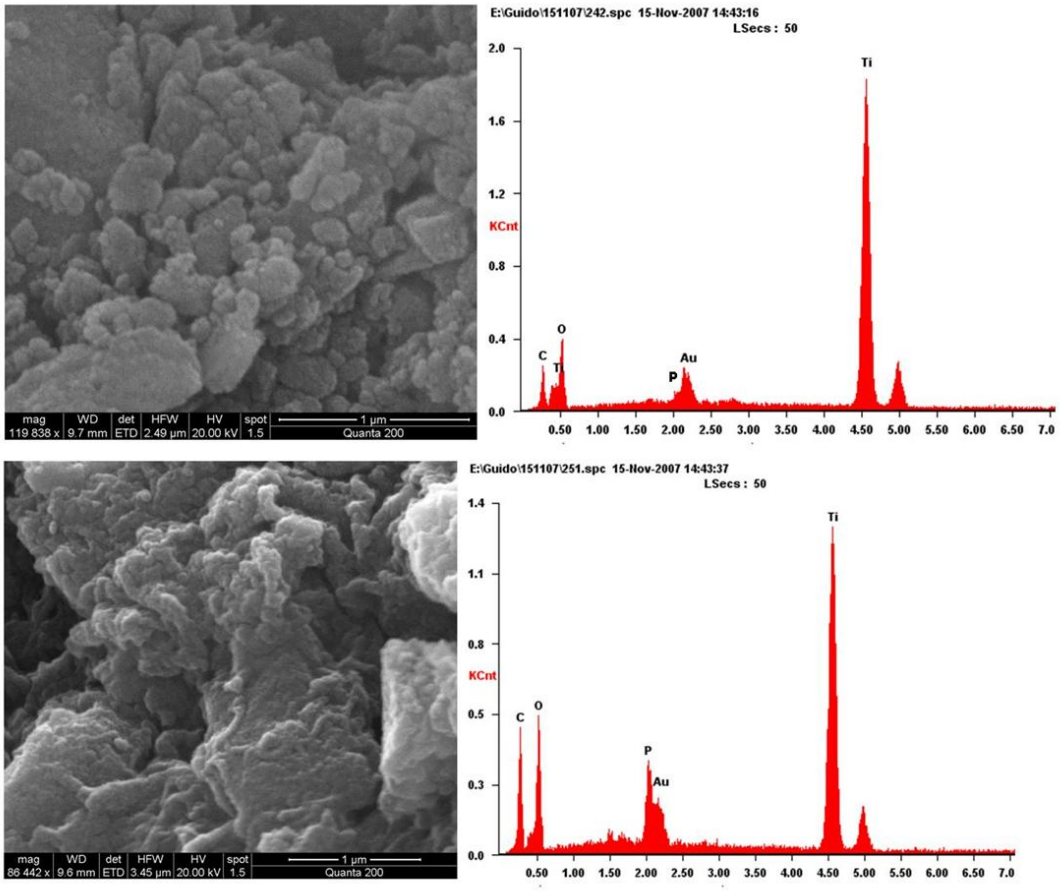

Figure 95. Upper part: SEM of TiO_2 - MetC5PA-Et particles formed from S242 – o/w emulsion (H_2O – Cyclohexane 10 : 1 mL). Lower part: SEM of TiO_2 – MetC11PA-Et formed from s251 – o/w emulsion (H_2O – toluene 10:2.5 mL)

Similar observations could be made for the case of TiO_2@MetC11PA-Et obtained from a slightly different Pickering emulsion (0.1 g TiO_2 particles, 10 mL water, 2.5 mL toluene) (Figure 95, down). In this case a higher amount of phosphorus was observed, probably due to the increase of the oil fraction of the Pickering emulsion.

TEM

Transmission electron microscopy was further used to check the presence of spherical nanoparticles after the emulsion formation. In Figure 96 there are presented typical micrographs obtained for the Janus TiO_2-MetC5PA-Et obtained from sol-gel TiO_2 particles (Pickering emulsion formed from 0.4 g particles, 40 mL H_2O, 8 mL cyclohexane). One can see from the HRTEM that the particles exhibit mean diameters of about 8 nm which is in concordance with the DLS measurements of the pristine TiO2 nanoparticles and smaller than the diameters of the Janus particles obtained by DLS. The particles appeared to have a spherical shape and no presence of other morphologies was detected.

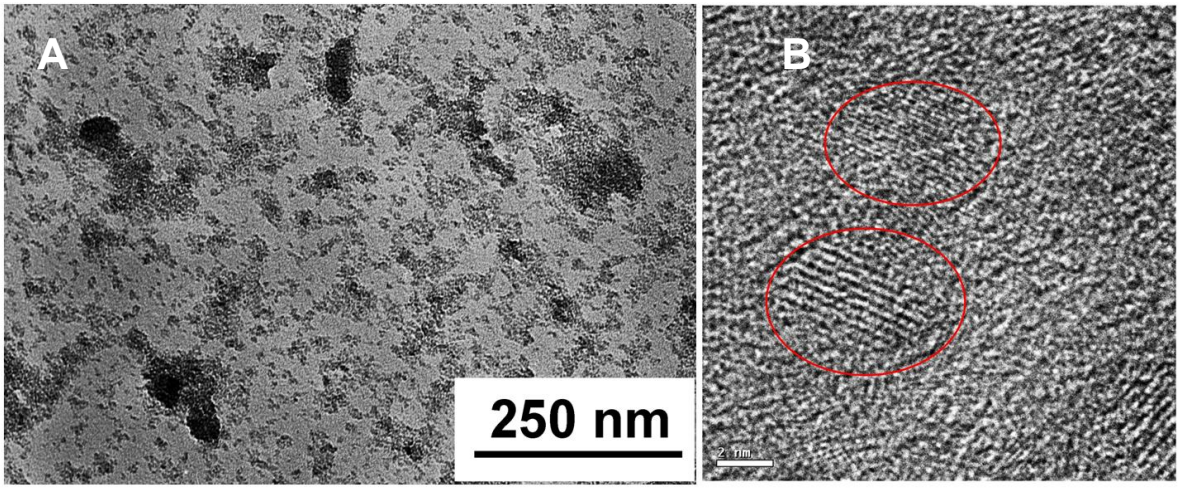

Figure 96. A) TEM micrographs and B) HRTEM of Janus TiO_2-MetC5PA-Et nanoparticles. Details of the emulsion: 0.4 g TiO_2 sol-gel particles with 8 nm diameters; cyclohexane: 8 mL; water: 40 mL; MetC5PA-Et: 0.24 g.

4.5. Synthesis of Hybrid Inorganic-Organic Materials Based on Pickering Emulsions

4.5.1. Polymerization inside the Emulsion Droplet

Emulsions were formed from 50 ml aqueous sol of particles containing 0.5 g TiO_2 and a total of 4 g oil phase containing the initiator and the organophosphourus ligand. Before the emulsion formation the pH in the water phase was maintained at pH = 3 at a value far from the point of zero charge (5.9 – 6.25 for TiO_2) so that the electrostatic repulsive forces due to charged surface sites can break the particles' aggregates. The phosphonate, the ethyl esters of the methacyrloyloxy pentyl phosphonic acid (MetC5PA) had a concentration in the oil phase of $1.5*10^{-3}$ mol/L. The emulsions were formed using an Ultraturrax at 20000 rpm for 15 min. The resulting material was separated from the liquid phase by centrifugation, dried and analyzed.

In order to fix the architecture of the Pickering emulsion, MMA as an organic monomer, the organophosphorus coupling agent containing polymerizable bonds (MetC5PA-Et) and AIBN as a common radical initiator were added to the oil phase. The water phase contained the TiO_2 particles. After mixing the two phases the emulsion was transferred into a closed flask which was subsequently evacuated and the mixture was polymerized at 85°C for various times (between 3 and 12 hours) (Scheme 16).

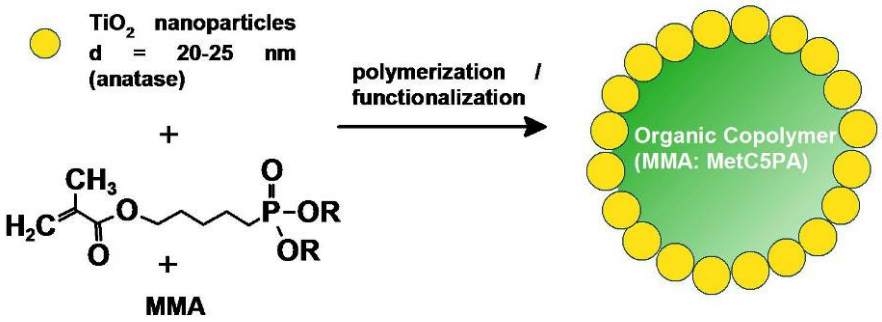

Scheme 16. Method for the formation of Pickering polymeric particles using an organophosphorus ligand as an extra stabilizer in the oil phase

Three different types of emulsions were prepared as typical examples. TiO_2 Degussa P25 with particle diameters of 21 nm ± 0.05 were used for the stabilization of emulsions containing either hexane, MetC5PA-Et and MMA (s261) as an oil phase or only organic monomer mixtures of MetC5PA-Et and MMA (s264). A third type of emulsion was prepared from sol-gel particles having a diameter of 8 nm ± 0.20 and an oil phase composed of the organic monomers MMA and MetC5PA-Et (s262). After the polymerization the hybrid polymer particles were filtrated, washed with water and dried in vacuum for 24 hours.

4.5.2. Spectroscopic Investigations

After drying of the hybrid Pickering polymers spectroscopic studies were carried out to determine the formation of the organic polymer as well as the attachment of the organophosphorus molecules on the TiO_2 surface. The FT-IR analyses of the obtained polymers using MetC5PA–Et esters are presented in Figure 97. A strong band at 1164 cm^{-1} which is characteristic for the P-alkyl groups is observed for the modified particles. The broad band between 930 and 1100 cm^{-1} corresponds to the P-O-(Ti) stretching vibration, proving the condensation of the ligand's OEt groups with Ti-OH groups from the particles' surface. The disappearance of the P=O signal of the phosphonic acid (1234 cm^{-1}) shows the coordination

of the P=O, proving that the phosphonates act as tridentate ligands. These results are consistent with earlier studies reported by *Guerrero et al*. who investigated the surface modification of TiO_2-P25 (Degussa) with phenyl phosphonic acid and esters[100]. Finally the presence of the P-alkyl vibration is evidenced by the band at 1171 cm^{-1}. The presence of PMMA is underpinned by the strong C-O band at 1725 cm^{-1} and the polymerization is demonstrated by the disappearance of the C=C vibration at 1637 cm^{-1}.

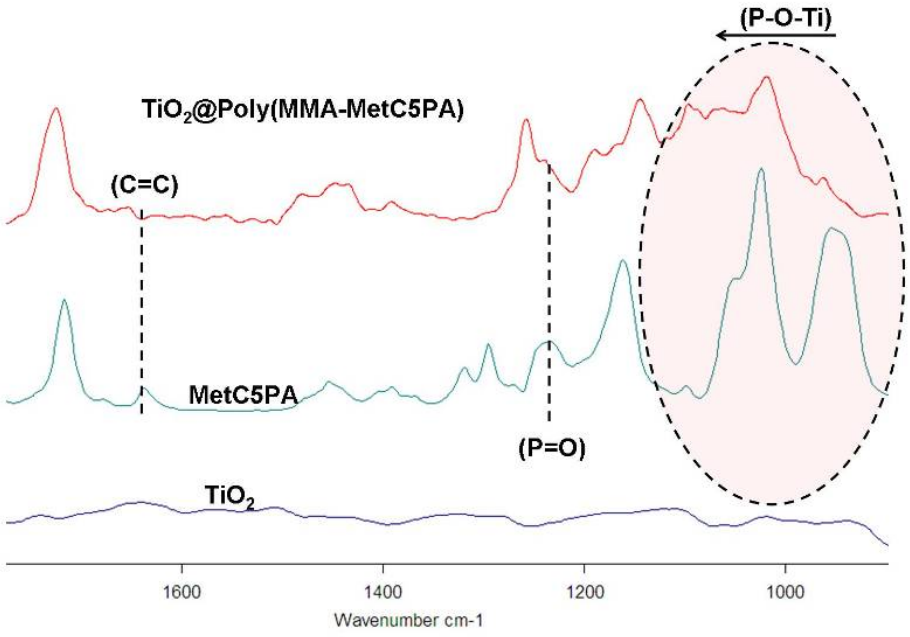

Figure 97. FT-IR spectra of the TiO_2@PMMA-MetC5PA hybrid particles prepared from Degussa P25 particles using an oil phase composed of MMA and Metc5PA

NMR studies confirmed the formation of the polymers and the subsequent connection of the organophosphorus on the TiO_2 particles' surface. The ^{31}P MAS NMR and the ^{13}C MAS NMR spectra of the polymers obtained with sol-gel particles or commercially available P25 particles are similar to each other (Figure 98). In the ^{31}P MAS NMR spectrum only one broad resonance is observed at 36 ppm. The disappearance of the P=O group in the FT-IR spectra led to the conclusion that this major resonance at 36 ppm is due to the tridentate phosphonate sites $PhP(OTi)_3$.[100] This chemical shift is also close to those found for phenylphosphonate/TiO_2 hybrids prepared by a sol-gel method.[195]

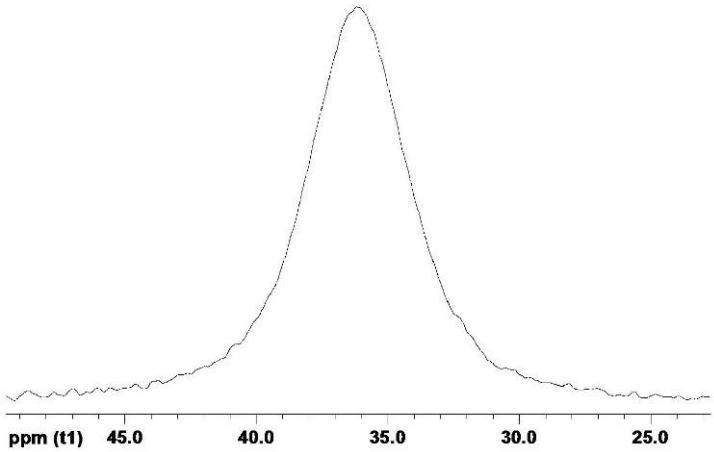

Figure 98. ^{31}P MAS NMR spectra of the TiO_2@PMMA-MetC5PA hybrid particles prepared from P25 particles using an oil phase composed of MMA and MetC5PA-Et

The ^{13}C MAS NMR (Figure 99) shows no trace of unreacted monomer as proven by the absence of any resonance in the double bond region (120 – 130 ppm). The carbonyl region shows a broad resonance for the carbonyl atoms of the methacrylic part at 169 ppm. The *CH_3* of the MMA ligand is located at 15 ppm. Evidence for the polymerization of the methacrylic parts is obtained by the signals at 37 and 44 ppm, corresponding to the quaternary carbon atoms of the polymer chains.

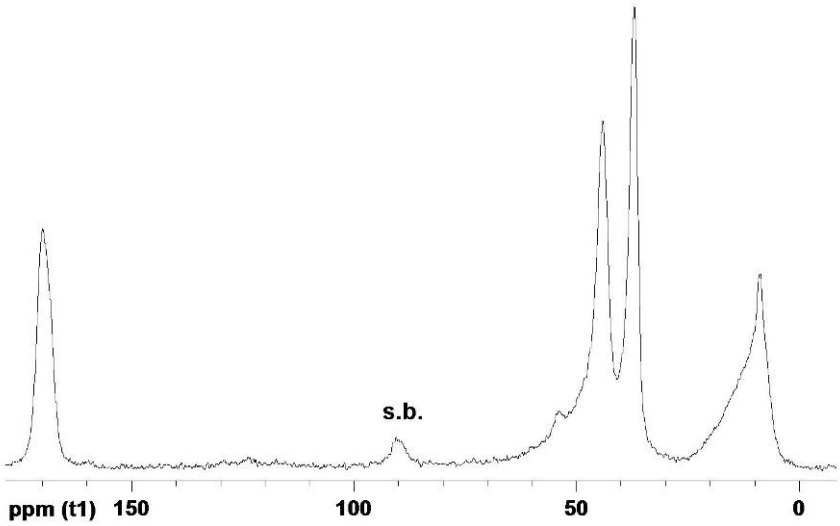

Figure 99. ^{13}C MAS NMR spectra of the TiO_2@PMMA-MetC5PA hybrid particles prepared from P25 particles using an oil phase composed of MMA and MetC5PA-Et (sb – side bands)

4.5.3. Thermogravimetric Analysis

TG analysis of the hybrid TiO_2@PMMA-MetC5PA Pickering particles were carried out in air with heating rate of 10°C per minute up to a temperature of 700°C in order to assure the

complete decomposition of the organic parts. Figure 100 presents the specific thermal behavior of Pickering polymers with TiO_2 as stabilizers and MetC5PA-Et as comonomer.
The pure MMA polymers synthesized in solution with similar amount of initiator shows an onset temperature of decomposition around 250ºC. The total mass change is more than 99% proving that the polymer completely decomposed at 700ºC. Contrary, the TiO_2@PMMA-MetC5PA Pickering particles showed an onset temperature at 300°C which is assigned to the decomposition of the main polymer chain. A second onset temperature appears after 400°C which is due to the decomposition of the organophosphorus based ligands. This is in agreement with earlier data about the decomposition temperatures of TiO_2 modified with phosphonate ligands. In all of the hybrid particles a residual mass remains at 700°C, which is due to the TiO_2 nanoparticles.

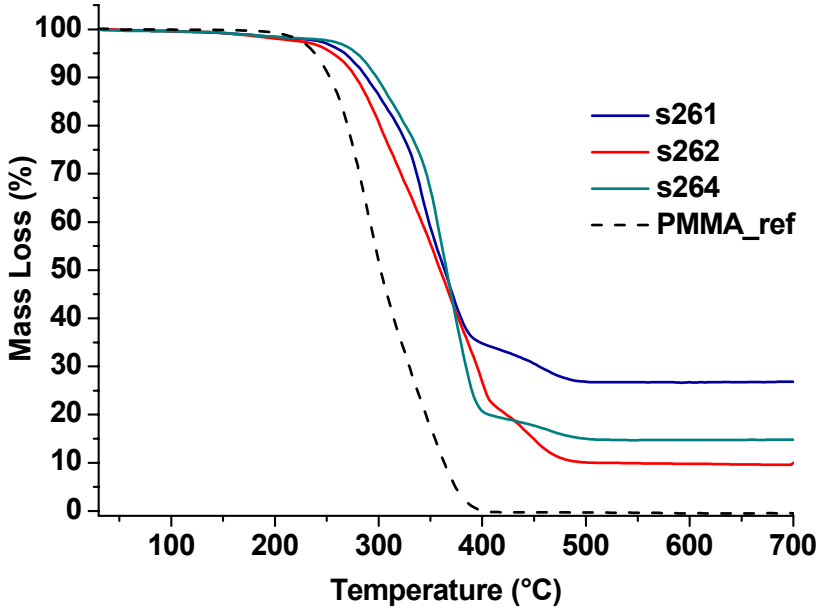

Figure 100. TGA of TiO_2@PMMA-MetC5PA hybrid particles

The decomposition profiles of all of the Pickering hybrid particles looked very similar. The only difference between the two TiO_2 P25 stabilized emulsions (s264, s261) appeared to be the amount of organic polymer. Both of them had the same volume fraction of oil phase but s261 contained 1.5 g of hexane. Considering that the particles were dried before the TG analysis, it was expectable that the s261 showed a higher residual mass than the s264, due to the less amount of organic polymer in the s261. A total relative residual mass had also the sample stabilized by the sol-gel particles even if here only the two organic monomers were used as the oil phase. This fact results from the lower total amount of particles used to

stabilize the Pickering emulsion due to the fact that they have smaller diameters, thus higher surface area.

4.5.4. Morphological Investigations

SEM

The morphology of the hybrid TiO_2@polymer spheres was investigated by SEM. In Figure 101 are presented three characteristic SEM images and the subsequent EDX spectra of one ball-like particle obtained from the Pickering emulsion stabilized by the P25 TiO_2 nanoparticles with the oil phase consisting only of the two comonomers, namely MMA and MetC5PA-Et.

Figure 101-A shows the presence of spherical particles. A small part of the particles seemed coagulated forming larger agglomerates. Most likely the agglomerates were formed in the emulsification process, as observed also in literature for the cases when TiO_2-polymer hollow spheres were synthesized by Pickering process.[149]

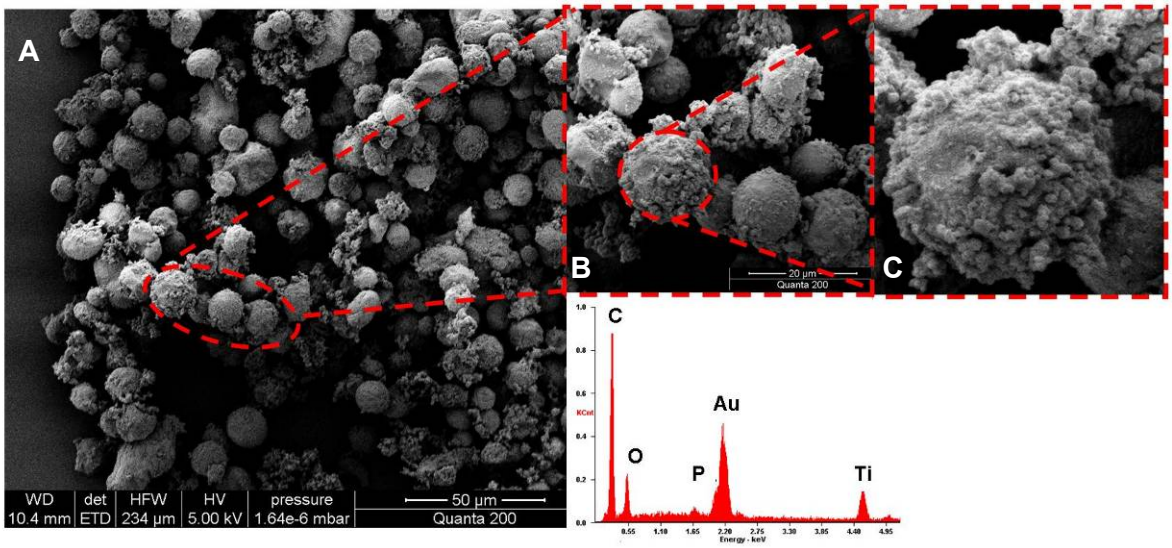

Figure 101. SEM images of TiO_2@PMMA-MetC5PA (s264) and the EDX analysis of one hybrid particle

Figure 101-B reveals that the Pickering spheres have diameters ranging from 10 to 15 µm. The particles show the presence of smaller particles on their surface as seen in the inset (Figure 101-C). When looking closer to the surfaces of the spheres it can be seen that the small spherical particles have 20-30 nanometer diameters, which is the size of the pristine TiO_2 Degussa P25 particles. Furthermore the EDX analysis of one of the Pickering hybrid spheres showed the presence of both Ti and O, proving the presence of the nanoparticles on

the polymer surface. Some residual signals of carbon and phosphorus were also detected. The origin of these signals is the bulk polymer. No quantification could be made due to the fact that the samples were sputtered with gold for better conductivity.

The sample prepared with an organic solvent in the oil phase (hexane) and the two monomers showed similar features (Figure 102-A). Here we could also observe the presence of spherical particles with a quite narrow size distribution together with few coagulated particles due to the emulsification process. The only difference seems to appear in the size of the Pickering spheres. Here the hybrid particles revealed smaller diameters with a mean of about 2 µm. Considering that the total amount of oil was kept constant, this difference could be directly connected to the smaller relative amount of monomer in the oil phase which may lead to smaller hybrid particles.

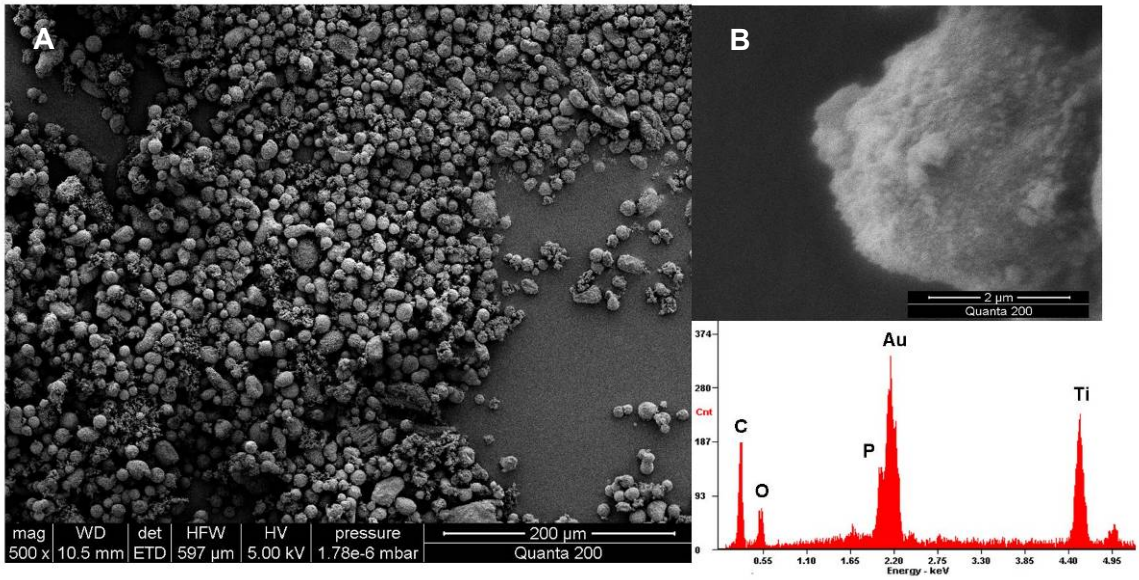

Figure 102 SEM images of TiO_2@PMMA-MetC5PA (s261) and the EDX analysis of one particle

The inset image (Figure 102-B) shows that the spheres were totally covered with small nanometer size spherical particles. Parts of the surface have some agglomerates of these particles. This fact comes most likely from the poor redispersion of the TiO_2 P25 in water. Even at low pH some of the particles were still aggregated, leading to regions of higher densities of the TiO_2 particles on the surface of the Pickering hybrid spheres after the Pickering emulsion separation. Furthermore EDX showed that the surface of the hybrid spheres had an intense band of Ti, proving that the small nanoparticles covering the hybrid particle are indeed the stabilizing P25.

Even smaller emulsion polymer spheres were obtained when sol-gel TiO_2 nanoparticles with diameters of 8 nm were used as stabilizing agents for the Pickering emulsions (Figure 103 -A and B). Here smaller spheres (1.5 µm diameter) were obtained but more of the spheres were coagulated due to emulsification.

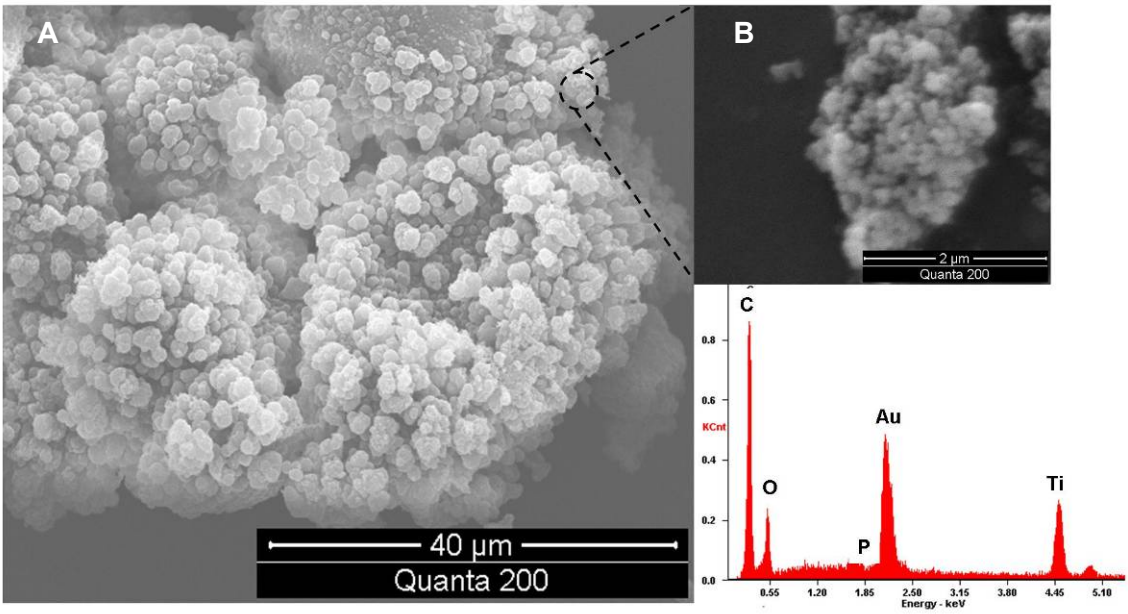

Figure 103. SEM images of TiO_2@PMMA-MetC5PA (s262) and the EDX analysis of one particle

EDX showed the presence of the Ti- and O-bands proving the presence of the TiO_2 on the surface of the particles.

Such hybrid spheres could be also formed when Pickering emulsions were formed from 12.5 ml H_2O containing 0.5 g TiO_2 (P25) and a total of 1 g oil phase containing the initiator and MetC11PA-Et as the organophosphourus ligand. The phosphonate had a concentration in the oil phase of $1.5*10^{-3}$ mol/L (0.25 g in this case). Similarly, the emulsions were formed using an Ultraturrax at 20k rot/min for 15 min. The particles were separated by centrifugation, dried and analyzed. Figure 104 reveals the formation of hybrid spheres prepared from this experiment. The surface shows the presence of small nanoparticles as seen before, while the EDX analysis confirmed the presence of the Ti and O. The presence of phosphorus is due to the fact that the EDX offers information from the whole hybrid particles and not only from the surface. However the morphological SEM investigation proves the presence of the small spherical nanoparticles on the surface of the polymer spheres.

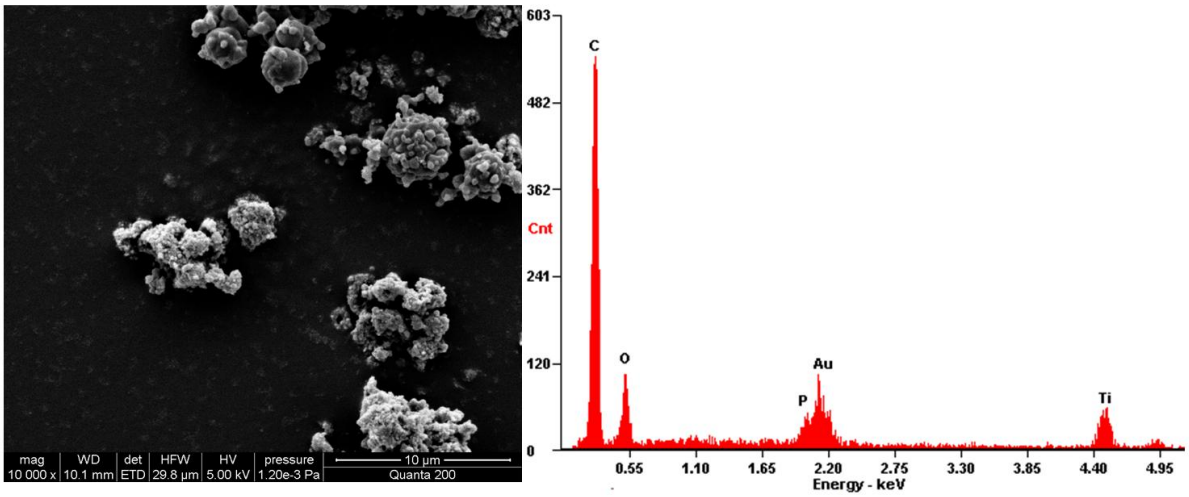

Figure 104. SEM images of TiO_2@PMMA-MetC5PA (s299) and the EDX analysis of one particle

TEM

Further proofs for the presence of the stabilizing TiO_2 nanoparticles on the Pickering polymeric spheres were gained from the TEM measurements of the hybrid polymers. Figure 105 presents a characteristic TEM micrograph of the samples s264 (TiO_2@PMMA-MetC5PA without hexane). The entire sample revealed the presence of spherical micron-sized particles with narrow size distribution. When zooming on the particles' edges we could see in the thinner regions the presence of monodisperse nanoparticles having a mean radius of about 21 nm and a morphology characteristic to the P25 Degussa particles. This proves the fact that the nanoparticles are retained at the surface of the Pickering emulsion after the polymerization process.

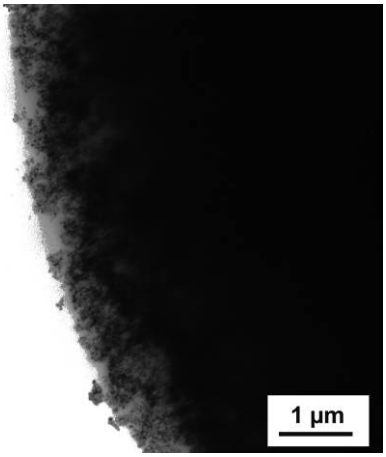

Figure 105. TEM image of TiO_2@PMMA-MetC5PA (s264)

4.5.5. X-ray Diffraction

Literature reports mentioned that the surface modification of TiO_2 with phosphonic acids is usually carried out in aqueous media at 100 °C[193, 194]. Depending on the reaction time and the phosphonic acid concentration, significant amounts of bulk titanium phosphonate can be formed. This means that the TiO_2 materials were partially or fully destroyed and titanium phosphonates were formed. The goal of this project however was only the surface-modification of TiO_2 nanoparticles without affecting their bulk structure. For example the TiO_2 Degussa P25 particles are standards in photocatalytic reactions carried out with TiO_2 as a photocatalyst. The disturbance of their crystalline phases by the formation of such bulk phosphonates can have drastic consequences on their photocatalytic activity and has to be avoided if further applications in this area are targeted. For this reason the crystalline phase has to be maintained. One problem is that the polymerization process requires temperatures of 85°C and reaction times of 3 to 12 hours. To prove the maintaining of the crystalline phases after the polymerization process we decided to investigate the hybrid Pickering polymer with X-ray powder diffraction. The XRD analyses were carried out in order to determine the crystalline phases of the resulting TiO_2@PMMA-MetC5PA hybrid polymers stabilized by the P25 nanoparticles. The XRD patterns of the hybrid polymer samples stabilized by the P25 particles were compared with the XRD pattern of the unmodified particles. No differences were detected when comparing the hybrid spheres with the pure particles. All of the patters proved the presence of the typical phases of the TiO_2 P25 (~ 90% anatase, 10% rutile) with the same composition (Figure 106).

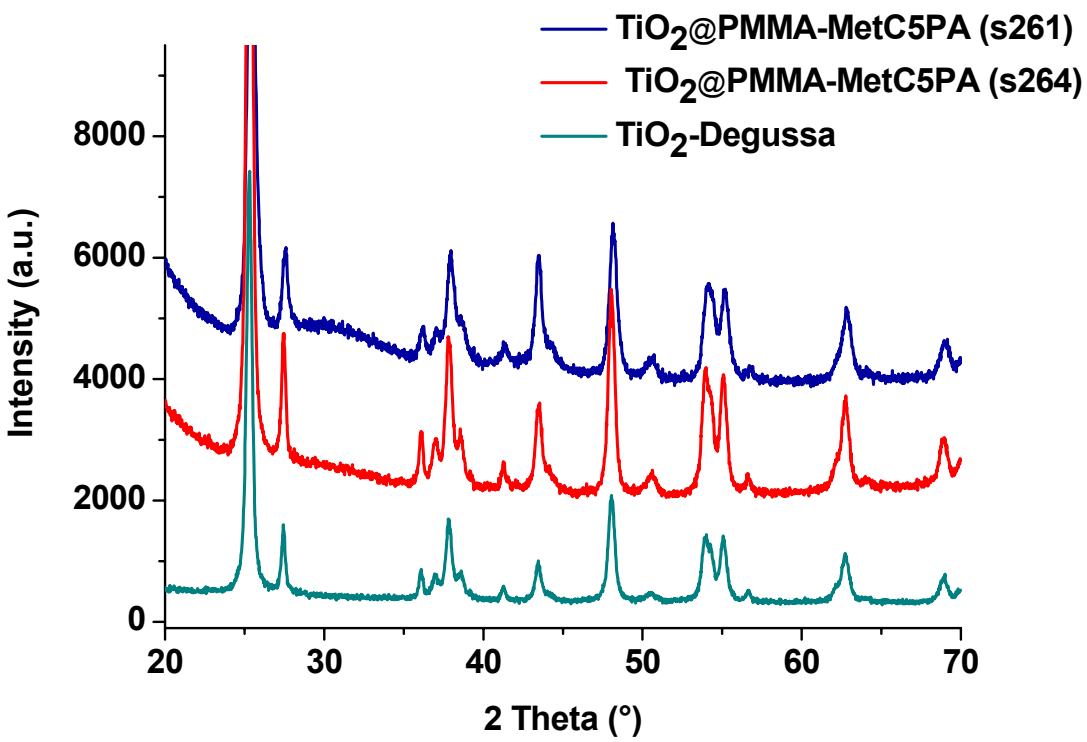

Figure 106. XRD patterns of pure TiO_2 P25 particles, and TiO_2@PMMA-MetC5PA (s264)

This proves that no bulk Ti-phosphonate phases were formed and the TiO_2 nanoparticles were still available for further reactions and applications.

4.5.6. X-Ray Photoelectron Spectroscopy

X-Ray Photoelectron Spectroscopy[205] was used to analyse the surface composition and the chemical state and environment of the different species in the 5 listed TiO_2-PMMA composite samples, characterized by different compositions and preparation routes.

This method was particularly used to prove the presence of titania on the surface of the nanoparticles and to obtain information on the chemical composition and the binding mode of the different species present.

In Figure 107, the survey spectra of the surface (before sputtering) of the sample 261_2 (Pickering emulsion. 50 mL H_20, TiO_2 P25 (d = 21 nm ± 0.05); oil: hexane, MetC5PA-Et, MMA) is exemplarily plotted, which shows the presence of all the expected species, i.e. Ti, O, P, C.

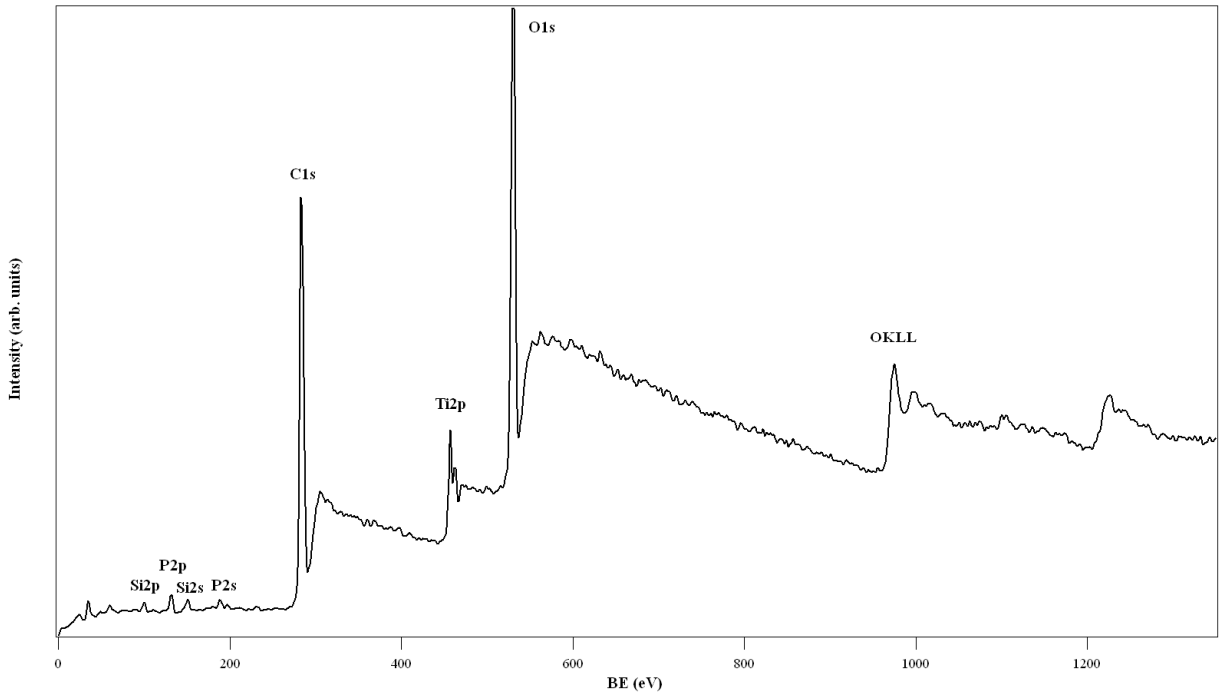

Figure 107. Survey spectrum of the sample 261_2 (Pickering emulsion. 50 mL H_20, TiO_2 P25 (d = 21 nm ± 0.05); oil: hexane, MetC5PA-Et, MMA)

Furthermore, the presence of low amounts of silicon was also detected, which can be ascribed to silicon grease impurities.

The composition in atomic percentages of the samples is reported in Table 10. As it can be seen, in all the samples both titanium as well phosphorous were detected in a Ti/P molar ratio of about 1.4-2.9, which is in aggrement with the EDX data, indicating a Ti/P atomic ratio of about 1.5-2.

Considering that the diameter of the titania nanoparticles is about 21 nm, which is a value much higher than the XPS sampling depth of about 10 nm, and that if the whole surface of the organic particle would be homogeneously covered with titania, no phosphorous should be seen (being completely "buried" under the titania nanoparticles), this finding suggests that either the coverage is not uniform or the amount of titania nanoparticles added is not enough to achieve a complete coverage of the underlying polymer particles. This latter case is also revealed by the SEM images.

Table 10. Atomic percentages and BE values (the BE of Ti, O, Au are corrected for charging effects)

Sample	%O	%P	%Ti	%C	Ti/P
261_1	**32.9**	**1.6**	**3.4**	**62.1**	**2.1**
261_2	**62.90**	**2.2**	**3**	**31.90**	**1.4**
262_1	**32.2**	**1.1**	**3.2**	**63.5**	**2.9**
264_1	**29.2**	**1.1**	**2**	**67.7**	**1.8**
264_2	**31.2**	**1.1**	**2.1**	**65.8**	**1.9**

All the samples are characterized by a high carbon content ranging between 60-68 atomic %, which has to be ascribed both to adventitious carbon contamination but mainly to the organic core of the core-shell produced nanoparticles. Again, this finding has to be ascribed to the not homogeneous coverage of the core PMMA particles by the TiO_2 nanoparticles and to the detection of the core PMMA particle. This is confirmed by the fact that the C1s region is broadened and, after deconvolution, it presents two components: the first one peaked at 284.5 eV, and ascribed to graphitic or aliphatic carbon, and the second one at 288.3 eV, which is a value typical for carbon in a ester[206-208].

The only exception to this common trend is represented by sample 261_1, in which the amount of detected carbon is about one half of the amounts detected in the other four samples. A possible explanation of this experimental evidence could be the higher TiO_2 amount used for the stabilization of the emulsions, which leads to a better coverage of the composite spheres. This is also sustained by the lower Ti/P ratio.

As far as the chemical state of the different species is concerned, the BE values of Ti2p region (Figure 108) are in the range 458.0-458.7 eV, values similar to those reported in literature for TiO_2 (458.7-458.8 eV).

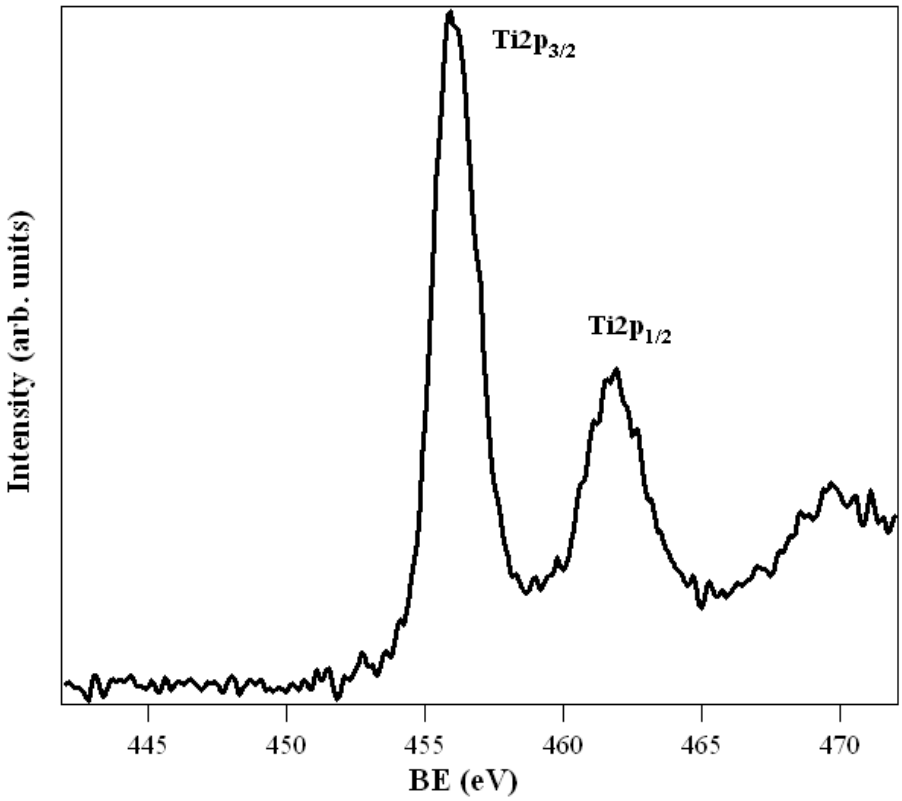

Figure 108. Ti2p spectrum of the sample 261_2

The BE values of the O1s region are located in the interval 531.9-532.1 eV, which are higher than the values for titania and more similar to BEs of oxygen in ester groups (532.0-533.0 eV), i.e. in agreement with the presence of methacrylate. The values detected for phosphorus are in agreement with those reported for phosphate groups

4.5.7. General Remarks

Anatase nanoparticles can be easily synthesized by the sol-gel process, having controlled sizes and crystallinity. For example, by changing the precursor's concentration the particle size were varied. XRD and HR TEM studies showed that the particles are fully crystalline, and the crystal phase was assigned to anatase.

These particles were surface-functionalized in suspension using previously synthesized organophosphorus coupling agents. The spectroscopic studies (NMR, FT-IR) showed the TiO_2 nanoparticles were surface-modified with various phosphonates and phosphates. The binding mode of the coupling agents on the surface of the particles was predominately tridentating. The amount of phosphonates or phosphates linked to the particle surface was tailored from thermogavrimetric analysis, ranging from full particles coverage to

partially coverage. TEM and SEM analyses showed that the particles were spherical and still in the nanosize region. Furthermore EDX confirmed the presence of phosphorus atoms.

The pristine TiO_2 nanoparticles were be applied as stabilizers in the formation of o/w Pickering emulsions. Various emulsions using either the sol-gel or the commercially available TiO_2 Degussa P25 nanoparticles were obtained. The oil phase contained the organophosphorus coupling agent which coordinated on the surface of the anatase nanoparticles while on the other chain-end has a methacrylic group for further modification. In such a way an isotropic surface modification of the particles was achieved. Spectroscopic studies showed the presence of tridentate organophosphorus coupling agents on the particles' surfaces. Thermogravimetric analyses also confirmed that the amount of coupling agent bonded to the particles surface was significantly lower than in the cases of the suspension modification.

By simply using such organophosphorus coupling agents together with MMA in the oil phase, the Pickering emulsion architecture was fixed giving rise to hybrid inorganic-organic Pickering spheres. Spectroscopic studies showed that after the polymerization the phosphonates acted as tridentate ligands bonded to the surface of the oxide particles. Furthermore, the copolymerization of the phosphonate with the MMA was also proven by ^{13}C NMR and FT-IR analyses. TG analysis showed a considerable increase in the thermal stability of the hybrid spheres compared to pure methacrylic polymers. SEM and EDX analysis gave insights in the morphology of the hybrids. As seen from the images narrow monodisperse polymer spheres were obtained for all the Pickering emulsions. The higher magnification photographs showed that the polymer spheres had the stabilizing TiO_2 nanoparticles on their surface. EDX revealed that the surface of the hybrid spheres contained mostly Ti. The presence of the small anatase nanoparticles on the surface of the hybrid Pickering spheres was confirmed also by the TEM measurements. As detected by XRD, the crystallinity of the TiO_2 nanoparticles was not affected by the polymerization process. These results have proven that the anatase nanoparticles were located at the surface and were still available for further applications.

4.6. Synthesis of Transparent Nanocomposites Based on Surface-Modified TiO_2 Nanoparticles

As mentioned in the *Introduction*, the last years showed an increased interest in the synthesis of inorganic-organic hybrid materials and nanocomposites based on metal oxides and organic polymers, due to the clear advantages of combining the two opposite worlds in one and thus obtaining new materials with enhanced properties.

Another approach of the research work was the use of TiO_2 nanoparticles surface–modified with organophosphorus coupling agents in suspension as the inorganic moieties and their inclusion in organic polymeric matrices.

In Scheme 17 is presented the theoretical pathway for the synthesis of nanocomposites based on surface–modified TiO_2 and organic monomers. In a first step TiO_2 nanoparticles were modified with dodecyl phosphonic acid. The ligand does not carry any reactive moiety for the incorporation in the polymer matrix. However, the long alkyl chain protects the particles from aggregation and provides a good dispersibility of the inorganics in the respective organic monomers, leading to transparent materials. This pathway should lead to the formation of nanocomposites without any covalent bonds. The second pathway was represented by the surface modification of the TiO_2 nanoparticles with organophosphorus coupling agents carrying a second methacrylic bond which would allow not only the good dispersion of the particles in the corresponding monomer, but also their chemical attachment to the polymer backbone by the subsequent copolymerization with the organic monomer. As seen from Scheme 17, this pathway should lead to the formation of nanocomposite materials with covalent bonds between the inorganic and the polymeric moieties.

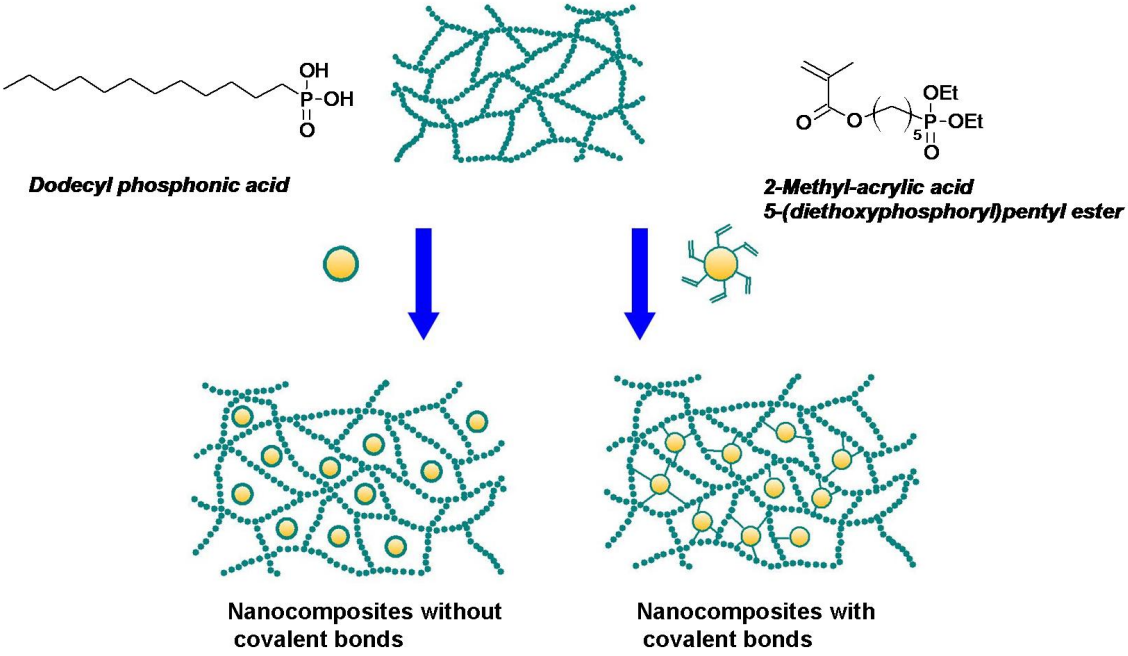

Scheme 17. Possible pathways for the synthesis of nanocomposite materials based on surface modified TiO_2 nanoparticles without or with covalent bonds between the inorganic and organic moieties

4.6.1. Dispersibility Tests of the Surface-Modified TiO_2 Nanoparticles

The first goal in this approach was to find suitable inorganic particles/monomer mixtures for both of the pathways. There were two main requirements for a dispersion of surface–modified TiO_2 nanoparticles in organic solvents/monomers:

- formation of a stable dispersion, without particle agglomeration, sedimentation, or phase separation in any way;
- formation of a highly transparent dispersion.

DLS was used to characterize the dispersibility of some of the modified particles. The main focus was on the dodecyl, phenyl, and methacrylate modified particles due to their similarity with the further on used organic monomers, MMA and styrene. For reasons of comparison the dispersibility was also investigated in different organic solvents.

Samples were prepared using 1 mg particles / mL solvent. The suspensions were dispersed using an ultrasound bath for 15 minutes and measured after 15 minutes standing time in order to avoid errors induced by dust particles.

Table 11 summarizes all the results obtained from the DLS measurements in different solvents. The dodecyl modified particles showed good dispersibility not only in styrene but also in apolar solvents like heptane and toluene, which make them also attractive for their incorporation in the oil phase of a Pickering emulsion. On the other hand, they are not dispersible at all in alcohol solvents or in water. The methacrylate modified particles were not good dispersible in both the apolar and polar solvents applied. However, they are well dispersible in MMA and thus, could be used for the formation of nanocomposite materials with covalent bonds between the inorganic and organic moieties.

Table 11. Dispersibility test of various surface modified TiO_2 nanoparticles in organic solvents and monomers.

Solvent/Particles	***Toluene***	***Heptane***	***MMA***	***Styrene***	***EtOH***	***H_2O***
TiO_2@DPA	+ +	+ +	-	+ +	-	-
TiO_2@MetC5PA-Et	-	- -	+	-	- -	-
TiO_2@PPA	+	- -	- -	-	-	-
TiO_2	- -	- -	- -	- -	+	+ +

Figure 109 presents the obtained size distributions as measured from DLS in the two monomers (styrene and MMA) for all of the particles. The DLS studies revealed that the TiO_2@DPA nanoparticles are very good dispersible in styrene, showing a size distribution of particles with a radius of about 6 nm ± 0.11. Some agglomerates were also observed. However the solution was clear and colorless, fulfilling all the requirements for their usage as precursors for transparent materials. TiO_2@MetC5PA-Et in MMA showed the presence of particles having 12 nm ± 0.045 radii, and also some bigger agglomerates.

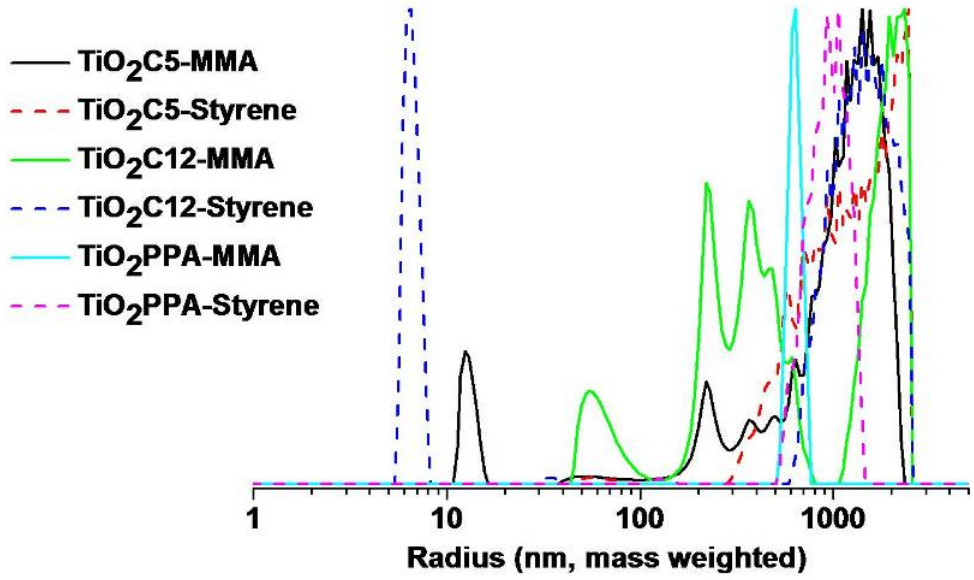

Figure 109. DLS size distribution of various surface modified TiO_2 nanoparticles in MMA and styrene

A third system was chosen based on PPA modified particles in styrene. Even if the light scattering studies showed only the presence of large agglomerates with radii of 121 nm ± 0.12, the solutions were rather clear and transparent and no precipitation of the particles was observed.

As shown already in the cases of PPA modified particles TEM was used to investigate the morphology of the surface modified nanoparticles. The samples measured in TEM were prepared after the drying of the particles and redispersion in ethanol. Both the DPA and the MetC5PA-Et modified particles appeared as small spherical nanoparticles together with larger aggregates (Figure 110). However the latter also consisted of small nanoparticles and were formed during the solvent evaporation. The measurement of the particles present on the TEM micrographs demonstrated that they have radii with a mean diameter of about 10 to 20 nm.

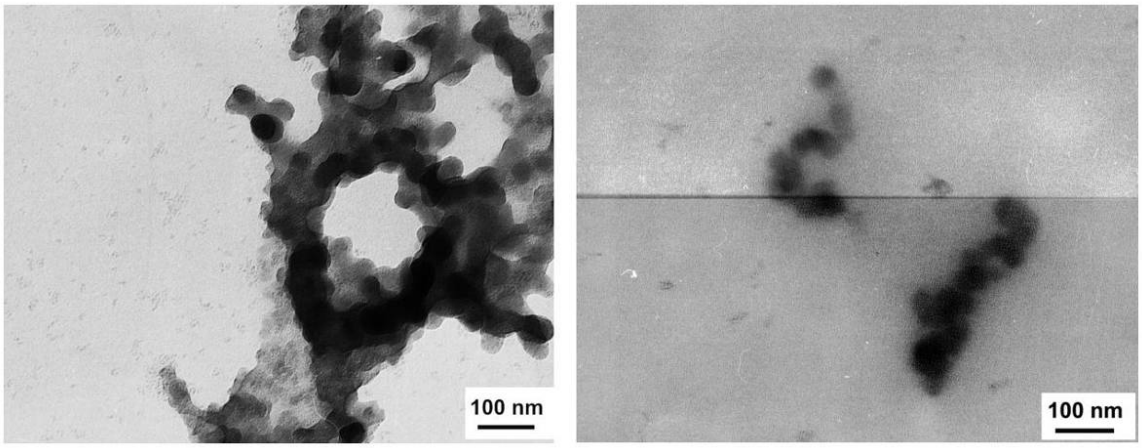

Figure 110. TEM analyses of TiO_2@DPA (left) and TiO_2@MetC5PA-Et nanoparticles (right)

4.6.2. Nanocomposites without Covalent Bond between the Matrix and the Nanoparticles

After the dispersion of the particles the solutions were polymerized in bulk at 80°C using BPO (1 wt%) as initiator. The polymerizations were carried out in close 10 mL vials under an argon atmosphere. The polymerizations were carried out for 12 hours to assure a full conversion of the monomers.

4.6.2.1 Spectroscopic Studies

FT-IR analyses (Figure 111) revealed no differences between the spectra of the PS reference and the PS having 5% TiO_2@DPA particles inside. The phenyl ring stretching vibrations were present in both of the samples at the same wavenumbers (1491, 1447, 753, 695 cm^{-1}). This is not unexpected considering that there are no chemical bonds between the particles and the polymer matrix, rather only weak physical interactions. The absence of the double bonds proves the full polymerization of the styrene.

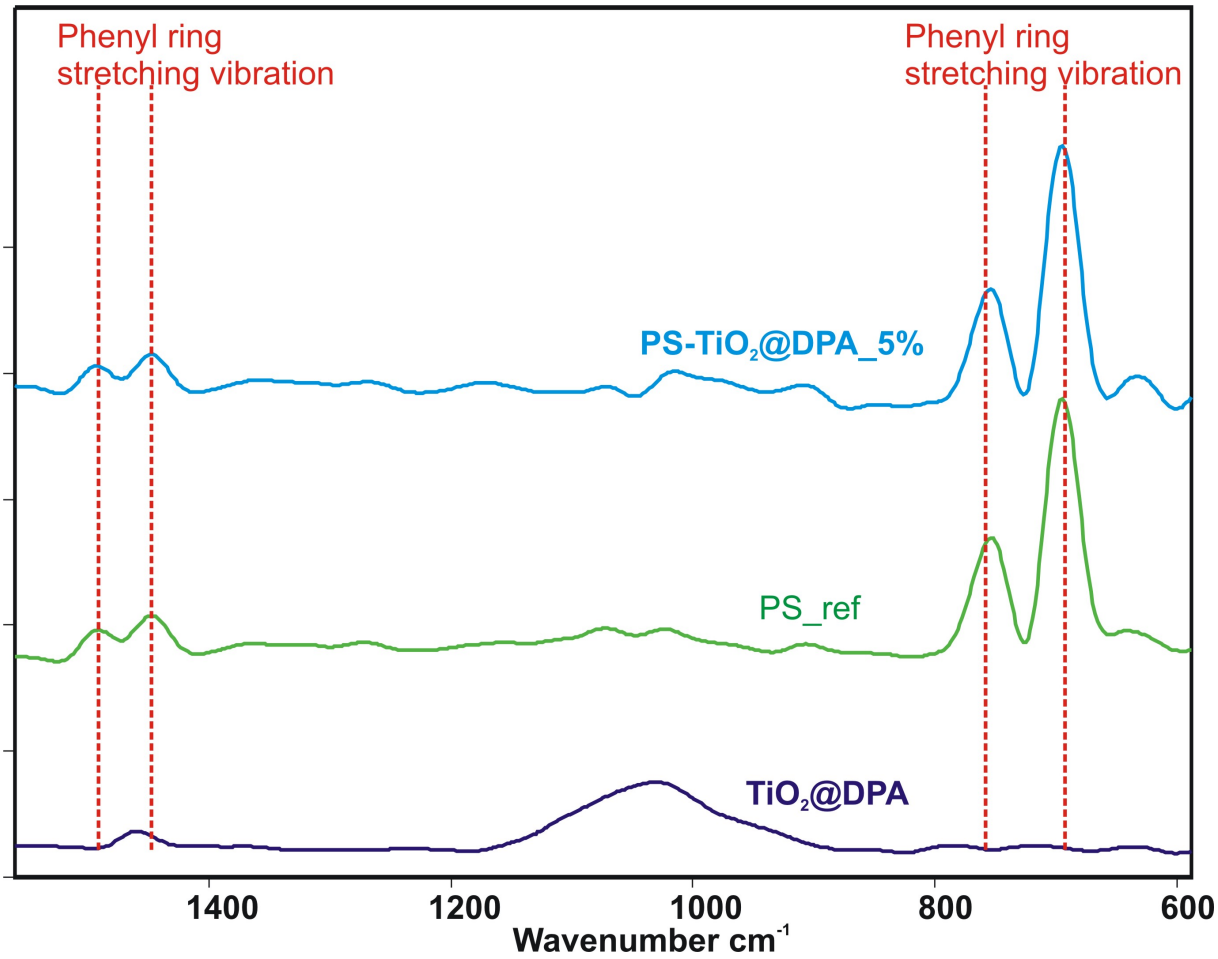

Figure 111. FT-IR analysis of the TiO_2@DPA, PS, and PS having 5% DPA-TiO_2

4.6.2.2. SEC Studies

The polymerization process was monitored using SEC, to detect if the molecular masses of the resulted doped polymers are in agreement with the reference samples. SEC results show that the molecular weights were monomodal for all of the doped samples (Figure 112). Molecular weight distributions of the resulting polymers showed values between 2 and 2.8, which are typical for radical polymerizations carried out in the absence of any chain controllers. The long polymerization times (typically 12 hours) can also explain the increase in the MWDs of the polymers. These facts proved that the particles have no influence on the polymerization process at these low contents. No effect was observed like the one reported by *Demir et al.*[103]. In this paper, TiO_2 particles with a mean diameter of 200 nm were surface-modified with octyl phosphonates and then dispersed in MMA. The weight fraction of particles was kept constant at 0.06 (120 mg particle in 2 mL of MMA). When the bulk free-radical polymerization of methyl methacrylate in the presence of the particles was carried out, it was observed that the nanoparticles suppress the autoacceleration (which would otherwise occur) resulting in a better control of heat dissipation and MWDs.

High MWDs were also obtained when bulk polymerization of styrene was carried out in the presence of zirconium clusters with non-polymerizable ligands[209]. No clear correlation between the gelation time and the molecular masses could be made because of the different carboxylate ligands of the clusters and because there was no information whether or to what extent the clusters interact with the polymers.

Polystyrene - TiO_2 nanocomposite particles were also synthesized by *in-situ* polymerization of styrene in the presence of silane coupling agent surface –modified TiO_2 nanoparticles. The molecular weights were increasing with the increase of the monomer amount, while all of the samples presented MWDs between 1.4 and 2.4[210].

However, high MWDs were obtained even when ATRP was employed for the *in-situ* polymerization of styrene in the presence of a layered silicate[211]. This was due to the long reaction times (22 hours) which lead to an increased importance of chain-transfer and termination reactions at high monomer conversions.

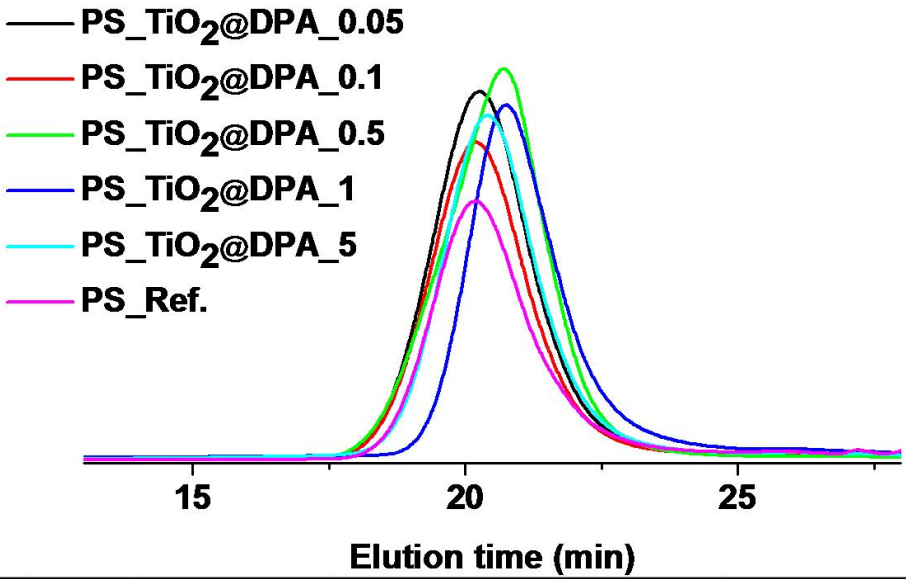

Sample	PS	PS-TiO_2@DPA_0.05	PS-TiO_2@DPA_0.1	PS-TiO_2@DPA_0.5	PS-TiO_2@DPA_1	PS-TiO_2@DPA_5
Mn	51033	55593	57393	45472	35360	48684
Mw/Mn	2.6	2.6	2.6	2.8	2	2.3

Figure 112. SEC analysis of the PS, and PS having various amount of DPA-TiO_2 particles

4.6.2.3. Thermal Properties

Information about the particles incorporation in the polymer matrices was also obtained by thermogravimetric analysis (TGA). The TG analyses were carried out in air with 10°C per minute up to a temperature of 700°C in order to assure the complete decomposition of the organic parts. Figure 113 presents the specific thermal behaviors of the PS series with TiO_2@DPA nanoparticles incorporated.

The DPA surface - modified TiO_2 nanoparticles exhibit two mass losses. The first one, with an onset temperature at 68 °C is due to volatiles adsorbed on the particles surfaces. The second one, with an onset temperature at 368 °C is due to the decomposition of the organophosphorus coupling agents. This latter effect exhibits a mass loss of 30 %. On one hand, the reference PS sample (no inorganic) exhibits an onset temperature at 330°C. This major mass loss was shifted from 330 °C as observed for the neat polystyrene to higher values for the doped samples (Onset 1, Table 12). This is in agreement with previously reported thermal decomposition of polystyrene prepared in bulk[209, 212]. An increase of the thermal stability with about 20 °C of the sample containing modified TiO_2 nanoparticles compared to the neat PS was observed. For example, when PS was in-situ polymerized in the presence of zirconium clusters with polymerizable or inert ligand, an increase in the thermal stability of all of the samples compared to the neat PS was evidenced. The shifts in the samples containing zirconium clusters with inert ligands were of the same order as for the samples where crosslinking occurred via the reactive zirconium clusters[209].

Samples containing higher amounts of particles present a second onset temperature around 440°C. There are two possibilities for assigning this. The first possibility is that this effect describes the oxidative volatilization of organic char which was produced in the step 1. A trend in the amount of formed char was clearly visible: by increasing the amount of particles in the samples and thus the loading of inorganic moieties, also the char yield increased. This is in accordance with earlier reports about PS-Zr oxocluster doped materials[209, 213-215]. A second possibility is that this onset is due to the decomposition of the organophosphorus groups from the surface of the particles. Due to the decomposition of the polymer chain, the onset could be shifted to higher values, and thus explain the higher onset present in the polymer samples compared to the modified particles. However, the first pathway is more likely to occur.

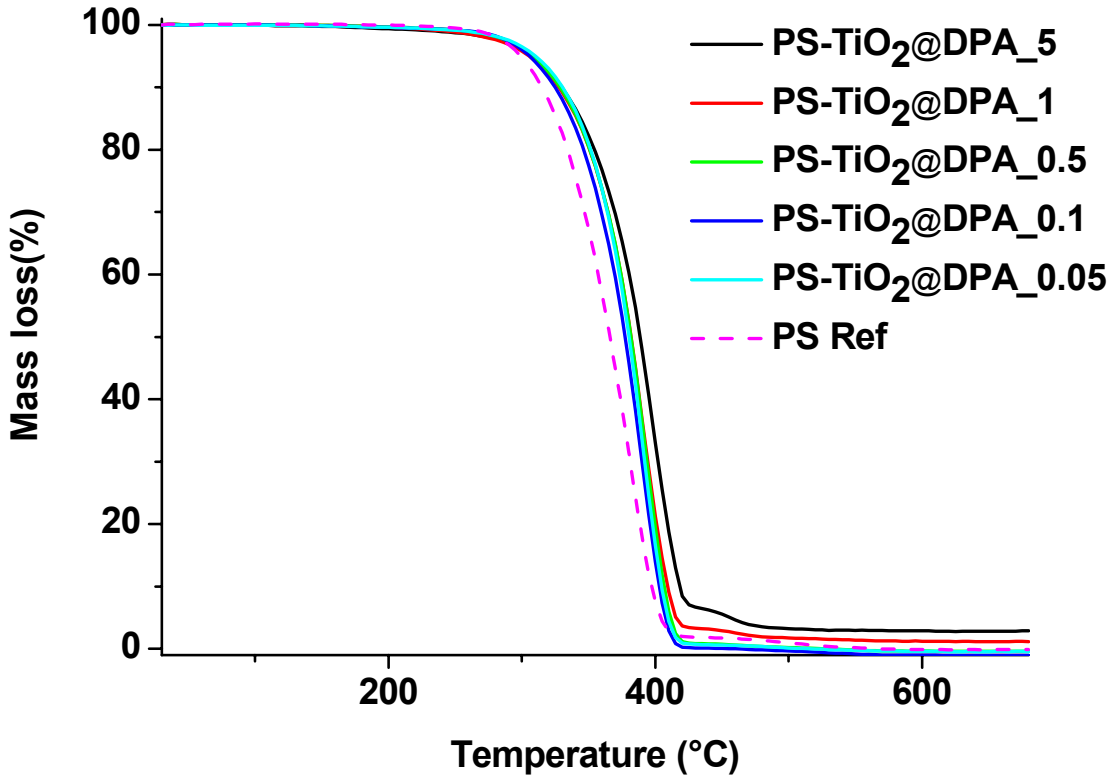

Figure 113. TG analysis of the PS series having TiO_2DPA between 0 and 5%

Table 12. The decomposition onsets and mass losses calculated from TGA for the PS doped with various amounts of TiO_2-DPA nanoparticles

Sample	Onset 1 (T°C)	Mass Loss 1 (%)	Onset 2 (T°C)	Mass Loss 2 (%)	Residual Mass (%)
PS-R	330	100	-	-	0
PS-0.05	356	100	-	-	0
PS-0.1	350	100	-	-	0
PS-0.5	356	99.41	-	-	0.59
PS-1	354	96	446	2.2	1.8
PS-5	359	92	447	4.3	3.7

Due to the low amount of particle loadings in the first samples the residual mass could not be determined. However, the residual mass was clearly identified for the samples containing a higher amount of particles (typically between 1 and 5%). After the subtraction of the relative amount due to the decomposition of the surface modifier, the total residual

amount fits well with the calculated amount of metal oxide present in the hybrid polymer.

DSC measurements of the hybrid polymers were conducted in nitrogen atmosphere in aluminum pans with sample masses between 4 and 8 mg. Glass transition temperatures (T_g) were determined by first removing thermal history of the samples in a heating run with a ramp of 10 °C/min. After cooling the samples, they were heated again with a ramp of 10 °C/min. Figure 114 presents the DSC curves together with their T_g 's values. The pristine PS sample presents a T_g with an onset temperature of 99°C, which is in accordance with literature reports[216]. All of the samples present T_g temperatures between 97 and 92 °C, without a dependence of the amount of particles incorporated. It is important to mention that in all of the samples only one T_g was observed, which indicates molecular homogeneity on a scale of about 10–30 nm[217]. Another conclusion that can be drawn is that the T_g temperatures of the doped samples decreased slightly compared to the T_g of the neat PS. The few °C difference compared to the neat PS is probably due to different chain lengths, as seen in the SEC analysis, which cause small differences in the thermal behavior. However, there is no real trend of this effect with the amount of particles, so an interpretation is rather hard to make. Most likely the T_g is not really affected by the incorporation of the inorganics.

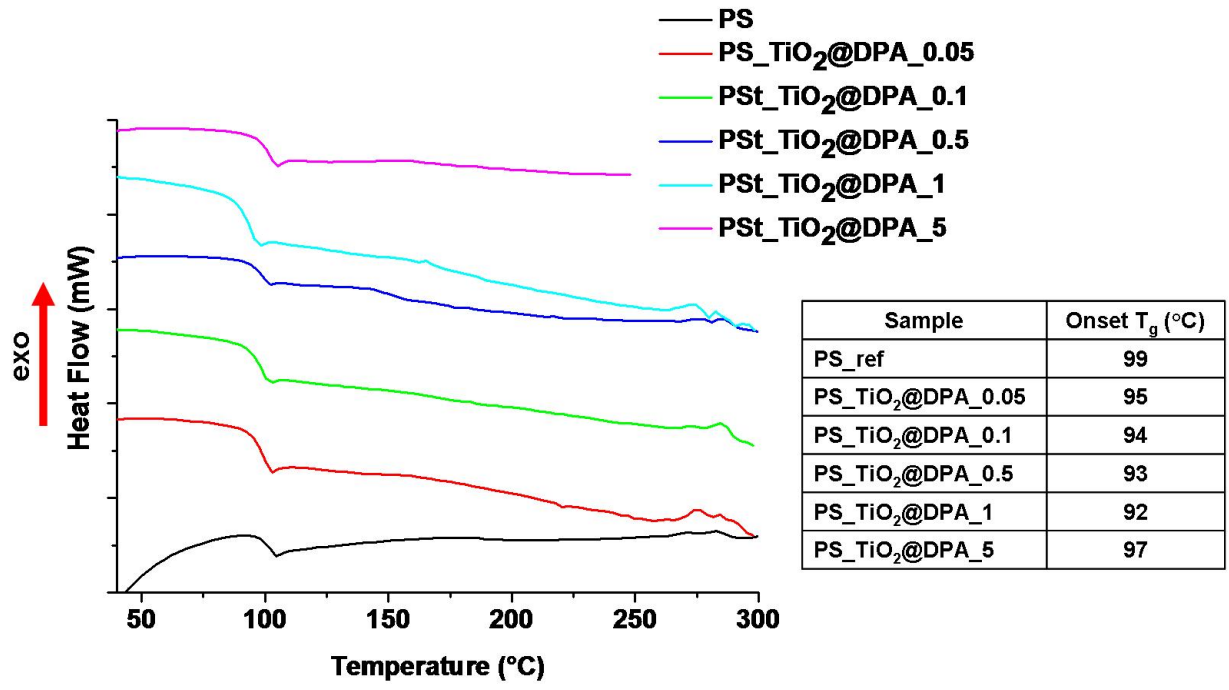

Sample	Onset T_g (°C)
PS_ref	99
PS_TiO$_2$@DPA_0.05	95
PS_TiO$_2$@DPA_0.1	94
PS_TiO$_2$@DPA_0.5	93
PS_TiO$_2$@DPA_1	92
PS_TiO$_2$@DPA_5	97

Figure 114. DSC curves and the respective T_g's for the PS doped with various amounts of TiO_2-DPA nanoparticles

Similar, no significant changes in the T_g temperatures were observed also when a PS matrix was filled with 50 vol% of glass beads with the mean diameter of 5 μm[218], or when PS matrix was filled with 5 vol% of 2 to 4 μm CdS particles[219].

A small shift of the T_g towards higher temperatures was observed for PS matrix filled with Fe_2O_3 particles of about 0.5 μm. This suggests a weak interaction between the filler particles and the PS matrix[220]. This interaction is furthermore proved by decreasing the particles surface, thus increasing the surface. In this later case a high increase in the T_g of about 17 °C was observed when a PS matrix filled with 3.7 wt% of Fe_2O_3 particles of 5 nm was prepared[221].

Shift of the T_g to slightly higher values was also observed by the incorporation of zirconium clusters into PS[215].

4.6.2.4. Transparency

The relative transparency of the materials can be visualized from Figure 115. The neat polystyrene is highly transparent. When doping the polymer with the DPA-modified particles, even at low ratio (0.05 %) the transparency decreases significantly. The hybrid polymers became slightly opaque but still maintained a reasonable transparency up to loadings of 0.5 %. Above this value the color changes from a slightly opaque material to a yellow opaque polymeric material, as it can be seen from Figure 115. This can be an effect of different refractive indeces of the two materials (PS ~ 1.58, anatase ~ 2.49) or can be due to some agglomeration of the particles in the polymer matrix. However, the agglomeration was excluded as proven in the next chapter (Chapter 4.6.6.).

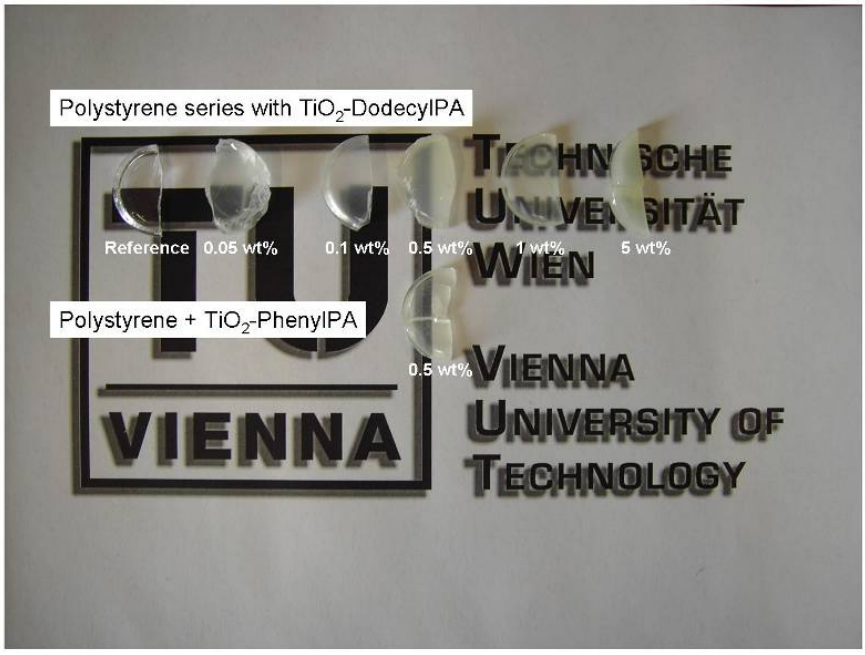

Figure 115. PS doped with various amounts of TiO_2@DPA nanoparticles (upper row) or with TiO_2-PPA nanoparticles (lower row)

4.6.3. Nanocomposites with Covalent Bonding between Matrix and Nanoparticles

Similar as seen for the synthesis of the nanocomposites based on PS and TiO_2@DPA, where no covalent bonding between the matrix and the fillers was presented, nanocomposites with a covalent bonding between the two parts could also be prepared based on TiO_2@MetC5PA-Et and MMA as the organic monomer.

The surface-functionalized TiO_2 nanoparticles were dispersed in MMA (1 mg/mL) using an ultrasound bath for 15 minutes. After the dispersion of the particles in MMA the solutions were polymerized at 80°C using BPO (1 wt.%) as initiator. The polymerizations were carried out in closed 10 mL vials under an argon atmosphere. Two different cases of polymerization were investigated: in the presence or the absence of an additional organic crosslinker (trimethoylolpropane trimethacrylate).

4.6.3.1. Spectroscopic Studies

The FT-IR analyses of the obtained polymers doped with TiO_2-MetC5PA-Et are presented in Figure 116. The FT-IR analyses for the obtained TiO_2-MetC5PA-Et have been already reported in Chapter 4.3.1. In the case of the doped polymers no remaining double bonds are present. However, it is hard to state that they do not exist anymore, due to the low content of inorganic particles. The carbonyl moiety of the PMMA is evidenced by the strong C-O band at 1740 cm^{-1}. Due to the very low content of phosphonate molecules and to the overlapping of their specific bands with the ones obtained from the organophosphorus coupling agent no real conclusions about the incorporation of the particles can be drawn from the FT-IR analysis.

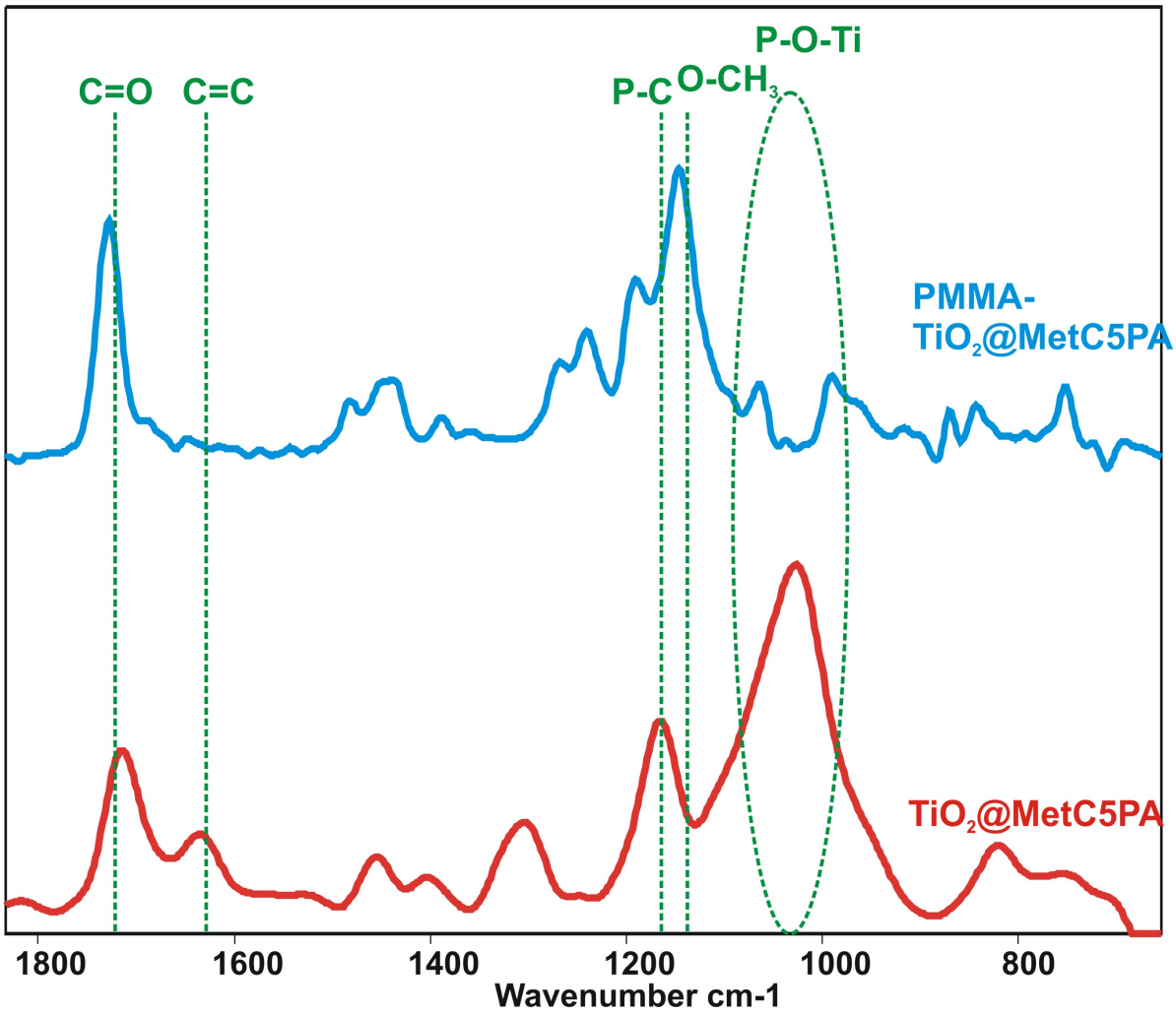

Figure 116. FT-IR analysis of the TiO_2@MetC5PA-Et and PMMA having 1% TiO_2@MetC5PA-Et

4.6.3.2. SEC Studies

The polymerizing process of styrene in the presence of dodecyl phosphonic acid modified particles was not affected by the presence of the particles.

The nanocomposites prepared from the TiO_2@MetC5PA-Et and MMA were also analyzed by SEC. Due to some degree of crosslinking induced by the double bonds present on the surface-modified particles, not the entire sample was soluble in THF. This fact makes the SEC data to have only a qualitative value, to detect if the molecular masses of the resulted doped polymers are in agreement with the reference samples.

SEC results show that the molecular weight distributions were monomodal for all of the doped samples (Figure 117). The MWDs of the resulting polymers were higher in this case, between 4.7 and 6.6. In the absence of chain controllers, these rather high values are normal. As mentioned before, the higher indices can result also from the crosslinking effect of

the methacrylate modified particles. This led to differences in the growing chains and thus increasing of polydispersity. However, no correlations between the amount of particles and the MWDs of the polymers or their molecular masses can be made, proving that the particles have no real influence on the polymerization process at these low contents.

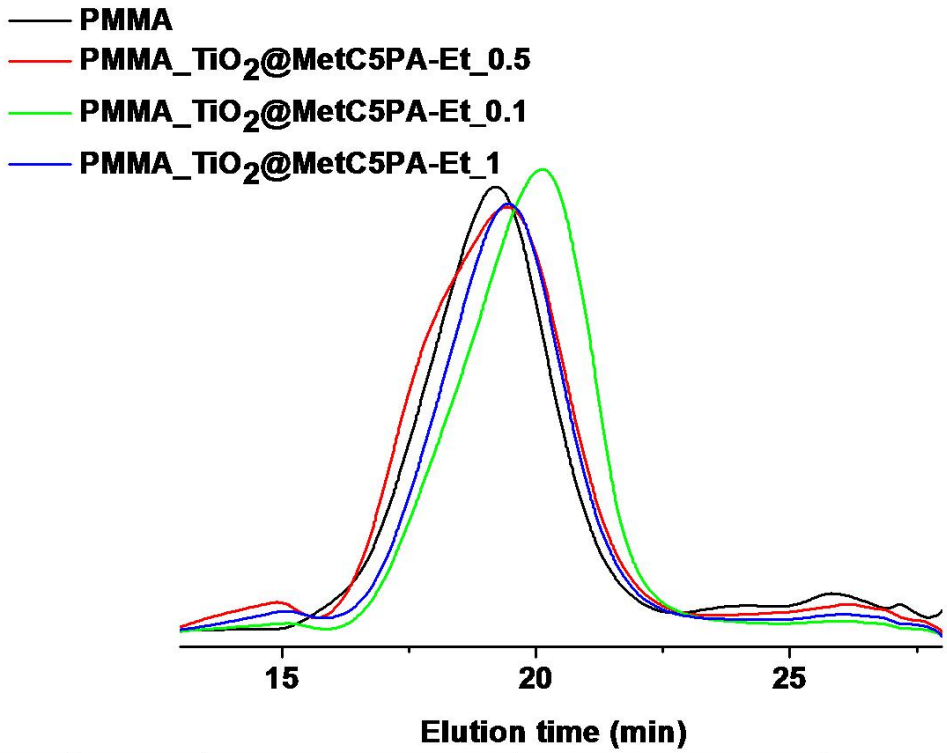

Sample	PMMA	PMMA_ TiO_2@MetC5PA-Et_0.1	PMMA_ TiO_2@MetC5PA-Et_0.5	PMMA_ TiO_2@MetC5PA-Et_1
Mn	186308	92407	147904	134343
Mw/Mn	6.6	5.2	6.4	4.7

Figure 117. SEC analysis of the PMMA and PMMA having various amounts of TiO_2-MetC5PA-Et

No effect was observed like the one reported by *Demir et al*[103], where TiO_2 particles surface-modified with octyl phosphonates were incorporated in PMMA. They observed that the nanoparticles suppress the autoacceleration which would otherwise occur, resulting in a better control of heat dissipation and MWDs.

PMMA/TiO_2 composites prepared from the in-situ grafting polymerization of MMA from TiO_2 surface-modified with silane coupling agents showed higher molecular weights and MWDs for the composites compared to the pure PMMA[96]. TiO_2 nanoparticles (d = 4.5 nm) surface-modified with 6-palmitate ascorbic acid were also incorporated in PMMA

matrices in weight ratios between 0.95 and 3.9 %[88]. No significant changes of the molecular masses and the MWDs were observed between the nanocomposites and the pristine PMMA samples.

4.6.3.3. Thermal Properties

Aditional information about the particles incorporation in the polymer matrices was obtained by the thermal analysis (TGA). The TG analyses were carried out similar as in the cases of the PS nanocomposites (air, 10°C / minute, up to a temperature of 700°C). Figure 118 presents the specific thermal behaviors of the PMMA series with TiO_2@MetC5PA-Et nanoparticles incorporated in the absence of an organic crosslinker.

The thermal decomposition in air of the reference PMMA sample proceeds at an onset temperature of 248°C through the depolymerization of the macromolecular chains. The mechanism of thermo-oxidative degradation of PMMA is much more complex than the mechanism of degradation in nitrogen. The oxygen suppresses degradation of free radical polymerized PMMA caused by the presence of the weak linkages in the PMMA chains at the low temperature but it enhances PMMA degradation at higher temperatures[88]. Kinetic analysis suggests that the initial rates of degradation under nitrogen and air are respectively controlled by the unzipping of the polymer chain and by degradation initiated by random scission. At the later stage the thermal degradation is controlled by random scission under both air and nitrogen[222].

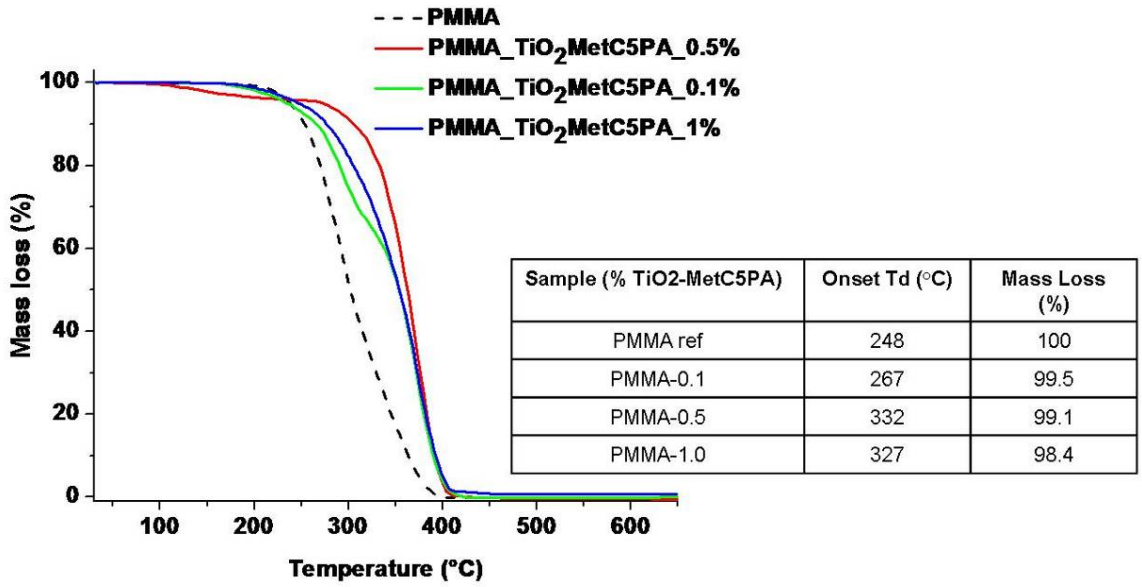

Sample (% TiO2-MetC5PA)	Onset Td (°C)	Mass Loss (%)
PMMA ref	248	100
PMMA-0.1	267	99.5
PMMA-0.5	332	99.1
PMMA-1.0	327	98.4

Figure 118. TG analysis of the PMMA series having TiO_2-MetC5PA-Et between 0 and 1%

With the incorporation of the modified TiO_2 nanoparticles inside the polymer matrices, the thermal decomposition temperature increases. With the incorporation of only 0.1 % TiO_2@MetC5PA-Et nanoparticles the onset decomposition temperature is increasead by almost 20°C. The shift of the decomposition onset temperature to higher values was earlier observed in similar PMMA/TiO_2 nanocomposites[89, 96] and indicates the enhancement of the thermal stability of the composite compared to the neat polymer. This thermal behavior of the composite provided a strong support that the methacrylic bonds of the the particles are copolymerized with the PMMA matrix, so that the TiO_2 particles act as crosslinkers in the polymerization process, which leads to a higher decomposition temperature. This fact is also supported by the further increase in the amount of particles which led to an onset temperature of about 330°C (for 0.5 % TiO_2-MetC5PA), due to more crosslinking sites. However, further increase in the amount of particles incorporated in the matrix (1%) does not lead to a further enhancement of the thermal stability anymore, showing a saturation of this effect. The residual mass after the decomposition of the polymers fits reasonable with the amount of nanoparticles incorporated, considering that char is also created during the thermo-oxidative combustion of the hybrid materials.

Similar as for the PS studies, DSC measurements of the hybrid polymers were conducted in nitrogen atmosphere in aluminum pans, with a sample mass between 4 and 8 mg. Glass transition temperatures were determined by first removing thermal history of the samples in a heating run with a ramp of 10 °C/min. After cooling the samples, they were heated again with a ramp of 10 °C/min. Figure 119 presents the DSC curves together with their T_g values.

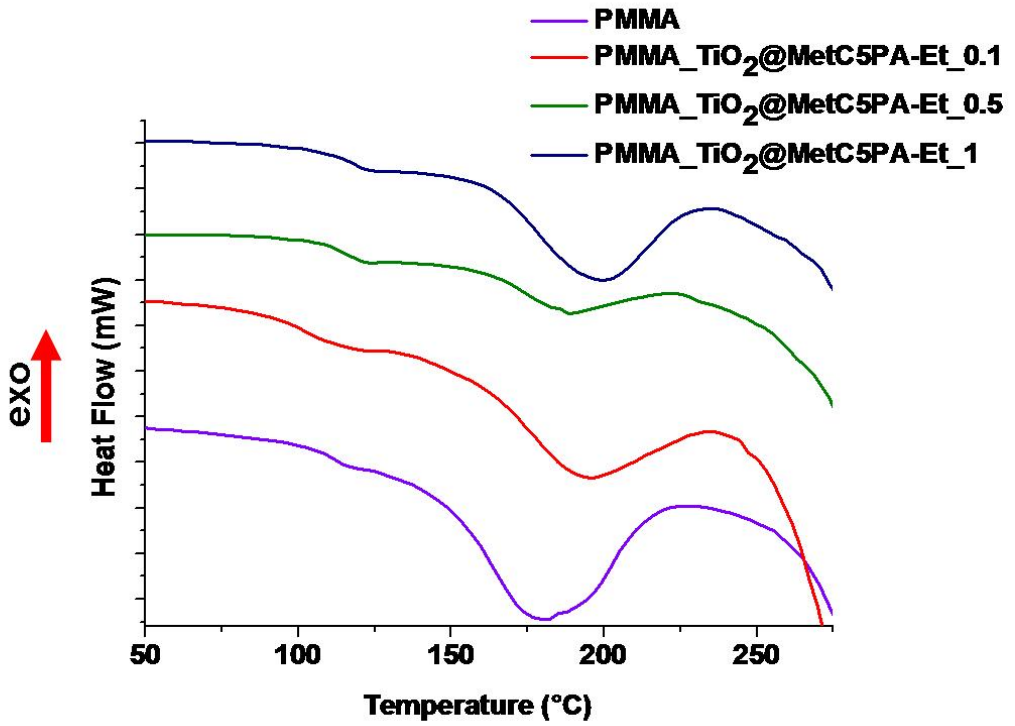

Sample	Onset T_g (°C)	Onset T_m (°C)	Onset T_d (°C)
PMMA_ref	109	151	258
PMMA_TiO_2MetC5PA-E_5_0.1	101	160	262
PMMA_TiO_2MetC5PA-Et_0.5	110	157	267
PMMA_TiO_2MetC5PA-Et_1	109	164	254

Figure 119. DSC analysis of the PMMA series having TiO_2-MetC5PA-Et between 0 and 1%

The pure PMMA matrix exhibited a glass transition temperature (T_g) of 109 °C, while the PMMA-functionalized titania nanocomposites prepared by bulk polymerization exhibited T_g values ranging from 101 to 110 °C. The smaller T_g obtained for a loading of 0.1% nanoparticles could also be linked to the lower molecular weights obtained for this sample. It was observed for composites consisting of Fe_2O_3 nanorods and PMMA that low molecular components can act as plasticizers, reducing the T_g of PMMA[223]. It was also shown that the thermal transitions depend on the molecular masses for the pristine PMMA[224]. However, in the absence of further data about the polymer tacticity and considering the fact that the particles are copolymerized with the MMA and induce some degree of crosslinking no real correlation can be made. For a loading of 0.5 and 1 % nanoparticles the onset temperatures of the T_g were basically unchanged, revealing that the glass transition is most likely not affected by the grafting of the particles. Hybrid materials synthesized from TiO_2/PMMA using methacrylic acid as coupling agent[89] showed an increase of the T_g starting with 3.5% particle

incorporation. Thus, it is reasonable to sustain that here the amount of particles is not high enough to affect glass transition of the matrix.

A second endothermic peak appears at values around 151°C for the neat PMMA and around 160°C for the composites. This could be assigned to the melting of some of the polymeric chains which were maybe not crosslinked by the nanoparticles[225]. The small enhance (10°C compared with the pure polymers) may be due to the crosslinking effect induced by the nanoparticles. This is sustained by the small increase observed in the decomposition temperatures.

4.6.4. Nanocomposites with Covalent Bond between the Matrix and the Nanoparticles with Additional Organic Crosslinker

Hybrid polymers were also prepared using 1 wt % trimethoyloylpropane trimethacrylate (Scheme 18) as an organic crosslinker. The concentration of crosslinker was maintained constant and was not increased to avoid fast gelation. The organic molecule is widely used for the synthesis of highly crosslinked polymers with improved thermal and mechanical stability. The effect of this additionally crosslinker on the nanocomposite properties was investigated.

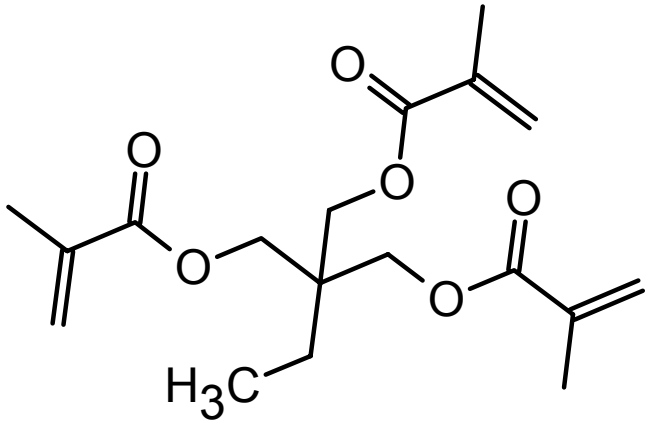

Scheme 18. The chemical structure of trimethoylolpropane trimethacrylate

4.6.4.1. Thermal Properties

Thermogravimetric analyses were carried out in air with 10°C per minute up to a temperature of 700°C in order to assure the complete decomposition of the organic content. Figure 120 presents the specific thermal behavior of the PMMA series with TiO_2@MetC5PA-Et nanoparticles incorporated in the presence of the organic crosslinker.

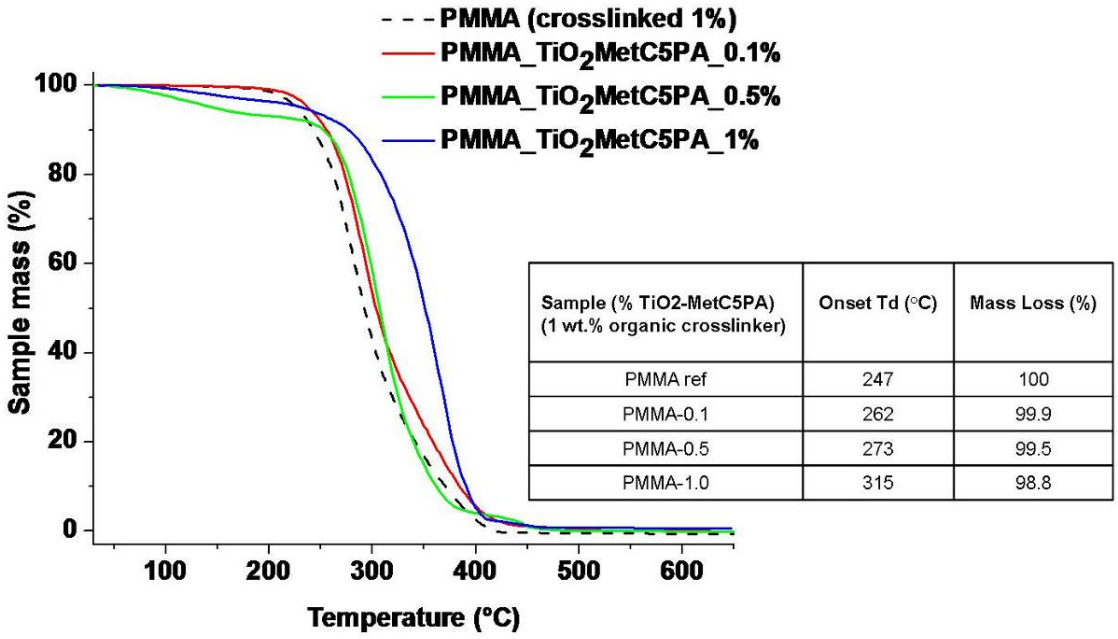

Sample (% TiO2-MetC5PA) (1 wt.% organic crosslinker)	Onset Td (°C)	Mass Loss (%)
PMMA ref	247	100
PMMA-0.1	262	99.9
PMMA-0.5	273	99.5
PMMA-1.0	315	98.8

Figure 120. TG analysis of the PMMA series having TiO_2@MetC5PA-Et between 0 and 1% with additional 1 wt % organic crosslinker

The thermal decomposition in air of the reference PMMA crosslinked by 1 wt.% trimethoylolpropane trimethacrylate takes place at an onset temperature of 247°C through the depolymerization of the macromolecular chains. This is virtually the same as for the pure PMMA in the absence of the crosslinker, which might appear awkward. However, in the case of PMMA crosslinked by various methacrylates, *Levchik et al.* showed that the crosslinking density depends on the amount of crosslinking agents but that the crosslinked polymers might undergo thermal degradation more easily than the homopolymers without crosslinkers[214]. This was observed also for high wt % of crosslinkers, typically between 5 and 40 wt %. With the incorporation of the modified TiO_2 nanoparticles in the polymer matrices, the thermal decomposition step moves to higher values. For the incorporation of only 0.1 % TiO_2-MetC5PA nanoparticles the onset decomposition temperature is increased by almost 15°C. As presented in the chapter before, this shift indicates the enhancement of the thermal stability of the composite. Further increase in the amount of particles (for 0.5 % TiO_2-MetC5PA) leads to an onset temperature of about 273°C, due to more crosslinking sites. An increase in the particle amount (1 %) enhances the thermal stability more pronounced showing an onset decomposition temperature of about 315°C. However, as stated before, it has to be considered that the addition of the organic crosslinker leads to a decrease of the thermal stability of the

polymer, when compared with the sample having 1 wt % nanoparticles without further organic crosslinker (327°C). Further increase in the amount of the particles was not carried out due to the low dispersibility of the particles in the organic monomer (MMA). The residual mass after the complete decomposition of the polymers fits better in this case with the amount of nanoparticles incorporated.

DSC measurements were also carried out for this series of samples (Figure 121). A remarkable difference compared to the previously discussed samples is the fact that there is no significant thermal transition peak that can be attributed to a glass transition. This might be due to two reasons: (i) either the combination of both crosslinkers makes the polymer chain segment immobile, and thus, the glass transition temperature is probably close to the decomposition temperature as observed before by *Lee et al.*[226], or (ii) due to various crosslinking effects which create a heterogeneous system, thus the glass transition is not well defined.

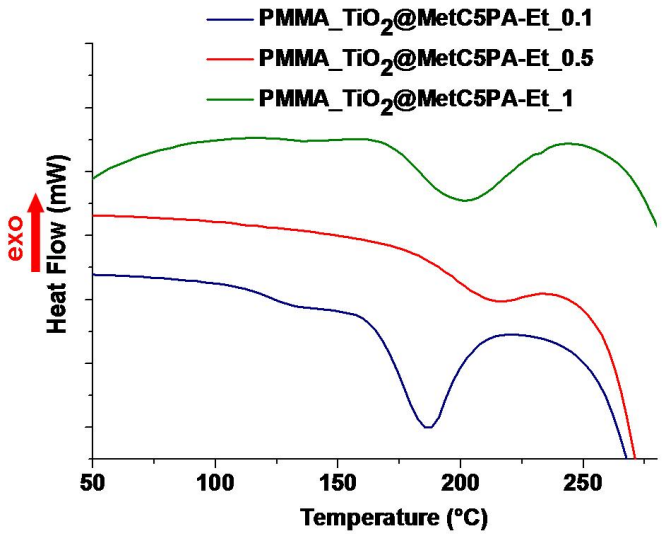

Figure 121. DSC analysis of the PMMA series having TiO_2@MetC5PA-Et between 0 and 1 % with additional 1 wt. % organic crosslinker

4.6.5. Transparency

Similar as observed in the case of the nanocomposites without covalent bonding between the particles and the matrix, the bulk hybrid polymers were removed from the glass vials and their relative transparency was compared to the pure PMMA samples (Figure 122).

In the absence of the organic crosslinker the neat PMMA is highly transparent. Up to 0.1 wt. % TiO_2-MetC5PA-Et doping the hybrid material maintains its transparency without any visible change.

Starting with loadings of 0.5 % particles, the nanocomposites revealed a yellow color but still maintained a high transparency. As presented in the case of the PS nanocomposites, this is an effect of different refractive indeces of the two materials (PMMA ~ 1.49, anatase ~ 2.49). By increasing the amount of particles to 1 % the yellowing of the hybrids becomes clear, sustaining a difference in the refractive indices of the two materials.

When using 1 % trimethoylolpropane trimethacrylate, the neat PMMA, prepared in the absence of any inorganics, appears already little opaque (Figure 122). Another observation is the fact that the edges of the sample have a ripple texture. This is due to the fast gelation in this case, induced by the organic crosslinking. In this case also the nanocomposites maintain their transparency without any visible change up to 0.1 wt. % TiO_2@MetC5PA-Et doping. However, at higher amounts of particles, the yellowing effect is present as well, similar to the samples prepared without any organic crosslinker.

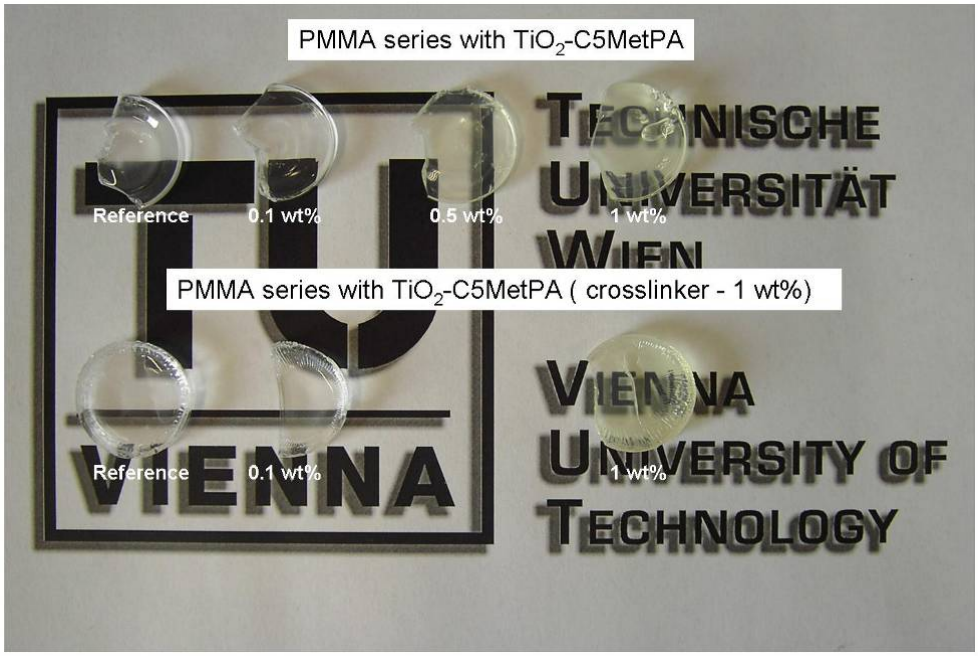

Figure 122. PMMA doped with various amounts of TiO_2-MetC5PA-Et nanoparticles without organic crosslinker (upper row) or with organic crosslinker (lower row)

4.6.6. Small Angle X-ray Scattering Investigations

SAXS studies were carried out on both PS and PMMA samples with the highest content of particles (PS-5 %, PMMA-1%) to investigate potential particle agglomeration in the polymer matrix. The powdered samples were measured and compared with the references, PS

respectively PMMA without any particles incorporated (Figure 123). Both the PS and PMMA reference samples present peaks at high q values (between 6 and 20, q/nm^{-1}). The data obtained from the samples containing nanoparticles were normalized to these peaks, in order to subtract the polymer background. The nanocomposites presented some shoulders at low q values which were assigned to the presence of the nanoparticles.

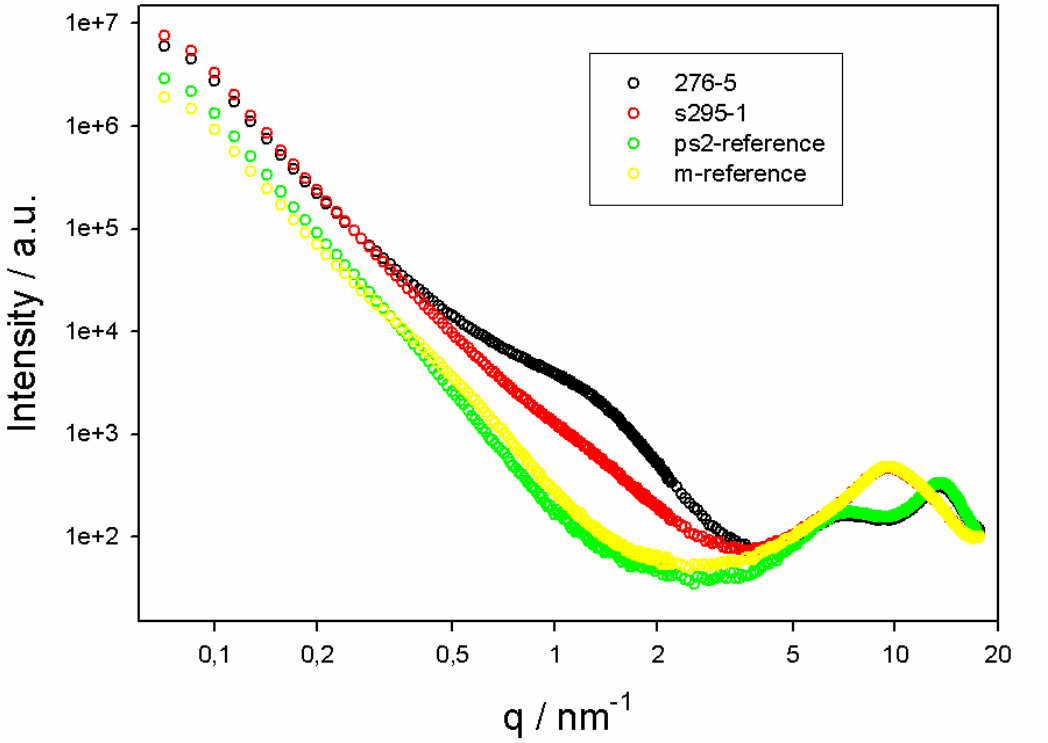

Figure 123. SAXS data for the PS and PMMA samples (references, s276 – 5 = PS – 5%, s295 – 1 = PMMA – 1%)

Information about the nanoparticles was obtained after the subtraction of the pure polymer and of the background resulting from the large units (> 100 nm). The points in Figure 124 show the obtained data, while the lines are the fits to the data, with a Gaussian distribution of randomly distributed spheres. The numerical data obtained after the fitting of the points are in good agreement with the size of the nanoparticles before their incorporation. For the PS hybrids, the numerical data obtained for the radius of the TiO_2-DPA particles is 2.12 nm, with an error of 0.57 nm. The PMMA hybrid exhibit radii of the TiO_2-MetC5PA-Et particles of 1.88 nm, with an error of 0.57 nm. Both values prove that the particles are not agglomerated in the polymer matrices, and they are randomly dispersed. This shows that the shading and the yellowing of the hybrid materials is induced not by agglomeration but most likely from the differences in the refractive indices of the two components or interactions between the polymer and the particle surfaces.

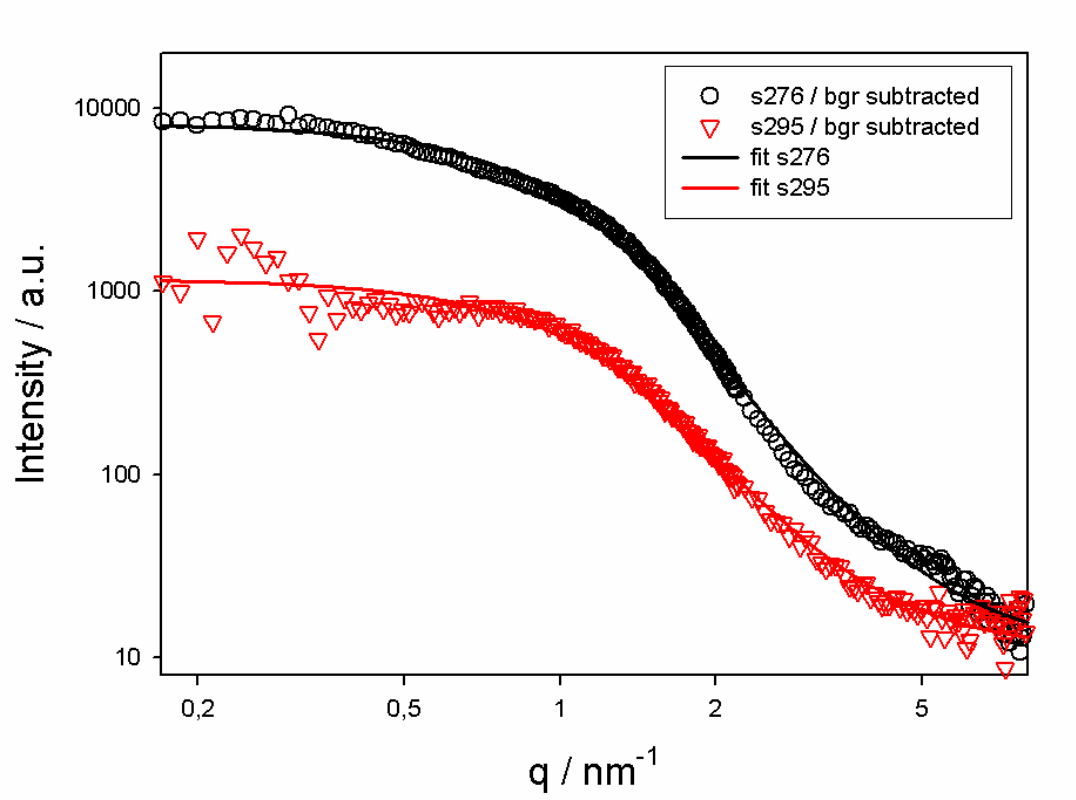

Figure 124. SAXS data (sign) and the Gaussian fits (lines) for the PS and PMMA samples (s276 – 5 = PS – 5% TiO_2@DPA, s295 – 1 = PMMA – 1% TiO_2@MetC5PA-Et)

4.6.7. General Remarks

TiO_2 nanoparticles surface-modified with organophosphorus coupling agents were easily dispersed in common organic monomers. Light scattering studies revealed that TiO_2 nanoparticles modified with phosphonates containing long alkyl chains (e.g. dodecylphosphonic acid) were easily dispersed in styrene, while TiO_2 nanoparticles modified with phosphonates having methacrylate double bonds (e.g. 2-Methyl-acrylic acid 5-(diethoxy-phosphoryl)-pentyl ester) were easily dispersed in methyl metharcylate.

Nanocomposites without covalent bonds between the matrix and the fillers were prepared by the in-situ polymerization of styrene in the presence of TiO_2 nanoparticles surface-modified with dodecylphosphonic acid. The SEC studies revealed that the radical polymerization process was not affected by the incorporation of the particles, monomodal molecular weight distributions being obtained even at high loading degrees (5 wt % particles). The FT-IR showed the full conversion of the styrene double bonds. Thermogravimetric analysis showed that the nanocomposites exhibit enhanced thermal stability compared to the pristine polystyrene. By the incorporation of the particles DSC results revealed that the glass transition temperatures were slightly smaller compared to the neat polystyrene. This was

explained by the fact that no covalent interactions are present between the matrix and the inorganic fillers. Thus, the particles had a plasticizers effect, increasing the chain mobility. The final nanocomposites showed a good transparency up to 5 wt % loadings. Above this value the nanocomposites became opaque due to the differences in the refractive indices of the two materials.

Nanocomposites with covalent bonds between the matrix and the fillers were prepared by the in-situ polymerization of methyl methacrylate in the presence of TiO_2 nanoparticles surface-modified with 2-Methyl-acrylic acid 5-(diethoxy-phosphoryl)-pentyl ester. FT-IR analysis revealed both the incorporation of the modified particles and the copolymerization of the organophosphorus coupling agent double bonds with the double bonds of the monomers. SEC showed that the polymerization was not affected by the particles and monomodal molecular distributions were obtained even at high loading degrees. The nanocomposites presented an enhanced thermal stability compared to the neat polymer, which was increasing with the increase of the amount of particles. The glass transition temperatures were not affected by the incorporation of the particles. The final nanocomposites revealed good transparency up to 1 wt % loadings. Above this value the nanocomposites became yellow opaque due to the differences in the refractive indices of the two materials.

Similar nanocomposites were obtained with the addition of an organic crosslinker to the MMA/TiO_2@MetC5PA-Et mixtures. The materials were highly crosslinked and insoluble in common organic solvents. Furthermore the thermal stability was increased by the incorporation of the particles compared to the PMMA systems crosslinked only by the organic agent.

Small angle X-ray scattering revealed that in both the nanocomposites (with or without covalent bonds between the fillers and the matrix) the TiO_2 surface-modified particles were randomly dispersed in the polymeric matrix.

5. Experimental Part

5.1 Materials

Titanium tetraisopropoxide ($Ti(O^iPr)_4$, 97%, Aldrich), titanium tetraethoxide ($Ti(OEt)_4$, purum, Fluka), zirconium isopropoxides (ABCR; 70-75 % in heptane), allyl acetoacetate (AAA, 98%, Aldrich), poly(dimethylsiloxane-*co*-methylhydrosiloxane) 50:50 (PDMS-co-PMHS, average M_n ~ 950, methylhydrosiloxane 50 mol %, Aldrich), polyhydromethylsiloxane (PMHS, 97%, average M_n = 1,700-3,200, Aldrich), Pt(0) (Platinum(0)-1,3-divinyl-1,1,3,3-tetramethyldisiloxane complex solution, 0.1 M in poly(dimethylsiloxane), vinyl terminated, Aldrich) catalyst were used as received. Toluene was dried over sodium metal and distilled freshly before usage. Ethanol was dried using magnesium and distilled afterwards. CuBr (Fulka, purum, p.a., ≥ 98.0%) was stirred overnight with concentrated acetic acid, washed with absolute ethanol and dried in vacuum. Pentamethyldiethylene triamine (PMDETA, Aldrich, 99%) and ethyl α-bromoisobutyrate (Aldrich, 98%) were distilled and kept under an argon atmosphere. Methyl methacrylate (Fluka, purum, ≥ 99.0%) and styrene (99% Aldrich) were dried over CaH_2, distilled under argon and kept at -20ºC. 2-(Methacryloyloxy)ethyl acetoacetate (Aldrich, 95%) was distilled under argon. Benzoyl peroxides (BO, 98%, Aldrich) and azobisisobutyronitril (AIBN, ≥ 98%, Alrdich) were used as received and stored at -20 °C.

The solvents used for reactions where the absence of water was required were dried with standard procedures and stored under an argon atmosphere[227]. Operations where the absence of humidity or oxygen was required, e.g. the handling of metal alkoxides and the polymerization procedures, were carried out under argon atmosphere using Schlenk techniques.

5.2 Analytical techniques

5.2.1 Nuclear Magnetic Resonance Spectroscopy (NMR)

NMR spectra were recorded on a Bruker Avance 300 (1H: 300.13 MHz, 13C: 75.47 MHz) equipped with a 5 mm broadband probe head and a z-gradient unit. 2D spectra[228] were measured with Bruker standard pulse sequences:

COSY (Correlated Spectroscopy)

The two-dimensional homonuclear (H, H)-correlated NMR experiment yields NMR spectra in which ^{1}H chemical shifts along both frequency axes are correlated with each other. Magnetization is transferred by scalar coupling.

TOCSY (Total Correlated Spectroscopy)

In the TOCSY experiment, magnetization is dispersed over a complete spin system by successive scalar coupling. In contrast to COSY, the TOCSY experiment correlates allprotons of a spin system. The mixing time was usually 160 ms.

HSQC (Heteronuclear Single Quantum Coherence)

HSQC is the most important inverse 2D heteronuclear (H, C)-correlated experiment. The strategy is to transfer magnetization from a proton to a carbon nucleus. Magnetization vectors are allowed to develop for a time and ^{13}C polarization is transferred back to the proton where the resonance is recorded.

^{1}H / ^{13}C HMBC (Heteronuclear Multiple Bond Correlation)

In this experiment, cross-peaks are observed connecting carbon signals to signals for protons two or more bonds away. Thus, HMBC spectra can be used to assign, inter alia, quaternary carbons.

5.2.2 Fourier Transformed Infrared Spectroscopy (FT-IR)

FT-IR spectra were recorded on a Bruker Tensor 27 instrument working in ATR MicroFocusing MVP-QL with a ZnSe crystal. The software used for analysis was OPUS^{TM} version 4.0.

5.2.3 Elemental Analysis

Elemental analyses were carried out at the Microanalytical Laboratory at the Institute of Physical Chemistry, University of Vienna, on a 2400 CHN Elemental Analyzer by Perkin Elmer.

5.2.4 Size Exclusion Chromatography (SEC)

Size exclusion chromatography (SEC), also known as Gel Permeation Chromatography (GPC), is a method used to separate solutions of (polymer) mixtures according to the molecular size of the components. The mixtures are dissolved in adequate solvents and then passed through columns filled with gel particles swollen in organic solvents. The gel particles are porous, and the pore diameters vary in size. When gels of appropriate pore size distributions have been properly matched with molecular weight ranges of materials to be separated, larger molecules do not enter the gel pores, but pass through the gel columns between particles. Unlike most chromatographic methods, larger entities elute first. The smaller molecules, depending on their size, spend varying amounts of time within the gel particles during an SEC separation. The smallest molecules enter all pores in gel particles and are not separated[229].

Relative size exclusion chromatography (SEC) measurements in tetrahydrofuran were performed using a Waters system including a 515 HPLC pump, a 717 autosampler, a 2410 differential refractive index detector and Styragel columns (HR 0.5, 3, and 4, linear and GPC PHASE SDV 50/100/10E5A) at 40ºC at a rate of 1 ml/min, applying linear polystyrene standards. Molecular weight analyses were calculated using Waters Millennium software including the GPC/V option and related to an internal standard (biphenyl ether).

5.2.5 Thermogravimetric Analysis (TGA)

Thermogravimetric analysis is a technique in which the mass change of a substance is measured as a function of the heating temperature while the substance is subjected to a controlled temperature program. Results are presented as a plot of mass against temperature or time[230]. Mass changes of the samples as functions of temperature were determined on a Netzsch TG 209C Iris thermal analyzer in synthetic air atmosphere at a flow rate of 30 ml/min. Samples were measured in an open platinum pan from 30 °C to a temperature, where complete thermo-oxidative decomposition was assured (~ 700 °C). Initial masses in measurements were kept in the range of 10 mg. A correction curve measured in the same conditions as the samples was subtracted from each thermogram to make allowance for buoyancy and gas viscosity.

5.2.6 Differential Scanning Calorimetry (DSC)

In heat flux differential scanning calorimetry, a temperature difference between sample and reference is measured as the reference is heated at the required rate[231]. This temperature difference is then converted into a heat flow by means of the appropriate conversion factor. The heat flow signal is composed of two parts: one is the heat flow required to raise the sample temperature at the programmed rate, and is directly related to the intrinsic heat capacity of the sample, and the other is the heat flow arising from kinetic processes that may occur during the heating scan, for example phase changes such as melting and crystallization, liquid crystalline transitions or second order transitions such as glass transition.
DSC measurements were performed on a DSC823^e with liquid nitrogen cooling from Mettler Toledo. The polymer samples were powdered and filled into 40µl aluminium crucibles. Measurements were carried out under N_2 atmosphere and a typical temperature program consisted of cooling with 20°C/min to 50°C and a subsequent heating with 20°C/min to 200°C.

5.2.7 Transmission Electron Microscopy (TEM)

Investigations were performed in TEM and scanning TEM (STEM) mode[232]. In TEM the image is formed by a wide beam of electrons which passes through a thin sample. This microscope is analogous to a standard upright or inverted light microscope. Stained areas of the sample absorb or scatter the beam, producing dark spots, unstained areas appear light. STEM uses a focused beam of electrons scanning through the specimen to form an image. Images are produced as in scanning electron microscopy one spot a time. Stained areas of the sample produce light spots in the image, unstained areas remain dark.
Samples for transmission electron microscopy (TEM) measurements were prepared by ultrasonically dispersing the particles in ethanol prior to deposition on a carbon coated TEM Cu grid. TEM measurements were performed on a JEOL JEM-200CX or a JEOL JEM-100CX (USTEM, Vienna University of Technology).

5.2.8 Small Angle X-Ray Scattering (SAXS)

Small-Angle X-ray Scattering (SAXS) is al tool for studying structures in the size range typically between 1 and 100 nm. This includes microstructures in materials, microporosity, micro emulsions and many other questions.

Small-angle scattering considers a range of sizes sufficiently larger than inter atomic distances, so that the scattering length density $\rho(r)$ can be approximated as a continuous variable of the position r in the specimen[233, 234]. The general equation for the SAXS intensity $I(q)$ can be written as

$$I(q) = I_0 \left| \int_V \rho(r) \cdot e^{i \cdot q \cdot r} d^3 r \right|^2$$

where q is the scattering vector, V the specimen volume illuminated by the X-ray beam and I_0 a constant defined by the conditions of the instrument.

SAXS was performed using a pinhole camera with a rotating anode generator (Nanostar from Bruker AXS, Karlsruhe, with CuKα radiation from crossed Göbel mirrors). The X-ray patterns were radially averaged to obtain the intensity in dependence on the scattering vector $q = \frac{4\pi}{\lambda} \sin\theta$, with 2θ being the scattering angle.

5.2.9 X-Ray Diffraction

Single Crystal

A selected crystal was mounted on a Bruker-AXS SMART diffractometer with an APEX CCD area detector. Graphite-monochromated Mo-K_α radiation (71.073 pm) was used for all measurements. The nominal crystal–to–detector distance was 5.00 cm. A hemisphere of data was collected by a combination of three sets of exposures at 173 K. Each set had a different ϕ angle for the crystal, and each exposure took 20 s and covered 0.3° in ω. The data were corrected for polarization and Lorentz effects, and an empirical absorption correction (SADABS) was applied[235]. The cell dimensions were refined with all unique reflections. The structure was solved by direct methods (SHELXS97)[236]. Refinement was carried out with the full-matrix least-squares method based on F^2 (SHELXL97)[236] with anisotropic thermal

parameters for all non-hydrogen atoms. Hydrogen atoms were inserted in calculated positions and refined riding with the corresponding atom.

Powder Diffraction

The crystallinity and the phase composition of the dried samples were examined by powder diffractometry (XRD) on a Philips X'Pert diffractometer using the Cu Kα line as X-ray source.

5.2.10 Dynamic Light Scattering (DLS)

The DLS measurement is based on the autocorrelation function, which basically relates the correlation of the system at one time with itself at a different time. Initially, envision setting up a very long line of microspheres and then releasing them simultaneously at time t_0 which would cause each of them to scatter the incident electric field of the laser. The superposition of the scattered fields at the detector results in an electric field of the value E_0. After a certain period of time the spheres have moved a sufficiently large distance. Afterwards, no coherence to the initial positions, where the spheres were lined up, is present. The movement of the spheres results into the independence of the scattered electric fields superposition of the initiating position and thus no correlation would be obtained. If the period of time is sufficiently short ($t = t_0 + \Delta t$), all of the spheres would have moved a small distance in a random direction due to Brownian motion. The correlation is still similar to the initial line of spheres. In this situation, the electric field at the detector is similar to E_0 which correlates the fields at t_0 and $t_0 + \Delta t$. The autocorrelation function describes the correlation of the system that can be written in the following form:

$$g_1(t) = e^{\frac{-t}{\tau}}$$

where τ is the decay time of the system[237].

It is important to mention that it is not possible to align the microspheres straight and release them simultaneously. This situation is also referred to as an average, where many systems are taken and observed at one time[238]. A complication that arises is that light detectors cannot measure electric fields but light impulses which are related to the electric field via the equation:

$$I = \left(\sum E^*\right) \cdot \left(\sum E\right)$$

where I is the intensity, Σ indicates a sum over all scatters, E is the electric field, and * indicates the complex conjugate. Normally the multiplication of a number by its complex conjugate results in a scalar and not a vector which would lead to the loss of the phase information. *Siegert*, however proved that the phase information is still retained and the autocorrelation function of the intensity obeys the relation

$$g_2(t) = < I_t^{\,2} > \cdot g_1^{\,2}(t) + < I_t >^2$$

where < > indicates an average. Instead of observing the intensity signal in the time domain, a spectrum analyzer will measure the signal in the frequency domain. After performing Fourier transformation, the diffusion coefficient can be calculated using the following equation

$$D^{-1} = \left[\frac{4 n_0 \pi \cdot \sin \frac{\theta}{2}}{\lambda} \right]^2 \cdot \tau$$

where n_0 is the refractive index of the solution, λ is the wavelength, τ is the decay time of the system and θ is the scattering angle[237].
The hydrodynamic radius can be calculated using the Stokes-Einstein relationship

$$R_h = \frac{kT}{6\pi\eta D}$$

where k is the Bolzmann constant, T the absolute temperature, and η is the solvents viscosity. The DLS measurements were performed with an ALV/CGS-3 compact goniometer system with an ALV/LSE-5003 light scattering electronics and multiple τ digital correlator at 25 °C. If not otherwise mentioned a 90° angle was used for the measurements.

5.2.11 Atomic Force Microscopy (AFM)

Samples for AFM were prepared by ultrasonically dispersing the particles in ethanol prior to deposition on a freshly cleaved mica surface. AFM images were recorded using a NanoScope

III Multimode SPM by Veeco Instruments. Measurements were performed in air in tapping, constant amplitude mode using silicon cantilevers with integrated silicon tips (NanoWorld, spring constant 42 N/m, resonance frequency ~285 kHz). All images were recorded with a resolution of 512x512 pixels at scanning rates of 0.5-5.0 Hz, depending on the size of the selected scan area. Data analysis was performed using the commercial NanoScope software.

5.2.12 Scanning electron microscopy (SEM)

SEM imagines were recorded on a Philips XL-30. The samples were sputtered on the surface with a thin gold layer prior to SEM imaging. For measurements secondary electrons were used. The typical conditions (accelerating voltage, magnification etc.) can be seen on the pictures.

5.2.13 X-Ray Photoelectron Spectroscopy (XPS)

The composition of the composite powders was investigated by XPS. XP spectra were run on a Perkin-Elmer Φ5600ci spectrometer using Al monochromatized radiation (1486.6 eV) working at 350 W. The working pressure was $< 5 \cdot 10^{-8}$ Pa. The spectrometer was calibrated by assuming the binding energy (BE) of the $Au4f_{7/2}$ line at 83.9 eV with respect to the Fermi level. The standard deviation for the BE values was 0.15 eV. The reported BE were corrected for the charging effects, assigning, in the outer layers where contamination carbon is still present, to the C1s line of carbon the BE value of 284.6 eV[205, 207]. Survey scans (187.85 pass energy, 1 eV/step, 25 ms per step) were obtained in the 0-1300 eV range. Detailed scans (58.7 eV pass energy, 0.05-0.1 eV/step, 100 ms per step) were recorded for the O1s, C1s, P2p, TiKLL and Ti2p regions. The atomic composition, after a Shirley type background subtraction (D.A. Shirley, Phys. Rev. 55 (1972) 4709) was evaluated using sensivity factors supplied by Perkin-Elmer[207]. Samples were introduced directly, by a fast entry lock system, into the XPS analytical chamber. The assignments of the peaks was carried out by using the values reported in the reference textbook[207, 208].

5.2.14 Photocatalytic studies

The photocatalytic studies were carried out at ARCS Seibersdorf.

A typical solution for photocatalytic test comprises of 200 mL solution of MB (conc. 20μM) and 0.05 g TiO_2 catalyst (with a concentration of 0.25 g/L). The pH was equal with pH = 4. The solution was stirred for 30 minutes at 300 rpm before the reaction start. The solutions

were irradiated with a UVA black light (Sylvania BLB, wavelength 350 – 400 nm). The initial temperature was 20°C and increased up to 23°C after one hour of illumination. Samples of 2mL solution were extracted at 0, 5, 10 minutes and then every 10 minutes up to one hour. Before the analysis the suspension was centrifuged 15 min at 4000 rpm to remove the catalyst. UV measurements of the purified solutions were carried out over the 190–800 nm range to determine the residual concentration of MB and to follow its kinetics of disappearance. A Beer–Lambert diagram was established to correlate the absorbance at 670 nm to MB concentration. Figure 125 shows an image of the photocatalytic reactor used.

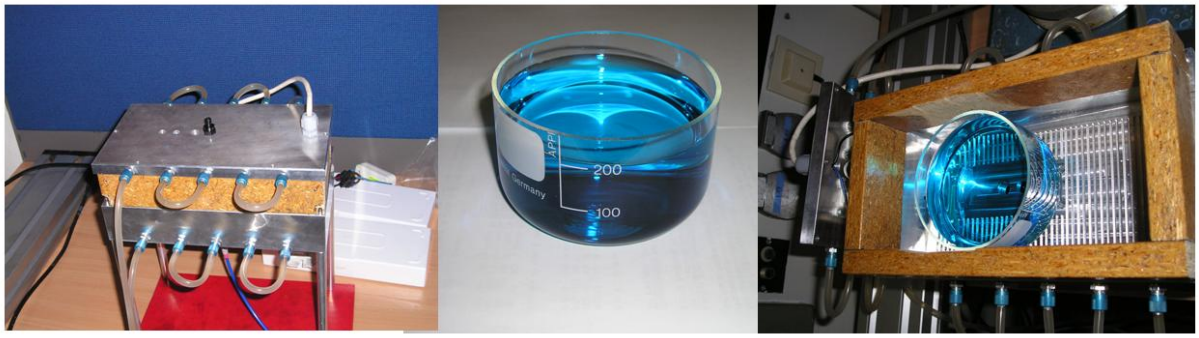

Figure 125. The UVA black light photocatalytic reactor and a typical MB/TiO_2 suspension

5.2.15 Raman

The Raman spectroscopy measurements were carried out at University of Stuttgart, Institute of Physical Chemistry, Group of Prof. Dr. H. Bertagnolli. The used spectrometer was a Bruker RFS 100/S Raman spectrometer with a spectral resolution of 4 cm^{-1}. Samples were excited with a Nd-YAG laser of 1064 nm wavelength.

5.2.16 Nitrogen Sorption

Nitrogen sorption measurements were carried out on an ASAP 2020 M (Micrometrics) instrument. Prior to each measurement the samples were degassed for 12 hours at temperatures between 40 and 120 °C, depending on their composition. The theoretical model used for the interpretation of the data was the Brunauer, Emmett, and Teller (BET) model[239].

5.3 Experimental Part I

5.3.1 Synthesis of Hydroxypropyl Methacrylate and Hydroxybutyl Methacrylate

Hydroxypropyl methacrylate and hydroxybutyl methacrylate were synthesized following published procedures[240]. A solution of 1,3-propanediol (15.0 g, 197 mmol) or 1,4-butandiol (197 mmol) and NEt_3 (33.1 g, 45.6 mL, 327 mmol) in 200 mL of dry THF was cooled with ice. Methacryloyl chloride (20.6 g, 197 mmol) was added dropwise over a period of 1 h with stirring, keeping the temperature between 0 and 3 °C. The reaction mixture was allowed to warm to 50 °C and kept at this temperature for 2 h. After this period, the reaction mixture was cooled and the precipitate filtered. The solvent was evaporated under reduced pressure and the residue redissolved in ethyl acetate (150 mL). The organic phase was washed with 0.5 M $NaHCO_3$ (2*100 mL) and 0.5 M sodium citrate (2*100 mL), dried over $MgSO_4$, and filtered and the solvent evaporated under vacuum. The residue was purified by flash chromatography on silica gel sequentially using the eluents ethyl acetate/hexane 20/80, and then 50/50, to give a colorless liquid.

HPMA. (37 % yield)

FT-IR (ATR, cm^{-1}): υ = 3420 (OH), 2964, 2926, 2892 (CH) 1717 (C=O), 1638 (C=C).

^1H NMR ($CDCl_3$, 25°C, ppm): δ = 5.98-5.99, 5.44, 4.14- 4.19, 3.51-3.6, 3.3 (broad), 1.77-1.85 (m). ^{13}C NMR ($CDCl_3$, 25°C, ppm): δ = 165.2, 135.5, 124.7, 62, 59.6, 32, 18.5.

HBMA. (34 % yield)

FT-IR (ATR, cm^{-1}): υ = 3383 (OH), 2960, 2919 (CH), 1715 (C=O), 1640 (C=C).

^1H NMR ($CDCl_3$, 25°C, ppm): δ = 6.1-5.9, 5.5, 4.2- 4.1, 3.6 - 3.4, 3.1 (broad), 1.9-1.73 (m).

^{13}C NMR ($CDCl_3$, 25°C, ppm): δ = 164, 136, 125.2, 61.5, 58.2, 32, 29. 18.5.

5.3.2 Synthesis of 3-(Methacryloyloxy)propyl Acetoacetate (HAAPMA) and 4-(Methacryloyloxy)butyl Acetoacetate (HAABMA)

6.43 g (0.075 mol) diketene were added under argon to a solution of 7.00 g (0.05 mol) 3-hydroxypropyl methacrylate (or 4-hydroxybutyl methacrylate, 0.05 mole) and 0.50 mL triethylamine (0.0036 mol) in 30 mL dichloromethane keeping the temperature between 0 and 5°C. The mixture was allowed to warm up at room temperature overnight under vigorous stirring. The reaction mixture was extracted several times with water. The organic layer was

dried over Na_2SO_4 and the solvent was removed under reduced pressure. The residue was purified by column chromatography on silica gel using hexane: ethyl acetate.

HAAPMA: Yellowish liquid, 6.65 g, yield 60%.
FT-IR (ATR, cm^{-1}): υ = 1637 (C=C), 1716 (C=O) cm^{-1}.
^{1}H NMR ($CDCl_3$, 25°C, ppm): δ = 1.93 (m, 2H, $CH_2CH_2CH_2$), 2.03 (s, 3H, CH_3C=), 2.26 (s, 3H, CH_3CO), 3.46 (s, 2H, $(CO)_2CH_2$), 4.22 (t, 2H, J = 6.20 Hz, OCH_2), 4.24 (t, 2H, J = 6.27 Hz, CH_2O), 5.57 (s, 1H, CH_2 = $C(CH_3)$), 6.09 (s, 1H, CH_2=$C(CH_3)$).
^{13}C NMR ($CDCl_3$, 25°C, ppm): δ = 16.7 (CH_3C=), 28.1 ($CH_2CH_2CH_2$), 28.7 ($COCH_3$), 48.0 ($COCH_2CO$), 61.4 (CH_2O), 62.9 (OCH_2), 123.5 (CH_2=C), 134.3 (CH_2=*C*), 165.4 (=$C(CH_3)$*C*OO), 170.8 (O*C*O), 198.7 (H_2CO).

HAABMA: Yellowish liquid, 7.17 g, yield: 61%.
FT-IR (ATR, cm^{-1}), ν = 1636 (C=C); 1718 (C=O).
^{1}H NMR ($CDCl_3$, 25ºC, ppm) δ = $CH_2CH_2CH_2CH_2$: 1.63-1.72 (m, 4H, overlapped), $CH_2CH_2CH_2CH_2$: 1.63-1.72 (m, 4H, overlapped), CH_3C=: 1.89(s, 3H), CH_3CO: 2.3(s, 3H), $(CO)_2CH_2$ 3.62(s, 2H), OCH_2: 4.12 (broad, overlapped, 2H), CH_2O: 4.13(broad, overlapped, 2H), CH_2=$C(CH_3)$: 5.51(s, 1H), 6.05(s, 1H).
^{13}C NMR ($CDCl_3$, 25ºC, δ, ppm), CH_3C=: 16.2, $CH_2CH_2CH_2CH_2$: 25.2, $CH_2CH_2CH_2CH_2$: 25.3, $COCH_3$: 28.3, $COCH_2CO$: 50.1, CH_2O: 60.3, OCH_2: 62.8, CH_2=C: 123.4, CH_2=*C*: 136.1, =$C(CH_3)$*C*OO: 165.2, O*C*O: 168.1, CH_2CO: 198.6.

5.3.3 Synthesis of β-Keto Esters Modified Metal Alkoxides

The *β*-keto ester ligand was added dropwise to a solution of a metal alkoxide in an absolute solvent (n-heptane, dichloromethane, toluene, alcohol) in ratios between 1:1 and 4:1 under stirring. The reaction was carried out overnight and the solvent was evaporated afterwards under reduced pressure. The resulting product was either an oily liquid (Ti compounds) or a solid (Zr compounds) soluble in most organic solvents (dichloromethane, n-heptane, toluene). Elemental analyses were carried out only in the cases of the well-defined Ti-ethyl acetoacetate for which also X-ray structures were obtained. The spectroscopic analyses were fitting well with previous data, so no further elemental analyses were carried out due to the fact that the compounds are very moisture sensitive. The yields were calculated only for the crystalline products obtained.

5.3.4 Synthesis of $[Ti(O^iPr)_3(EAA)]_2$ Crystals

Ethyl acetoacetate (10 mmol, 1.26ml) in 5 mL n-heptane was added dropwise to a solution of $Ti(O^iPr)_4$ (10 mmol) in 20 mL n-heptane in a 1:1 ratio and the mixture was stirred overnight. The solution was concentrated under reduced pressure and colorless crystals were obtained by cooling the solution at -20ºC overnight. $C_{30}H_{60}O_{12}Ti_2$, Yield: 2.68 g (76%) colorless crystals. Elemental anal.: calc.: C: 50.85%, H 7.94% found: C 49.63%, H: 6.54% (the differences due to the fact that the compounds are highly moisture sensitive, leading to small decomposition when exposed to air).

$Ti_2(O^iPr)_6(EAA)_2$

FT-IR (ATR): υ = 1633, 1610 (C=C), 1520 (C=O) cm^{-1};

^{1}H NMR ($CDCl_3$, 25°C): δ = 1.21 (m, overlapped, CH_3CH_2O), 1.21 (m, overlapped, 36H, CH_3^{OiPr}), 1.81 (s, 2H, CH_3CO), 1.95 (s, 6H, CH_3CO), 4.04 (q, J = 6.75, 13.40 Hz, 4H, CH_2O) 4.23 (br, 1H, CH_2O), 4.50 (sept, 4H, J = 5.91, 12.05 Hz, CH^{OiPr}), 4.77 (sept, 2H, J = 6.07, 11.97Hz, CH^{OiPr}), 4.97 (s, 2H, CO*CH*CO) ppm.

^{13}C NMR ($CDCl_3$, 25°C): δ = 14.4 (CH_3CH_2), 25.0 (CH_3CO), 60.4 (CH_2O), 87.2, 88.6 ($(CO)_2CH$), 172.4 (*C*OO), 184.7 (CH_3CO); O^iPr: 26.6 (CH_3), 76.2, 79.3 (*CH*) ppm.

$Ti(O^iPr)_2(EAA)_2$

FT-IR (ATR, cm^{-1}): υ = 1637, 1614 (C=C), 1525 (C=O).

^{1}H NMR ($CDCl_3$, 25°C, ppm): δ = 1.21 (br, overlapped, 6H, CH_3CH_2O) 1.21 (br, overlapped, 36H, CH_3^{OiPr}), 1.93 (s, 6H, 1.81, 2H, CH_3CO), 4.02 (br, 4H, CH_2O), 4.23 (br, 1H, CH_2O), 4.48 (sept, 2H, J = 5.37 Hz, CH^{OiPr}), 4.76 (sept, 4H, J = 5.96, 11.68Hz, CH^{OiPr}), 4.93 (s, 2H(s), CO*CH*CO).

^{13}C NMR ($CDCl_3$, 25°C, ppm): δ = 14.1 (CH_3CH_2), 25.0, 25.6 (CH_3CO), 60.2 (CH_2O), 88.1, 86.6 ($(CO)_2CH$), 172.3 (*C*OO), 184.6 (CH_3CO); O^iPr: 24.8 (CH_3), 77.1, 78.8 (*CH*).

$Ti_2(O^iPr)_6(AAEMA)_2$

FT-IR (ATR, cm^{-1}): υ = 1634, 1609 (C=C), 1519 (C=O).

^{1}H NMR ($CDCl_3$, 25°C, ppm): δ = 1.22 (d, 24H, J = 6.05 Hz, CH_3^{OiPr}), 1.91,1.97 (br, CH_3CO), 1.95 (br, overlapped, 6H, CH_3C=), 4.23 (m, br, OCH_2), 4.29 (m, br, CH_2O), 4.51 (br, CH^{OiPr}), 4.77 (br, overlapped region, 8H, CH^{OiPr}), 5.02 (s, 1H, $(CO)_2CH$), 5.59 (1H, CH_2=C(CH_3)–), 6.12 (s, 1H, CH_2=C(CH_3)–).

^{13}C NMR ($CDCl_3$, 25°C, ppm): δ = 18.2 (*CH_3*C), 25.2 (*CH_3*CO), 62.1 (O*CH_2*CH_2O), 62.3 (OCH$_2$*CH_2*O), 86.5, 87.9 ((CO)$_2$*CH*), 172.2 (OCO*CH*CO), 167.0 (*C*OO), 125.9 (*CH_2*=), 136.9 (CH$_3$*C*=), 185.8 (CH$_3$*CO*); O^{i}Pr: 25.0 (*CH_3*), 76.2, 79.3 (*CH*).

Ti(O^{i}Pr)$_2$(AAEMA)$_2$

FT-IR (ATR, cm^{-1}): υ = 1637, 1615 (C=C), 1525 (C=O).

^{1}H NMR ($CDCl_3$, 25°C, ppm): δ = 1.22 (br, 18H, *CH_3^{OiPr}*), 1.80 (s, br, *CH_3*CO), 1.87 (s, br, overlapped, *CH_3*CO), 1.88 (s, overlapped, *CH_3*C=), 4.17 (m, O*CH_2*), 4.20 (m, *CH_2*O), 4.71 (m, br, overlapped region, *CH^{OiPr}*), 4.95, 4.98 (s, 1H, (CO)$_2$*CH*), 5.52 (s, 1H, *CH_2*=C(CH$_3$)–), 6.05 (s, 1H, *CH_2*=C(CH$_3$)–).

^{13}C NMR ($CDCl_3$, 25°C, ppm): δ = 18.2 (*CH_3*C), 25.2 (*CH_3*CO), 62.2 (O*CH_2*CH_2O), 65.3 (OCH$_2$*CH_2*O), 87.7, 86.3 ((CO)$_2$*CH*), 166.8(*C*OO), 125.6 (*CH_2*=), 135.6 (CH$_3$*C*=), 173.4 (O*C*OCHCO), 185.7 (CH$_3$*C*O); O^{i}Pr: 24.9 (*CH_3*), 77.5, 79.3 (*CH*).

Ti$_2$(O^{i}Pr)$_6$(AAPMA)$_2$

FT-IR (ATR, cm^{-1}): ν = 1629, 1610 (C=C), 1525 (C=O).

^{1}H NMR ($CDCl_3$, 25°C, ppm): δ = 1.3 (d, J = 5.89 Hz, 18H, *CH_3^{OiPr}*), 1.25 (m, 2H, OCH$_2$*CH_2*CH$_2$O), 1.92, 1.97 (s, *CH_3*CO), 1.96 (s, *CH_3*C=), 4.01 (m, *CH_2*O), 4.17 (t, J = 5.93 Hz, *OCH_2*), 4.48, 4.75, (m, J = 5.78, 11.40 Hz, overlapped region, O*CH^{OiPr}*), 4.94, 4.96 (s, 1H, (CO)$_2$*CH*), 5.56 (s, 1H, *CH_2*=C(CH$_3$)), 6.08 (s, 1H, *CH_2*=C(CH$_3$)).

Ti$_2$(O^{i}Pr)$_6$(AABMA)$_2$

FT-IR (ATR, cm^{-1}): υ = 1630, 1609 (C=C), 1524 (C=O).

^{1}H NMR ($CDCl_3$, 25°C, ppm): δ = 1.21 (m, 18H, *CH_3^{OiPr}*), 1.35 (m, 2H, (CH$_2$)$_2$*CH_2*CH$_2$), 1.65 (m, 2H, CH$_2$*CH_2*(CH$_2$)$_2$), 1.93 (br, *CH_3*CO), 1.93 (m, *CH_3*C=), 4.02 (t, *CH_2*O); 4.12 (t, J = 5.68 Hz, O*CH_2*), 4.48 (sept, 2H, J = 6.04, 11.96 Hz, O*CH^{OiPr}*), 4.75 (sept, 1H, J = 6.04, 12.06 Hz, O*CH^{OiPr}*), 4.95 (s, 1H, (CO)$_2$*CH*), 6.08, 5.55 (s, 1H, *CH_2*=C(CH$_3$)).

Ti$_2$(OEt)$_6$(EAA)$_2$

FT-IR (ATR, cm^{-1}): υ = 1630, 1613 (C=C), 1523 (C=O).

^{1}H NMR ($CDCl_3$, 25°C, ppm): δ = 1.22 (m, br, *CH_3^{OEt}*), 1.22 (m, br, overlapped signals, 12H, *CH_3*CH$_2$), 1.89 (s, *CH_3*CO), 1.96 (s, 3H, *CH_3*CO), 4.05 (m, *CH_2*O), 4.43 (m, overlapped signals, 8H, O*CH_2^{OEt}*), 4.97 (s, 1H, (CO)$_2$*CH*).

^{13}C NMR ($CDCl_3$, 25°C, ppm): δ = 14.9 (*CH_3*CH_2), 24.7 (*CH_3*CO), 60.4 (*CH_2*O), 86.3, 88.7 ((CO)$_2$*CH*), 172.4 (*C*OO), 184.7 (CH_3*C*O); O^{i}Pr: 24.7 (*CH_3*), 77.1, 78.8 (*CH*).

$Ti_2(OEt)_6(AAEMA)_2$

FT-IR (ATR, cm^{-1}): υ = 1634, 1609 (C=C), 1519 (C=O).

^{1}H NMR ($CDCl_3$, 25°C, ppm): δ = 1.23 (t, 9H, J = 6.84 Hz, *CH_3^{OEt}*), 1.91 (s, *CH_3*CO), 1.98 (s, 3H, *CH_3*CO), 1.94 (s, 3H, *CH_3*C=), 4.23 (br, O*CH_2*); 4.27 (br, *CH_2*O), 4.36 (br, O*CH_2^{OEt}*), 4.45 (br, overlapped region, 10H, O*CH_2^{OEt}*) 5.02 (s, (CO)$_2$*CH*), 5.04 (s, 1H, (CO)$_2$*CH*), 5.58 (s, 1H, *CH_2*=C(CH_3)), 6.12 (s, 1H, *CH_2*=C(CH_3).

^{13}C NMR ($CDCl_3$, 25°C, ppm): δ = 18.2 (CH_3C=), 25.4 (*CH_3*CO), 62.3 (O*CH_2*CH_2O), 62.7 (OCH_2*CH_2*O), 87.0, 88.2 ((CO)$_2$*CH*), 125.0 (*CH_2*=), 135.8 (CH_3*C*=), 167.1 (*C*OO), 171.5 (OCOCH*C*O), 185.7 (CH_3*C*O); OEt: 18.4 (*CH_3*), 71.1, 73.2 (*CH_2*).

$Ti(OBu)_6(AAEMA)_2$

FT-IR (ATR, cm^{-1}): υ = 1631, 1608 (C=C), 1523 (C=O).

^{1}H NMR ($CDCl_3$, 25°C, ppm): δ = 1.88 (s, *CH_3*CO), 1.97 (s, 3H, *CH_3*CO), 1.93 (s, 3H, *CH_3*C=), 4.44 (m, overlapped, O*CH_2**CH_2*O), 5 (s, (CO)$_2$*CH*)), 5.03 (s, 1H, (CO)$_2$*CH*)), 5.53, 5.58 (s, 1H, CH_2=C(CH_3)), 6.1, 6.13 (s, 1H, CH_2=C(CH_3), Butoxy: 0.89 (t, 9H, *CH_3*), 1.36 (m, *CH_2*CH_3), 1.54 (m, overlapped signals, 10H, OCH_2*CH_2*), 4.46 (m, overlapped, 10H, O*CH_2*).

^{13}C NMR ($CDCl_3$, 25°C, ppm): δ = 18.2 (*CH_3*C), 25.5 (*CH_3*CO), 62.3 (O*CH_2*CH_2O), 62.7 (OCH_2*CH_2*O), 88.3, 88.8 ((CO)$_2$*CH*), 126.0 (*CH_2*=)), 136.0 (CH_3C=), 167.2 (*C*OO), 170.5 (OCOCH*C*O), 186.1 (CH_3*C*O); OBu: 14.1 (*CH_3*), 19.1 (*CH_2*CH_3), 34.5 (OCH_2*CH_2*), 75.6, 77.7 (O*CH_2*).

$Zr_2(O^iPr)_6(AAEMA)_2$

FT-IR (ATR, cm^{-1}): υ = 1615 (C=C), 1521 (C=O).

^{1}H NMR ($CDCl_3$, 25°C, ppm): δ = 1.24 (m, br, *CH_3^{OiPr}*), 1.91, 1.96 (br, *CH_3*CO), 1.93 (br, *CH_3*C=), 4.06 (m, br, O*CH^{OiPr}*); 4.30 (br, O*CH_2*); 4.33 (br, *CH_2*O), 5.06 (m, br, (CO)$_2$*CH*)), 5.54, 5.59 (s, *CH_2*=C(CH_3)), 6.09, 6.14 (s, overlapping signals, no integration possible, *CH_2*=C(CH_3)).

^{13}C NMR ($CDCl_3$, 25°C, ppm): δ = 18.5 (*CH_3*C), 25.7 (CH_3CO), 60.4 (O*CH_2*CH_2O), 62.3 (OCH_2*CH_2*O), 88.1 ((CO)$_2$*CH*), 125.8 (*CH_2*=), 135.8 (CH_3*C*=), 167.1 (*C*OO), 173.0 (O*C*OCHCO), 187.5 (CH_3*CO*); O^{i}Pr: 21.9 (*CH_3*), 71.0, 71.1 (*CH*).

$Zr_2(OBu)_6(EAA)_2$)

FT-IR (ATR, cm^{-1}): υ = 1609 (C=C), 1573, 1520 (C=O).

^{1}H NMR ($CDCl_3$, 25°C, ppm): δ = 1.14–1.28 (m, *CH_3*CH_2), 1.89, 1.92, 1.96 (s, *CH_3*CO), 4.33–4.04 (m, *CH_2*O), 5.05, 5.06 (s, $(CO)_2$*CH*), Butoxy: 0.89 (m, 9H, *CH_3*), 1.41 (m, *CH_2*CH_3), 1.60 (m, OCH_2*CH_2*), 3.99 (t, overlapping signals, no integration possible, J = 6.63 Hz, O*CH_2*) ppm; ^{13}C NMR ($CDCl_3$, 25°C): δ = 14.2 (*CH_3*CH_2), 25.4 (*CH_3*CO), 60.4 (*CH_2*O), 88.2, 86.7 ($(CO)_2$*CH*), 171.9 (*C*OO), 185.7 (CH_3*C*O); OBu: 14.0 (*CH_3*), 19.1 (*CH_2*), 36.3 (*CH_2*), 69.4 (O*CH_2*).

$Zr_2(OBu)_6(AAEMA)_2$)

FT-IR (ATR, cm^{-1}): υ = 1615 (C=C), 1571, 1519 (C=O).

^{1}H NMR ($CDCl_3$, 25°C, ppm): δ = 1.90, 1.96 (s, *CH_3*CO), 1.94 (s, *CH_3*C=), 3.98 (m, broad, O*CH_2CH_2*O), 5.01, 5.04 (br, $(CO)_2$*CH*), 5.56 (s, *CH_2*=C), 6.11 (s, 1H, *CH_2*=C), Butoxy: 0.89 (m, *CH_3*), 1.37 (br, overlapped, *CH_2*CH_3), 1.67 (m, br, overlapped, OCH_2*CH_2*), 4.17 (t, overlapping signals, no integration possible, J = 6.59 Hz, O*CH_2*).

^{13}C NMR ($CDCl_3$, 25°C, ppm): δ = (*CH_3*C), 25.9 (*CH_3*CO), 62.4 (O*CH_2*CH_2O), 64.4 (OCH_2*CH_2*O), 89.4, 88.2 ($(CO)_2$*CH*), 125.1, 126.0 (*CH_2*=), 136.9 (CH_3*C*=), 167.6 (*C*OO), 173.4 (O*C*OCHCO), 185.9 (CH_3*CO*); OBu: 14.2 (CH_3), 19.4 (*CH_2*CH_3), 36.5 (OCH_2*CH_2*), 69.7 (O*CH_2*).

5.3.5 (Co)Polymerization

All polymerizations were carried out according to standard ATRP procedures described in literature[31]. Copolymerizations were carried out in toluene or in bulk using CuBr catalyst, PMDETA ligand and ethyl-bromoisobutyrate as initiator at 85ºC (monomer:CuBr:PMDETA:Initiator = 200:1:1:2). The ratio between the HAAEMA type monomers and MMA were 1:1, 1:5 and 1:10. Pure HAAEMA monomer was also copolymerized with MMA to compare the results of uncoordinated ligands with those of metal complexes. The polymerization time was between 4 and 6 hours. The reactions were quenched by precipitating the reaction mixture in petroleum ether. In Table 13 are presented some example of prepared polymers.

5.3.6 Typical Example for Homopolymerization of HAAEMA. 5 mL (0.026 mol) HAAEMA, 0.019 g ($0.13\cdot10^{-3}$ mol) CuBr and 0.039 mL ($0.262\cdot10^{-3}$ mol) ethyl 2-bromoisobutyrate were added to a dry flask under inert gas atmosphere. The flask was freeze-

dried three times and filled with Argon. 0.028 mL ($0.13 \cdot 10^{-3}$ mol) PMDETA were added and the reaction flask was placed in an oil bath at 85°C. The mixture was stirred at this temperature for 6 hours. The polymer was precipitated in petroleum ether, washed, and dried under vacuum.Yield (gravimetric calculated): 73%.

^{1}H NMR ($CDCl_3$, 25°C, ppm): δ = 12.01 (OH^{enol}), 5.04 ($(CO)_2CH^{enol}$), 4.30-4.15 (br, 4H, OCH_2CH_2O), 3.55 (br, 2H, $(CO)_2CH_2$), 2.3 (s, 3H, CH_3CO), 1.94 (s, 1H, CH_3C), 1.91-1.62 (br, $CH_2C(CH_3)$-).

5.3.7 Typical Example for Copolymerization of HAAEMA with MMA (1:5). 2 mL (0.011 mol) HAAEMA, 5.55 mL (0.053 mol) MMA, 0.030 g ($0.21 \cdot 10^{-3}$ mol) CuBr and 0.062 mL ($0.420 \cdot 10^{-3}$ mol) ethyl 2-bromoisobutyrate were added to a dry flask under inert gas atmosphere. The flask was freeze-dried three times and filled with Argon. 0.044 mL ($0.21 \cdot 10^{-3}$ mol) PMDETA were added and the reaction was placed in an oil bath at 85°C. The mixture was stirred at this temperature for 6 hours. The polymer was precipitated in petroleum ether, washed, and dried under vacuum. Yield (gravimetric calculated): 79%.

^{1}H NMR ($CDCl_3$, 25°C, ppm): δ = 12.01 (OH^{enol}), 4.99 ($(CO)_2CH^{enol}$), 4.29-4.14 (br, OCH_2CH_2O), 3.67 (CH_3C), 3.55 (br, $(CO)_2CH_2$), 2.3 (br, CH_3CO), 1.95 (s, CH_3C), 1.92-1.43(br, $CH_2C(CH_3)$-).

^{13}C NMR ($CDCl_3$, 25°C, ppm): δ = 202.1 (CH_3CO), 176.1 (CH_3OCO-), 168 ($OCOCH_2CO$), 167.1 (COO), 63.1 (OCH_2CH_2O), 62.1 (OCH_2CH_2O), 43.1 ($CH_2C(CH_3)$-), 42.3 ($CH_2C(CH_3)$-), 51.1 ($(CO)_2CH_2$), 25.4 (CH_3CO), 18.2 ($CH_3C(CH_2)$-).

Table 13. Homopolymers and copolymers, experimental details

Sample	HAAEMA	MMA	CuBr	PMDETA	Initiator (ethyl-2-bromoisobutyrate)	Yield
PHAAEMA	200 eq (5.6 g)	0	1 (0.019 g)	1 (0.028 mL)	2 (0.038 mL)	68
PMMA	-	100 eq (6.78 g)	0.097	0.14 mL	0.1 mL	83
PHAAEMA-co-MMA 1:1	2 mL	1,11 mL	0.030 g	0.044 mL	0.062 mL	74
PHAAEMA-co-MMA 1:5	2 mL	5.55 mL	0.03 g	0.044 mL	0.062 mL	79
PHAAEMA-coMMA 1:10	1.33 mL	7.41 mL	0.02 g	0.03 mL	0.041 mL	76

5.3.8 Typical Example for Copolymerization of M(OR)$_3$AAEMA (M=Ti, Zr; R=Et, ^{i}Pr) with MMA. (1:5): 3.98 g (0.011 mol) Ti(OEt)$_3$AAEMA, 5.55 mL (0.053 mol) MMA, 0.030 g ($0.21 \cdot 10^{-3}$ mol) CuBr and 0.062 mL ($0.420 \cdot 10^{-3}$ mol) ethyl 2-bromoisobutyrate were dissolved in 25 mL solvent (toluene, dichlorobenzene) in a dry flask under inert gas atmosphere. The flask was freeze-dried three times and filled with argon. 0.044 mL ($0.21*10^{-3}$ mol) PMDETA were added and the reaction was placed in an oil bath at 85°C. The mixture was stirred at this temperature for 6 hours. The polymer was precipitated in dry petroleum ether, washed, and dried under vacuum. The copolymers were insoluble in common organic solvents. Yield (gravimetric calculated): 81%. In Table 14 the experimental details of various hybrid copolymers are presented.

^{13}C CP MAS NMR (25°C, ppm): δ = 188.7 (CH_3CO), 176.1 (CH_3OCO-), 166.8 (OCOCHCO), 167.1 (COO), 88.2 ($(CO)_2CH$), 73.2 (CH^{OEt}), 63.1 (OCH_2CH_2O), 62.1 (OCH_2CH_2O), 42.5 ($CH_2C(CH_3)$-), 41 ($CH_2C(CH_3)$-), 25.4 (CH_3CO), 18.4 (CH_3^{OEt}), 18.2 ($CH_3C(CH_2)$-).

Table 14. Hybrid copolymers, experimental details

Complex	Amount	MMA	CuBr	PMDETA	Initiator
Poly[Ti(O^{i}Pr)$_3$AAEMAcoMMA] 1:5	4.58 g	5.55 mL	0.03 g	0.044 mL	0.062 mL
Poly[Ti(OEt)$_3$AAEMAcoMMA] 1:5	4.14 g	5.55 mL	0.03 g	0.044 mL	0.062 mL
Poly[Ti(O^{i}Pr)$_3$AAEMAcoMMA] 1:10	2.29 g	5.55 mL	0.03 g	0.044 mL	0.065 mL
Poly[Ti(OEt)$_3$AAEMAcoMMA] 1:10	1.05 g	2.8 mL	0.008 g	0.011 mL	0.015 mL
Poly[Zr(O^{i}Pr)$_3$AAEMAcoMMA] 1:5	0.85 mL	2.36	0.013 g	0.019 mL	0.026 mL
Poly[Zr(O^{i}Pr)$_3$AAEMAcoMMA] 1:10	0.85 mL	4.73 mL	0.013 g	0.019 mL	0.026 mL

5.3.9 Sol-gel Process

The purified copolymers containing Ti and Zr alkoxides were precipitated in petroleum ether, dried, washed with heptane, powdered, and kept under inert atmosphere. For the sol-gel process the copolymers (approximately 1 g copolymer) were powdered and transferred into a desiccator under a saturated water atmosphere and kept for 7 days, either at room temperature or at 40°C. Afterwards, the polymers were dried under reduced pressure. Yield (gravimetric calculated): 81%.

^{13}C CP MAS (25°C, ppm): δ = 196 (CH_3CO), 175 (CH_3OCO-), 168 (OCOCHCO), 167 (COO), 87.7 ($(CO)_2CH$), 63 (OCH_2CH_2O), 62.4 (OCH_2CH_2O), 48.5 ($CH_2C(CH_3)$-), 42.6 ($CH_2C(CH_3)$-), 25.4 (CH_3CO), 18.2 ($CH_3C(CH_2)$-).

5.3.10 Coordination of Ti alkoxides with AAA

The synthesis was based upon a literature known procedure[153]. AAA (1.58 mL, 11.5 mmol) was added to a solution of $Ti(OEt)_4$ (2.62 g , 11.5 mmol) or $Ti(O^iPr)_4$ (3.26 g, 11.5 mmol) in 20 mL of hexane. The reaction was stirred over night. Removal of the solvent in vacuum gave 1 and 2 as yellow solids

(1): [Ti(OEt)$_3$CH$_3$C(O)CHC(O)OCH$_2$CH=CH$_2$]$_2$. (Yield: 75%).

^{1}H NMR (25°C, $CDCl_3$, δ/ppm). CH_3CH_2O-: 1.22(t), J = 6.75 Hz, CH_3CO: 1.98(s), 1.91(s), OCH_2CH_3: 4.47(m), 4.79(m,br) CH_2CO: 4.63-4.74(m,br), COCHCO: 5.02(s), $=CH_2$: 5.17-5.33(m), -CH=: 5.78-5.99(m).

^{13}C NMR ($CDCl_3$, 25°C, δ/ppm): CH_3CH_2O-: 18.2; CH_3CO: 25.0; OCH_2CH_3: 71.3; CH_2O: 72.8; $(CO)_2CH$: 88.6; $=CH_2$: 117.5; CH=: 133.8; CH_3CO: 174.8; COO: 185.3.

Selected FT-IR bands (ATR, υ, cm^{-1}): (νC=C): 1634/1611, (νC=O): 1574/1524.

(2): [Ti(O^{i}Pr)$_3$CH$_3$C(O)CHC(O)OCH$_2$CH=CH$_2$]). (Yield: 68%)

^{1}H NMR (25°C, $CDCl_3$, δ/ppm). $(CH_3)_2$CHO: 1.24(d), J = 6.1 Hz, CH_3CO: 1.94(s), 1.85(s), $(CH_3)_2CH$: 4.46 (sept), J = 5.7, 11.87 Hz, CH_2O: 4.76(d), J = 6.06 Hz, COCHCO: 4.98(s), $=CH_2$: 5.26(m), -CH=: 5.76-5.92(m).

^{13}C NMR ($CDCl_3$, 25°C, δ/ppm): $(CH_3)_2$CHO: 22.0; CH_3CO: 25.12; =CHCH_2O: 73.2; $(CH_3)_2CH$: 79.2; $(CO)_2CH$: 88.7; $=CH_2$: 117.8; CH=: 133.4; CH_3CO: 174.0; COO: 184.7.

Selected FT-IR bands (ATR, υ, cm^{-1}): (νC=C): 1636/1612, (νC=O): 1576/1529.

Zr(O^{i}Pr)$_6$AAA$_2$. AAA was added to a solution of $Zr(O^iPr)_4$ in 1:1 molar ratio hexane. The reaction was stirred out over night. The solvent was removed in vacuum giving rise to compound ***Zr(O^{i}Pr)$_6$AAA$_2$*** as solid.

5.3.11 Hydrosilation of PDMS-co-PMHS with AAA and coordination with Ti(OR)$_4$

A solution of Si-H functionalized polysiloxanes and allyl acetoacetate (1 mol/mol Si-H groups) in dry THF was stirred at room temperature under argon atmosphere. The coupling reaction was carried out adding 10^{-4} mol Pt(0) catalyst (Karstedt catalyst). The reaction was

further on stirred over night. After the analysis of the product $Ti(O^iPr)_4$ was added (1:1 ratio with respect to the ligand) and the solution was stirred further on overnight. The results for the formation of the polymers are given in the next paragraph.

5.3.12 Hydrosilation of $[Ti(OR)_3AAA]_2$ with PDMS-co-PMHS

To a solution of $[Ti(OR)_3AAA]_2$ (7.98 g, 10.9 mmol) and polysiloxane containing Si-H bonds (2 mL, 2.08 mmol) in dry toluene a few drops of Karstedt catalyst were added (10^{-4} mol). The reaction was stirred overnight and the solvent was removed under vacuum. The reaction was monitored by the disappearance of the Si-H signal in FT-IR and NMR (described in the Results and Discussions part).

$[Ti(OEt)_3AAA]$@PDMS-co-PMHS. (Yield: 79 %)

^{1}H NMR ($CDCl_3$, 25°C, δ/ppm). *CH_3*Si: 0.08(s, br), Si*CH_2*: 0.51(m), *CH_3*CH_2O-: 1.20-1.23(m, br), $SiCH_2$*CH_2*: 1.60-1.88(m, br), *CH_3*CO1.91(s), *CH_2*CO: 3.71-3.82 (m, br), CH_3*CH_2*O-: 4.47(m), CO*CH*CO: 4.98(s).

^{13}C-NMR ($CDCl_3$, 25°C, δ/ppm): *CH_3*SiO: -0.689; CH_2*CH_2*Si: 11.7; *CH_3*CH_2O- 18.2; $SiCH_2$*CH_2*: 22.4; *CH_3*CO: 25.0; $SiCH_2CH_2$*CH_2*: 66.9; CH_3*CH_2*O: 73.1; $(CO)_2$*CH*: 88.7/90.8; CH_3*CO*: 174.2; *COO*: 185.1.

^{29}Si NMR, (CDCl3, 25°C, δ/ppm): $(CH_3)_3SiO$: 6.12, OSiO: -22.78. Selected FT-IR bands (ATR, υ, cm^{-1}): (C=C): 1638/1610, (C-O): 1570/1524, (CH): 1258, (Si-O-Si): 1023, (C-Si-C): 788.

$[Ti(O^iPr)_3AAA]$@PDMS-co-PMHS. (Yield: 81 %)

^{1}H NMR ($CDCl_3$, 25°C, δ/ppm). *CH_3*Si: 0.09(s, br), Si*CH_2*: 0.56(m), *$(CH_3)_2$*CHO- 1.19-1.26(m, br), $SiCH_2$*CH_2*: 1.51-1.68(m, br), *CH_3*CO: 1.93(s), *CH_2*CO: 4.02-4.27(m, br), $(CH_3)_2$*CH*: 4.49(sept), J = 6.01, 11.78 Hz, 4.75(sept), J = 5.21, 11.45 Hz, CO*CH*CO: 4.95(s).

^{13}C-NMR ($CDCl_3$, 25°C, δ/ppm): *CH_3*SiO: -2.18; CH_2*CH_2*Si: 13.3; *$(CH_3)_2$*CHO-: 22.0; $SiCH_2$*CH_2*: 22.6; *CH_3*CO: 25.12; $SiCH_2CH_2$*CH_2*: 64.76; $(CH_3)_2$*CH*: 79.2; $(CO)_2$*CH*: 86.8/88.6; CH_3*CO*: 174.1; *COO*: 184.4.

^{29}Si NMR, (CDCl3, 25°C, δ/ppm): $(CH_3)_3SiO$: 6.4, OSiO: -22.85.

Selected FT-IR bands (ATR, υ, cm^{-1}): (C=C): 1633/1610, (C-O): 1574/1524, (CH): 1259, (Si-O-Si): 1023, (C-Si-C): 788.

5.3.13 Hydrosilation Reaction of $[Zr(O^iPr)_3AAA]_2$ with PDMS-co-PMHS (50:50). To a solution of $[Zr(O^iPr)_3AAA]_2$ (10.9 mmol) and polysiloxane containing Si-H bonds (2.08 mmol, M_n = 950) in dry toluene a few drops of Karstedt catalyst were added (10^{-4} mol). The reaction was stirred over night and the solvent was removed under vacuum. (Yield: 67 %)

5.3.14 Synthesis of MO_2-Polysiloxane (M = Ti, Zr) Hybrid Nanoparticles

The Ti-modified polysiloxanes (typically between 0.1 and 0.6 mmol modified polymer) were dissolved in dry ethanol (THF was also successfully used) and water was added under vigorous stirring in different ratios (from 1:1.5 to 1:3) with regard to the Ti content. The solution was stirred overnight (12 hours). The products were centrifuged, washed three times with methanol and water and redispersed in ethanol or dried and analyzed by NMR and FT-IR.

^{13}C CP/MAS (25°C, δ/ppm): *CH_3*SiO: -6.4; CH_2*CH_2*Si: 14.1; $SiCH_2$*CH_2*: 18.3; *CH_3*CO: 22.2; $SiCH_2CH_2$*CH_2*: 57.1; $(CO)_2$*CH*: 81.8; CH_3*CO*: 165.7; *COO*: 177.2.

^{29}Si CP/MAS (25°C, δ/ppm): (CH_3)SiO: 6.7, OSi(Me $)_2$O: -22.5.

FT-IR (25°C, ATR, υ, cm^{-1}): (C=C): 1610, (C-O): 1528, (CH): 1260, (Si-O-Si): 1025, (C-Si-C): 792.

5.3.15 Synthesis of Hybrid Gels

TiO_2 modified polysiloxane gels were obtained when the sol-gel reaction of the alkoxide modified polysiloxanes was carried out in toluene as solvent using the same water ratio as for the synthesis of the nanoparticles. The sol-gel reactions were carried out over night and the mixtures were placed in cylindrical glass vials for gelation. Gels were obtained at room temperature after two days.

5.3.16 Synthesis of TiO_2-Polysiloxane Xerogels

The TiO_2-polysiloxanes hybrid gels were dried at room temperature for several days.

^{13}C CP/MAS (25°C, δ/ppm): *CH_3*SiO: -0.4; CH_2*CH_2*Si: 16.0; $SiCH_2$*CH_2*: 23.7; *CH_3*CO: 26.7; $SiCH_2CH_2$*CH_2*: 61.5; $(CO)_2$*CH*: 85.7; CH_3*CO*: 171.4; *COO*: 181.7.

^{29}Si CP/MAS (25°C, δ/ppm): (CH_3)SiO: 6.73, OSi(Me $)_2$O: -22.75.

FT-IR (25°C, ATR, υ, cm^{-1}): (C=C): 1635/1611, (C-O): 1576/1529, (CH): 1260, (Si-O-Si): 1025, (C-Si-C): 792.

5.3.17 Hydrosilation Reaction of Vinyl Triethoxysilane with PDMS-co-PMHS

A mixture of vinyl triethoxysilane (0.01 mol, 2.3 mL) and the Si-H functionalized polysiloxane (2.08 mmol, 2 mL) in 20 mL dry toluene was stirred and three drops of Karstedt catalyst were added. The reaction was stirred overnight and the solvent was removed under reduce pressure. [$Si(OEt)_3CH_2CH_2$]@PDMS-*co*-PMHS.

^{1}H NMR ($CDCl_3$, 25°C, δ/ppm). *CH_3*Si: 0.08(s, br); Si*CH_2CH_2*Si: 0.55 (s, br); *CH_3*CH_2O: 1.21 (tr, J = 6.76 Hz); CH_3*CH_2*O: 3.8 (qt, J = 6.85, 19.84 Hz).

^{13}C NMR ($CDCl_3$, 25°C, δ/ppm): *CH_3*SiO: -0.7; *CH_2CH_2*Si: 11.7; CH_3*CH_2*O: 18; CH_3*CH_2*O: 73.1.

Selected FT-IR bands (ATR, υ, cm^{-1}): ν($Si(CH_3)_3$), δs (CH_3-Si-): 1260; (Si-O-Si): 1027; ν ($Si(CH_3)_3$): 794.

5.3.18 Synthesis of SiO_2@PDMS-co-PMHS Nanoparticles. The synthesis was carried out under typical Stöber conditions[165]. s108_1. 0.62 g (0.32 mmol) [$Si(OEt)_3CH_2CH_2$]@PDMS-*co*-PMHS were dissolved in 2 mL EtOH. 0.1 mL (1.65 mmol) NH_3 32% and 0.06 mL H_20 were added to this solution and the reaction was stirred for 12 hours. The molar ratios between the reactants were: EtOH : NH_3 : H_2O : Si-modified polysiloxane = 108 : 5.2 : 10.5 : 1. S108_2. 0.5 g (0.25 mmol) [$Si(OEt)_3CH_2CH_2$]@PDMS-*co*-PMHS were dissolved in 2.35 mL EtOH. 0.19 mL (3.16 mmol) NH_3 32% and 0.24 mL H_2O were added to this solution and the reaction was stirred overnight. The molar ratios between the reactants were: EtOH : NH_3 : H_2O : Si-modified polysiloxane = 157 : 12.43 : 77.6 : 1. S109_2. 0.66 g (0.34 mmol) [$Si(OEt)_3CH_2CH_2$]@PDMS-*co*-PMHS and 0.07 g (0.34 mmol) TEOS were dissolved in 4.35 mL EtOH. 0.22 mL (3.54 mmol) NH_3 32% were added to this solution and the reaction was stirred for 12 hours. The molar ratios between the reactants were: EtOH : NH_3 : H_2O : Si-modified polysiloxane : TEOS = 108 : 5.2 : 10.5 : 0.5 : 0.5.

^{29}Si CP/MAS (25°C, δ/ppm): (CH_3)SiO: 6.8; OSi(Me)$_2$O: -22.6; -Si(O-)$_3$: T^1- 46.2, T^2- 53.1.

Selected FT-IR bands (ATR, υ, cm^{-1}): ν($Si(CH_3)_3$), δs (CH_3-Si-): 1260; (Si-O-Si): 1028; ν ($Si(CH_3)_3$): 792.

Table 15. Various MO_x-polysiloxanes nanoaprticles prepared

Name	***Description***	***Ti:H_2O ratio***	***T,ºC***	***Radius [nm] (number weight)***
PDMS-co-PMHS	PDMS-co-PMHS in EtOH, before functionalization	-	25	1.2
S97	PDMS-co-PMHS@Ti(O^iPr)$_4$ before sol-gel reaction in EtOH	-	25	1.55
S44	TiO_2@PDMS-co-PMHS	1:1.5	25	3.32
S51	TiO_2@PDMS-co-PMHS in 2-propanol	1:1.5	25	2.716
S56	Ti(O^iPr)$_4$ modified polysiloxane copolymerized with Ti(O^iPr)$_4$ in 1:1 ratio with respect for Ti after sol-gel in 2-propanol	1:1.5	25	1.385E+002 1.618E+003 broad peaks
S58	TiO_2@PDMS-co-PMHS in EtOH	1:1.5	25	50.1 191.6
S65	TiO_2@PDMS-co-PMHS in EtOH	1:1.5	25	72.8 (60%) 453.9 (40%)
S70	PDMS-co-PMHS@AAA before coordination with Ti alkoxide in EtOH	1:1.5	25	3.35
S71	PDMS-co-PMHS@Ti(O^iPr)$_4$ before sol-gel reaction in EtOH	1:1.5	25	3.1
S73	S71 after sol-gel in 2-propanol	1:1.5	50	18
S74	S71 after sol-gel in 2-propanol	1:1.5	70	Broad band-
S108_1	SiO_2@PDMS-co-PMHS		25	3.6
S108_2	SiO_2@PDMS-co-PMHS		25	3.73
S109_2	SiO_2@PDMS-co-PMHS		25	2.6 (60%) 8.13 (40%)
s174	Zr(O^iPr)$_4$@PDMS-co-PMHS	-	25	28.7 (95 %) 260 (5%)
S175_1	ZrO_2@PDMS-co-PMHS in EtOH	1:1.5	25	60 (79 %) 299 (21 %)

5.4 Experimental Part II

5.4.1 Synthesis of TiO_2 by the Hydrothermal Approach (s161)

5 mL (0.017 mol) of $Ti(O^iPr)_4$ were slowly added to a 4:1 mixture of EtOH and H_2O previously acidified with HNO_3 (pH 0.7). The reaction mixture was stirred over night and then introduced into a teflon capped autoclave. The autoclave was heated at 200°C for 4 hours. The particles were isolated by centrifugation, dried under vacuum, and redispersed in water. DLS: Peak 1: 58 nm ± 0.12, 78.1 %. Peak 2, 230 nm ± 0.22, 21.9 %. XRD: Anatase: a (Å) = 0 3.78320, c (Å) = 9.45037 crystallite size = 7.4 nm[60].

5.4.2 Synthesis of TiO_2 by the Solvothermal Approach[189]

Different amounts of $Ti(O^iPr)_4$ were mixed with toluene under an argon atmosphere at the weight ratio of 5:100, 10:100, 20:100, 30:100 and 40:100, which makes 5, 9, 17, 23 and 29 wt% of $Ti(O^iPr)_4$ in solution, respectively. The mixture was vigorously stirred with a magnetic stirrer for 3 h and transferred into a stainless steel autoclave with teflon liner. The autoclave was then heated to 200°C with a rate of 10°C/min and maintained for 3 h at 200°C without stirring. The mixture was cooled to room temperature and the precipitate was separated by centrifugation and then dried. DLS: Peak 1: 4.1 nm ± 0.11, 36 %. Peak 2: 32 nm ± 0.28, 64 %.

5.4.3 Synthesis of TiO_2 Nanoparticles by a Sol-Gel Approach[190]

1.25 mL (0.17 mol/L) of $Ti(O^iPr)_4$ were dissolved in 25 mL of dry ethanol and then added dropwise under vigorous stirring to 250 mL of distilled water (4 °C) adjusted to pH 1.5 with nitric acid. The resulting transparent colloidal suspension (1.34 g/L) was stirred overnight. To obtain powder sample, the solvent (H_2O) was evaporated (40°C) using a rotavapor and dried under vacuum. The powdered sample contained still some HNO_3. The particles are very good re-dispersible in water. XRD shows that they are 100% anatase, with a crystallite size of 3.4 nm. The particle diameter from DLS was 5 nm (mean) ± 0.18. Raman (υ, cm^{-1}): Ti – O stretching vib.: 643, TiO_2: 515, 406, 156. XRD: Anatase 100%: a (Å) = 3.79802, c (Å) = 9.51969; crystallite size: 3.4 nm. BET: 170.5612 m²/g.

5.4.4 Variations in the Synthesis of TiO_2 Nanoparticles

Amounts between 1.25 mL and 5.5 mL of $T(O^iPr)_4$ were dissolved in 25 mL of dry ethanol and then added dropwise under vigorous stirring to 250 mL of distilled water (4 °C) adjusted to pH 1.5 with nitric acid. The resulting transparent colloidal suspension was stirred

overnight. To obtain powder sample, the solution was evaporated (40°C) using a rotavapor and dried under vacuum. The particles are very good re-dispersible in water. XRD shows that they are 100% anatase, with a crystallite size of 3.4 nm and 3.7 nm.

- ***TiO_2 with 5 nm diameterr***

1.25 mL (0.17 mol/L) of $Ti(O^iPr)_4$ were dissolved in 25 mL of dry ethanol and then added dropwise under vigorous stirring to 250 mL of distilled water (4 °C) adjusted to pH 1.5 with nitric acid. DLS: 5 nm ± 0.18. TEM: 5 nm (Figure 126).

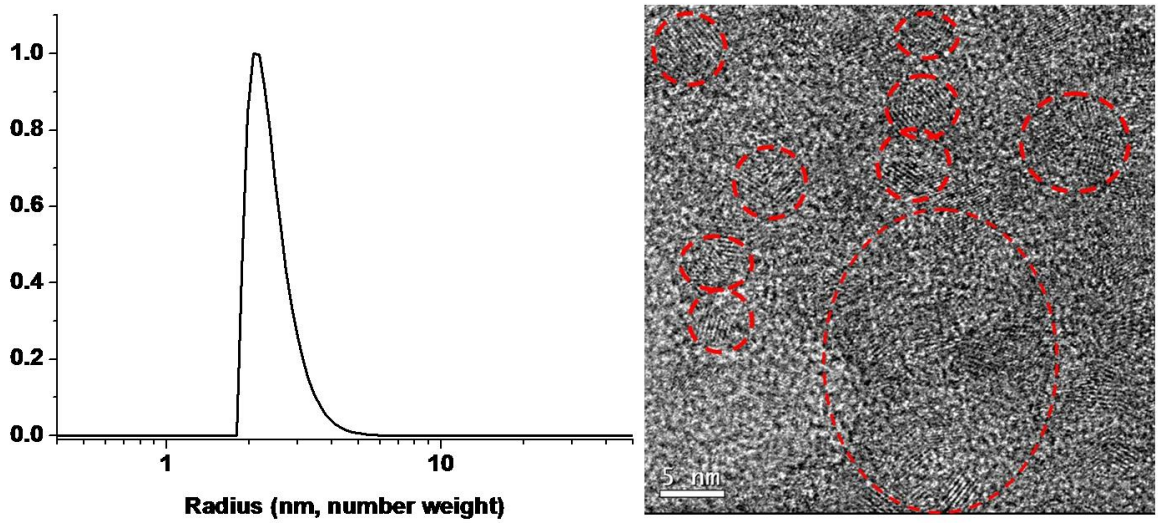

Figure 126. DLS (left side) and TEM (right side) analysis of TiO_2 synthesized from 0.17 mol/L $Ti(O^iPr)_4$

- ***TiO_2 with 8 nm diameter***

1.5 mL (0.34 mol/L) of $T(O^iPr)_4$ were dissolved in 25 mL of dry ethanol and then added dropwise under vigorous stirring to 250 mL of distilled water (4 °C) adjusted to pH 1.5 with nitric acid. DLS: 8 nm ± 0.20. TEM: 7.6 nm (Figure 127).

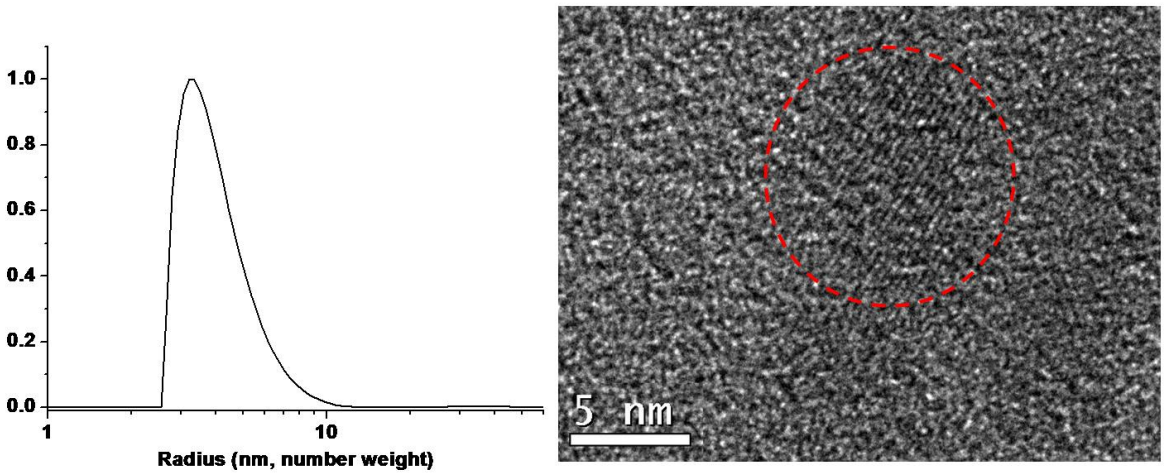

Figure 127. DLS (left side) and TEM (right side) analysis of TiO_2 synthesized from 0.34 mol/L $Ti(O^iPr)_4$

- ***TiO_2 with 12 nm diameter***

1.75 mL (0.51 mol/L) of $T(O^iPr)_4$ were dissolved in 25 mL of dry ethanol and then added dropwise under vigorous stirring to 250 mL of distilled water (4 °C) adjusted to pH 1.5 with nitric acid. DLS: 12 nm ± 0.18. TEM: 11.5 nm (Figure 128).

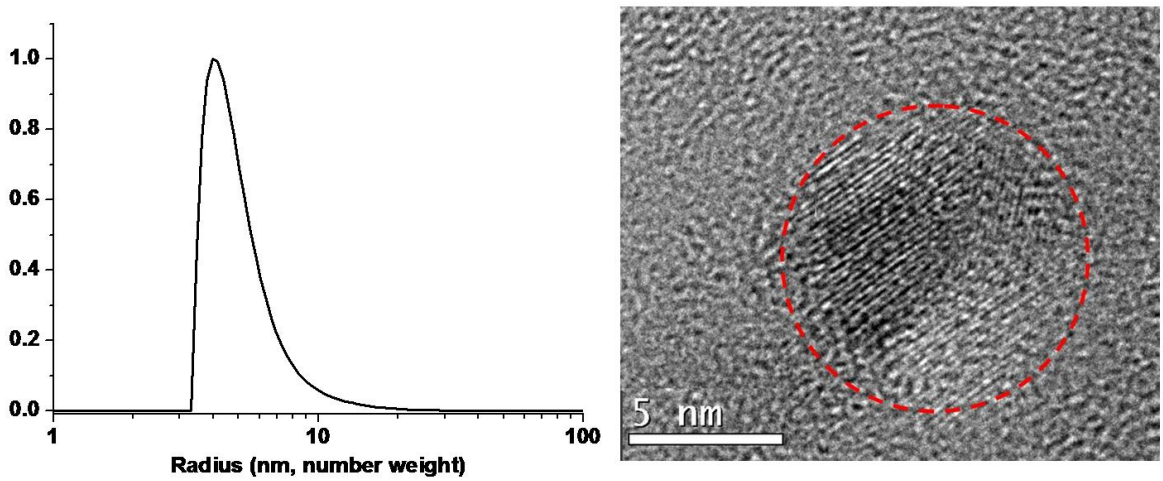

Figure 128. DLS (left side) and TEM (right side) analysis of TiO_2 synthesized from 0.51 mol/L $Ti(O^iPr)_4$

5.4.5 Synthesis of Phosphonates and Phosphates with Polymerizable Double Bonds

The synthesis of 2-methyl-acrylic acid (diethoxy-phosphoryl)-alkyl esters with a different length of the alkyl chain (Scheme 19) was carried out according to a procedure published by *Francova et al.*[192]

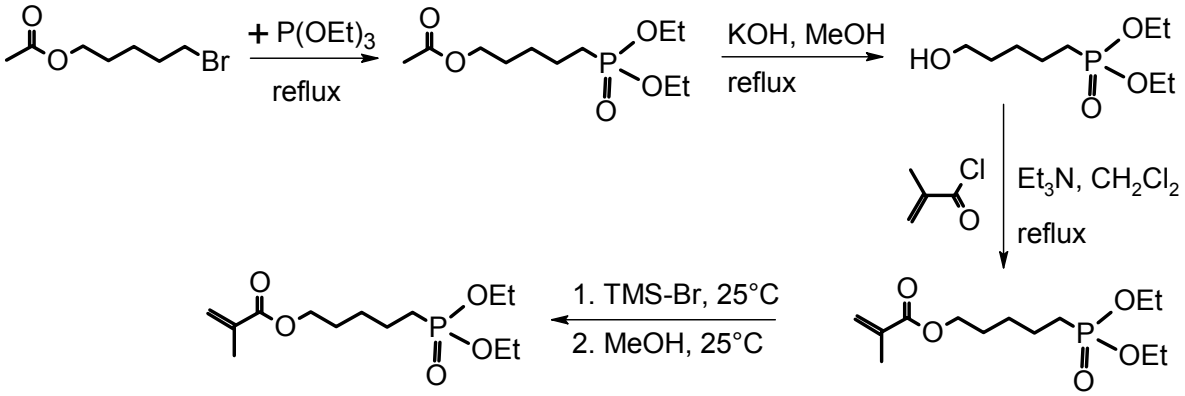

Scheme 19. Synthesis of 2-methyl-acrylic acid (diethoxy-phosphoryl)-alkyl esters with a different length of the alkyl chain

5.4.6 Synthesis of Acetic Acid (Diethoxy-phosphoryl)-Alkyl Ester[192]

In a 100 ml three-necked round bottom flask fitted with a condenser, a system of argon bubbling and a pressure-equalizing dropping funnel 47.4 g (0.343 mol) diethyl phosphite were introduced. Argon was bubbled through the reaction mixture using a capillary and the temperature was maintained at 120 °C during the whole reaction. The mixture of 9.3 g (0.093 mol) vinyl acetate, 0.8 g (4.9 mmol) AIBN and 13.4 g (0.097 mol) diethyl phosphite were dropwise introduced. The reaction mixture was kept under stirring at 120 °C for 2 hrs. The obtained reaction product was distilled under vacuum to eliminate the excess of diethyl phosphite and other potential side products, 21.9 g (99 % yield) of a colorless liquid was obtained.

Arbuzov reaction: In a 100 ml flask fitted with a condenser 40.4 g (0.243 mol) triethyl phosphite and 12.5 g (0.06 mol) 5-bromopentyl acetate were mixed and heated to reflux for 16 hrs. Afterwards the mixture was distilled under vacuum to eliminate the excess of triethyl phosphite and other side products, 13.4 g (76 % yield) of a colorless liquid was obtained.

Acetic acid 5-(diethoxy-phosphoryl)-pentyl ester.

^{1}H NMR ($CDCl_3$, 25°C, ppm): δ = 1.3 (t, 6H, J = 7.0 Hz), 1.4 (m, 2H), 1.7 (m, 6H), 2.0 (s, 3H), 4.1 (m, 6H);

^{31}P NMR ($CDCl_3$, 25°C, ppm): δ = 32.06 (R-P(O)$(OEt)_2$).

Acetic acid 11-(diethoxy-phosphoryl)-undecyl ester.

^{1}H NMR ($CDCl_3$, 25°C, ppm): δ = 1.3 (m, 20H), 1.6 (m, 6H), 2.0 (s, 3H), 4.1 (m, 6H);
^{31}P NMR ($CDCl_3$, 25°C, ppm): δ = 32.43 (R-P(O)$(OEt)_2$).

5.4.7 Synthesis of (Hydroxy-alkyl)-Phosphonic Acid Diethyl Ester[192]

In a 250 ml three-necked round bottom flask equipped with a reflux condenser 21.9 g (0.092 mol) acetic acid 3-(diethoxy-phosphoryl)-propyl ester and 1.0 g (0.018 mol) potassium hydroxide in 98.4 g (3.07 mol) methanol were mixed under an argon atmosphere. The mixture was stirred under reflux for 3 days. 18.0 g (99 % yield) of a colorless liquid was obtained.

(5-Hydroxy-pentyl)-phosphonic acid diethyl ester.

^{1}H NMR ($CDCl_3$, 25°C, ppm): δ = 1.3 (t, 6H, J = 7 Hz),), 1.4 (m, 2H), 1.7 (m, 6H), 3.6 (t, 2H, J = 6.2 Hz), 4.1 (m, 4H);
^{31}P NMR ($CDCl_3$, 25°C, ppm): δ = 32.47 (R-P(O)$(OEt)_2$).

(11-Hydroxy-undecyl)-phosphonic acid diethyl ester.

^{1}H NMR ($CDCl_3$, 25°C, ppm): δ = 1.3 (m, 20H), 1.6 (m, 6H), 3.6 (t, 2H, J = 6.5 Hz), 4.1 (m, 4H);
^{31}P NMR ($CDCl_3$, 25°C, ppm): δ = 32.81 (R-P(O)$(OEt)_2$)

5.4.8 Synthesis of 2-Methyl-Acrylic Acid (Diethoxy-phosphoryl)-Alkyl Ester[192]

In a 500 ml three-necked round bottom flask fitted with a reflux condenser, a system of argon bubbling and a pressure-equalizing dropping funnel 18.0 g (0,092 mol) (3-hydroxy-propyl)-phosphonic acid diethyl ester, 11.1 g (0.11 mol) triethylamine and 262.4 g (3.09 mol) dichloromethane were introduced. The reaction mixture was purged with argon and cooled to 0 °C in an ice-bath. Then 11.5 g (0.11 mol) methacryloyl chloride dissolved in 37.4 g (0.44 mol) dichloromethane was added dropwise to the mixture. At the end of the addition the reaction mixture was kept under stirring for 2 days at room temperature. After 2 days, a white precipitate was filtered. The solvent was evaporated and the crude reaction mixture was poured into diethyl ether. The organic phase was washed three times with water saturated with sodium chloride. After evaporation under vacuum 22.8 g (94 % yield) of pale yellow liquid 2-methyl-acrylic acid 3-(diethoxy-phosphoryl)-propyl ester was isolated.

2-Methyl-acrylic acid 5-(diethoxy-phosphoryl)-pentyl ester.

^{1}H NMR ($CDCl_3$, 25°C, ppm): δ = 1.3 (t, 6H, J = 7.0 Hz), 1.4 (m, 2H), 1.7 (m, 6H), 1.9 (s, 3H), 4.1 (m, 6H), 5.5 (s, 1H), 6.0 (s, 1H);
^{31}P NMR ($CDCl_3$, 25°C, ppm): δ = 32.49 (R-P(O)$(OEt)_2$);

^{13}C NMR ($CDCl_3$, 25°C, ppm): δ = 167.46, 136.37, 125.33, 64.18, 61.68, 61.58 (J = 7.5 Hz), 28.16, 27.15, 26.88, 26.63, 24.69 (J = 145 Hz), 22.17, 22.09 (J = 6 Hz), 18.31, 16.47, 16.38 (J = 7.2 Hz).

FT-IR (ATR, cm^{-1}): υ = 2982, 2954, 1716 (C=O), 1636 (C=C), 1455, 1320, 1296, 1229 (P=O), 1162, 1024 (P-O), 957, 814, 787.

Elemental analysis: $C_{13}H_{25}O_5P$: calculated: C 53.42, H 8.62; found: C 53.50, H 8.11.

2-Methyl-acrylic acid 11-(diethoxy-phosphoryl)-undecyl ester.

^{1}H NMR ($CDCl_3$, 25°C, ppm): δ = 1.3 (m, 20H), 1.6 (m, 6H), 1.9 (s, 3H), 4.1 (m, 6H), 5.5 (s, 1H), 6.0 (s, 1H);

^{31}P NMR ($CDCl_3$, 25°C, ppm): δ = 32.76 (R-P(O)$(OEt)_2$);

^{13}C NMR ($CDCl_3$, 25°C, ppm): δ = 167.66, 136.51, 125.16, 64.82, 61.59, 61.49 (J = 7.5 Hz), 29.45, 29.21, 28.57, 26.39, 24.46 (J = 145 Hz), 25.95, 22.36, 22.28 (J = 6.2 Hz), 18.34, 16.50, 16.40 (J = 7.2 Hz).

FT-IR (ATR, cm^{-1}): υ = 2928, 2855, 1717 (C=O), 1636 (C=C), 1455, 1320, 1296, 1243 (P=O), 1162, 1055, 1025 (P-O), 957, 814, 786.

Elemental analysis: $C_{19}H_{37}O_5P$: calculated: C 60.62, H 9.91; found: C 60.24, H 10.00.

5.4.9 Synthesis of 2-Methyl-Acrylic Acid Hydroxy-Alkyl Ester[192]

In the first step, 7.5 g (0.069 mol) sodium methacrylate and 4.7 g (0.050 mol) 3-chloro-1-propanol in 117.8 g (2.87 mol) acetonitrile were introduced in a 250 ml round bottom flask supplied with a reflux condenser. The methacrylate was stabilized with hydroquinone monomethylether 14 mg (0.11 mmol). As a catalyst tricaprylylmethylammonium chloride (Aliquat®336) was used (5 % by weight) (Scheme 20). The mixture was refluxed for 24 hrs. After cooling, the mixture was filtered and extracted with CH_2Cl_2. The organic phase was washed with water, dried with $MgSO_4$ and concentrated. The residue was purified by distillation under reduced pressure and by column chromatography with the system of solvents dichlormethane: methanol (100: 1). 4.3 g (60 % yields) of a colorless liquid was obtained.

2-Methyl-acrylic acid 8-hydroxy-octyl ester.

^{1}H NMR ($CDCl_3$, 25°C, ppm): δ = 1.45 (m, 12H), 1.9 (s, 3H), 3.7 (t, 2H, J = 6.5 Hz), 4.3 (t, 2H, J = 6.7 Hz), 5.5 (s, 1H), 6.1 (s, 1H).

5.4.10 Synthesis of 2-Methyl-Acrylic Acid (Diethoxy-phosphoryloxy)-Alkyl Ester[192]

In a 100 ml three-necked round bottom flask supplied with a condenser and a pressure-equalizing dropping funnel 4.3 g (0.03 mol) 2-methyl-acrylic acid 3-hydroxy-propyl ester and

2.1 g (0.021 mol) triethylamine solubilized in 51.0 g (0.6 mol) dichloromethane were mixed under an argon atmosphere (Scheme 20). The reaction mixture was cooled at 0 °C in an ice-bath. Then 3.8 g (0.022 mol) diethyl chlorophosphate dissolved in 7.3 g (0.086 mol) CH_2Cl_2 were added dropwise. 0.95 g (0.012 mol) of pyridine was added to the reaction mixture and the solution was stirred for 3 days at room temperature. The formed white precipitate was filtered and the solvent was evaporated. The crude reaction mixture was poured into diethyl ether. The organic phase was washed three times with distilled water saturated with sodium chloride. After distillation under vacuum 5.8 g (71 % yield) of a pale yellow liquid 2-methyl-acrylic acid *3*-(diethoxy-phosphoryloxy)-propyl ester was obtained.

2-Methyl-Acrylic Acid 8-(Diethoxy-Phosphoryloxy)-Octyl Ester.

^{1}H NMR ($CDCl_3$, 25°C, ppm): δ = 1.3 (m, 20H), 1.7 (m, 6H), 1.9 (s, 3H), 4.2 (m, 8H), 5.5 (s, 1H), 6.0 (s, 1H);

^{31}P NMR ($CDCl_3$, 25°C, ppm): δ = -0.71 (R(O)-P(O)$(OEt)_2$);

^{13}C NMR ($CDCl_3$, 25°C,ppm): δ = 167.54, 136.50, 125.17, 67.54, 67.64 (J = 7.3 Hz), 64.72, 63.68, 63.59 (J = 6.9 Hz), 30.27, 30.16, 29.09, 28.54, 25.87, 25.34, 18.31, 16.18, 16.07 (J = 8 Hz). FT-IR (ATR, cm^{-1}): υ = 2931, 2857, 1717 (C=O), 1637 (C=C), 1455, 1321, 1296, 1261 (P=O), 1163, 1026 (P-O), 975, 814.

Elemental analysis: $C_{16}H_{31}O_6P$: calculated: C 54.85, H 8.92; found: C 55.03, H 8.87.

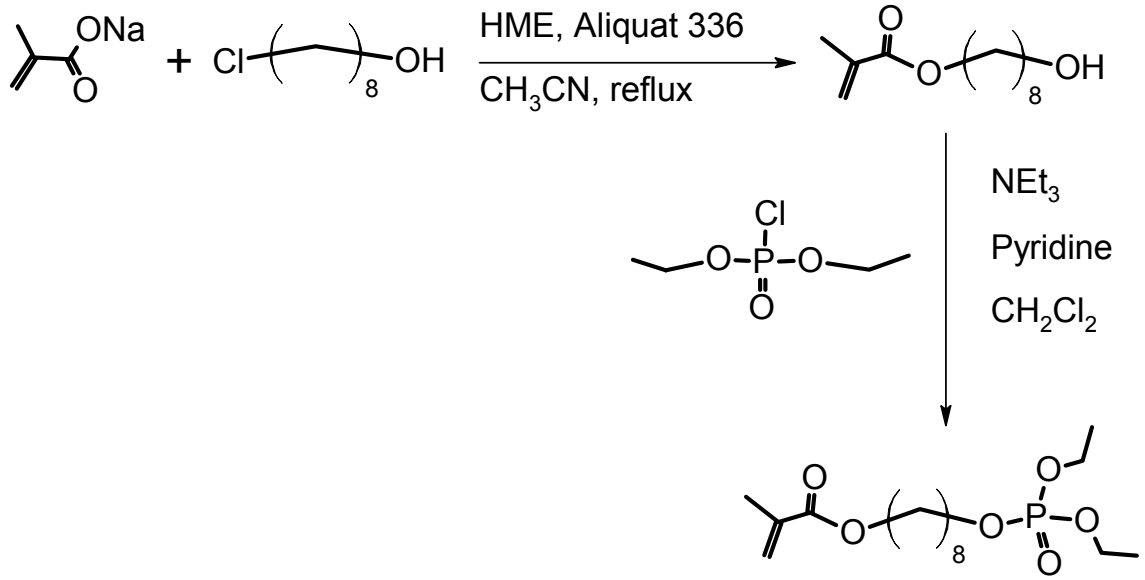

Scheme 20. Synthesis of 2-Methyl-acrylic acid (diethoxy-phosphoryloxy)-alkyl ester

5.4.11 Cleavage of Phosphonic and Phosphoric Esters[192]

The cleavage of esters was carried out following a procedure published by *Francova et al.*[192] In the first step, 2.5 g (6.6 mmol) 2-methyl-acrylic acid 11-(diethoxy-phosphoryl)-undecyl ester or 2.3 g 2-methyl-acrylic acid 8-(diethoxy-phosphoryloxy)-octyl ester and 53 mg (0.6 mmol) ethylacetate in 5.3 g (0.062 mol) dichloromethane were stirred at 25 °C in a 10 ml round bottom flask supplied with a precision seal septum. 2.1 g (0.014 mol) trimethylbromosilane was slowly added by a syringe through the septum into solution. At the end of addition, the reaction mixture was stirred for 1 h at room temperature. The second step was carried out in the same round bottom flask after evaporation of the solvent. 4.2 g (9.1 mmol) bis-trimethylsilyl (methacryloyloxyalkyl) phosphonate or 4.0 g bis-trimethylsilyl (methacryloyloxyalkyl) phosphate were dissolved in 2.1 g (0.064 mol) methanol and the reaction mixture was kept under stirring at room temperature for 1 hour. 2.0 g and 1.85 g (95 % yield) of viscous yellow liquid 2-methyl-acrylic acid 11-phosphono-undecyl ester and 2-methyl-acrylic acid 8-phosphonooxy-octyl ester was obtained, respectively.

2-Methyl-Acrylic Acid 8-Phosphonooxy-Octyl Ester.

^{1}H NMR ($CDCl_3$, 25°C, ppm): δ = 1.3 (m, 8H), 1.7 (m, 4H), 1.9 (s, 3H), 3.6 (t, 2H, J= 6.7 Hz), 4.1 (t, 2H, J= 6.5 Hz), 5.5 (s, 1H), 6.0 (s, 1H);

^{31}P NMR ($CDCl_3$, 25°C, ppm): δ = -51.13 ($R(O)-P(O)(OH)_2$);

^{13}C NMR ($CDCl_3$, 25°C, ppm): δ = 167.57, 136.49, 125.27, 64.74, 63.42, 63.31 (J = 8.0 Hz), 32.73, 29.03, 28.62, 28.54, 28.047, 25.84, 18.34.

FT-IR (ATR, cm^{-1}): υ = 2932, 2857, 1717 (C=O), 1636 (C=C), 1454, 1320, 1296 (P=O), 1163, 1010 (P-O), 957, 849, 814.

Elemental analysis:$C_{12}H_{23}O_6P$: calculated C 48.98, H 7.88; found: C 48.98, H 8.04.

2-Methyl-Acrylic Acid 11-Phosphono-Undecyl Ester.

^{1}H NMR ($CDCl_3$, 25°C, ppm): δ = 1.3 (m, 18H), 1.6 (m, 2H), 1.9 (s, 3H), 4.1 (t, 2H, J= 6.5 Hz), 5.5 (s, 1H), 6.0 (s, 1H);

^{31}P NMR ($CDCl_3$, 25°C, ppm): δ = 37.35 ($R-P(O)(OH)_2$);

^{13}C NMR ($CDCl_3$, 25°C, ppm): δ = 167.62, 136.50, 125.20, 64.84, 29.69, 29.43, 29.29, 29.20, 28.57, 25.94, 22.35, 22.24 (J = 6.2 Hz), 18.32.

FT-IR (ATR, cm^{-1}): υ = 2922, 2953, 1718 (C=O), 1636 (C=C), 1458, 1303 (P=O), 1149, 1063 (P-O), 990, 935, 716.

Elemental analysis: $C_{15}H_{29}O_5P$: calculated: C 56.24, H 9.12; found: C 56.51, H 9.22.

5.4.12 Synthesis of Dodecylphosphonic Acid Diethyl Ester[241-244]

15.6 mL (64 mmol) 1- bromdodecane were mixed with 12.4 mL (74 mmol) triethylphosphit and refluxed for 3.5 hours (Scheme 21). The by-products were removed by distillation at 100 °C. The excess of triethylphosphit was removed at 100 °C and 12 mbar. The dodecylphosphonic acid ethyl ester was a clear liquid (13.1 g, yield 66 %).

^{1}H NMR (DMSO-d6, 25 °C, ppm): δ = 0.82 (t, 3 H, *CH$_3$*); 1.18 – 1.23 (m, 24 H, *CH$_2$*, *CH$_3^{Et}$*); 1.67-1.82 (m, 4H, CH$_2$–*CH$_2$*–P); 3.93 (q, 4H, *CH$_2$O^{Et}*).

^{31}P NMR (DMSO-d6, 25 °C, ppm): δ = 33.4.

5.4.13 Synthesis of Dodecylphosphonic Acid

13.1 g (42 mmol) dodecylphosphonic acid ethyl esters were refluxed with 70 mL HCl conc. for 22 hours. The liquid was removed under reduced pressure using a rotavapor until a dry powder was obtained. The powder was washed several times with acetonitril and dried under vacuum. The dodecylphosphonic acid was crystallized from n-hexane and dried under vacuum to afford 9.5 g (38 mmol, 90 % yield) colorless, crystalline powder.

^{1}H NMR (CDCl$_3$, 25 °C, ppm): δ = 0.84 (t, 3 H, *CH$_3$*); 1.26 (m, 18 H, *CH$_2$*); 1.55 -1.82 (m, 4H, CH$_2$–*CH$_2$*–P); 8.56 (s, 2H, P-O*H*).

^{13}C NMR (CDCl$_3$, 25 °C, ppm): δ =31.8, 30.5, 29.7, 26.6, 23, 22.6, 14.2.

^{31}P NMR (CDCl$_3$, 25 °C, ppm): δ = 39.5.

FT–IR (ATR, υ, cm^{-1}): 2961 (C-H), 2851 (C-H), 1465 (C-H), 1209 (P=O), 1000 (P-O), 942 (P-OH).

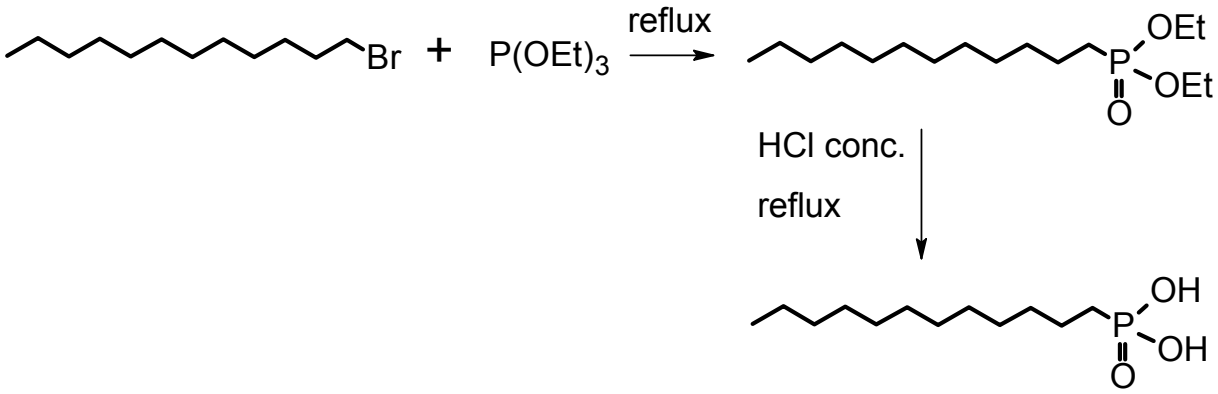

Scheme 21. Synthesis of dodecylphosphonic acid

5.4.14 Phosphonates and Phosphates Used and Their Source.

Table 16. Organophosphorus coupling agents used for the modification of the TiO_2 nanoparticles

Name	Structure	Short name	Source
Phenyl Phosphonic Acid	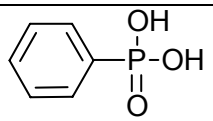	PPA	Aldrich
Allyl phosphonic acid	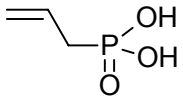	APA	Synthesis Arbuzov
Allyl phosphonic acid, iPr esters	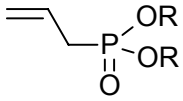	APA-iPr	Synthesis Arbuzov
2-Methyl-acrylic acid 5-(diethoxyphosphoryl)alkyl ester	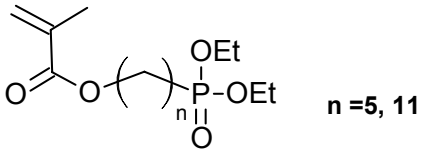 **n =5, 11**	MetC5PA-Et MetC11PA-Et	Synthesis radical addition
2-Methyl-acrylic acid 5-alkyl phosphonic acid	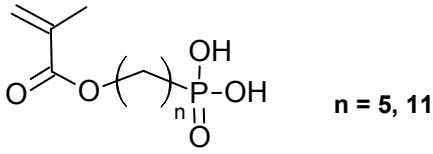 **n = 5, 11**	MetC5PA MetC11PA	Synthesis radical addition
Dodecyl phosphonic acid	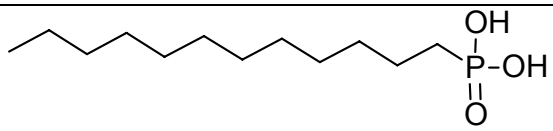	DPA	Synthesis Arbuzov
Dodecyl phosphonic acid, ethyl esters	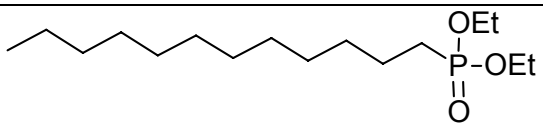	DPA-Et	Synthesis Arbuzov
Phenyl Phosphoric acid	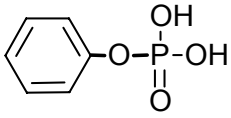	PPoA	Commercial
2-Methyl-acrylic acid 8-octyl phosphoric acid	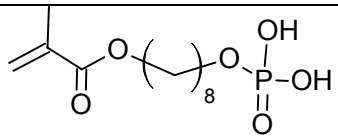	MetC8PoA	Synthesis
Poly(propylene oxide)phosphate- methacrylate terminated	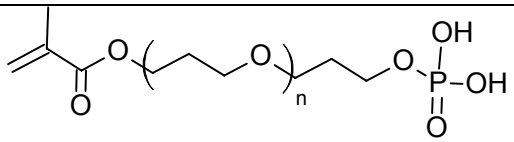	MetPPOPoA	Rhodia

5.4.15 Modification of the TiO_2 Nanoparticles with Phosphonic Acids

Various phosphonic acids (1.56 mmol, as reference phenyl phosphonic acid was used) were dissolved in a 3:1 mixture of methanol and water (500 ml). A suspension of 1 g TiO_2 in 100 mL of water was added to this solution. The suspension was stirred at room temperature for 3 days. The obtained modified particles were isolated via centrifugation, washed several times with ethanol, and dried at 120°C in vacuum. Commercially available TiO_2 nanoparticles (P25, Degussa) were also functionalized for reason of comparison.

TiO_2@PPA (TiO_2 d = 21 nm) (Figure 129)

FT-IR (ATR, υ , cm^{-1}): 1619, 1550, 1429, 1263, 1138, 1100-950, 798, 682. ^{31}P/MAS (δ, 25°C, ppm): 15.9. BET (m^2/g): 51.5687 m²/g. TGA (mass loss, %): 30 – 200 °C: 5.3 %, 200 – 600 °C: 20.7 %. Diameter. DLS (nm): 30 ± 5. TEM: 23 ± 5. Raman (υ, cm^{-1}): Ti – O stretching vib.: 631, TiO_2: 515, 405, 157.

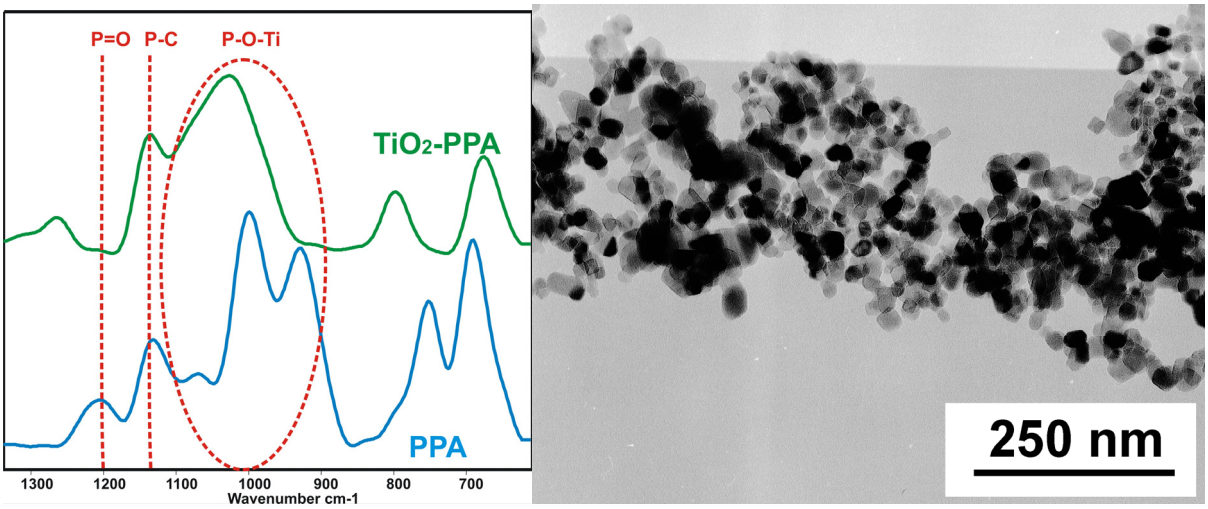

Figure 129. Left side: FT-IR spectra of PPA and TiO_2@PPA. Right side: TEM image of TiO_2@PPA

TiO_2@APA

FT-IR (ATR, υ , cm^{-1}): 2983, 2937, 1727, 1642, 1549, 1460, 1387, 1255, 1176, 1091-921, 801, 724, 682. ^{31}P/MAS (δ, 25°C, ppm): 31.43. TGA (mass loss, %): 30 – 200 °C: 8.8 %, 200 – 600 °C: 9.2 %. Diameter. DLS (nm): 18 ± 4 .

TiO_2@MetC11PA (Figure 130)

FT-IR (ATR, υ, cm^{-1}): 2981, 2922, 2852, 1713, 1647, 1514, 1459, 1418, 1316, 1173, 1100-950, 852, 756, 652, 607, 577. ^{31}P/MAS (δ, 25°C, ppm): 17.65. TGA (mass loss, %): 30 – 160 °C: 6.5 %, 160 – 700 °C: 15.5 %. Diameter. DLS (nm): 320 ± 120. TEM: 12 ± 3 nm.

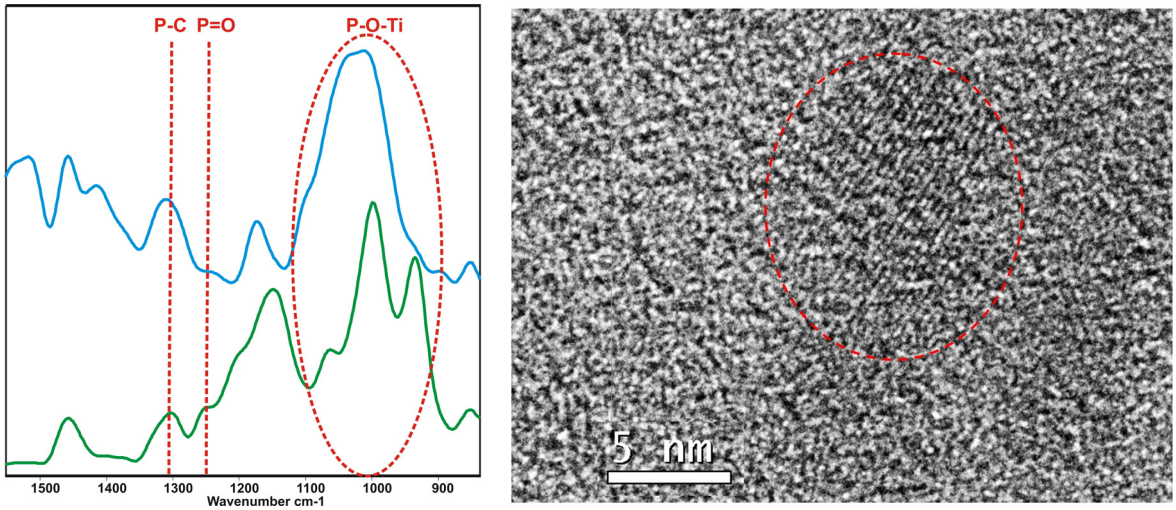

Figure 130. Left side: FT-IR spectra of MetC11PA and TiO_2@MetC11PA. Right side: TEM image of TiO_2@MetC11PA

TiO_2@DPA

FT-IR (ATR, υ, cm^{-1}): 2924, 2853, 1460, 1410, 1372, 1160-890, 672. ^{31}P/MAS (δ, 25°C, ppm): 30.6. TGA (mass loss, %): 30 – 200 °C: 4.6 %, 200 – 600 °C: 30.8 %. Diameter. DLS (nm): 9.8 ± 2.2. Raman (υ, cm^{-1}): Ti – O stretching vib.: 639, TiO_2: 508, 407, 160.

5.4.16 Modification of the TiO_2 Nanoparticles with Phosphoric Acids

Various phosphoric acids (1.56 mmol, as reference was used phenyl phosphonic acid) were dissolved in a 3:1 mixture of methanol and water (500 ml). A suspension of 1 g TiO_2 in 100 mL of water was added to this solution. The suspension was stirred at room temperature for 3 days. The obtained modified particles were isolated via centrifugation, washed several times with ethanol, and dried at 120°C in vacuum. Commercially available TiO_2 nanoparticles (P25, Degussa) were also functionalized for reason of comparison.

TiO_2@PPoA (TiO_2 d = 21 nm)

FT-IR (ATR, υ, cm^{-1}): 1649, 1597, 1489, 1325, 1222, 1124, 1100-925, 718. ^{31}P/MAS (25°C, δ, ppm): 1.2. ^{13}C CP/MAS NMR (25°C, δ, ppm): 121, 112. BET (m^2/g): . TGA (mass loss, %): 30 – 200 °C: 0.9 %, 200 – 600 °C: 2.5 %. Diameter. DLS (nm): 44 ± 6 .

TiO_2@MetC8PoA (TiO_2 d = 21 nm) (Figure 131)

FT-IR (ATR, υ, cm^{-1}): 1705, 1630, 1521, 1469, 1413, 1360, 1307, 1162-987, 807, 724. TGA (mass loss, %): 30 – 200 °C: 1 %, 200 – 600 °C: 2.6 %. Raman (υ, cm^{-1}): Ti – O stretching vib.: 638, TiO_2: 514, 398, 146. Diameter. DLS (nm): 38 ± 6 .

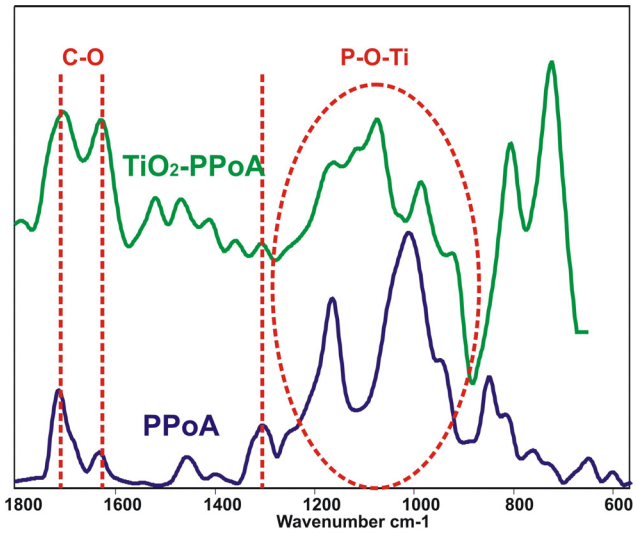

Figure 131. FT-IR spectra of PPoA and TiO_2@PPoA.

TiO_2@MetPPOPPoA (Figure 132)

FT-IR (ATR, υ, cm^{-1}): 2973, 2932, 2873, 1717, 1635, 1553, 1453, 1376, 1319, 1296, 1264, 1153, 1088-950, 850, 661. TGA (mass loss, %): 30 – 110 °C: 4.8 %, 110 – 310 °C: 30 %, 310 – 460 °C: 9.5 %, 460 – 600 °C: 2.7 %.

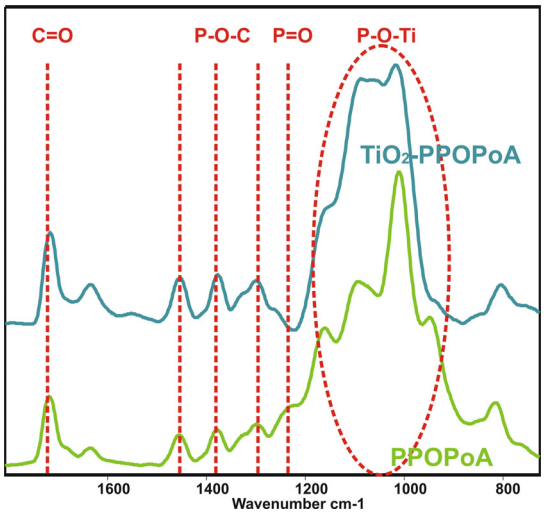

Figure 132. FT-IR spectra of PPOPoA and TiO_2☺PPOPoA

5.4.17 Modification of TiO_2 Nanoparticles with Alkyl Esters of the Phosphonic Acids

When alkyl esters of the phosphonic acid were used instead of the acids, methylene chloride was used as a solvent. The reaction was carried out at room temperature, over night.

TiO_2@MetC5PA-Et (Figure 133)

FT-IR (ATR, υ, cm^{-1}): 2984, 2940, 2871, 1772, 1641, 1557, 1449, 1402, 1300, 1171, 1099-948, 803. 755. ^{31}P/MAS (25°C, δ, ppm): 36.5. TGA (mass loss, %): 30 – 200 °C: 6.2 %, 200 – 600 °C: 27.8 %. Raman (υ, cm^{-1}): Ti – O stretching vib.: 642, TiO_2: 519, 403, 156. Diameter. DLS (nm): 52 ± 4. TEM (nm): 11 ± 2 nm.

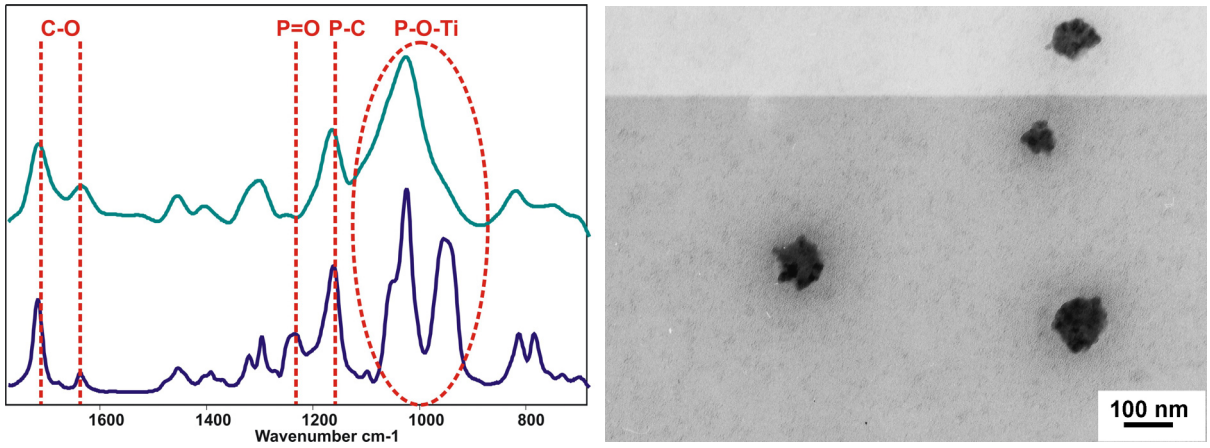

Figure 133. Left side: FT-IR spectra of Met5PA-Et and TiO_2@MetC5PA-Et. Right side: TEM image of TiO_2@MetC5PA-Et

TiO_2@MetC11PA-Et

FT-IR (ATR, υ, cm^{-1}): 2927, 2855, 1718, 1638, 1551, 1450, 1412, 1297, 1165, 1097-958, 795, . ^{31}P/MAS (25°C, δ, ppm): 17.7. TGA (mass loss, %): 30 – 200 °C: 7.7 %, 200 – 600 °C: 20.1 %. Raman (υ, cm^{-1}): Ti – O stretching vib.: 646, TiO_2: 515, 410, 156. Diameter. DLS (nm): 120 ± 24.

TiO_2@DPA-Et

FT-IR (ATR, υ, cm^{-1}): 2932, 2848, 1462, 1418 1368, 1170-900. TGA (mass loss, %): 30 – 180 °C: 7.6 %, 180 – 550 °C: 10.8 %. Diameter: DLS (nm): 9.8 ± 2.2.

5.4.18 Preparation of Pickering Emulsions Stabilized by SiO_2 or TiO_2

As a first model system toluene (cyclohexane) / H_2O emulsions were prepared containing between 0.125 and 2 wt. % SiO_2 or TiO_2. The pH was varied between 1 and 6. Sol-gel TiO_2 nanoparticles or commercially available TiO_2 and SiO_2 nanoparticles (Degussa) were used in the synthesis. The emulsions were formed from 20% toluene and 80% H_2O sol of particles. NaCl was used as an electrolyte in different concentration (0.1 – 2 M).

5.4.19 Preparation of Pickering Emulsions Stabilized by TiO_2

Model system emulsions were prepared containing various oils like toluene, cyclohexane, hexane 20% vol. and 80% vol. H_2O dispersion of the TiO_2 particles. The amount of TiO_2 containing in the emulsion was varied between 0.125 and 2 wt%. The pH was varied between 1 and 6. Sol-gel synthesized TiO_2 nanoparticles or commercially available TiO_2 P25 (Degussa) were used in the preparation of the emulsions. Stable Pickering emulsion were generated by agitation using an IKA Ultra-Turrax T 25 at 20000 rpm for 10 min by adding the oil phase dropwise to the water sol. NaCl was used as an electrolyte in different concentration (0.1 – 2 M). Emulsions containing MetC5PA were prepared similar with a concentration of MetC5PA of $1.5*10^{-3}$ mol/L in the oil phase.

5.4.20 Synthesis of TiO_2 'Janus' Nanoparticles

As a first model systems for Pickering emulsions cyclohexane/H_2O mixtures were used. The Pickering emulsions contained between 1wt.% TiO_2 (self-synthesized or Degussa P25). The pH was around 3. The emulsions were formed from 10 ml H_2O sol of particles and between 2.5 and 1 ml of cyclohexane. The cyclohexane contained the phosphonate (ethyl ester of methacyrloyloxy pentyl phosphonic acid – MetC5PA or isopropyl esters of ally phosphonic acid - APA). The concentration of the ligand in the oil phase was $1.5*10^{-3}$ mol/L (the same used for the surface-functionalization in solution). The emulsions were prepared using an Ultraturrax at 14k rot/min for 15 min. The oil phase was added to the water sol during mixing. The particles were separated by centrifugation, dried and analyzed. For DLS measurements a few drops of the emulsion were further on diluted with water and then analyzed. Typical Pickering emulsions are presented in Table 16.

Janus - TiO_2@MetC5PA-Et

FT-IR (ATR, υ, cm^{-1}): 2961, 1725,1641, 1557, 1449, 1436, 1300, 1259, 1241, 1189-963, 795. ^{31}P/MAS (25°C, δ, ppm): 37.2. BET (m^2/g): . TGA (mass loss, %): 30 – 170 °C: 5.2 %, 170 – 260: 4%; 260 – 600 °C: 10.3 %. Raman (υ, cm^{-1}): Ti – O stretching vib.: 645, TiO_2: 517, 403, 153. Diameter. DLS (nm): 9.27 nm ± 0.05. TEM (nm): 11 nm.

Janus - TiO_2@DPA

FT-IR (ATR, υ, cm^{-1}): 2983, 2955, 2858, 1463, 1175-910. ^{31}P/MAS (25°C, δ, ppm): 37, 30. BET (m^2/g): . TGA (mass loss, %): 30 – 200 °C: 5.9 %, 200 – 650 °C: 24 %. Diameter. DLS (nm): 10.1 nm ± 0.05.TEM: 12 nm.

Janus - TiO_2@MetC11PA-Et

FT-IR (ATR, υ, cm^{-1}): 2927, 2855, 1716, 1638, 1536, 1482, 1447, 1388, 1293, 1188, 1151, 1037, 962. ^{31}P/MAS (25°C, δ, ppm): 17.6. TGA (mass loss, %): 30 – 250 °C: 6 %, 250 – 600 °C: 25 %.

Sample	*TiO_2H_2O 10 mL*	*Ligand($1.5*10^{-3}$ mol/L)*	*Oil(mL)*
Se234	P25	APA_^{i}Pr	2.5 cyclohexane
Se235	P25	APA_^{i}Pr	1 cyclohexane
Se236	P25	MetC5PA_Et	2.5 cyclohexane
Se237	P25	MetC5PA_Et	1 cyclohexane
Se241	s227	MetC5PA_Et	2.5 cyclohexane
Se242	s217	MetC5PA_Et	1 cyclohexane
Se243	s227	APA_^{i}Pr	2.5 cyclohexane
Se244	s217	APA_^{i}Pr	1 cyclohexane
Se245	s225	MetC5PA_Et	2.5 cyclohexane
Se246	s225	MetC11PA_Et	1.5 cyclohexane
Se247	s225	Pyrene	3 cyclohexane
Se248	s225	DPA_Et	2 cyclohexane
Se250	s249	MetC11PA_Et	2.5 toluene
Se251	s249	MetC11PA_Et	2.5 toluene
Se252	s249	DPA	2 cyclohexane
Se253	s249	DPA	2 toluene
Se254	s249	DPA	1 toluene
Se255	s249	DPA	1.5 toluene
Se256	s249	DPA	1.5 cyclohexane
Se257	s249	DPA_Et	1 cyclohexane
Se258	s249	DPA_Et	2.5 cyclohexane
Se259	s249	MetC5PA_Et	2.5 cyclohexane

Table 16. Typical Pickering emulsions prepared from H_2O sol (10 ml, 1 wt.% TiO_2 nanoparticles) and cyclohexane

5.4.21 Preparation of polymer–TiO_2 hybrid particles

s264. 0.5 g TiO_2 (21 nm) were dispersed in 50 mL distilled water using an ultrasonic processor with a digital sonifier for 4 min at 70% amplitude and with a 30 sec pause every minute. 3 mL MMA (0.028 mol) were mixed with 1.0 g of MetC5PA (0.0034 mol) and 0.02 g AIBN ($1.2*10^{-3}$ mol); this solution was subsequently mixed with the TiO_2 dispersion. A stable Pickering emulsion was generated by agitation using an IKA Ultra-Turrax T 25 at 20000 rpm for 10 min. The resulting emulsion was poured into a 100 mL Schlenk flask, sealed with a rubber seal, and degassed. The reaction mixture was heated to 85°C and was subsequently polymerized at that temperature for 3 hours. The polymers were separated by filtration and dried in vacuum. Due to the fact that the TiO_2 stabilizing particles were covering the surface of the polymer spheres no yield of the polymerization reaction could be calculated.

FT-IR (ATR, υ, cm^{-1}): 2961, 1725, 1673, 1514, 1448, 1437, 1392, 1259, 1243, 1189, 1145, 1095, 1066, 1019, 795. ^{31}P/MAS (25°C, δ, ppm): 36.2. ^{13}C/CP/MAS (25°C, δ, ppm): 169.9, 54.5, 44.1, 37, 8.8. TGA (mass loss, %): 30 – 210 °C: 2 %, 210 – 410 °C: 80 %, 410 – 600°C: 4 %.

s261. 0.5 g TiO_2 (21 nm) were dispersed in 50 mL distilled water using an ultrasonic processor with a digital sonifier for 4 min at 70% amplitude and with a 30 sec pause every minute. 1.5 g MMA (0.015 mol) were mixed with 1.0 g of MetC5PA (0.0034 mol), 1.5 g hexane and 0.0125 g ($0.7*10^{-3}$ mol) AIBN; this solution was subsequently mixed with the TiO_2 dispersion. A stable Pickering emulsion was generated by agitation using an IKA Ultra-Turrax T 25 at 20000 rpm for 10 min. The resulting emulsion was poured into a 100 mL Schlenk flask, sealed with a rubber seal, and degassed. The reaction mixture was heated to 85°C and was subsequently polymerized at that temperature for three hours. The polymers were separated by filtration and dried in vacuum. Due to the fact that the TiO_2 stabilizing particles were covering the surface of the polymer spheres no yield of the polymerization reaction could be calculated.

FT-IR (ATR, υ, cm^{-1}): 1728, 1539, 1520, 1478, 1443, 1241, 1187, 1149, 1095, 1066, 1040, 959. ^{31}P/MAS (25°C, δ, ppm): 35.2. ^{13}C/CP/MAS (25°C, δ, ppm): 169.7, 53.5, 44, 37, 19.4, 8.8. TGA (mass loss, %): 30 – 210 °C: 2 %, 210 – 410 °C: 66.4 %, 410 – 600°C: 6.2 %.

s262. 0.5 g TiO_2 (8 nm) were dispersed in 50 mL distilled water using an ultrasonic processor with a digital sonifier for 4 min at 70% amplitude and with a 30 sec pause every minute. 1.5 g MMA (0.015 mol) were mixed with 1.0 g of MetC5PA (0.0034 mol), 1.5 g hexane and 0.0125 g ($0.7*10^{-3}$ mol) AIBN; this solution was subsequently mixed with the TiO_2 dispersion. A stable Pickering emulsion was generated by agitation using an IKA Ultra-Turrax T 25 at 20000 rpm for 10 min. The resulting emulsion was poured into a 100 mL Schlenk flask, sealed with a rubber seal, and degassed. The reaction mixture was heated to 85°C and was subsequently polymerized at that temperature for three hours. The polymers were separated by filtration and dried in vacuum. Due to the fact that the TiO_2 stabilizing particles were covering the surface of the polymer spheres no yield of the polymerization reaction could be calculated.

FT-IR (ATR, υ, cm^{-1}): 2985, 2948, 1729, 1449, 1389, 1243, 1152, 1035, 964, 817, 752. TGA (mass loss, %): 30 – 210 °C: 2.3 %, 210 – 410 °C: 77 %, 410 – 600°C: 11 %.

s298 – MetC11PA

0.5 g TiO_2 (21 nm) were dispersed in 12.5 mL distilled water (acidified before with few drops of HNO_3 conc.) using a Ultrasonic Processor with a digital sonifier for 4 min at 70% amplitude and with a 30 sec pause every minute. 0.38 g MMA were mixed with 0.25 ($0.78*10^{-3}$ mol) g of MetC11PA, 0.38 g hexane and 0.0031 g AIBN; this solution was subsequently mixed with the TiO_2 dispersion. A stable Pickering emulsion was generated by agitation using an IKA Ultra-Turrax T 25 at 20000 rpm for 10 min. The resulting emulsion was poured into a 100 mL Schlenk flask, sealed with a rubber seal, and degassed. The reaction mixture was heated to 85°C and was subsequently polymerized at that temperature for three hours. The polymers were separated by filtration and dried in vacuum. Due to the fact that the TiO_2 stabilizing particles were covering the surface of the polymer spheres no yield of the polymerization reaction could be calculated.

s299 – MetC11PA

0.5 g TiO_2 (21 nm) were dispersed in 12.5 mL distilled water (acidified before with few drops of HNO_3 conc.) using a Ultrasonic Processor with a digital sonifier for 4 min at 70% amplitude and with a 30 sec pause every minute. 0.75 g MMA were mixed with 0.25 g ($0.78*10^{-3}$ mol) of MetC11PA and 0.005 g AIBN; this solution was subsequently mixed with the TiO_2 dispersion. A stable Pickering emulsion was generated by agitation using an IKA

Ultra-Turrax T 25 at 20000 rpm for 10 min. The resulting emulsion was poured into a 100 mL Schlenk flask, sealed with a rubber seal, and degassed. The reaction mixture was heated to 85°C and was subsequently polymerized at that temperature for three hours. The polymers were separated by filtration and dried in vacuum. Due to the fact that the TiO_2 stabilizing particles were covering the surface of the polymer spheres no yield of the polymerization reaction could be calculated.

FT-IR (ATR, υ, cm^{-1}): 2999, 2952, 1726, 1658, 1450, 1386, 1241, 1153, 1041, 961, 752. ^{31}P/MAS (25°C, δ, ppm): 36. ^{13}C CP MAS NMR (25°C, δ, ppm): 171.5, 55.1, 45.6, 38.6, 10.5. TGA (mass loss, %): 30 – 210 °C: 5.1 %, 210 – 410 °C: 52 %, 410 – 600°C: 9.7 %.

5.4.22 Nanocomposites without Covalent Bonds between the Matrix and the Nanoparticles

Nanocomposites without covalent bonds between the matrix and the nanoparticles were prepared based on dodecyl phosphonic acid modified TiO_2 nanoparticles and styrene. The surface modified particles were dispersed under inert atmosphere into the required quantity of organic monomer (styrene), previously degassed (Table 17). The initiator, peroxide benzoyl (PBO) was added to this mixture. The dispersion was sonificated for 10 minutes using an ultrasonic bath. The obtained clear solution was then introduced into an oven at 85°C and polymerized for 10 hours.

Typical example for the polymerization of styrene in the presence of TiO_2@DPA nanoparticles

s276_5. FT-IR (ATR, υ, cm^{-1}): 3061, 3025, 2919, 2854, 1492, 1448, 1072, 1024, 753, 696. SEC: Mn = 226827 g/mol; PDI = 2.1. TGA (air, 30 – 700 °C): onset 1 = 359 °C, 92 %; onset 2 = 447 °C, 4.3 %. DSC (N_2, 30 – 200 °C): T_g = 97 °C. Yield: 96 %.

Table 17. Nanocomposites based on PS and TiO_2-DPA

Sample	Styrene (mL)	Initiator (PBO) (g)	TiO_2-DPA (g)
PSref	1.1	0.013	-
s279_0.05	2.2	0.026	0.001
s278_0.1	2.2	0.026	0.002
s277_0.5	2.2	0.026	0.010
s274_1	1.1	0.013	0.010
s276_5	1.1	0.013	0.050

5.4.23 Nanocomposites with Covalent Bonds between the Matrix and the Nanoparticles

In a similar manner, nanocomposites with covalent bonds between the matrix and the nanoparticles were prepared based on methacryloyloxy pentyl phosphonic ester modified TiO_2 nanoparticles and methyl methacrylate. The surface modified particles were dispersed under inert atmosphere into the required quantity of organic monomer (styrene), previously degassed (Table 18). The initiator, peroxide benzoyl (PBO) and the crosslinker (when required) were added to this mixture. The dispersion was sonificated for 10 minutes using an ultrasonic bath. The obtained clear solution was then introduced into an oven at 85°C and polymerized for 10 hours.

Typical example for the polymerization of styrene in the presence of TiO_2@MetC5PA nanoparticles

s295_1. FT-IR (ATR, υ, cm^{-1}): 2998, 2947, 2846, 1728, 1443, 1388, 1240, 1186, 1146, 1067, 1027, 985, 838, 753. SEC: Mn = 231005 g/mol; PDI = 4.4. TGA (air, 30 – 700 °C): 327 °C, 98.4 %. DSC (N_2, 30 – 200 °C): T_g = 109 °C. Yield: 98 %.

Table 18. Nanocomposites based on PMMA and TiO_2-MetC5PA-Et

Sample	MMA (mL)	Initiator (PBO) (g)	TiO_2-MetC5PA (g)	TMPTMA (mL)
PMMAref_1	1.1	0.013	-	-
s293_0.1	1.1	0.013	0.001	-
s291_0.5	1.1	0.013	0.005	-
s295_1	1.1	0.013	0.010	
PMMAref_2	1.1	0.013	-	0.030
s294_0.1	1.1	0.013	0.001	0.030
s292_0.5	1.1	0.013	0.005	0.030
s296_1	1.1	0.013	0.010	0.030

6. Summary

Recently hybrid materials gained much attention because of their synergetic properties arising from the combination of both inorganic and organic components. An important challenge in their formation is the prevention of agglomeration of the inorganic components in the polymer matrix, which can be reached by a covalent connection between the inorganic and the organic moieties, limiting the diffusion of the formed inorganic particles in the organic network. Furthermore, a stable connection between the organic matrix and the inorganic fillers hinders microphase separation, which is regularly observed when particles and clays are used for the reinforcement of the polymer materials

In a first part of the work hybrid materials were prepared from well-defined building blocks which were acting as single source precursors for the formation of both the inorganic and organic polymers. One of the research goals was the synthesis of structured inorganic-organic nanocomposites by the combination of atom transfer radical polymerization (ATRP) and sol-gel chemistry. First the synthesis of β-keto esters, such as 2-(methacryloyloxy)ethyl acetoacetate (HAAEMA), ethyl acetoacetate (EAA), 3-(methacryloyloxy)propyl acetoacetate (HAAPMA) and 4-(methacryloyloxy)butyl acetoacetate (HAABMA) was carried out (Scheme 22).

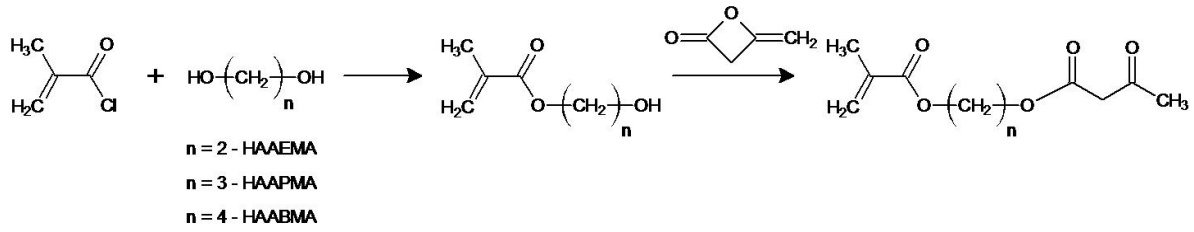

Scheme 22. The general pathway for the synthesis of β-keto esters with attached polymerizable groups

For the synthesis of hybrid materials in a first step the coordination behavior of the β-keto esters to titanium and zirconium alkoxides was investigated. In a second step, the complexes were used as monomers in ATRP leading to well-defined metal alkoxide-containing polymers, which were transformed into nanocomposites by the sol-gel reaction of the alkoxide precursors (Scheme 23).

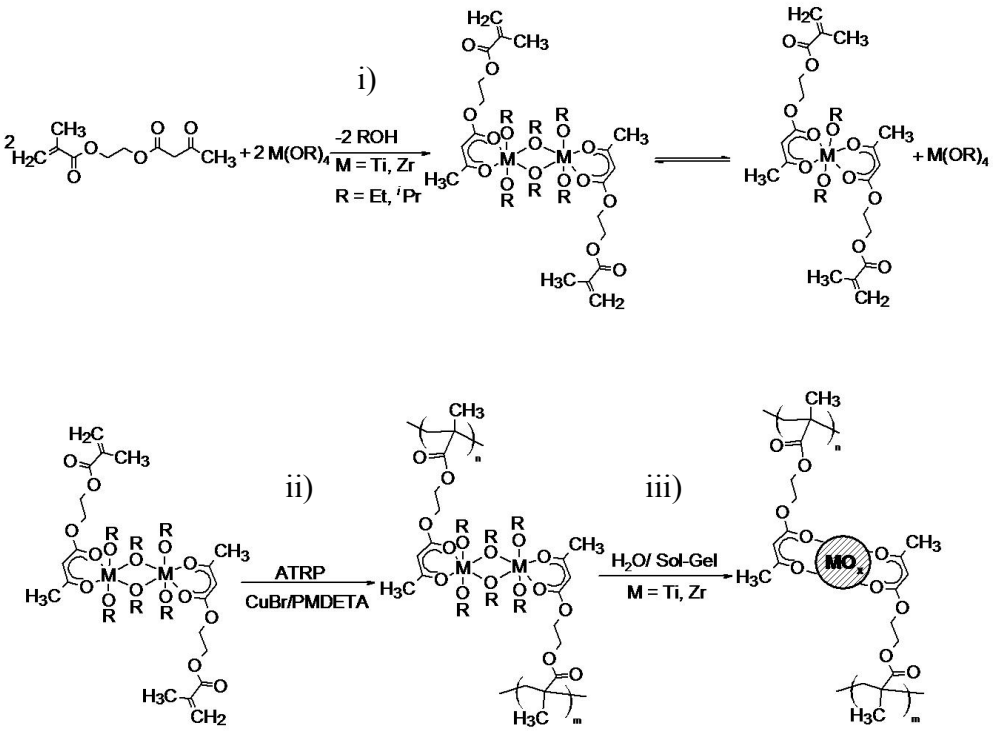

Scheme 23. Presentation of the synthetic pathway: i) coordination of Ti and Zr alkoxides with HAAEMA, ii) polymerization, iii) sol-gel process

Coordination between Ti alkoxides and β-keto esters led to well defined complexes as show by investigations in the solid state as well as in the liquid state. From single crystal X-ray diffraction analysis the coordination compounds obtained from Ti ethoxides or *iso*propoxides and EAA in a 1:1 ratio appeared as alkoxide-bridged dimers with chelating ethyl acetoacetate ligands, presenting a centrosymmetric structure (Figure 134). In these structures the metal center was six-fold coordinated.

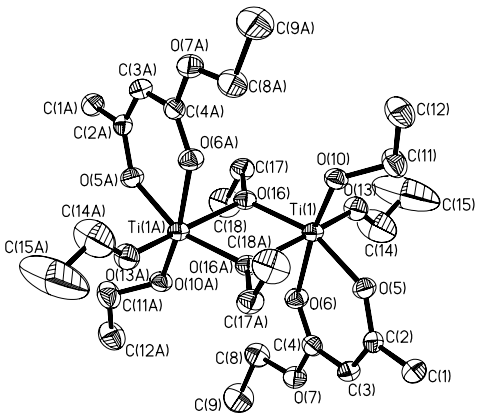

Figure 134. ORTEP plot of the structure of $Ti_2(\mu_2\text{-}OEt)(OEt)_2(EAA)_2$. Thermal ellipsoids are at a 50% probability level. H-atoms were omitted for clarity

In solution the complexes exhibited ligand exchange reactions which made the structure assignments difficult. However, 2D NMR analysis supported a full coordination of β-keto esters in the case of Ti alkoxides. Investigation of the spacer length between coordinating part and polymerizable group shows that this parameter does not have an influence on the coordination behavior. Contrary to the preferentially six coordinated Ti, Zr offers an expandable coordination sphere with potential coordination numbers between 6 and 9. The coordination of Zr alkoxides with β-keto esters was investigated using 2D NMR and FT-IR techniques. The Zr *iso*propoxide complexes showed a full coordination of the β-keto esters, similar as seen for the Ti-complexes. However, when Zr butoxides were used, transesterification reaction of the β-keto esters with the butoxy groups of the alkoxide occurred, leading to the decomposition of the β-keto esters ligands and the breaking of the covalent binding between the acetylacetonate part and the methacrylate part (Scheme 24). For this reason, the Zr butoxides were not used further for the synthesis of hybrid materials.

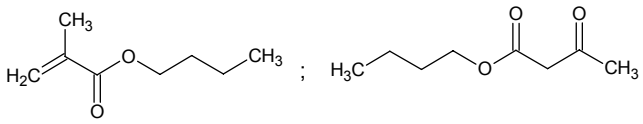

Scheme 24. Transesterification products of HAAEMA with $Zr(OBu)_4$

ATRP was applied to the well-defined coordination compounds which did not show metal alkoxide catalyzed transesterification reactions ($[Ti(OEt)_3AAEMA]_2$, $[Ti(O^iPr)_3AAEMA]_2$ and $[Zr(O^iPr)_3AAEMA]_2$), resulting in hybrid polymers. When an organic monomer (MMA) was used in combination with the complexes, hybrid copolymers were synthesized. Spectroscopic methods such as ^{13}C CP/MAS NMR and FT-IR proved the successful incorporation of the complexes in the polymers. SEC studies revealed that in all of the (co)polymerization cases monodispersed molecular weights and narrow molecular weight distributions (MWDs) were obtained, showing that the polymerization was controlled. Electron microscopy measurements showed that the hybrid materials were homogeneous, which was in concordance with an even distribution of the metal alkoxide complexes throughout the (co)polymer matrix. Furthermore SAXS studies revealed that the titanium alkoxide clusters were regularly aligned in one-dimensional chains inside the polymer matrix (Scheme 25). The chains containing the clusters also presented a short range order. The ordering in the case of the zirconium alkoxides was less visible.

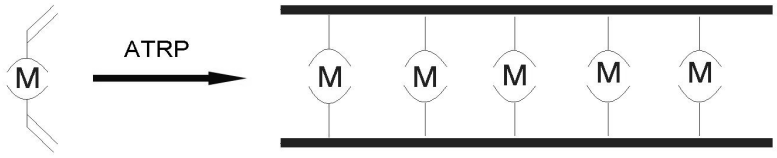

Scheme 25. Hybrid polymers having the metal alkoxide clusters regularly aligned in one-dimensional chains inside the polymer matrix

The thus prepared metal alkoxide-containing polymers were further on used as precursors in an aqueous sol-gel process. The alkoxides were converted into the respective oxide by exposing the hybrid polymers to water vapors. This way the formation of TiO_2 or ZrO_2 nanoparticles with diameters between 3 and 20 nm inside the polymer matrix was achieved (Figure 135). TEM studies proved that the particles were not agglomerated and randomly dispersed in the matrix. The formation of the particles was also evidenced by SAXS analysis which revealed the disappearance of the metal alkoxide ordering and the formation of randomly dispersed nanoparticles.

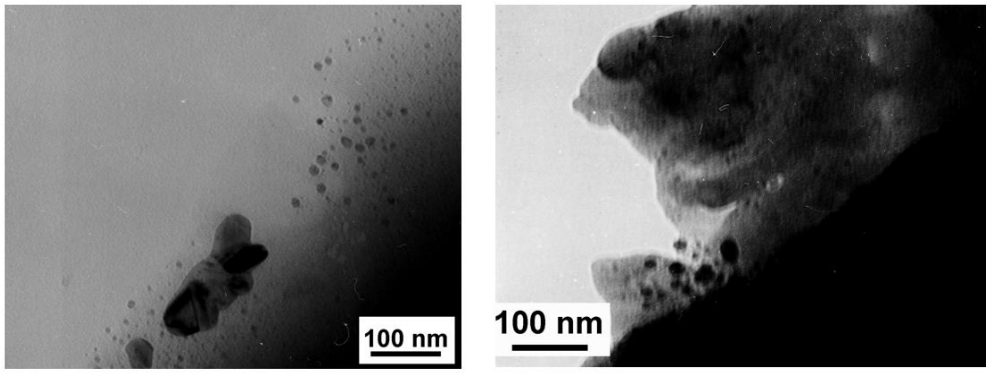

Figure 135. TEM micrographs of the TiO_2-polyAAEMAcoMMA and ZrO_2-polyAAEMAcoMMA (1:10)

In a second approach hybrid materials based on various polysiloxanes and metal oxides were prepared (Scheme 26). Starting compounds were preformed copolymers like PDMS-co-PMHS containing reactive groups and metal alkoxides modified with ligands containing coupling units. A β-keto ester, allyl acetoacetate, was reacted with titanium or zirconium alkoxides to afford well-defined complexs. These complexes were linked to the PDMS-co-PMHS polymer chains via hydrosilation reactions of the allyl double bond and the Si-H groups available in the copolymer. Spectroscopic investigations (e.g. NMR, FT-IR) showed that the coordination between the β-keto esters and the Ti or Zr alkoxides was successful resulting in alkoxide-bridged dimers with chelating allyl acetoacetate ligands. The

complex structure was not disturbed by the hydrosilation reaction with the polysiloxanes. The alkoxide-modified copolymers could still be used as a macromolecular precursor in the sol-gel process. Applying the sol-gel reaction to the thus formed macromolecular precursors in ethanol resulted in the formation of hybrid nanoparticles. This was due to the fact that the PDMS chains display a poor solubility in polar solvents and they formed micellar aggregates as shown by DLS studies.

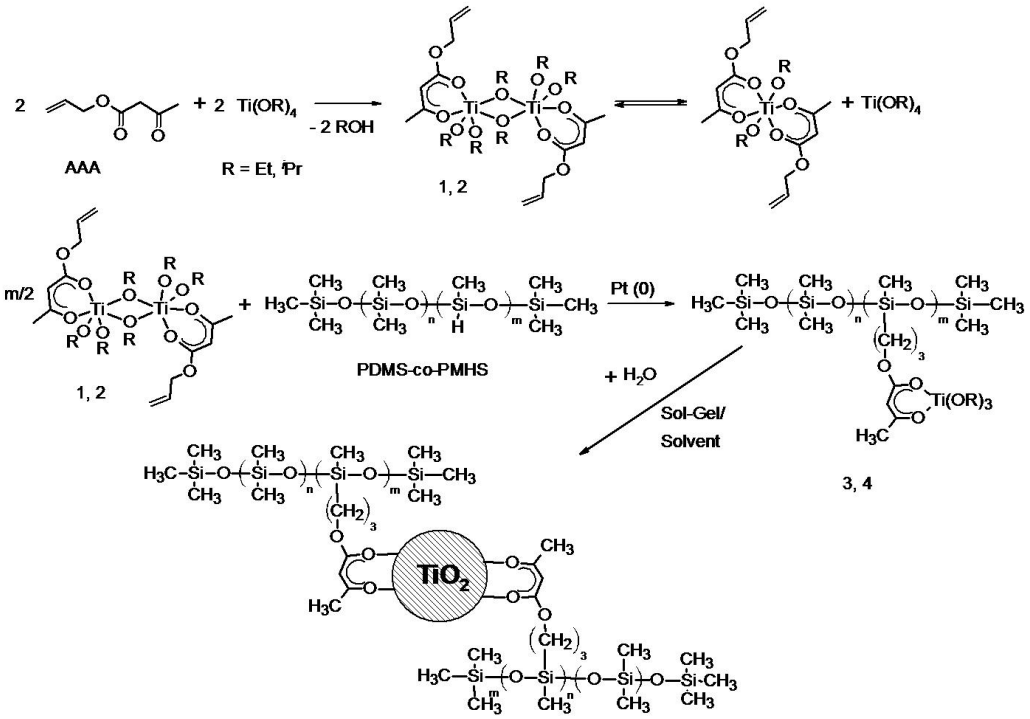

Scheme 26. General pathway for obtaining TiO_2-polysiloxanes hybrid materials (similar for ZrO_2-polysiloxanes): first coordination and then hydrosilation

The investigation of the structure of the nanoparticles by FT-IR and solid-state NMR showed that the linkage between the polymer chains and the metal oxide was maintained via the coordinative β-keto esters. The DLS measurements revealed that the particles had a radius between 3 and 15 nm. Most of the samples presented a bimodal size distribution, with a second distribution function between 70 and 100 nm radii. The percentage of the second, larger-size distribution mode was very low at small concentrations of precursor and increased with higher concentrations of the precursor. The TEM, SEM, and AFM analyses sustained the formation of hybrid nanoparticles. The chemical structure was also proved by EDX studies, which showed that the hybrid nanoparticles contained both Si derived from the polymer and Ti or Zr from the metal alkoxides.

Hybrid gels were obtained when toluene was employed as a solvent in the sol-gel process. This was due to the fact that the PDMS chains were well soluble and the nucleation centers could grow to form a homogeneous, continuous phase. EDX analyses showed that the polysiloxane was incorporated in the oxide matrix. The SEM analyses of the xerogels revealed uniform surfaces with no presence of pores.

In the last decade TiO_2 nanomaterials were extensively studied for their photocatalytical properties which led to many applications such as self-cleaning surfaces or waste water treatment. However, if organic substrates are targeted, it has to be avoided that the particles induce as well the decomposition of the organic substrate under the exposure of light. Thus, the second part of the research was focused on the synthesis of TiO_2 nanoparticles active for photocatalysis and their anisotropically functionalization with organophosphorus coupling agents. Such Janus particles could be used for the attachment to organic substrates. The bare TiO_2 surface would be available for photocatalysis, while the organophosphorus coupling agents should protect the organic substrate from decomposition.

Anatase nanoparticles were synthesized by the sol-gel process that allowed the control over the size and crystallinity of the particles. In such a way, TiO_2 nanoparticles having mean diameters of 5 nm were synthesized (Figure 136). The XRD and HR TEM analysis showed that the particles were fully crystalline. The crystal phase was assigned to anatase, with primary crystallite sizes of 3.4 nm.

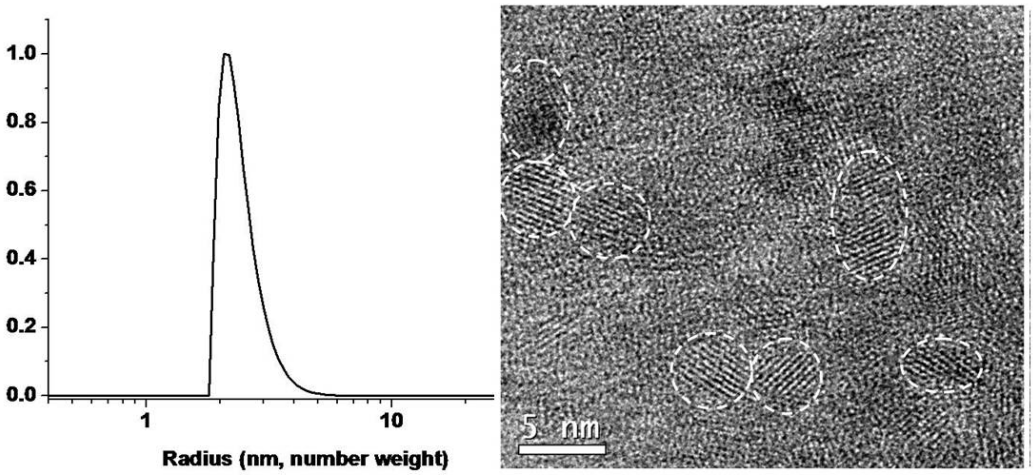

Figure 136. DLS (left side) and TEM (right side) analysis of TiO_2 synthesized from 0.17 mol/L $Ti(O^iPr)_4$

By changing the parameters of the sol-gel process like the precursor concentration or the aging time, the particle size could be increased from 5 to 12 nm. The increase of the particle size did not affect the crystallinity of the particles. XRD and HR TEM studies showed that the particles were still fully crystalline, and the crystal phase was assigned to anatase. All of the particles obtained through the sol-gel process were redispersible in water. The particles showed little photocatalytic activity in the decomposition reaction of methylene blue compared to the commercially available systems. However, the photocatalytic activity could be enhanced when the TiO_2 particles were heat treated at 400 °C.

The prepared TiO_2 particles were surface-functionalized in suspension using previously synthesized or commercially available organophosphorus coupling agents. The phosphonates and phosphates used had second organic moieties like methacrylic bonds (2-methyl-acrylic acid 5-(diethoxy-phosphoryl)-pentyl ester, 2-methyl-acrylic acid 11-(diethoxy-phosphoryl)-undecyl ester, and their acid homologues), long alkyl chains (dodecylphosphonic acid), phenyl rings (phenyl phosphonic acid, phenyl phosphoric acid), etc. The spectroscopic studies (^{31}P NMR, ^{13}C NMR) showed the TiO_2 nanoparticles could be surface-modified with various phosphonates and phosphates, either the free acids or their alkyl esters. FT-IR measurements evidenced the formation of Ti-O-P bonds and the disappearance of the P=O bonds. These results revealed that the binding mode of the coupling agents on the surface of the particles was predominately tridentate (Scheme 27).

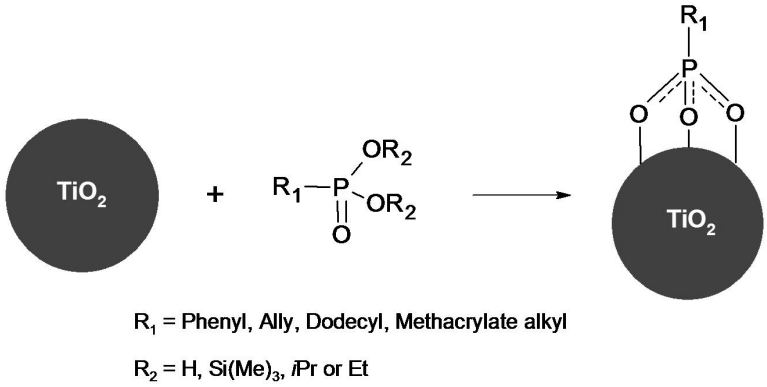

Scheme 27. The surface-modification of TiO2 nanoparticles with organophosphorus coupling agents

The amount of phosphonates or phosphates linked to the particle surface was dependent on the concentration of the organophosphorus coupling agent used for the modification of the particles, as calculated using thermogavrimetric analysis. In such a way the surface coverage of the particles could be tailored, ranging from partial to full coverage of the particle surface. TEM and SEM analyses showed that the particles were spherical and still

in the nanosize regim. Raman analysis proved that the particles maintained their anatase structure upon modification. Furthermore EDX confirmed the presence of phosphorus atoms. The modified particles still showed good photocatalytic activity for the decomposition reaction of methylene blue under UV light.

The pristine TiO_2 nanoparticles could also be applied as stabilizers in the formation of oil-in-water Pickering emulsions. Various emulsions stabilized by either the sol-gel or the commercially available TiO_2 Degussa P25 nanoparticles were obtained using organic solvents like cyclohexane and toluene for the oil phase. The emulsions were stable over a wide range of compositions, pH and salt concentrations. When the oil phase contained additionally an organophosphorus coupling agent, this was attached to the nanoparticle surface in contact with the oil phase in a similar manner as seen for the suspension modifications. Thus, an anisotropic surface modification of the particles was achieved (Scheme 28).

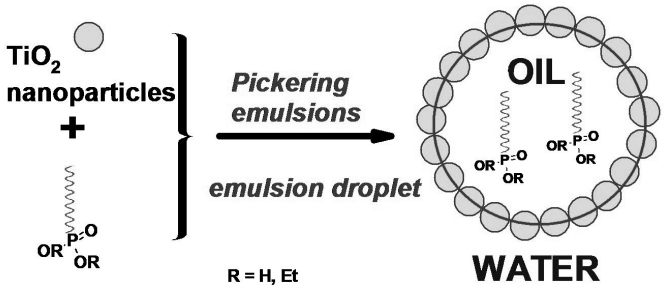

Scheme 28. O/w Pickering emulsion stabilized by TiO_2 nanoparticles. The oil phase contained an organophosphorus coupling agent

Spectroscopic studies showed the presence of tridentate organophosphorus coupling agents on the particle surfaces as seen for the samples modified in suspension. Thermogravimetric analyses were used to compare the amount of coupling agent bonded to the surface of particles which were modified in the Pickering emulsion and in suspension. When using the same relative concentration of the organophosphorus coupling agent for both of the modifications, the TG analysis revealed that the amount of organics was significantly lower for the samples prepared in Pickering emulsion compared to the ones modified in suspension. This was in agreement with an anisotropic surface functionalization, when only a part of the surface was covered by the phosphonates. After their modification the particles still maintained their anatase structure as showed by the Raman analysis. Light scattering studies and TEM analyses showed that the particles were spherical and still in the nanosize region, with sizes in the range of 10 to 30 nm. EDX confirmed the presence of phosphorus atoms and proved that the weight ratio of the phosphorus was lower than in the case of

surface-functionalization in suspension. All these results sustained an anisotropic surface-modification of the anatase particles with the organophosphorus coupling agents.

By simply using such organophosphorus coupling agents having a methacrylate moiety together with MMA in the oil phase, the Pickering emulsion architecture was fixed giving rise to hybrid inorganic-organic spheres. Several Pickering emulsions were prepared stabilized by different TiO_2 nanoparticles. The oil phase contained either only the polymerizable organophosphonate and MMA, or the two comonomers and a volatile organic solvent like cyclohexane or toluene. Spectroscopic studies showed that after the polymerization the phosphonates acted as tridentate ligands that bonded to the surface of the oxide particles. Furthermore, the copolymerization of the phosphonate double bonds with the MMA was also proven by ^{13}C NMR and FT-IR analyses. TG analysis showed a considerable increase in the thermal stability of the hybrid spheres compared with pristine PMMA. The hybrid spheres revealed an onset decomposition temperature at about 300°, which was 50 °C higher than the decomposition temperature of the pristine PMMA. SEM revealed that narrow monodisperse polymer spheres were obtained for all Pickering emulsions (Figure 137). The higher magnification photographs showed that the polymer spheres had the stabilizing TiO_2 nanoparticles on their surface. EDX revealed that the surface of the hybrid spheres contained mostly Ti. The presence of the small anatase nanoparticles on the surface of the hybrid Pickering spheres was confirmed also by the TEM measurements. These results have proven that the anatase nanoparticles were located at the surface of the polymer spheres. As detected by XRD, the crystallinity of the TiO_2 nanoparticles was not affected by the polymerization process, so the surface of the particles was still available for photocatalytic reactions.

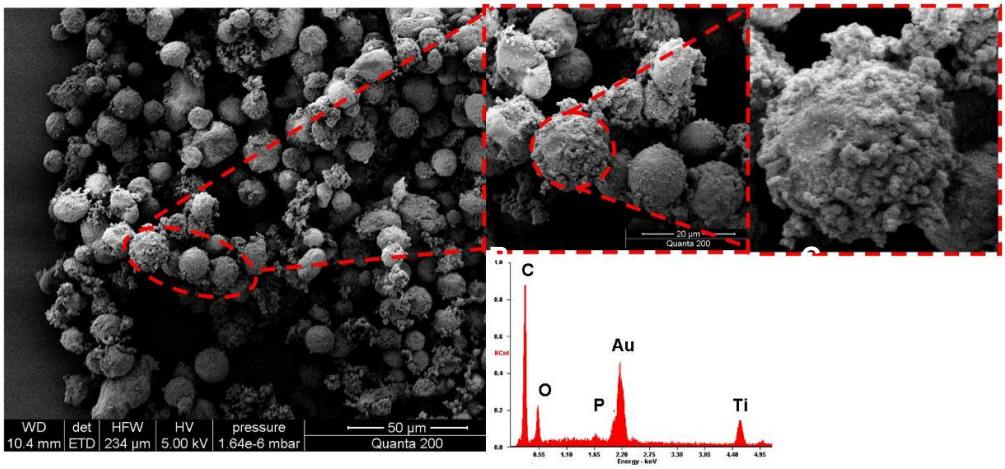

Figure 137. SEM images of TiO_2@PMMA-MetC5PA (s264) and the EDX analysis of one hybrid particle

Another approach leading to nanocomposites which are optically transparent waa based on the use of fully surface-functionalized anatase nanoparticles.

The TiO_2 nanoparticles surface-modified with organophosphorus coupling agents in suspension were good dispersible in common organic monomers. Light scattering studies revealed that TiO_2 nanoparticles modified with phosphonates containing long alkyl chains (e.g. dodecylphosphonic acid) or phenyl groups (phenyl phosphonic acid) were easily dispersed in styrene, while TiO_2 nanoparticles modified with phosphonates that had also methacrylate double bonds (e.g. 2-Methyl-acrylic acid 5-(diethoxy-phosphoryl)-pentyl ester) were good dispersed in methyl metharcylate.

Nanocomposites without covalent bonds between the matrix and the fillers were prepared by *in-situ* polymerization of styrene in the presence of TiO_2 nanoparticles surface-modified with dodecylphosphonic acid (Scheme 29).

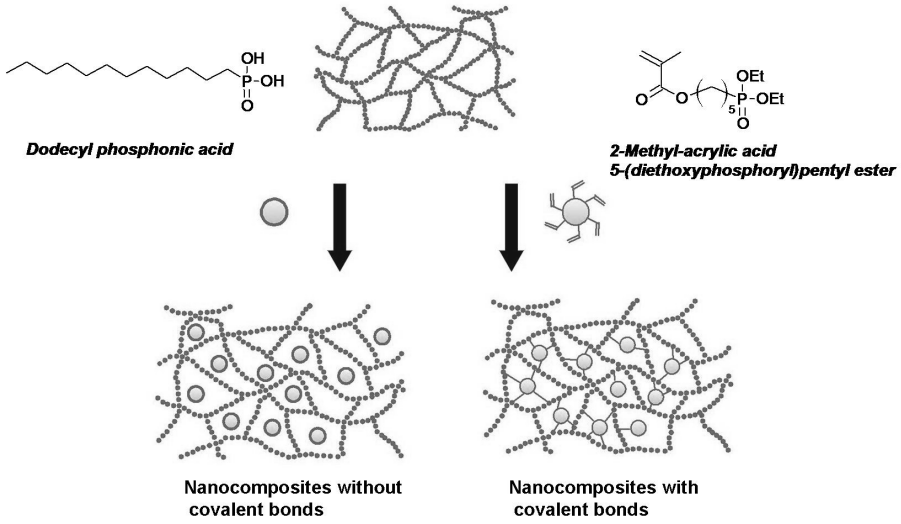

Scheme 29. Possible pathways for the synthesis of nanocomposite materials based on surface modified TiO_2 nanoparticles without or with covalent bonds between the inorganic and organic moieties

The SEC studies revealed that the radical polymerization process was not affected by the incorporation of the particles, monomodal molecular weight distributions were obtained even at high loading degrees (5 wt % particles). The molecular weight distributions (MWD) of the resulting polymers showed values between 2 and 2.8, which are typical for radical polymerizations carried out in the absence of any chain controllers. The FT-IR showed the full conversion of the styrene double bonds. Thermogravimetric analysis showed that the nanocomposites exhibit enhanced thermal stability compared to the pristine polystyrene. An increase of the thermal stability of about 20 °C when modified TiO_2 nanoparticles were

incorporated in the PS was observed. DSC measurements showed that the glass transition temperatures were slightly reduced compared to the neat polystyrene. This could be explained by the fact that no covalent interactions are present between the matrix and the inorganic fillers. Thus, the particles had a plasticizer effect, increasing the chain mobility. The final nanocomposites showed a good transparency up to 5 wt % loadings. At higher values the nanocomposites became opaque probably due to the differences in the refractive indices of the two materials.

Nanocomposites with covalent bonds between the matrix and the fillers were prepared by *in-situ* polymerization of methyl methacrylate in the presence of TiO_2 nanoparticles surface-modified with 2-methyl-acrylic acid 5-(diethoxy-phosphoryl)-pentyl ester. FT-IR analysis revealed the presence of the specific P-O-Ti vibration mode which proved that the particles were incorporated into the polymer matrices. Furthermore no signal of the organophosphorus coupling agent double bonds was detected which proved that the ligand was copolymerized with the organic monomers. SEC showed that the polymerization was not affected by the particles, monomodal molecular distributions being obtained even at high loading degrees. The MWDs of the resulting polymers were higher in this case, between 4.7 and 6.6. The higher indices were probably also the result of the crosslinking effect of the methacrylate modified particles. This could lead to differences in the growing chains and thus increasing of polydispersity. With the incorporation of only 0.1 % TiO_2@MetC5PA-Et nanoparticles inside the polymer matrices the onset decomposition temperature increased by almost 20°C. Higher TiO_2 contents resulted in a further increase of the decomposition onset temperature. This thermal behavior of the composite provided a strong support that the surface-modification of the particles was copolymerized with the PMMA matrix, so that the TiO_2 particles acted as crosslinkers in the polymerization process, leading to a higher decomposition temperature. This fact was also supported by the further increase in the amount of particles which led to an onset temperature of about 330°C (for 0.5 % TiO_2-MetC5PA), due to more crosslinking sites. The glass transition temperatures were not affected by the incorporation of the particles. The final nanocomposites presented good transparency up to 1 wt % loadings, while higher values yielded yellow opaque nanocomposites.

Similar nanocomposites were obtained through the addition of an organic crosslinker to the MMA/TiO_2@MetC5PA-Et mixtures. The materials were highly crosslinked and insoluble in common organic solvents. Furthermore the thermal stability was increased by the incorporation of the particles compared to the PMMA systems crosslinked only by the organic agent.

Small angle X–ray scattering measurements revealed that in both types of nanocomposites (with or without covalent bonds between the fillers and the matrix) the TiO_2 surface-modified particles were randomly dispersed in the polymeric matrix without formation of large aggregates.

7. Bibliography

1 G. Kickelbick and Editor, *Hybrid Materials: Synthesis, Characterization, and Applications*, 2007.
2 P. Gomez-Romero and C. Sanchez, *New J. Chem.*, 2005, 29, 57-58.
3 Brinker C.J. and S. G.W., *Sol-Gel Science: The Physics and Chemistry of Sol-Gel Processing*, Academic Press 1990.
4 C. Sanchez and F. Ribot, *New J. Chem.*, 1994, 18, 1007-47.
5 J. Livage, M. Henry and C. Sanchez, *Prog. Solid State Chem.*, 1988, 18, 259-341.
6 Schubert U. and Huesing N., *Synthesis of Inorganic Materials*, Wiley-Vch, 2004.
7 U. Schubert, *J. Sol-Gel Sci. Technol.*, 2003, 26, 47-55.
8 U. Schubert, *J. Mater. Chem.*, 2005, 15, 3701-15.
9 G. Kickelbick and U. Schubert, *Monatsh. Chem.*, 2001, 132, 13-30.
10 C. Sanchez, B. Lebeau, F. Ribot and M. In, *J. Sol-Gel Sci. Technol.*, 2000, 19, 31-38.
11 B. Moraru, N. Huesing, G. Kickelbick, U. Schubert, P. Fratzl and H. Peterlik, *Chem. Mater.*, 2002, 14, 2732-40.
12 G. Kickelbick, P. Wiede and U. Schubert, *Inorg. Chim. Acta*, 1999, 284, 1-7.
13 G. Kickelbick and U. Schubert, *Chem. Ber.*, 1997, 130, 473-77.
14 F. R. Kogler, M. Jupa, M. Puchberger and U. Schubert, *J. Mater. Chem.*, 2004, 14, 3133-38.
15 M. Jupa, G. Kickelbick and U. Schubert, *Eur. J. Inorg. Chem.*, 2004, 1835-39.
16 N. Miele-Pajot, L. G. Hubert-Pfalzgraf, R. Papiernik, J. Vaissermann and R. Collier, *J. Mater. Chem.*, 1999, 9, 3027-33.
17 C. Barglik-Chory and U. Schubert, *J. Sol-Gel Sci. Technol.*, 1995, 5, 135-42.
18 J. Mendez-Vivar, P. Bosch, V. H. Lara and R. Mendoza-Serna, *J. Sol-Gel Sci. Technol.*, 2002, 25, 249-54.
19 M. S. M. Saifullah, D.-J. Kang, K. R. V. Subramanian, M. E. Welland, K. Yamazaki and K. Kurihara, *J. Sol-Gel Sci. Technol.*, 2004, 29, 5-10.
20 U. Gbureck, J. Probst and R. Thull, *J. Sol-Gel Sci. Technol.*, 2003, 27, 157-62.
21 U. Patil, M. Winter, H.-W. Becker and A. Devi, *J. Mater. Chem.*, 2003, 13, 2177-84.
22 A. Baunemann, R. Thomas, R. Becker, M. Winter, R. A. Fischer, P. Ehrhart, R. Waser and A. Devi, *J. Chem. Soc., Chem. Commun.*, 2004, 1610-11.
23 B. Corain, M. Zecca, P. Mastrorilli, S. Lora and G. Palma, *Makromol. Chem., Rapid Commun.*, 1993, 14, 799-805.
24 G. Moad and D. H. Solomon, *The chemistry of free radical polymerization*, Pergamon, 1995.
25 D. Holzinger and G. Kickelbick, *J. Mater. Chem.*, 2004, 14, 2017-23.
26 Y. Wei, D. Jin, C. Yang and G. Wei, *J. Sol-Gel Sci. Technol.*, 1996, 7, 191-201.
27 G. Luciani, A. Costantini, B. Silvestri, F. Tescione, F. Branda and A. Pezzella, *J. Sol-Gel Sci. Technol.*, 2008, 46, 166-75.
28 R. Di Maggio, L. Fambri and A. Guerriero, *Chem. Mater.*, 1998, 10, 1777-84.
29 S. Trabelsi, A. Janke, R. Haessler, N. E. Zafeiropoulos, G. Fornasieri, S. Bocchini, L. Rozes, M. Stamm, J.-F. Gerard and C. Sanchez, *Macromolecules*, 2005, 38, 6068-78.
30 L. Chen, J. Zhu, Q. Li, S. Chen and Y. Wang, *Eur. Polym. J.*, 2007, 43, 4593-601.
31 K. Matyjaszewski and J. Xia, *Chem. Rev.*, 2001, 101, 2921-90.
32 H. Fischer, *J. Polym. Sci., Part A: Polym. Chem.*, 1999, 37, 1885-901.
33 T. E. Patten and K. Matyjaszewski, *Adv. Mater.*, 1998, 10, 901-15.
34 K. Matyjaszewski, *Chem.--Eur. J.*, 1999, 5, 3095-102.
35 T. E. Patten and K. Matyjaszewski, *Acc. Chem. Res.*, 1999, 32, 895-903.
36 J. Xia, X. Zhang and K. Matyjaszewski, *ACS Symp.Ser.*, 2000, 760, 207-23.

37 J. Pyun and K. Matyjaszewski, *Chem. Mater.*, 2001, 13, 3436-48.
38 D. Holzinger and G. Kickelbick, *J. Polym. Sci., Part A: Polym. Chem.*, 2002, 40, 3858-72.
39 R. O. R. Costa, W. L. Vasconcelos, R. Tamaki and R. M. Laine, *Macromolecules*, 2001, 34, 5398-407.
40 D. Holzinger and G. Kickelbick, *Chem. Mater.*, 2003, 15, 4944-48.
41 D. Holzinger, L. M. Liz-Marzan and G. Kickelbick, *J. Nanosci. Nanotechnol.*, 2006, 6, 445-52.
42 J. Pyun and K. Matyjaszewski, *Macromolecules*, 2000, 33, 217-20.
43 R. Chen, W. Feng, S. Zhu, G. Botton, B. Ong and Y. Wu, *Polymer*, 2006, 47, 1119-23.
44 G. Pfaff and P. Reynders, *Chem. Rev.*, 1999, 99, 1963-81.
45 A. Salvador, M. C. Pascual-Marti, J. R. Adell, A. Requeni and J. G. March, *J. Pharm. Biomed. Anal.*, 2000, 22, 301-06.
46 R. Zallen and M. P. Moret, *Solid State Commun.*, 2006, 137, 154-57.
47 J. H. Braun, A. Baidins and R. E. Marganski, *Prog. Org. Coat.*, 1992, 20, 105-38.
48 A. Fujishima and K. Honda, *Nature*, 1972, 238, 37-8.
49 A. Fujishima, T. N. Rao and D. A. Tryk, *J. Photochem. Photobiol., C*, 2000, 1, 1-21.
50 D. A. Tryk, A. Fujishima and K. Honda, *Electrochim. Acta*, 2000, 45, 2363-76.
51 X. Chen and S. Mao Samuel, *Chem. Rev.*, 2007, 107, 2891-959.
52 G. Schmid, *Nanoparticles: From Theory to Application*, 2004.
53 A. L. Linsebigler, G. Lu and J. T. Yates, Jr., *Chem. Rev.*, 1995, 95, 735-58.
54 E. Roduner, *Chem. Soc. Rev.*, 2006, 35, 583-92.
55 C. Burda, X. Chen, R. Narayanan and A. El-Sayed Mostafa, *Chem. Rev.*, 2005, 105, 1025-102.
56 S.-S. Hong, M. S. Lee, S. S. Park and G.-D. Lee, *Catal. Today*, 2003, 87, 99-105.
57 K. D. Kim, S. H. Kim and H. T. Kim, *Colloids Surf., A*, 2005, 254, 99-105.
58 J. Lin, Y. Lin, P. Liu, M. J. Meziani, L. F. Allard and Y.-P. Sun, *J. Am. Chem. Soc.*, 2002, 124, 11514-18.
59 M. Andersson, L. Oesterlund, S. Ljungstroem and A. Palmqvist, *J. Phys. Chem. B*, 2002, 106, 10674-79.
60 S. Y. Chae, M. K. Park, S. K. Lee, T. Y. Kim, S. K. Kim and W. I. Lee, *Chem. Mater.*, 2003, 15, 3326-31.
61 F. Cot, A. Larbot, G. Nabias and L. Cot, *J. Eur. Ceram. Soc.*, 1998, 18, 2175-81.
62 X. Wang, J. Zhuang, Q. Peng and Y. Li, *Nature*, 2005, 437, 121-24.
63 J.-M. Wu, *J. Cryst. Growth*, 2004, 269, 347-55.
64 S. K. Pradhan, P. J. Reucroft, F. Yang and A. Dozier, *J. Cryst. Growth*, 2003, 256, 83-88.
65 S. Seifried, M. Winterer and H. Hahn, *Chem. Vap. Deposition*, 2000, 6, 239-44.
66 J.-M. Wu, H. C. Shih and W.-T. Wu, *Chem. Phys. Lett.*, 2005, 413, 490-94.
67 B. Xiang, Y. Zhang, Z. Wang, X. H. Luo, Y. W. Zhu, H. Z. Zhang and D. P. Yu, *J. Phys. D: Appl. Phys.*, 2005, 38, 1152-55.
68 Y. Lei, L. D. Zhang and J. C. Fan, *Chem. Phys. Lett.*, 2001, 338, 231-36.
69 M. D. Blesic, Z. V. Saponjic, J. M. Nedeljkovic and D. P. Uskokovic, *Mater. Lett.*, 2002, 54, 298-302.
70 E. Gressel-Michel, D. Chaumont and D. Stuerga, *J. Colloid Interface Sci.*, 2005, 285, 674-79.
71 C. B. Almquist and P. Biswas, *J. Catal.*, 2002, 212, 145-56.
72 P. Arnal, R. J. P. Corriu, D. Leclercq, P. H. Mutin and A. Vioux, *J. Mater. Chem.*, 1996, 6, 1925-32.

73 Y. Bessekhouad, D. Robert and J. V. Weber, *J. Photochem. Photobiol.*, 2003, 157, 47-53.
74 G. Oskam, A. Nellore, R. L. Penn and P. C. Searson, *J. Phys. Chem. B*, 2003, 107, 1734-38.
75 T. Sugimoto, K. Okada and H. Itoh, *J. Colloid Interface Sci.*, 1997, 193, 140-43.
76 C. J. Barbe, F. Arendse, P. Comte, M. Jirousek, F. Lenzmann, V. Shklover and M. Gratzel, *J. Am. Ceram. Soc.*, 1997, 80, 3157-71.
77 E. A. Barringer and H. K. Bowen, *Langmuir*, 1985, 1, 414-20.
78 E. A. Barringer and H. K. Bowen, *Langmuir*, 1985, 1, 420-8.
79 J. H. Jean and T. A. Ring, *Langmuir*, 1986, 2, 251-5.
80 C. Kormann, D. W. Bahnemann and M. R. Hoffmann, *J. Phys. Chem.*, 1988, 92, 5196-201.
81 D. Vorkapic and T. Matsoukas, *J. Colloid Interface Sci.*, 1999, 214, 283-91.
82 A. Chemseddine and T. Moritz, *Eur. J. Inorg. Chem.*, 1999, 235-45.
83 T. Moritz, J. Reiss, K. Diesner, D. Su and A. Chemseddine, *J. Phys. Chem. B*, 1997, 101, 8052-53.
84 M. R. Hoffmann, S. T. Martin, W. Choi and D. W. Bahnemann, *Chem. Rev.*, 1995, 95, 69-96.
85 J. Jordan, K. I. Jacob, R. Tannenbaum, M. A. Sharaf and I. Jasiuk, *Mater. Sci. Eng., A*, 2005, A393, 1-11.
86 J. E. Mark, *Prog. Polym. Sci.*, 2003, 28, 1205-21.
87 H. Althues, J. Henle and S. Kaskel, *Chem. Soc. Rev.*, 2007, 36, 1454-65.
88 E. Dzunuzovic, K. Jeremic and J. M. Nedeljkovic, *Eur. Polym. J.*, 2007, 43, 3719-26.
89 S. M. Khaled, R. Sui, P. A. Charpentier and A. S. Rizkalla, *Langmuir*, 2007, 23, 3988-95.
90 Y. Zhang, G. E. Zhou, Y. H. Zhang, L. Li, L. Z. Yao and C. M. Mo, *Mater. Res. Bull.*, 1999, 34, 701-09.
91 A. P. Wight and M. E. Davis, *Chem. Rev.*, 2002, 102, 3589-613.
92 W. Yoshida, R. P. Castro, J.-D. Jou and Y. Cohen, *Langmuir*, 2001, 17, 5882-88.
93 A. Van Blaaderen and A. Vrij, *J. Colloid Interface Sci.*, 1993, 156, 1-18.
94 M. Z. Rong, Q. L. Ji, M. Q. Zhang and K. Friedrich, *Eur. Polym. J.*, 2002, 38, 1573-82.
95 G. Kickelbick and L. M. Liz-Marzan, *Encycl. Nanosci. Nanotechnol.*, 2004, 2, 199-220.
96 M. Yang and Y. Dan, *Colloid Polym. Sci.*, 2005, 284, 243-50.
97 M. Niederberger, G. Garnweitner, F. Krumeich, R. Nesper, H. Coelfen and M. Antonietti, *Chem. Mater.*, 2004, 16, 1202-08.
98 J. M. Notestein, E. Iglesia and A. Katz, *Chem. Mater.*, 2007, 19, 4998-5005.
99 P. H. Mutin, G. Guerrero and A. Vioux, *J. Mater. Chem.*, 2005, 15, 3761-68.
100 G. Guerrero, P. H. Mutin and A. Vioux, *Chem. Mater.*, 2001, 13, 4367-73.
101 C. N. Rusu and J. T. Yates, Jr., *J. Phys. Chem. B*, 2000, 104, 12299-305.
102 R. Hofer, M. Textor and N. D. Spencer, *Langmuir*, 2001, 17, 4014-20.
103 M. M. Demir, P. Castignolles, U. Akbey and G. Wegner, *Macromolecules*, 2007, 40, 4190-98.
104 Y. Abe and T. Gunji, *Prog. Polym. Sci.*, 2004, 29, 149-82.
105 J. E. Mark, *Acc. Chem. Res.*, 2004, 37, 946-53.
106 C. Guermeur, J. Lambard, J.-F. Gerard and C. Sanchez, *J. Mater. Chem.*, 1999, 9, 769-78.
107 M. Nakade, K. Ichihashi and M. Ogawa, *J. Porous Mater.*, 2005, 12, 79-85.
108 M. Nakade, K. Ichihashi and M. Ogawa, *J. Sol-Gel Sci. Technol.*, 2005, 36, 257-64.
109 M. Nakade, K. Kameyama and M. Ogawa, *J. Mater. Sci.*, 2004, 39, 4131-37.

110 B. Julian, C. Gervais, E. Cordoncillo, P. Escribano, F. Babonneau and C. Sanchez, *Chem. Mater.*, 2003, 15, 3026-34.
111 B. Julian, C. Gervais, M.-N. Rager, J. Maquet, E. Cordoncillo, P. Escribano, F. Babonneau and C. Sanchez, *Chem. Mater.*, 2004, 16, 521-29.
112 A. Perro, S. Reculusa, S. Ravaine, E. Bourgeat-Lami and E. Duguet, *J. Mater. Chem.*, 2005, 15, 3745-60.
113 N. Glaser, D. J. Adams, A. Boeker and G. Krausch, *Langmuir*, 2006, 22, 5227-29.
114 H. Takei and N. Shimizu, *Langmuir*, 1997, 13, 1865-68.
115 A. Walther and A. H. E. Mueller, *Soft Matter*, 2008, 4, 663-68.
116 V. N. Paunov and O. J. Cayre, *Adv. Mater.*, 2004, 16, 788-91.
117 I. K. Voets, A. de Keizer, P. de Waard, P. M. Frederik, P. H. H. Bomans, H. Schmalz, A. Walther, S. M. King, F. A. M. Leermakers and M. A. Cohen Stuart, *Angew. Chem., Int. Ed.*, 2006, 45, 6673-76.
118 K.-H. Roh, D. C. Martin and J. Lahann, *Nat. Mater.*, 2005, 4, 759-63.
119 T. Nisisako and T. Torii, *Adv. Mater.*, 2007, 19, 1489-93.
120 L. Hong, S. Jiang and S. Granick, *Langmuir*, 2006, 22, 9495-99.
121 B. P. Binks, *Curr. Opin. Colloid Interface Sci.*, 2002, 7, 21-41.
122 S. U. Pickering, *J. Chem. Soc., Trans.*, 1907, 91, 2001-21.
123 W. Ramsden, *Proc. R. Soc. London, Ser. A*, 1903, 72, 156-64.
124 D. Wang, H. Duan and H. Moehwald, *Soft Matter*, 2005, 1, 412-16.
125 B. P. Binks and S. O. Lumsdon, *Langmuir*, 2000, 16, 8622-31.
126 B. P. Binks and S. O. Lumsdon, *Langmuir*, 2001, 17, 4540-47.
127 P. Finkle, H. D. Draper and J. H. Hildebrand, *J. Am. Chem. Soc.*, 1923, 45, 2780-8.
128 R. Aveyard, B. P. Binks and J. H. Clint, *Adv. Colloid Interface Sci.*, 2003, 100-102, 503-46.
129 A. Boeker, J. He, T. Emrick and T. P. Russell, *Soft Matter*, 2007, 3, 1231-48.
130 S. Stiller, H. Gers-Barlag, M. Lergenmueller, F. Pfluecker, J. Schulz, K. P. Wittern and R. Daniels, *Colloids Surf., A*, 2004, 232, 261-67.
131 S. Sacanna, W. K. Kegel and A. P. Philipse, *Phys. Rev. Lett.*, 2007, 98, 158301.
132 S. Melle, M. Lask and G. G. Fuller, *Langmuir*, 2005, 21, 2158-62.
133 N. P. Ashby and B. P. Binks, *Phys. Chem. Chem. Phys.*, 2000, 2, 5640-46.
134 F. Yang, S. Liu, J. Xu, Q. Lan, F. Wei and D. Sun, *J. Colloid Interface Sci.*, 2006, 302, 159-69.
135 Y. He and K. Li, *J. Colloid Interface Sci.*, 2007, 306, 296-99.
136 H. Hassander, B. Johansson and B. Toernell, *Colloids Surf.*, 1989, 40, 93-105.
137 B. R. Midmore, *Colloids Surf., A*, 1998, 132, 257-65.
138 B. P. Binks and S. O. Lumsdon, *Phys. Chem. Chem. Phys.*, 1999, 1, 3007-16.
139 B. P. Binks and C. P. Whitby, *Colloids Surf., A*, 2005, 253, 105-15.
140 H. Strohm, M. Sgraja, J. Bertling and P. Loebmann, *J. Mater. Sci.*, 2003, 38, 1605-09.
141 Y. Yin, Y. Lu, B. Gates and Y. Xia, *Chem. Mater.*, 2001, 13, 1146-48.
142 H. Strohm and P. Loebmann, *J. Mater. Chem.*, 2004, 14, 2667-73.
143 D. Wang, R. A. Caruso and F. Caruso, *Chem. Mater.*, 2001, 13, 364-71.
144 D. Wang and F. Caruso, *Chem. Mater.*, 2002, 14, 1909-13.
145 O. D. Velev, K. Furusawa and K. Nagayama, *Langmuir*, 1996, 12, 2374-84.
146 A. D. Dinsmore, M. F. Hsu, M. G. Nikolaides, M. Marquez, A. R. Bausch and D. A. Weitz, *Science*, 2002, 298, 1006-09.
147 S. Cauvin, P. J. Colver and S. A. F. Bon, *Macromolecules*, 2005, 38, 7887-89.
148 J. Yang, T. Hasell, W. Wang, J. Li, P. D. Brown, M. Poliakoff, E. Lester and S. M. Howdle, *J. Mater. Chem.*, 2008, 18, 998-1001.
149 T. Chen, P. J. Colver and S. A. F. Bon, *Adv. Mater. (Weinheim, Ger.) FIELD Full Journal Title:Advanced Materials (Weinheim, Germany)*, 2007, 19, 2286-89.

150 P. Mastrorilli, C. F. Nobile, G. P. Suranna, M. R. Taurino and M. Latronico, *Inorg. Chim. Acta*, 2002, 335, 107-12.
151 D. Hoebbel, T. Reinert, H. Schmidt and E. Arpac, *J. Sol-Gel Sci. Technol.*, 1997, 10, 115-26.
152 R. J. Errington, J. Ridland, W. Clegg, R. A. Coxall and J. M. Sherwood, *Polyhedron*, 1998, 17, 659-74.
153 L. C. Cauro-Gamet, L. G. Hubert-Pfalzgraf and S. Lecocq, *Z. Anorg. Allg. Chem.*, 2004, 630, 2071-77.
154 J. Blanchard, S. Barboux-Doeuef, J. Maquet and C. Sanchez, *New J. Chem.*, 1995, 19, 929-41.
155 D. Seebach, E. Hungerbuehler, R. Naef, P. Schnurrenberger, B. Weidmann and M. Zueger, *Synthesis*, 1982, 138-41.
156 N. Pajot, R. Papiernik, L. G. Hubert-Pfalzgraf, J. Vaissermann and S. Parraud, *J. Chem. Soc., Chem. Commun.*, 1995, 1817-19.
157 T. Krasia, R. Soula, G. Borner Hans and H. Schlaad, *Chem. Commun.*, 2003, 538-9.
158 H. Schlaad, T. Krasia and M. Antonietti, *J. Am. Chem. Soc.*, 2004, 126, 11307-10.
159 G. Kickelbick, D. Holzinger, D. Rutzinger and S. Ivanovici, *Controlled/Living Radical Polymerization. From Synthesis to Materials*, American Chemical Society, 2006.
160 J. Du and Y. Chen, *Macromolecules*, 2004, 37, 6322-28.
161 S. Ivanovici, M. Puchberger, H. Fric and G. Kickelbick, *Monatsh. Chem.*, 2007, 138, 529-39.
162 M. In, C. Gerardin, J. Lambard and C. Sanchez, *J. Sol-Gel Sci. Technol.*, 1995, 5, 101-14.
163 C. Sanchez and M. In, *J. Non-Cryst. Solids*, 1992, 147-148, 1-12.
164 T. C. Chang, Y. T. Wang, Y. S. Hong and Y. S. Chiu, *Thermochim. Acta*, 2002, 390, 93-102.
165 W. Stoeber, A. Fink and E. Bohn, *J. Colloid Interface Sci.*, 1968, 26, 62-9.
166 N. Huesing, J. Bauer, G. Kalss, G. Garnweitner and G. Kickelbick, *J. Sol-Gel Sci. Technol.*, 2003, 26, 73-76.
167 C. Zhang and R. M. Laine, *J. Am. Chem. Soc.*, 2000, 122, 6979-88.
168 B.-H. Kim, M.-S. Cho and H.-G. Woo, *Synlett*, 2004, 761-72.
169 G. Kickelbick, J. Bauer, N. Huesing, M. Andersson and K. Holmberg, *Langmuir*, 2003, 19, 10073-76.
170 G. Kickelbick, J. Bauer, N. Huesing, M. Andersson and A. Palmqvist, *Langmuir*, 2003, 19, 3198-201.
171 G. J. d. A. A. Soler-Illia, E. L. Crepaldi, D. Grosso and C. Sanchez, *Curr. Opin. Colloid Interface Sci.*, 2003, 8, 109-26.
172 D. Zhao, Q. Huo, J. Feng, B. F. Chmelka and G. D. Stucky, *J. Am. Chem. Soc.*, 1998, 120, 6024-36.
173 R. C. Hayward, B. F. Chmelka and E. J. Kramer, *Adv. Mater.*, 2005, 17, 2591-95.
174 H. Zhu, Z. Pan, B. Chen, B. Lee, S. M. Mahurin, S. H. Overbury and S. Dai, *J. Phys. Chem. B*, 2004, 108, 20038-44.
175 Y. Chen, J. Du, M. Xiong, K. Zhang and H. Zhu, *Macromol. Rapid Commun.*, 2006, 27, 741-50.
176 A. H. Yuwono, Y. Zhang, J. Wang, X. H. Zhang, H. Fan and W. Ji, *Chem. Mater.*, 2006, 18, 5876-89.
177 J. N. Lee, C. Park and G. M. Whitesides, *Anal. Chem.*, 2003, 75, 6544-54.
178 V. Gualandris, D. Hourlier-Bahloul and F. Babonneau, *J. Sol-Gel Sci. Technol.*, 1999, 14, 39-48.

179 L. Bois, J. Maquet, F. Babonneau, H. Mutin and D. Bahloul, *Chem. Mater.*, 1994, 6, 796-802.
180 K. Noble, A. B. Seddon, M. L. Turner, P. Chevalier and I. A. Mackinnon, *J. Sol-Gel Sci. Technol.*, 2000, 19, 807-10.
181 V. Belot, R. J. P. Corriu, D. Leclercq, P. H. Mutin and A. Vioux, *J. Polym. Sci., Part A: Polym. Chem.*, 1992, 30, 613-23.
182 W. H. Cho, D. J. Kang and S. G. Kim, *J. Mater. Sci.*, 2003, 38, 2619-25.
183 Y. Oguri, R. E. Riman and H. K. Bowen, *J. Mater. Sci.*, 1988, 23, 2897-904.
184 B. L. Cushing, V. L. Kolesnichenko and C. J. O'Connor, *Chem. Rev.*, 2004, 104, 3893-946.
185 G. Demazeau, *J. Mater. Chem.*, 1999, 9, 15-18.
186 F. Cansell, B. Chevalier, A. Demourgues, J. Etourneau, C. Even, V. Pessey, S. Petit, A. Tressaud and F. Weill, *J. Mater. Chem.*, 1999, 9, 67-75.
187 H. Y. Ha, S. W. Nam, T. H. Lim, I.-H. Oh and S.-A. Hong, *J. Membr. Sci.*, 1996, 111, 81-92.
188 N. Kaliwoh, J.-Y. Zhang and I. W. Boyd, *Appl. Surf. Sci.*, 2002, 186, 241-45.
189 C.-S. Kim, B. K. Moon, J.-H. Park, S. T. Chung and S.-M. Son, *J. Cryst. Growth*, 2003, 254, 405-10.
190 W. Choi, A. Termin and M. R. Hoffmann, *J. Phys. Chem.*, 1994, 98, 13669-79.
191 A. K. Bhattacharya and G. Thyagarajan, *Chem. Rev.*, 1981, 81, 415-30.
192 D. Francova and G. Kickerlbick, *in press*, 2008.
193 W. Gao, L. Dickinson, C. Grozinger, F. G. Morin and L. Reven, *Langmuir*, 1996, 12, 6429-35.
194 J. Randon, P. Blanc and R. Paterson, *J. Membr. Sci.*, 1995, 98, 119-29.
195 G. Guerrero, P. H. Mutin and A. Vioux, *Chem. Mater.*, 2000, 12, 1268-72.
196 A. Houas, H. Lachheb, M. Ksibi, E. Elaloui, C. Guillard and J. M. Herrmann, *Appl. Catal., B*, 2001, 31, 145-57.
197 H. Gnaser, M. R. Savina, W. F. Calaway, C. E. Tripa, I. V. Veryovkin and M. J. Pellin, *Int. J. Mass Spectrom.*, 2005, 245, 61-67.
198 K. V. Baiju, S. Shukla, K. S. Sandhya, J. James and K. G. K. Warrier, *J. Phys. Chem. C*, 2007, 111, 7612-22.
199 Y.-h. Xu, H.-r. Chen, Z.-x. Zeng and B. Lei, *Appl. Surf. Sci.*, 2006, 252, 8565-70.
200 M. B. Mitchell, V. N. Sheinker and E. A. Mintz, *J. Phys. Chem. B*, 1997, 101, 11192-203.
201 I. Langmuir, *J. Am. Chem. Soc.*, 1918, 40, 1361-402.
202 A. Wei, *Chem. Commun.*, 2006, 1581-91.
203 L. H. Allen and E. Matijevic, *J. Colloid Interface Sci.*, 1969, 31, 287-96.
204 M. D. Chadwick, J. W. Goodwin, E. J. Lawson, P. D. A. Mills and B. Vincent, *Colloids Surf., A*, 2002, 203, 229-36.
205 D. Briggs and M. P. Seah, *Practical Surface Analysis - Second Edition*, J. Wiley & Sons, New York, 1990.
206 P. Louette, F. Bodino and J.-J. Pireaux, *Surf. Sci. Spectra*, 2006, 12, 69-73.
207 J. F. Moulder, W. F. Stickle, P. E. Sobol and K. D. Bomben, in *Handbook of X-Ray Photoelectron Spectroscopy*, ed. J. Chastain, Eden Prairie, 1992.
208 in *NIST XPS Database, X-ray Photoelectron Spectroscopy Database 20, Version 3.0,*, National Institute of Standards and Technology, Gaithersburg.
209 F. R. Kogler and U. Schubert, *Polymer*, 2007, 48, 4990-95.
210 Y. Rong, H.-Z. Chen, G. Wu and M. Wang, *Mater. Chem. Phys.*, 2005, 91, 370-74.
211 H. Zhao, S. D. Argoti, B. P. Farrell and D. A. Shipp, *J. Polym. Sci., Part A: Polym. Chem.*, 2004, 42, 916-24.
212 D. Wang, J. Zhu, Q. Yao and C. A. Wilkie, *Chem. Mater.*, 2002, 14, 3837-43.

213 Y. Gao, F. R. Kogler and U. Schubert, *J. Polym. Sci., Part A: Polym. Chem.*, 2005, 43, 6586-91.
214 G. F. Levchik, K. Si, S. V. Levchik, G. Camino and C. A. Wilkie, *Polym. Degrad. Stab.*, 1999, 65, 395-403.
215 F. R. Kogler, T. Koch, H. Peterlik, S. Seidler and U. Schubert, *J. Polym. Sci., Part B: Polym. Phys.*, 2007, 45, 2215-31.
216 N. Guo, L. Li and T. J. Marks, *J. Am. Chem. Soc.*, 2004, 126, 6542-43.
217 Q. R. Huang, H.-C. Kim, E. Huang, D. Mecerreyes, J. L. Hedrick, W. Volksen, C. W. Frank and R. D. Miller, *Macromolecules*, 2003, 36, 7661-71.
218 A. Bergeret and N. Alberola, *Polymer*, 1996, 37, 2759-65.
219 J. Kuljanin, M. Vuckovic, M. I. Comor, N. Bibic, V. Djokovic and J. M. Nedeljkovic, *Eur. Polym. J.*, 2002, 38, 1659-62.
220 J. Kuljanin, M. Marinovic-Cincovic, S. Zec, M. I. Comor and J. M. Nedeljkovic, *J. Mater. Sci. Lett.*, 2003, 22, 235-37.
221 V. Djokovic and J. M. Nedeljkovic, *Macromol. Rapid Commun.*, 2000, 21, 994-97.
222 J. D. Peterson, S. Vyazovkin and C. A. Wight, *J. Phys. Chem. B*, 1999, 103, 8087-92.
223 E. Dzunuzovic, M. Marinovic-Cincovic, K. Jeremic, J. Vukovic and J. Nedeljkovic, *Polym. Degrad. Stab.*, 2008, 93, 77-83.
224 L. Andreozzi, M. Faetti, M. Giordano and F. Zulli, *Macromolecules*, 2005, 38, 6056-67.
225 K. Ute, N. Miyatake and K. Hatada, *Polymer*, 1995, 36, 1415-19.
226 L.-H. Lee and W.-C. Chen, *Chem. Mater.*, 2001, 13, 1137-42.
227 Armarego WLF and Perrin DD, *Purification of Laboratory Chemicals*, Reed Educational and Professional Publishing, 1996.
228 H. Friebolin, *Basic One- and Two- Dimensional NMR Spectroscopy. 4th Completely Revised and Expanded Edition*, 2004.
229 S. Mori and H. G. Barth, *Size Exclusion Chromatography*, Springer, Berlin, 1999.
230 G. R. Heal, *Princ. Therm. Anal. Calorim.*, 2002, 10-54.
231 P. G. Laye, *Princ. Therm. Anal. Calorim.*, 2002, 55-93.
232 D. B. Williams and C. B. Carter, *Transmission Electron Microscopy*, Plenum Press, 1996.
233 O. Glatter, O. Kratky and Editors, *Small Angle X-ray Scattering*, 1982.
234 A. Guinier and G. Fournet, *Small-Angle Scattering of X-rays*, 1955.
235 G. M. Sheldrick, ed. G. University of Göttingen, 1996.
236 G. M. Sheldrick, ed. G. University of Göttingen, 1997.
237 N. C. Santos and M. A. R. B. Castanho, *Biophys. J.*, 1996, 71, 1641-50.
238 B. J. Berne and R. Pecora, *Dynamic Light Scattering: with Applications to Chemistry, Biology, and Physics*, 1975.
239 S. Brunauer, P. H. Emmett and E. Teller, *J. Am. Chem. Soc.*, 1938, 60, 309-19.
240 M. Sibrian-Vazquez and D. A. Spivak, *J. Org. Chem.*, 2003, 68, 9604-11.
241 G. M. Kosolapoff, *J. Am. Chem. Soc.*, 1944, 66, 109-11.
242 G. M. Kosolapoff, *J. Am. Chem. Soc.*, 1944, 66, 1511-12.
243 G. M. Kosolapoff, *J. Am. Chem. Soc.*, 1945, 67, 1180-2.
244 T. Vallant, H. Brunner, U. Mayer and H. Hoffmann, *Langmuir*, 1998, 14, 5826-33.

Curiculum Vitae

Dipl. Ing. Sorin Ivanovici
Schlüsselgasse 2/16
A-1040 Vienna, Austria
Tel.: +43-(0)650-6421767
Email: sorin.ivanovici@gmail.com
Born: April 4th 1980 in Bucharest, Romania
Citizenship: Romanian
Unmarried, no children

EDUCATION

11/2004 – 06/2008	**Vienna University of Technology, Austria** PhD in Materials Chemistry
2/2004 – 8/2004	**University of Ghent, Faculty of Science, Department of Inorganic and Physical Chemistry, Belgium** Research project
10/1999 – 9/2004	**University 'Politehnica' of Bucharest, Faculty of Chemistry, Romania** Chemistry studies with emphasis on polymer chemistry and materials chemistry Degree: Dipl. Ing. with distinction
1995 - 1999	**National College ‚Gheorghe Lazar'** High school degree ('Bacalaureat') with distinction

RESEARCH EXPERIENCE

11/2004 – present	**PhD, Vienna University of Technology** Title: *Synthetic Methods to Control the Structure of Titania – Polymer Hybrid Materials and Nanocomposites* under the supervision of Prof. Guido Kickelbick
09/2004	**Diploma Thesis, University 'Politehnica' Bucharest,** Topic: *Synthesis and Characterization of Polydicyclopentadiene* under supervision of Prof. Horia Iovu at the University 'Politehnica' of Bucharest and Prof. Francis Verpoort at University Gent
02/2004 - 08/2004	**Research project, University of Ghent,** Topic: *Synthesis and Characterization of Polydicyclopentadiene* under supervision of Prof. Francis Verpoort
07/2003-08/2003	**Trainee in R&D,** S.C. CHIMCOLOR S.A., quality control of resins and dyes
07/2002-08/2002	**Trainee in R&D,** S.C. DANUBIANA S.A., quality control

HONORS & GRANTS

02/2004 Erasmus Scholarship
1999-2004 University 'Politehnica' of Bucharest – Scholarship for outstanding Students

PUBLICATIONS and PRESENTATIONS

4 publications in international peer-reviewed journals, 2 submitted, 2 in preparation (pdf copies are available on request). Chapter contribution in two books (in print).
Various oral presentations and posters at international and national conferences. Participation in various trainings and summer schools (Training in Electron Microscopy, TU Vienna, 2006, 2007; Sol-gel summer school, September 2006, Seefeld; Light-scattering workshop, Vienna 2006)

PROFESSIONAL ACTIVITIES

- Member of the GÖCH (Gesellschaft Österreichischer Chemiker)
- Member of the ISGS (International Sol-Gel Society)

PERSONAL SKILLS AND INTERESTS

- Languages: Romanian (mother tongue), English (excellent), German (good), French (basic)
- Computer Skills: MS Windows; MS Office
- Recreation activities: music, travel, literature, sport

Publications in International Peer-Reviewed Journals

1. Guido Kickelbick, Dieter Holzinger, Dieter Rutzinger, Sorin Ivanovici: "*Synthesis of inorganic-polymer nanocomposites by atom transfer radical polymerization using initiators or polymerizable groups attached to transition metals via bidentate ligands"* ACS Symposium Series (2006), 944(Controlled/Living Radical Polymerization), 269-278. ISSN:0097-6156. AN 2007:1005516.

2. Sorin Ivanovici, Michael Puchberger, Helmut Fric, Guido Kickelbick: "*Coordi nation Behavior of Acetoacetate Ligands with Attached Methacrylate Groups Containing Alkyl-Spacers of Different Length to Titanium and Zirconium Alkoxides*"; Monatshefte für Chemie, **138** (2007), 6; S. 529 - 539.

3. Sorin Ivanovici, Christoph Rill, Claudia Feldgitscher, Guido Kickelbick: *"Hybrid Nanocomposites Based on Metal Oxides and Polysiloxanes with Controlled Morphology"*; *Organic/Inorganic Hybrid Materials—2007*, edited by R.M. Laine, C. Sanchez, C. Barbé , U. Schubert (Mater. Res. Soc. Symp. Proc. **Volume 1007**, Warrendale, PA, 2007)

4. Sorin Ivanovici, Herwig Peterlik, Claudia Feldgitscher, Michael Puchberger, Guido Kickelbick: "*Atom Transfer Radical Polymerizations of Complexes Based on Ti and Zr Alkoxides Modified with β-Keto Ester Ligands and Transformation of the Resulting Polymers in Nanocomposites*"; Macromolecules, **41** (2008), S. 1131 – 1139

5. Sorin Ivanovici, Guido Kickelbick: *"Synthesis of hybrid polysiloxane-MO_2 (M = Si, Ti, Zr) nanoparticles through a sol–gel route"*; J Sol-Gel Sci Technol, (2008), 46(3), 273-280

6. Sorin Ivanovici, Christoph Rill, Thomas Koch, Michael Puchberger, Guido Kickelbick: *"Solvent effects in the formation of hybrid materials based on titanium alkoxide-polysiloxane precursors"*; New Journal of Chemistry, (2008), 32(7), 1243-1252

7. Claudia Feldgitscher, Sorin Ivanovici, Guido Kickelbick: *"Versatile Hybrid Polymers as Matrices for Nanoparticle Preparation"; Organic/Inorganic Hybrid Materials—2007*, edited by R.M. Laine, C. Sanchez, C. Barbé , U. Schubert (Mater. Res. Soc. Symp. Proc. **Volume 1007**, Warrendale, PA, 2007)

8. Christoph Rill, Sorin Ivanovici, Guido Kickelbick: *"Hybrid Nanoparticles Prepared by In-situ and Post-synthetic Surface Modification of Lanthanide-Based Nanoparticles with Phosphonic Acid Derivatives"; Organic/Inorganic Hybrid Materials—2007*, edited by R.M. Laine, C. Sanchez, C. Barbé , U. Schubert (Mater. Res. Soc. Symp. Proc. **Volume 1007**, Warrendale, PA, 2007

Book contributions

1. Guido Kickelbick, Claudia Feldgitscher, Sorin Ivanovici: "*Polysiloxane Based Polymer Nanocomposites"* in Polymer Nanocomposite Research Advances; in press. 2008

2. Guido Kickelbick, Dieter Holzinger, Sorin Ivanovici: *"Organically Functionalized Silica Nanoparticles"* in Material Synthesis; in press. 2008

Selected Oral Presentations and Posters

1. S. Ivanovici, M. Puchberger, G. Kickelbick:
"*β-keto esters bearing polymerizable groups as precursors for hybrid inorganic-organic materials*";
Poster: 11. Austrian Chemistry Days, Montanuniversität Leoben; 19.09.2005 - 22.09.2005.

2. S. Ivanovici, G. Kickelbick:
"*Synthesis of molecular building blocks as precursor for nanocomposite materials*";
Oral Presentation: 4. Workshop Inorganic Chemistry in Austria (4.WACÖ), Eisenstadt; 10.04.2006 - 11.04.2006.

3. S. Ivanovici, M. Puchberger, G. Kickelbick:
"*Hybrid Inorganic-Organic Materials by Coordinative Linkage between Polymers and Metal Alkoxides*";
Poster: Junior Scientist Conference, Vienna University of Technology; 19.04.2006 - 21.04.2006; in: "*Junior Scientist Conference 2006*", (2006), ISBN: 3-902463-05-8; S. 133 - 134.

4. S. Ivanovici, C. Rill, C. Feldgitscher, M. Puchberger, T. Koch, G. Kickelbick:
"*Hybrid nanocomposites based on metal oxides and polysiloxanes with controlled morphology*"; Poster: MRS Spring Meeting, San Francisco; 09.04.2007 - 13.04.2007.

5. G. Kickelbick, S. Ivanovici, F. Hamza:
"*Giving a Structure to Soft Matter - Synthesis and Properties of Inorganic-organic*

Hybrid Materials Combining Metal Complexes and Polysiloxanes."; MRS Spring Meeting, San Francisco; 09.04.2007 - 13.04.2007.

6. C. Rill, S. Ivanovici, G. Kickelbick:
"*Hybrid Nanoparticles Prepared by In-situ and Post-synthetic Surface Modification of Neodymium-based Nanoparticles with Phosphonic Acid Derivatives*";
Poster: MRS Spring Meeting, San Francisco; 09.04.2007 - 13.04.2007.

7. S. Ivanovici, G. Kickelbick:
"*Click chemistry im materials science: modified spherosilicates as building blocks for hybrid inorganic-organic nanocomposites*";
Poster: 9th FIGIPAS, Vienna University of Technology; 04.07.2007 - 07.07.2007; in: "*9th FIGIPAS, Meeting in Inorganic Chemistry*", (2007), ISBN: 978-80-227-2680-1; S. 203.

8. S. Ivanovici, D. Francová, M. Raza, G. Kickelbick:
"*Synthesis of anisotropically modified anatase nanoparticles ba a sol-gel approach*";
Poster: XIV International Sol-Gel Conference, Montpellier, France; 02.09.2007 - 07.09.2007; in: "*XIV International Sol-Gel Conference - Abstracts*", (2007), S. 318.

9. S. Ivanovici, G. Kickelbick:
"*Synthesis of Anisotropically Modified Anatase Nanoparticles by a Sol-Gel Approach*"; Oral Presentation: 12. Austrian Chemistry Days, Klagenfurt; 10.09.2007 - 13.09.2007; in: "*12. Austrian Chemistry Days - Abstracts*", (2007), ISBN: 978-3-900554-61-3; S. 45.

10. A. Bachinger, S. Ivanovici, G. Kickelbick:
"*A Click Chemistry Approach to the Incorporation of Modified Spherosilicates to Organic and Inorganic Polymers*"; Poster: 12. Austrian Chemistry Days; 10.09.2007 - 13.09.2007; in: "*12. Austrian Chemistry Days - Abstracts* ", (2007), ISBN: 978-3-900554-61-3; S. 75.

11. F. Hamza, S. Ivanovici, G. Kickelbick:
"*Preparation of Copper(II) Carboxylate Core-shell Nanoparticles*";
Poster: 12. Austrian Chemistry Days, Klagenfurt; 10.09.2007 - 13.09.2007; in: "*12. Austrian Chemistry Days - Abstracts* ", (2007), ISBN: 978-3-900554-61-3; S. 28.

12. M. Raza, S. Ivanovici, G. Kickelbick:
"*Anisotropic Surface Functionalization of Titania Nanoparticles by a Silica Shell*";
Poster: 12. Austrian Chemistry Days, Klagenfurt; 10.09.2007 - 13.09.2007; in: "*12. Austrian Chemistry Days - Abstracts* ", (2007), ISBN: 978-3-900554-61-3; S. 62.